Detrital zircon fission-track thermochronology and U-Pb geochronology of syn-rift, Lower Cretaceous Hibernia Formation strata, Jeanne d'Arc basin, offshore Newfoundland

By Emily Johns-Buss

A Thesis submitted to the School of Graduate Studies in partial fulfillment

of the requirements for the degree of

Master of Science, Department of Earth Sciences

Memorial University of Newfoundland

December 2021

St. John's, Newfoundland and Labrador

GENERAL SUMMARY

The Newfoundland margin was established after Mesozoic continental rifting broke up supercontinent Pangea and opened the North Atlantic Ocean between North America and Europe. Normal faults cut through the lithosphere to accommodate extension and created a dynamic landscape that shifted as the rift system evolved over ~150 million years. Upper Triassic to Upper Cretaceous sedimentary rock units of the Jeanne d'Arc basin, Grand Banks, offshore Newfoundland, have been broadly correlated to rift processes, however, the precise timing of rift-related exhumation and details of ancient drainage systems were uncertain. New stratigraphic and sediment provenance results for Lower Cretaceous Hibernia Formation strata, including those that are known reservoir units at the Hibernia oil field, confirm rift-related exhumation was occurring in the Grand Banks during the Triassic to Jurassic and Early Cretaceous and can be tied to rift processes occurring further offshore in deep-water settings. North-flowing, Early Cretaceous rivers and delta systems drained highlands that were located south of the Jeanne d'Arc basin and comprised both uplifted rocks of the Appalachian orogen and active, syn-rift volcanic centers.

ACKNOWLEDGEMENTS

Throughout the writing of this thesis I have received a great deal of support and assistance. I would first like to thank my supervisor, Dr. Luke Beranek, for providing the opportunity for this project. His unwavering patience, engaging scientific discussions, and countless revisions allowed this thesis to come to life and brought my work to a higher level. Thank you to Dr. Eva Enkelmann, Dr. Scott Jess, and Dr. William Matthews from the Geo- and Thermochronology Laboratory for their assistance during my time at the University of Calgary. Dr. Eva Enkelmann provided instrument guidance and supervision of my lab work and data interpretation. Her willingness to take time and provide insightful feedback throughout the writing process accelerated the evolution of my ideas and understanding of thermochronology. I would also like to thank Dr. Scott Jess and Dr. William Matthews for daily discussions and problem solving during my time at the University of Calgary and quickly running my final samples only days before the COVID-19 shutdown. A huge thank you to Matthew Crocker and Adam Wiest for the training and support during the tight time window I had for completing the detrital zircon separation. Thank you to Dr. Stephen Piercey for being on my committee and reviewing this thesis. I could not have completed this project without the support of fellow students Adam Wiest, Maya Soukup, and Gabriel Sindol for the many virtual meetings, quality conversations about our research and happy distractions that kept me on track over the last two years. Finally, thank you to the Geo- and Thermochronology Research Group for welcoming me in their meetings and providing weekly inspiration.

This project was supported by NSERC Discovery Grants to Luke Beranek. I would also like to acknowledge financial support during my thesis from the Canadian Society of Petroleum Geologist Regional Graduate Student Scholarship, Husky Education Fund Scholarship, and Chevron Canada Limited Rising Star Award.

CO-AUTHORSHIP STATEMENT

The design of this research project is accredited to Dr. Luke Beranek. The author conducted the primary research that included core logging, sample collection and preparation, laboratory analysis, and data interpretation. Drillcore viewing and sample collection were conducted at the Canada-Newfoundland and Labrador Offshore Petroleum Board Core Storage and Research Centre in St. John's. All samples were crushed, milled, and density separated at Memorial University of Newfoundland by the author in CREAIT labs run by Matthew Crocker. Detrital zircon U-Pb and fission-track double-dating was performed by the author under supervision of Dr. Eva Enkelmann, Dr. Scott Jess, and Dr. William Matthews in the University of Calgary Geo- and Thermochronology Laboratory. Age determinations and data-filtering were completed by Dr. William Matthews and the author. The primary editor of this manuscript is Dr. Luke Beranek, with secondary editing performed by Dr. Stephen Piercey.

TABLE OF CONTENTS

LIST OF TABLES

LIST OF FIGURES

LIST OF APPENDICES

CHAPTER 1: OVERVIEW

1.1 Introduction

Passive margins have likely existed on Earth since the Neoarchean era and modern examples account for ~105,000 km of present coastlines, which are greater than the lengths of mid-ocean spreading ridges (~65,000 km) and convergent (~53,000 km) plate boundaries (e.g., Bradley, 2008). Passive margins result from extensional processes that affect the entire lithosphere and provide insights into the nature of continental rifting, lithospheric breakup, and formation of divergent plate boundaries (e.g., McKenzie, 1978; Lister et al., 1986; Bradley, 2008). Although early rift models were based on tectonic scenarios where stretching is instantaneous and uniform for all layers of the lithosphere (McKenzie, 1978), there is now consensus that non-plume-related rifting includes polyphase, depth-dependent stretching that is decoupled between lithospheric layers (e.g., Davis and Kusznir et al., 2004, Lavier and Manatschal 2006, Huismans and Beaumont, 2014). Continental extension in polyphase rift scenarios takes place over >100 Myr and includes discrete modes of lithospheric stretching and thinning, hyperextension and mantle exhumation, and lithospheric breakup (e.g., Péron-Pinvidic and Manatschal, 2009). Stepwise progression through these extensional modes results in a complex transition zone between highly extended continental lithosphere and oceanic lithosphere with margin-parallel domains (proximal, necking, distal, outer, and oceanic domains) that collectively record continental margin development (e.g., Lavier and Manatschal, 2006, Péron-Pinvidic and Manatschal, 2009; Péron-Pinvidic et al., 2013; Huismans and Beaumont, 2014). The Newfoundland (SE Grand Banks)-Iberia conjugate margins (Fig. 1-1A) record the evolution of the Newfoundland-Iberia magma-poor rift system that developed during the protracted breakup of supercontinent Pangea and opening of the North Atlantic Ocean. The Newfoundland-Iberia rift system is used as the basis for modern theoretical

models of magma-poor rift evolution, largely constrained by marine seismic and scientific drilling data in the offshore regions (e.g., Boillot et al., 1980; Jagoutz et al., 2007; Péron-Pinvidic et al., 2013; Sutra et al., 2013; Haupert et al., 2016). Triassic to Jurassic stretching and thinning (proximal and necking domains), Early to mid-Cretaceous hyperextension and mantle exhumation (distal domain), and mid-Cretaceous breakup-related (outer domain) events characterize the main phases of Newfoundland-Iberia rift evolution (Fig. 1-1B; e.g., Péron-Pinvidic et al., 2013). Mesozoic basins with predominantly clastic basin fill occur along both margins and indicate that significant exhumation and erosion in the proximal domain occurred during Mesozoic rifting (e.g., Hiscott et al., 1990a), however, the predicted exhumation histories during Triassic to Cretaceous rift development have yet to be tested.

The Jeanne d'Arc basin is an asymmetric graben in the proximal domain (Grand Banks) of the Newfoundland margin and contains up to 18 km of syn-rift to post-rift strata (Fig. 1-1B; Enachescu, 1988). Upper Triassic to Upper Cretaceous rocks of the Jeanne d'Arc basin have been broadly correlated with rift episodes in the North Atlantic region (e.g., Hiscott et al., 1990; Shannon et al., 1995; Williams et al., 1999; Tucholke et al., 2007). However, the precise depositional age, provenance, and tectonic significance of these proximal domain units with respect to coincident Late Jurassic to Cretaceous growth of outboard (necking, distal, outer) domains and Mesozoic paleodrainage evolution are uncertain (e.g., Hutter and Beranek, 2020). Upper Jurassic to Lower Cretaceous braided fluvial strata of the Jeanne d'Arc Formation were sourced from volcanic centers along the SW Grand Banks transform fault and Appalachian highlands within the Avalon Uplift to the south of the Jeanne d'Arc basin as a result of rift-related tectonism in the proximal domain during the necking phase (Fig. 1-1B; e.g., Hutter and Beranek, 2020). Overlying Lower Cretaceous shallow-marine strata of the Hibernia Formation have

untested source-to-sink histories and geological connections with deformation events that involved hyperextension and mantle exhumation (distal domain) outboard of the modern Grand Banks.

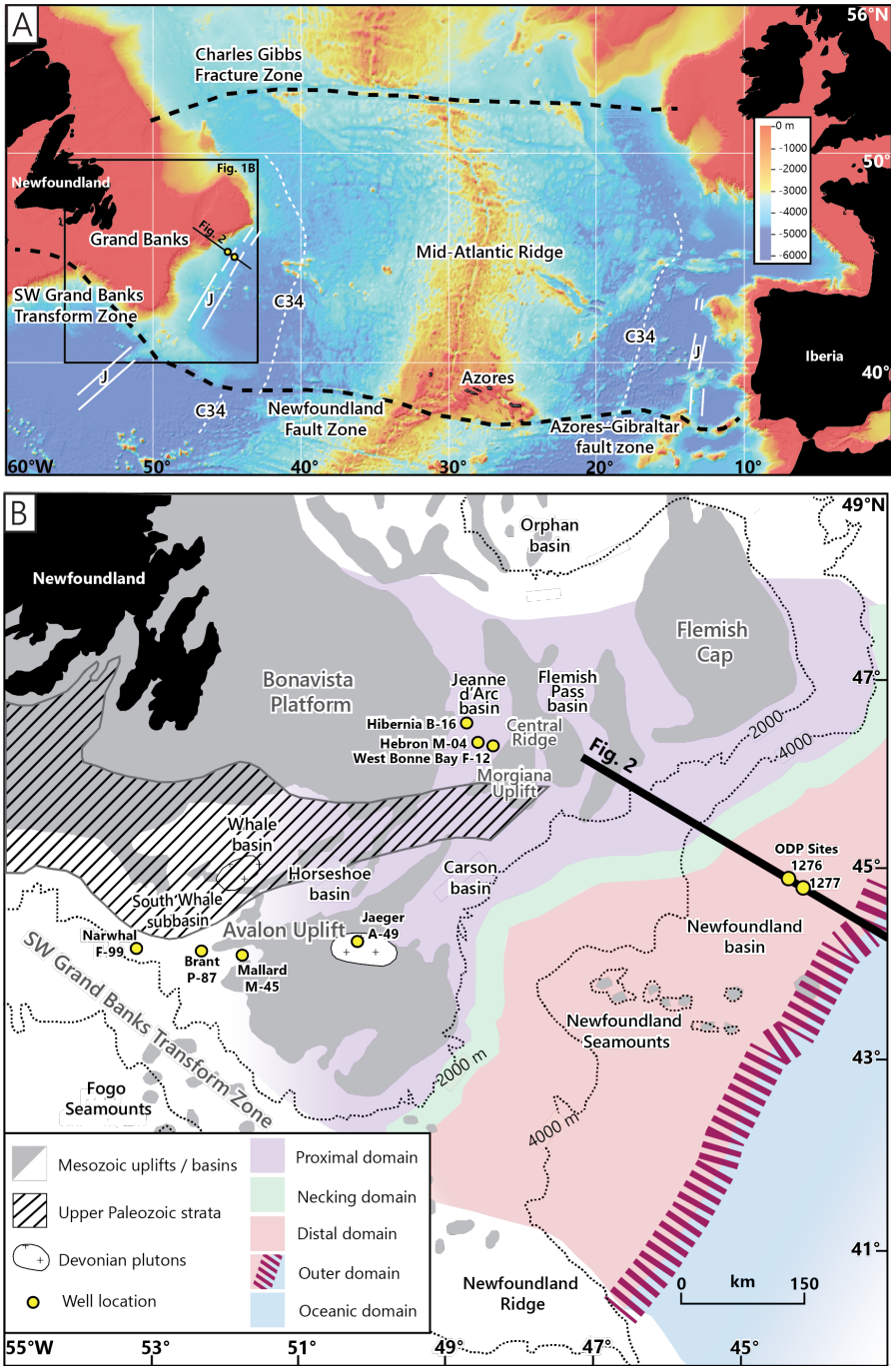

Figure 1-1: (a) Bathymetric map of the southern North Atlantic Ocean and primary features of the Newfoundland-Iberia rift system compiled from Ryan et al. (2009) and Bronner et al. (2011), (b) Locations of Mesozoic architectural elements, upper Paleozoic strata, and Devonian plutons in the Grand Banks and nearby regions after Grant and McAlpine (1990), Bell and Howie (1990) and Péron-Pinvidic et al. (2013).

New studies of Jeanne d'Arc basin strata are required to identify the timing of regional exhumation and source-to-sink connections along this archetypal magma-poor rift system. In this thesis, detrital zircon U-Pb and fission-track double-dating investigations of Hibernia Formation strata are used to constrain Early Cretaceous and older exhumation- and magmatic-cooling events (e.g., Carter and Moss, 1999; Montario and Garver, 2009; Enkelmann et al., 2019), sediment provenance signatures, and maximum depositional ages of syn-rift rocks deposited in a proximal domain setting. The results allowed published rift models for the Newfoundland margin to be tested, including predictions for proximal domain evolution during hyperextension and mantle exhumation (e.g., Péron-Pinvidic et al., 2013; Sutra et al., 2013), Berriasian to Valanginian depositional ages for Hibernia Formation strata to be established, and working hypotheses for the Early Cretaceous paleogeography of the Grand Banks region to be developed to include north-flowing fluvial and deltaic systems that drained exhumed Appalachian cover assemblages of the Avalon Uplift and coeval, syn-rift volcanic-plutonic complexes along the SW Grand Banks transform fault.

1.2 Geological Background

1.2.1 North Atlantic rift evolution

Magma-poor rift systems are underlain by several margin-parallel architectural domains that have predictable geological elements and geophysical signatures worldwide (e.g., Péron-Pinvidic et al., 2013). In the southern North Atlantic Ocean, the Newfoundland and Iberian margins transition seaward from thick, undisturbed continental crust into proximal, necking, distal, outer, and oceanic domains that progressively developed during the Late Triassic to Late Cretaceous periods (Fig. 1-2; Péron-Pinvidic et al., 2013; Sutra et al., 2013). The Jeanne d'Arc basin, located in the Grand Banks of Newfoundland (proximal domain), records a polyphase subsidence history

that resulted from episodic tectonism during the breakup of eastern North America, Africa, UK, Ireland, and Iberia (Sinclair, 1988; Tankard et al., 1989; Soares et al., 2012; Péron-Pinvidic et al., 2013; Sutra et al., 2013; Nirrengarten et al., 2018). The proximal domains of the Newfoundland-Iberia system initially formed by widely distributed, upper crustal extension that resulted in the formation of intracontinental rift basins, including the Jeanne d'Arc basin, over a vast region without significant thinning (Tucholke et al., 2007). Thermal subsidence and slow extensional motion between Newfoundland and Iberia (<2.0 cm/year) subsequently occurred during the Early Jurassic following the breakup of North Africa and eastern North America near present-day Nova Scotia further south (Tankard et al., 1989; Sinclair, 1988; Nirrengarten et al., 2018). The transition from decoupled to coupled deformation and early development of the necking domain at the outer edge of the Grand Banks began by the early Late Jurassic (Péron-Pinvidic et al., 2013; Sutra et al., 2013). Renewed tectonic exhumation and subsidence in the Jeanne d'Arc basin and adjacent rift grabens at this time were accommodated by north- to north-northeast-trending normal faults (Tankard et al., 1989, Sinclair, 1988). The necking phase culminated with Early Cretaceous hyperextension and/or mantle exhumation episodes, which promoted the development of the distal domain and penetration of faults through the entire crust and mantle lithosphere (Fig. 1-2; Péron-Pinvidic et al., 2013). Berriasian and Hauterivian rift episodes recognized in the Jeanne d'Arc basin may correlate with the rupture of crust in the southern and northern parts of the Newfoundland-Iberia rift system, respectively (Tucholke et al., 2007; Nirrengarten et al., 2018).

Early to mid-Cretaceous exhumation of continental mantle lithosphere resulted in wide transition zones of serpentinized mafic-ultramafic rocks in the distal and outer domains prior to lithospheric breakup (Fig. 1-2; Péron-Pinvidic et al., 2013). The principal stress orientation in the Jeanne d'Arc basin shifted to a northeast-southwest direction by the mid-Cretaceous and drove

dip-slip motion along transfer faults that previously accommodated strike-slip displacement (Tankard et al., 1989). Final lithospheric breakup between Newfoundland and Iberia occurred by the late Aptian (e.g., Tankard et al., 1989; Sutra et al., 2013; Eddy et al., 2017) and was in part triggered by a high-volume magmatic event in the outer domain, a region with high relief that includes thickened crust and underplated, exhumed mantle lithosphere (Fig. 1-2; Bronner et al., 2011). This magmatic event produced a large-magnitude, linear magnetic anomaly (J anomaly; Fig. 1-1A) that has a long-lived and complicated history of syn- to post-breakup magmatism (Nirrengarten et al., 2018).

Lithospheric breakup and the onset of seafloor spreading in the southern North Atlantic Ocean likely began in the south near the Newfoundland-Azores-Gibraltar fracture zone and propagated northwards (e.g., Alves et al., 2006; Bronner et al., 2011). The C34 anomaly (~85 Ma) represents the oceanward extent of the outer domain and is the oldest undisputed seafloor spreading isochron in the modern oceanic domain (Fig. 1-1A; Bronner et al., 2011). Syn-breakup

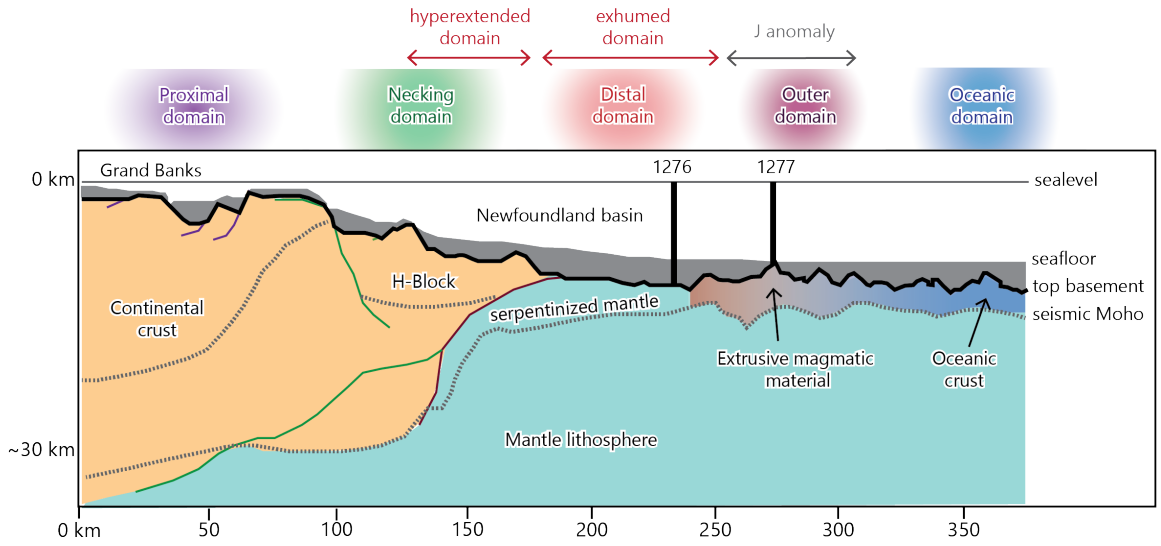

Figure 1-2: Schematic cross-section of the Newfoundland margin after Péron-Pinvidic et al. (2013). Location of J anomaly from Bronner et al. (2011).

and off-axis, post-breakup magmatism persisted in the outer domain until at least 70 Ma (e.g., Jagoutz et al., 2007; Nirrengarten et al., 2018). Lithospheric breakup in the proximal domain is manifested by an unconformity referred to as the U reflection, a prominent seismic reflector at the Aptian-Albian boundary in the Jeanne d'Arc basin and elsewhere (Tankard et al., 1989; Péron-Pinvidic et al., 2013; Sutra et al., 2013; Nirrengarten et al., 2018). Thermal subsidence dominated the Jeanne d'Arc basin after regional breakup-related uplift (e.g., Soares et al., 2014) and extension in the adjacent Orphan basin (Sinclair, 1988, Tucholke et al., 2007).

1.2.2 Newfoundland margin

The Newfoundland margin is underlain by Proterozoic to Paleozoic rocks of the Appalachian orogen that span the onshore and offshore portions of eastern North America and record the accretion of arcs and microcontinents prior to the final Laurentia-Gondwana collision and assembly of supercontinent Pangea (Fig. 1-3; e.g., van Staal and Barr, 2012). The Canadian Appalachians comprise the northern extent of the orogen and are subdivided into several lithotectonic components that from west to east represent the ancient Laurentian margin, peri-Laurentian arc and ophiolite fragments, peri-Gondwanan arc fragments, and the peri-Gondwanan Gander, Avalon, and Meguma terranes (e.g., Williams, 1979). Paleozoic events associated with the Taconic (500-450 Ma), Salinic (440-420 Ma), Acadian (420-400 Ma), Neoacadian (400-350 Ma), and Alleghenian (340-260 Ma) orogenies generated collision-related igneous suites and orogen-proximal basins that record Appalachian evolution (e.g., van Staal and Barr, 2012). In Atlantic Canada, the late Paleozoic Alleghenian orogeny included dextral-oblique convergence and filling of strike-slip basins with Upper Devonian to Permian strata (Fig. 1-3; van de Poll et al., 1995; Gibling et al., 2008; Waldron et al., 2015). Proterozoic to Paleozoic rocks in central and western Newfoundland yield Late Triassic zircon fission-track (Willner et al., 2019) and Jurassic

and older apatite fission-track (Hendriks et al., 1993) ages, respectively, that are consistent with Mesozoic exhumation of Appalachian infrastructure and recycling of basement and cover assemblages into the Jeanne d'Arc and related rift basins.

The Grand Banks is a ~500 km-wide platform of submerged continental crust that consists of Neoproterozoic (760-550 Ma) igneous and meta-sedimentary basement units assigned to Avalonia and Cambrian to Ordovician (537-475 Ma) meta-sedimentary strata and Late Devonian plutons assigned to Meguma (Fig. 1-3; Bell and Howie, 1990; Tucholke et al., 2007; van Staal and Barr, 2012). The SW Grand Banks fault zone is part of a margin-normal, strike-slip fault system that transitions onshore into the Cobequid-Chedabucto or Minas fault zone in Nova Scotia that bounds Avalonia and Meguma (Fig. 1-3; Pe-Piper and Piper, 2004; Murphy et al., 2011).

Lower Paleozoic cover assemblages of Avalonia yield 550-750 Ma and 2000-2200 Ma detrital zircon age populations and indicate provenance from underlying arc basement and recycling of peri-Gondwanan cratonal signatures (e.g., Pollock et al., 2009, Barr et al., 2012). Cambrian to Ordovician cover assemblages in Meguma yield 550-750, 2000-2200, and 2500-3000 Ma detrital zircon age populations (e.g., Waldron et al., 2009, Krogh and Keppie, 1990) and are deformed and intruded by Late Devonian (ca. 375-370 Ma) plutons (e.g., Keppie and Krogh, 1999; Maclean et al., 2003; Kontak et al., 2004). Upper Paleozoic terrestrial to marine strata derived from the Canadian Appalachians represent overlap assemblages that sit unconformably on basement and may also have originally covered the Grand Banks region (Fig. 1-3; Bell and Howie, 1990; Gibling et al., 2008). Upper Paleozoic strata in Nova Scotia yield 370-380, 500-700, and 2000-2200 Ma detrital zircon populations that indicate recycling from clastic rocks of the Avalon and Meguma terranes with minor contributions from Appalachian igneous suites (e.g., Murphy and Hamilton, 2000; Force and Barr, 2012).

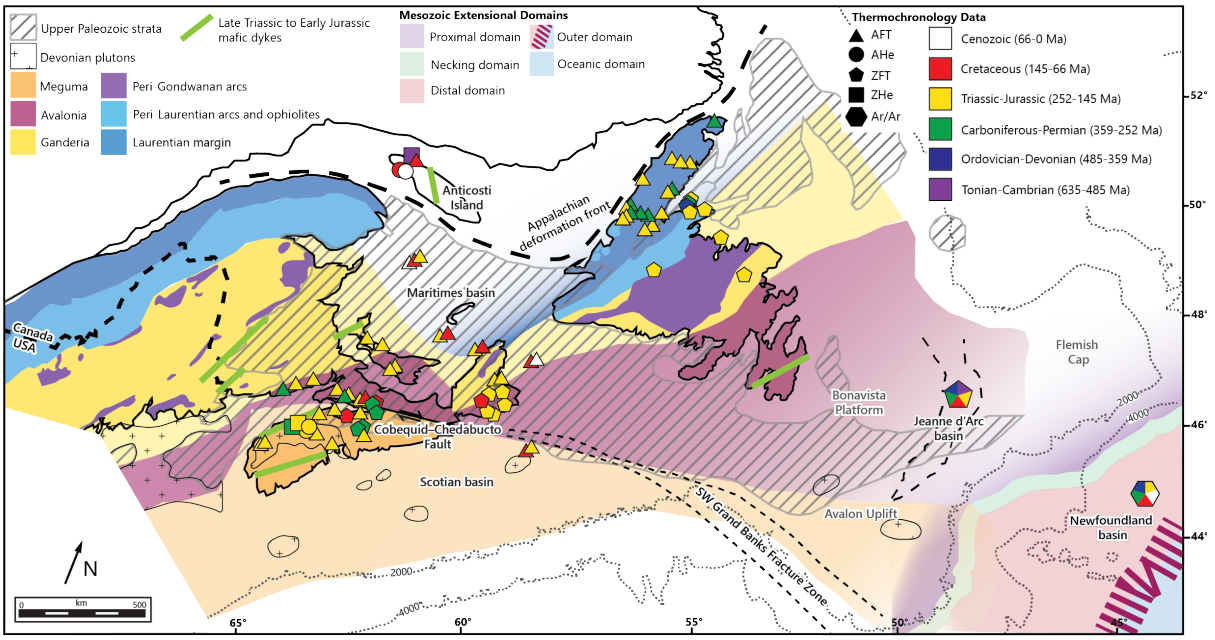

Figure 1-3: Compiled mica ^{40}Ar-^{39}Ar, zircon fission-track and (U-Th)/He, and apatite fission-track and (U-Th)/He ages from Cretaceous and older rocks in Atlantic Canada modified from Willner et al. (2019) and sources in Table 1-1. Tectonic map of northern Appalachians basement and early Paleozoic lithotectonic elements after van Staal and Barr (2012). Inferred extensions into offshore Nova Scotia and Newfoundland after Bell and Howie (1990). Early Triassic–Late Jurassic mafic dyke locations after Greenough (1995).

Triassic to Cretaceous syn-rift strata unconformably overlie upper Paleozoic and older rocks and filled multiple basins (e.g. Jeanne d'Arc, Flemish Pass, Whale, and Orphan basins) during North Atlantic rift evolution (e.g., Sinclair, 1988). Some syn-rift units are preserved on uplifted sediment ridges that now separate depocenters (e.g., Central Ridge, Morgiana Uplift; Enachescu, 1987, 1988). Extensional deformation and tectonic subsidence alternated with periods of thermal subsidence and can be tied to the development of the proximal, necking, distal, and outer domain phases (Fig. 1-4; e.g., Sinclair, 1988; Tankard et al., 1989; Tucholke et al., 2007). Late Jurassic to Early Cretaceous tectonic subsidence in the Jeanne d'Arc basin was episodic and evidenced by stacked depositional successions, intervening unconformities, and isopach-thickening toward extensional faults (Tankard et al., 1989; Shannon et al., 1995). Multiple erosional surfaces coalesce at the basin margins into a regional unconformity that records 50-60 Myr of rift-related

deformation, uplift, and erosion (Avalon unconformity, e.g., Grant and McAlpine, 1990). Sedimentary wedges were deposited above rotated fault blocks during the growth of north-northeast-trending normal faults and rotation of subsiding blocks (Shannon et al., 1995; Williams et al., 1999).

Table 1-1: Mica ^{40}Ar-^{39}Ar, zircon fission-track and (U-Th)/He, and apatite fission-track and (U-Th)/He ages from Cretaceous and older rocks in Atlantic Canada.

Dating Method	Mica $^{40}Ar/^{39}Ar$	Zircon fission-track (ZFT)	Zircon (U-Th)/He (ZHe)	Apatite fission-track (AFT)	Apatite (U-Th)/He (AHe)
Cooling Temperature (°C)	300-400°C[(1)]	210-290°C[(2)]	160-200°C[(3)]	100-120°C[(4)]	40-80°C[(5)]
Western & Central Newfoundland		235-212 Ma[(6)] ($\bar{x}$ = 227 Ma)		343-152 Ma[(7)] ($\bar{x}$ = 232 Ma)	
Offshore Newfoundland	50-430 Ma[(8)]	122-648 Ma			
Onshore Nova Scotia		342-217 Ma[(13)(14)] ($\bar{x}$ = 225 Ma)	290-192 Ma[(15)] ($\bar{x}$ = 220 Ma)	244-165 Ma[(9)(10)(11)(12)(13)] ($\bar{x}$ = 213 Ma)	211-165 Ma[(15)] ($\bar{x}$ = 180)
Offshore Nova Scotia				200 Ma[(16)]	
Anticosti Island			761-581 Ma[(17)] ($\bar{x}$ = 655 Ma)	125 Ma[(17)]	48-16 Ma[(17)] ($\bar{x}$ = 33 Ma)

(1) Hames and Bowring (1994); (2) Tagami et al. (1998); Tagami (2005); (3) Reiners et al. (2004); (4) Green et al. (1986); Ketcham et al. (1999); (5) Farley (2000); (6) Willner et al. (2019); (7) Hendriks et al. (1993); (8) Wilson and Hiscott (2007); (9) Ryan and Zentilli (2003); Ryan (1993); (10) Ravenhurst et al. (1990); (11) Arne et al. (1990); (12) Grist and Zentilli (2003); (13) Ravenhurst et al. (1989); (14) Willner et al. (2015); (15) Chang (2017); (16) Grist et al. (1991); (17) Powell et al., (2018).

Late Jurassic to Cretaceous igneous rocks locally crop out in onshore regions of Newfoundland (Peace et al., 2018) and western Portugal (Grange et al., 2008), and more prominently along the offshore SW Grand Banks fault zone where they include volcanic centers with mafic to felsic dykes, sills, and pyroclastic flows (e.g., Pe-Piper et al., 1994; e.g., Bowman et al., 2012). Upper Jurassic fluvial strata in the Jeanne d'Arc and Flemish Pass basins yield ca. 159-145 Ma detrital zircon grains that indicate sustained rift-related magmatism in the Grand Banks during the development of the necking and distal domains (Hutter and Beranek, 2020).

1.2.3 Jeanne d'Arc basin stratigraphy

Late Jurassic to Early Cretaceous regional unconformities are recognized along the Newfoundland margin and represent long-term, recurrent extensional deformation and resultant erosion-deposition events (Grant and McAlpine, 1990). Within the Jeanne d'Arc basin, the unconformities separate Upper Jurassic to Upper Cretaceous terrestrial to shallow-marine siliciclastic units that are important reservoirs in the Grand Banks (Fig. 1-4; Sinclair, 1988). Late Callovian to middle Kimmeridgian Rankin Formation strata consist of thick limestone units with interbeds of sandstone and shale, including the Egret Member shale, the main source rock for Jeanne d'Arc basin hydrocarbon systems (Sinclair, 1988; Shannon et al., 1995; Williams et al., 1999). A late Kimmeridgian unconformity marks base-level fall and north-south-trending valleys up to 400 m deep were cut into the underlying Rankin Formation with an erosion apex to the southern Avalon Uplift (Fig. 1-1B; Sinclair, 1988; Tankard et al., 1989; Hiscott et al., 1990a; Shannon et al., 1995; Williams et al., 1999). Rivers flowed north, longitudinally along the axis of the basin, from the southern Avalon Uplift and paleovalleys became back-filled with fluvial successions of the Tithonian to early Berriasian Jeanne d'Arc Formation (Fig. 1-1B; Tankard et al., 1989; Hiscott et al., 1990a; Shannon et al., 1995, Hutter and Beranek, 2020). Subsidence eventually outpaced sedimentation and a continued transgression deposited the Fortune Bay shales that overlie and cap the Jeanne d'Arc Formation.

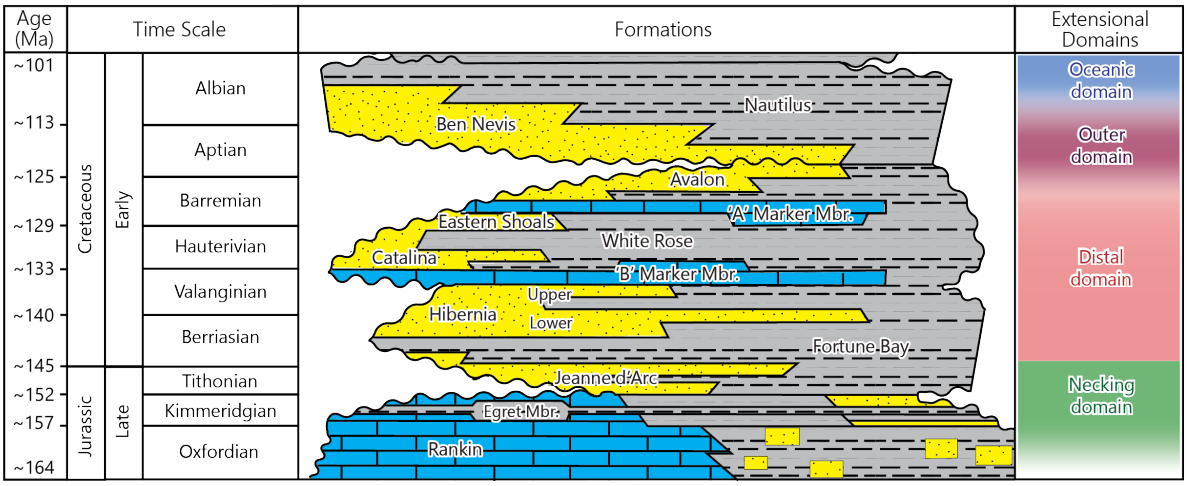

Figure 1-4: Upper Jurassic to Lower Cretaceous stratigraphy compiled by Sinclair et al. (1992) and Hutter & Beranek (2020) using the geological timescale of Cohen et al. (2013). Extensional domain development from Péron-Pinvidic et al. (2013).

Lower Cretaceous rock units of the Jeanne d'Arc basin mostly consist of nonmarine to shallow-marine siliciclastic strata (Tankard et al., 1989) that superseded north-directed, Upper Jurassic braided fluvial systems (Fig. 1-4; e.g., Hiscott et al., 1990a; Shannon et al., 1995). Early Cretaceous rise of the Avalon Uplift renewed the clastic source area and resulted in the northward progradation of Hibernia Formation deltaic successions (Sinclair, 1988; Tankard et al., 1989; Hiscott et al., 1990b; Williams et al., 1999). The lower member of the Hibernia Formation (Lower Hibernia) is comprised of stacked fluvial channels in the southwest to delta-front bar facies and coastal deposits in the northeast (Sinclair, 1988; Hiscott et al., 1990b). The upper member of the Hibernia Formation (Upper Hibernia) consists of fine-grained, shallow-marine sandstone and mudstone units that grade laterally to pro-delta shale in the northwest Hibernia oil field (Hiscott et al., 1990a). Biostratigraphic correlations based on palynomorphs, dinoflagellates, foraminifers, and ostracods indicate late Berriasian to Valanginian depositional ages in the type section of the Hibernia Formation (Williams et al., 1990).

A late Barremian to early Aptian hiatus in the stratigraphic record is marked by an unconformity that is recognized throughout the North Atlantic region (Tankard et al., 1989, Hiscott et al., 1990a). In the Jeanne d'Arc basin, the Aptian unconformity truncates underlying tilted and folded strata and is draped by Ben Nevis Formation sandstone units (Fig. 1-4; Hiscott et al., 1990a; Shannon et al., 1995; Williams et al., 1999). Ben Nevis Formation strata and laterally equivalent Nautilus Formation successions record an overall transgressive system with a large-scale fining upward character (Sinclair, 1988). Fluvial systems flowed northward along the basin axis and deposited coarse-grained sandstone, conglomerate, and organic debris (Sinclair, 1988; Hiscott et al., 1990a, 1990b; Shannon et al., 1995; Williams et al., 1999). These strata were overlain by fine-grained, beach-barrier bar sand and marine mud as the water depth continued to increase and fluvial systems retreated south (Sinclair, 1988).

1.3 Thesis Objectives

The aim of this project is to investigate the timing and spatial extent of tectonic exhumation and Early Cretaceous paleodrainage patterns in the Grand Banks region and their genetic connections to Newfoundland-Iberia rift system development. Specifically, this study analyzed syn-rift Lower Cretaceous Hibernia Formation sandstone units that were deposited in the proximal domain (Jeanne d'Arc basin) during the onset of hyperextension and mantle exhumation and development of the outboard distal domain. Detrital zircon U-Pb and fission-track (FT) signatures of Hibernia Formation strata provide new insights into magmatic- and exhumation-cooling events, sediment provenance, and Early Cretaceous landscape evolution. The following main objectives aim to address the above and are as follows:

- Constrain the lithology and physical and biogenic sedimentary structures of syn-rift, Lower Cretaceous strata in Hebron M-04, West Bonne Bay F-12, Hibernia B-16 55, and Hibernia B-16 54W drill core materials (Fig. 1-5);
- Use detrital zircon U-Pb geochronology to constrain the maximum depositional ages of Hibernia Formation strata and compare with known biostratigraphic information;
- Use detrital zircon U-Pb geochronology to identify age distributions and develop a new provenance reference frame for Hibernia Formation strata;
- Use detrital zircon fission-track thermochronology to constrain cooling age populations for Hibernia Formation strata. Specifically, investigate cooling ages that correspond to the timing of pre-rift, Appalachian-related tectonism, Triassic to Jurassic stretching and thinning, and Early Cretaceous mantle exhumation.
- Use the combination of U-Pb crystallization ages and fission-track cooling ages to identify cooling types of zircon grains (magmatic- or exhumation-cooled) and constrain the source regions contributing to basin-fill;
- Compare detrital mineral signatures to other syn-rift stratigraphic units and known source regions in Atlantic Canada and Iberia to constrain timing of exhumation, transport, and deposition patterns in the proximal domain during Early Cretaceous rift development.

1.4 Methods & Materials

1.4.1 Samples

Seven Hibernia Formation samples from the Hibernia B-16 55, Hibernia B-16 54W, Hebron M-04, and West Bonne Bay F-12 wells were analyzed for detrital zircon studies and approximately 300 meters of drillcore were described at the Canada-Newfoundland and Labrador Offshore Petroleum Board Core Storage and Research Centre in St. John's, Newfoundland and Labrador (Fig. 1-5). These include two samples of the Lower Hibernia Formation from the Hibernia oil field and five samples of the Upper Hibernia Formation in the Hebron oil field and nearby areas (Table 1-2). Each sample consisted of ~500 g of medium- to coarse-grained sandstone from full-diameter core. Zircon grains were isolated from the samples using standard crushing, milling, sieving, magnetic separation, and heavy liquid separation (methylene iodide) techniques at Memorial University of Newfoundland.

Table 1-2: Location and lithological descriptions for Hibernia Formation detrital zircon samples.

Sample	Well Name	Core - Box Numbers	Core Depth (mMD)	Approx. True Vertical Depth (mTVD)	Formation - Member	Sample Description
20EJ01	West Bonne Bay F-12	#1 - 110-113	4009-4013	3431	Upper Hibernia	medium- to coarse-grained, subrounded to rounded, moderately-sorted, massive to normally graded, quartz arenite
20EJ02	West Bonne Bay F-12	#1 - 92-96	3994-3998	3416	Upper Hibernia	fine- to medium-grained, subrounded to rounded, well-sorted, massive to planar crossbedded, sublithic arenite
20EJ03	West Bonne Bay F-12	#1 - 24-30	3941-3947	3364	Upper Hibernia	fine- to medium-grained, subrounded to rounded, well-sorted, massive to planar crossbedded, sublithic arenite
20EJ08	Hebron M-04	#3 - 37-42	3028-3037	3032	Upper Hibernia	fine- to medium-grained, subrounded to rounded, well-sorted, massive to normally graded, sublithic arenite
20EJ09	Hebron M-04	#3 - 26-33	3015-3025	3020	Upper Hibernia	fine- to medium-grained, subrounded to rounded, poor- to moderately-sorted, wavy bedded, sublithic arenite
20EJ05	Hibernia B-16 55	#2 - 3	7245-7246	4618	Lower Hibernia	medium- to coarse-grained, subrounded to rounded, well-sorted, massive to planar crossbedded, quartz arenite
20EJ06	Hibernia B-16 54W	#1 - 1-3	6989-6986	4445	Lower Hibernia	fine- to medium-grained, subrounded to rounded, moderately- to well-sorted, massive to planar crossbedded, sublithic arenite

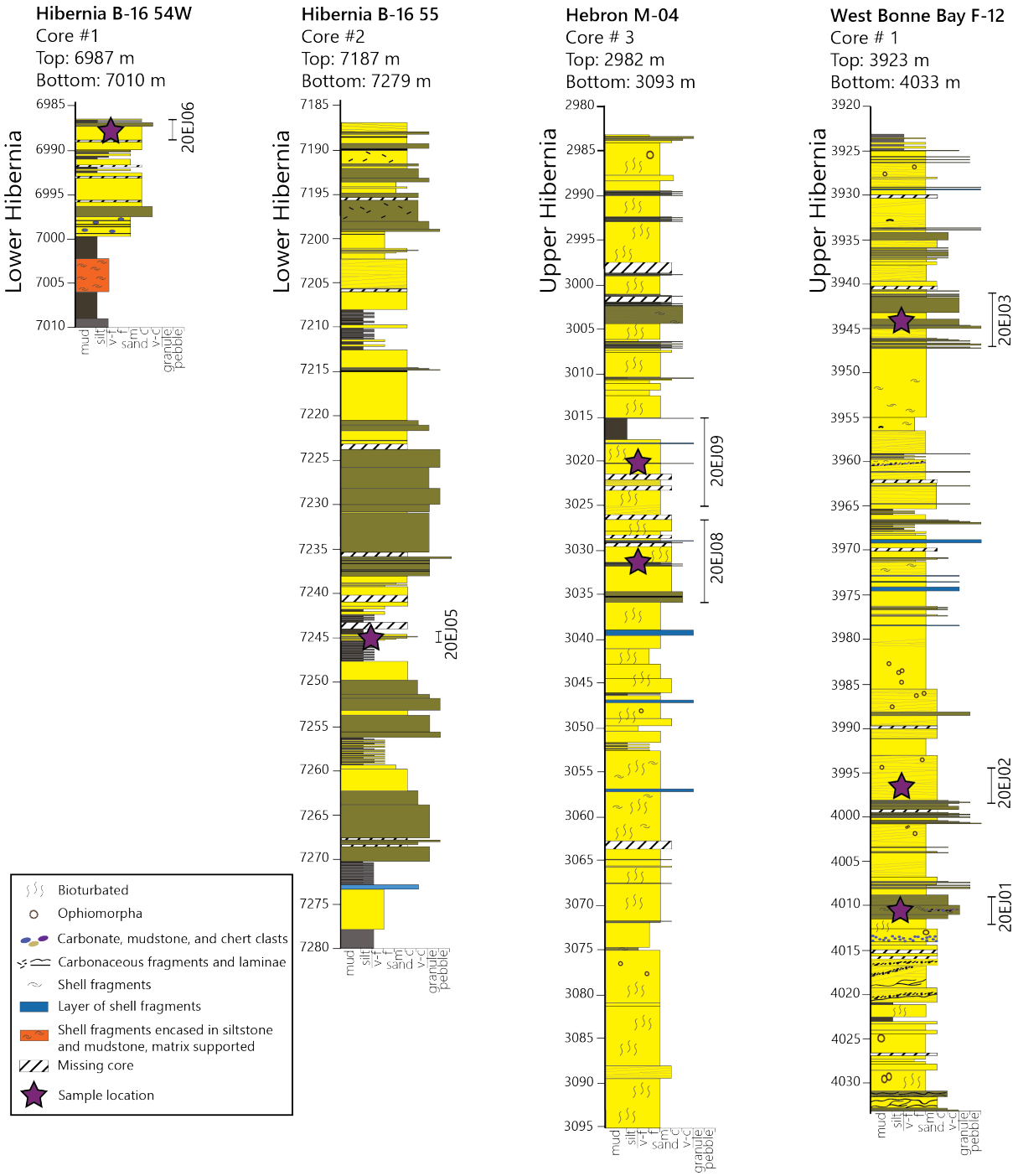

Figure 1-5: Stratigraphy and detrital zircon sample locations for Hibernia Formation samples in Hibernia B-16 55 and 54W, Hebron M-04, and West Bonne Bay F-12 wells.

1.4.2 Detrital zircon U-Pb and fission-track double-dating methods

Detrital zircon grains were analyzed using U-Pb and fission-track (FT) double-dating techniques at the Geo- and Thermochronology Laboratory, University of Calgary. Each rock sample was divided between two Teflon mounts and polished following the procedures of Tagami (2005). Mounts were polished with 6 μm, 3 μm, and 1 μm diamond paste and etched in a binary eutectic mixture of KOH:NaOH (in proportions by weight: 8.0 g KOH and 11.2 g NaOH) etchant at 228°C (Gleadow et al., 1976). Etching detrital zircon samples is a multi-step process devised to create as many countable grains as possible. Every zircon population has an unknown optimal etch time between 4-120+ hours dependent on variations in uranium concentration ([U]), radiation damage, and FT age (Garver and Brandon, 1994; Bernet and Garver, 2005; Kohn et al., 2019). In detrital samples, multiple zircon populations coexist and one etch time will not optimally etch all of the grains (Gleadow et al., 1976; Hasebe et al., 1994). One set of the mounts was etched for 10 hours before fission-track counting. At 10 h etch time, there were distinct populations of over-etched zircon (tracks were dense and uncountable; high [U] or old FT age) and under-etched zircon (tracks were too faint or infrequent to count; low [U] or young FT age). The second set of mounts was etched to 5, 7, and 12 hours, and counted at each etch point to capture these zircon populations.

Zircon samples were prepared for fission-track counting by cutting down to the size of a blank laser mount, marking with three reference points, flattening between glass for 20 minutes at 228°C, and allowed to cool for 45-60 minutes. After fission-track counting was completed, the samples were cleaned using 2% nitric acid (HNO_3) in a sonic bath for 30 minutes to remove surficial common Pb. A map of each sample mount was created using the three reference points and Trackworks program. A 30 μm grid was placed on each zircon under 160x magnification and the number of fission-tracks were recorded. The location of the grid was added to the mount map

and a photograph of the grain was saved to ensure the exact location was analyzed for U-Pb geochronology. Zircon grains with a crystal face large enough to fit a 30μm spot were mapped and photographed for U-Pb analysis only.

Six zircon reference materials were used for U-Pb dating by laser ablation inductively coupled plasma mass spectrometry (LA-ICP-MS) and a second mount of Fish Canyon Tuff was used for fission-track calibration. U-Pb age determinations and data-filtering followed procedures of Matthews and Guest (2016) and the reported measurement uncertainties include both random and systemic components. $^{206}Pb/^{238}U$ ages were used for dates <1.5 Ga and $^{207}Pb/^{206}Pb$ ages for dates >1.5 Ga, and analyses with a probability of concordance of <1% were eliminated from the dataset (Matthews and Guest, 2016). Fission-track ages were determined using the fundamental FT age equation modified for LA-ICP-MS-based data (Vermeesch, 2019):

$$t = \frac{1}{\lambda_D} \ln\left(1 + \frac{1}{2}\lambda_D \zeta \frac{N_s}{A[U]}\right)$$

Where λ_D is the decay constant of ^{238}U (1.55125 x 10-1 year-1; Jaffey et al., 1971), ζ is the zeta calibration calculated from Fish Canyon Tuff zircon standard, N_s is the counted fission tracks, A is the area of the analysis spot, and [U] is the uranium concentration (U/Si). FT analyses were eliminated that did not pass U-Pb data filtering protocols (Matthews and Guest, 2016) and three FT age outliers (819, 843, 899 Ma) were removed for age population analysis.

The youngest detrital zircon U-Pb age populations in each sample were statistically evaluated to constrain the maximum depositional age and compare to existing fossil constraints. Maximum depositional age (MDA) determinations vary and can be completed through a variety of statistical methods (e.g., Barbeau et al., 2009; Coutts et al., 2019; Vermeesch, 2021). MDA values were calculated using four methods: (1) the youngest statistical peak (YSP - Coutts et al.,

2019; Herriott et al., 2019) method, which calculates the MDA as the weighted average of the youngest sub-sample of two or more grains that yield a mean square weighted deviates (MSWD) of ~1; (2) the youngest grain cluster at 2σ method (YGC 2σ - Dickinson and Gehrels, 2009) method, which calculates the MDA from the youngest three or more ages that overlap within 2σ uncertainty; (3) the youngest graphical peak method (YPP - Dickinson and Gehrels, 2009), that uses the Age Pick macro (https://sites.google.com/laserchron.org/arizonalaserchroncenter/home) to calculate peaks for clusters of three or more overlapping ages at 2σ; and (4) the central value of the youngest peak determined by mixture modelling (Galbraith, 2005).

1.5 Thesis Presentation

This thesis is presented manuscript style and consists of three chapters with supplementary appendices. Chapter one serves as an overview and provides the relevant geological background, methods, and objectives of the thesis research. Chapter two is the main body of this thesis and is intended to be submitted to *Marine and Petroleum Geology* or similar peer-reviewed journal with co-authors Beranek, Enkelmann, Jess, and Matthews. This chapter provides the Hibernia Formation detrital zircon U-Pb and FT double-dating results and interpretation. Evidence for tectonic exhumation during Mesozoic extension (proximal, necking, and distal domain development), detrital zircon provenance, and Early Cretaceous paleogeography are discussed. Chapter three is a summary of thesis results, outlines unresolved questions, and provides areas for future research. Appendices provide supplementary material including a compilation of the U-Pb and FT data tables, maximum depositional age plots for each statistical routine, and RadialPlotter diagrams used for statistical analysis of fission-track ages.

1.6 References

Alves, T.M., Moita, C., Sandnes, F., Cunha, T., Monteiro, J.H., and Pinheiro, L.M., 2006, Mesozoic-Cenozoic evolution of North Atlantic continental-slope basins: The Peniche basin, western Iberian margin: AAPG Bulletin, v. 90, p. 31–60, doi:10.1306/08110504138.

Barbeau, D.L., Olivero, E.B., Swanson-Hysell, N.L., Zahid, K.M., Murray, K.E., and Gehrels, G.E., 2009, Detrital-zircon geochronology of the eastern Magallanes foreland basin: Implications for Eocene kinematics of the northern Scotia Arc and Drake Passage: Earth and Planetary Science Letters, v. 284, p. 489–503, doi:10.1016/j.epsl.2009.05.014.

Barr, S.M., Hamilton, M.A., Samson, S.D., Satkoski, A.M., and White, C.E., 2012, Provenance variations in northern Appalachian Avalonia based on detrital zircon age patterns in Ediacaran and Cambrian sedimentary rocks, New Brunswick and Nova Scotia, Canada: Canadian Journal of Earth Sciences, v. 49, p. 533–546, doi:10.1139/E11-070.

Bell, J.S., and Howie, R.D., 1990, Paleozoic geology, *in* Keen, M.J. and Williams, G.L. eds., Geology of the Continental Margin of Eastern Canada, Geological Survey of Canada, p. 141–165.

Bernet, M., and Garver, J.I., 2005, Fission-track analysis of detrital zircon: Reviews in Mineralogy and Geochemistry, v. 58, p. 205–238, doi:10.2138/rmg.2005.58.8.

Boillot, G., Grimaud, S., Mauffret, A., Mougenot, D., Kornprobst, J., Mergoil-Daniel, J., and Torrent, G., 1980, Ocean-continent boundary off the Iberian margin: a serpentinite diapir west of the Galicia Bank: Earth and Planetary Letters, v. 48, p. 23-34, doi: https://doi.org/10.1016/0012-821X(80)90166-1.

Bowman, S.J., Pe-Piper, G., Piper, D.J.W., Fensome, R.A., and King, E.L., 2012, Early cretaceous volcanism in the Scotian Basin: Canadian Journal of Earth Sciences, v. 49, p. 1523–1539, doi:10.1139/e2012-063.

Bradley, D.C., 2008, Passive margins through earth history: Earth-Science Reviews, v. 91, p. 1–26, doi:10.1016/j.earscirev.2008.08.001.

Bronner, A., Sauter, D., Manatschal, G., Péron-Pinvidic, G., and Munschy, M., 2011, Magmatic breakup as an explanation for magnetic anomalies at magma-poor rifted margins: Nature Geoscience, v. 4, p. 549–553, doi:10.1038/NGEO1201.

Carter, A., and Moss, S.J., 1999, Combined detrital-zircon fission-track and U-Pb dating: A new approach to understanding hinterland evolution: Geology, v. 27, p. 235–238, doi:https://doi.org/10.1130/0091-7613(1999)027<0235:CDZFTA>2.3.CO;2.

Cohen, K.M., Finney, S.C., Gibbard, P.L., and Fan, J.-X., 2013 (updated), The ICS International Chronostratigraphic Chart: Episodes, v. 36, p. 199-204.

Coutts, D.S., Matthews, W.A., and Hubbard, S.M., 2019, Assessment of widely used methods to derive depositional ages from detrital zircon populations: Geoscience Frontiers, v. 10, p. 1421–1435, doi:10.1016/j.gsf.2018.11.002.

Davis, M., and Kusznir, N., 2004, Depth-Dependent Lithospheric Stretching at Rifted

Continental Margins, *in* Karner, G.D. ed., Proceedings of NSF Rifted Margins Theoretical Institute, New York, Columbia University Press, p. 92–137, doi:10.7312/karn12738-005.

Dickinson, W.R., and Gehrels, G.E., 2009, Use of U-Pb ages of detrital zircons to infer maximum depositional ages of strata: A test against a Colorado Plateau Mesozoic database: Earth and Planetary Science Letters, v. 288, p. 115–125, doi:10.1016/j.epsl.2009.09.013.

Eddy, M.P., Jagoutz, O., and Ibañez-Mejia, M., 2017, Timing of initial seafloor spreading in the Newfoundland-Iberia rift: Geology, v. 45, p. 527–530, doi:10.1130/G38766.1.

Enachescu, M.E., 1988, Extended basement beneath the intracratonic rifted basins of the Grand Banks of Newfoundland: Canadian Journal of Exploration Geophysics, v. 24, p. 48–65.

Enachescu, M.E., 1987, Tectonic and Structural Framework of the Northeast Newfoundland Continental Margin, *in* Beaumont, C. and Tankard, A.J. eds., Sedimentary Basins and Basin-Forming Mechanisms, Canadian Society of Petroleum Geologists, Memoir 12, p. 117–146.

Enkelmann, E., Lohff, S.K.S., and Finzel, E.S., 2019, Detrital zircon double-dating of forearc basin strata reveals magmatic, exhumational, and thermal history of sediment source areas: Geological Society of America Bulletin, v. 131, p. 1364–1384, doi:10.1130/B35043.1.

Force, E.R., and Barr, S.M., 2012, Provenance of the Lower Carboniferous Horton Group, Petit-de-Grat Island, Nova Scotia, as revealed by detrital zircon ages: Atlantic Geology, v. 48, p. 137–145, doi:10.4138/atlgeol.2012.007.

Galbraith, R.F., 2005, Statistics for Fission Track Analysis (R. F. Galbraith, Ed.): Boca Raton, Florida, Chapman & Hall/CRC, 224 p.

Garver, J.I., and Brandon, M.T., 1994, Erosional denudation of the British Columbia Coast Ranges as determined from fission-track ages of detrital zircon from the Tofino Basin, Olympic Peninsula, Washington: Geological Society of America Bulletin, v. 106, p. 1398–1412, doi:10.1130/0016-7606(1994)106<1398:EDOTBC>2.3.CO;2.

Gibling, M.R., Culshaw, N., Rygel, M.C., and Pascucci, V., 2008, Chapter 6 The Maritimes Basin of Atlantic Canada: Basin Creation and Destruction in the Collisional Zone of Pangea: Elsevier, v. 5, 211–244 p., doi:10.1016/S1874-5997(08)00006-3.

Gleadow, A.J.W., Hurford, A.J., and Quaife, R.D., 1976, Fission track dating of zircon: Improved etching techniques: Earth and Planetary Science Letters, v. 33, p. 273–276, doi:10.1016/0012-821X(76)90235-1.

Grange, M., Schärer, U., Cornen, G., and Girardeau, J., 2008, First alkaline magmatism during Iberia-Newfoundland rifting: Terra Nova, v. 20, p. 494–503, doi:10.1111/j.1365-3121.2008.00847.x.

Grant, A.C., and McAlpine, K.D., 1990, The continental margin around Newfoundland, *in* Keen, M.J. and Williams, G.L. eds., Geology of the Continental Margin of Eastern Canada, Geological Survey of Canada, p. 239–292.

Hasebe, N., Tagami, T., and Nishimura, S., 1994, Towards zircon fission-track thermochronology: Reference framework for confined track length measurements:

Chemical Geology, v. 112, p. 169–178, doi:10.1016/0009-2541(94)90112-0.

Haupert, I., Manatschal, G., Decarlis, A., and Unternehr, P., 2016, Upper-plate magma-poor rifted margins: Stratigraphic architecture and structural evolution: Marine and Petroleum Geology, v. 69, p. 241–261, doi:10.1016/j.marpetgeo.2015.10.020.

Hendriks, M., Jamieson, R.A., Willett, S.D., and Zentilli, M., 1993, Burial and exhumation of the Long Range Inlier and its surroundings, western Newfoundland: results of an apatite fission-track study: Canadian Journal of Earth Sciences, v. 30, p. 1594–1606, doi:10.1139/e93-137.

Herriott, T.M., Crowley, J.L., Schmitz, M.D., Wartes, M.A., and Gillis, R.J., 2019, Exploring the law of detrital zircon: LA-ICP-MS and CA-TIMS geochronology of Jurassic forearc strata, Cook Inlet, Alaska, USA: Geology, v. 47, p. 1044–1048, doi:10.1130/G46312.1.

Hiscott, R.N., Marsaglia, K.M., Wilson, R.C.L., Robertson, A.H.F., Karner, G.D., Tucholke, B.E., Pletsch, T., and Petschick, R., 2008, Detrital sources and sediment delivery to the early post-rift (Albian-Cenomanian) Newfoundland Basin east of the Grand Banks: Results from ODP Leg 210: Bulletin of Canadian Petroleum Geology, v. 56, p. 69–92, doi:10.2113/gscpgbull.56.2.69.

Hiscott, R.N., Wilson, R.C.L., Gradstein, F.M., Pujalte, V., Garcia-Mondejar, J., Boudreau, R.R., and Wishart, H.A., 1990a, Comparative stratigraphy and subsidence history of Mesozoic rift basins of North Atlantic: AAPG Bulletin, v. 74, p. 60–76.

Hiscott, R.N., Wilson, R.C.L., Harding, S.C., Pujalte, V., and Kitson, D., 1990b, Contrasts in early Cretaceous depositional environments of marine sandbodies, Grand Banks-Iberian corridor: Bulletin of Canadian Petroleum Geology, v. 38, p. 203–214.

Huismans, R.S., and Beaumont, C., 2014, Rifted continental margins: The case for depth-dependent extension: Earth and Planetary Science Letters, v. 407, p. 148–162, doi:10.1016/j.epsl.2014.09.032.

Hutter, A., and Beranek, L., 2020, Provenance of Upper Jurassic to Lower Cretaceous synrift strata in the Terra Nova oil field, Jeanne d'Arc basin, offshore Newfoundland: A new detrital zircon U-Pb-Hf reference frame for the Atlantic Canadian margin: AAPG Bulletin, v. 104, p. 2325–2349, doi:10.1306/02232018241.

Jagoutz, O., Müntener, O., Manatschal, G., Rubatto, D., Péron-Pinvidic, G., Turrin, B.D., and Villa, I.M., 2007, The rift-to-drift transition in the North Altantic: A stuttering start of the MORB machine? Geology, v. 35, p. 1087–1090, doi:10.1130/G23613A.1.

Keppie, J.D., and Krogh, T.E., 1999, U-Pb Geochronology of Devonian Granites in the Meguma Terrane of Nova Scotia, Canada: Evidence for Hotspot Melting of a Neoproterozoic Source: Journal of Geology, v. 107, p. 555–568, doi:10.1086/314369.

Kohn, B., Chung, L., and Gleadow, A., 2019, Fission-Track Analysis: Field Collection, Sample Preparation and Data Acquisition, *in* Malusà, M.G. and Fitzgerald, P.G. eds., Fission-Track Thermochronology and its Application to Geology, Cham, Switzerland, Springer International Publishing AG, p. 25–48, doi:https://doi.org/10.1007/978-3-319-89421-8_2.

Kontak, D.J., Ham, L.J., and Dunning, G., 2004, U-Pb dating of the Musquodoboit Batholith,

southern Nova Scotia: Evidence for a protracted magmatic-hydrothermal event in a Devonian intrusion: Atlantic Geology, v. 40, p. 207–216, doi:10.4138/1040.

Krogh, T.E., and Keppie, J.D., 1990, Age of detrital zircon and titanite in the Meguma Group, southern Nova Scotia, Canada: Clues to the origin of the Meguma Terrane: Tectonophysics, v. 177, p. 307–323, doi:10.1016/0040-1951(90)90287-I.

Lavier, L.L., and Manatschal, G., 2006, A mechanism to thin the continental lithosphere at magma-poor margins: Nature, v. 440, p. 324–328, doi:10.1038/nature04608.

Lister, G.S., Etheridge, M.A., and Symonds, P.A., 1986, Detachment faulting and the evolution of passive continental margins: Geology, v. 14, p. 246–250, doi:10.1130/0091-7613(1986)14<890:CARODF>2.0.CO;2.

Lowe, D.G., Sylvester, P.J., and Enachescu, M.E., 2011, Provenance and paleodrainage patterns of Upper Jurassic and Lower Cretaceous synrift sandstones in the Flemish Pass Basin, offshore Newfoundland, east coast of Canada: AAPG Bulletin, v. 95, p. 1295–1320, doi:10.1306/12081010005.

Maclean, N.J., Barr, S.M., White, C.E., and Ketchum, J.W.F., 2003, New U-Pb (zircon) age and geochemistry of the Wedgeport pluton, Meguma terrane, Nova Scotia: Atlantic Geology, v. 39, p. 239–253.

Matthews, W.A., and Guest, B., 2016, A Practical Approach for Collecting Large-n Detrital Zircon U-Pb Data sets by Quadrupole LA-ICP-MS: Geostandards and Geoanalytical Research, v. 41, p. 161–180, doi:10.1111/ggr.12146.

Mattinson, J.M., 1987, U-Pb ages of zircons: A basic examination of error propagation: Chemical Geology: Isotope Geoscience Section, v. 66, p. 151–162, doi:10.1016/0168-9622(87)90037-6.

McKenzie, D., 1978, Some remarks on the development of sedimentary basins: Earth and Planetary Science Letters, v. 40, p. 25–32, doi:10.1016/0012-821X(78)90071-7.

Montario, M.J., and Garver, J.I., 2009, The thermal evolution of the grenville terrane revealed through U-Pb and fission-track analysis of detrital zircon from cambro-ordovician quartz arenites of the potsdam and galway formations: Journal of Geology, v. 117, p. 595–614, doi:10.1086/605778.

Murphy, J.B., and Hamilton, M.A., 2000, Orogenesis and Basin development: U-Pb detrital zircon age constraints on evolution of the Late Paleozoic St. Marys Basin, Central Mainland Nova Scotia: Journal of Geology, v. 108, p. 53–71, doi:10.1086/314384.

Murphy, J.B., Waldron, J.W.F., Kontak, D.J., Pe-Piper, G., and Piper, D.J.W., 2011, Minas Fault Zone: Late Paleozoic history of an intra-continental orogenic transform fault in the Canadian Appalachians: Journal of Structural Geology, v. 33, p. 312–328, doi:10.1016/j.jsg.2010.11.012.

Nirrengarten, M., Manatschal, G., Tugend, J., Kusznir, N., and Sauter, D., 2018, Kinematic Evolution of the Southern North Atlantic: Implications for the Formation of Hyperextended Rift Systems: Tectonics, v. 37, p. 89–118, doi:10.1002/2017TC004495.

Pe-Piper, G., Jansa, L.F., and Palacz, Z., 1994, Geochemistry and regional significance of the early Cretaceous bimodal basalt-felsic associations on Grand Banks, eastern Canada: Geological Society of America Bulletin, v. 106, p. 1319–1331, doi:10.1130/0016-7606(1994)106<1319:GARSOT>2.3.CO;2.

Pe-Piper, G., and Piper, D.J.W., 2004, The effects of strike-slip motion along the Cobequid - Chedabucto - Southwest Grand Banks fault system on the Cretaceous-Tertiary evolution of Atlantic Canada: Canadian Journal of Earth Sciences, v. 41, p. 799–808, doi:10.1139/E04-022.

Peace, A.L., Welford, J.K., Geng, M., Sandeman, H., Gaetz, B.D., and Ryan, S.S., 2018, Rift-related magmatism on magma-poor margins: Structural and potential-field analyses of the Mesozoic Notre Dame Bay intrusions, Newfoundland, Canada and their link to North Atlantic Opening: Tectonophysics, v. 745, p. 24–45, doi:10.1016/j.tecto.2018.07.025.

Péron-Pinvidic, G., and Manatschal, G., 2009, The final rifting evolution at deep magma-poor passive margins from Iberia-Newfoundland: A new point of view: International Journal of Earth Sciences, v. 98, p. 1581–1597, doi:10.1007/s00531-008-0337-9.

Péron-Pinvidic, G., Manatschal, G., and Osmundsen, P.T., 2013, Structural comparison of archetypal Atlantic rifted margins: A review of observations and concepts: Marine and Petroleum Geology, v. 43, p. 21–47, doi:10.1016/j.marpetgeo.2013.02.002.

Pollock, J.C., Hibbard, J.P., and Sylvester, P.J., 2009, Early Ordovician rifting of Avalonia and birth of the Rheic Ocean: U-Pb detrital zircon constraints from Newfoundland: Journal of the Geological Society, v. 166, p. 501–515, doi:10.1144/0016-76492008-088.

Ryan, W.B.F. et al., 2009, Global multi-resolution topography synthesis: Geochemistry, Geophysics, Geosystems, v. 10, p. 1–9, doi:10.1029/2008GC002332.

Shannon, P.M., Williams, B.P.J., and Sinclair, I.K., 1995, Tectonic controls on Upper Jurassic to Lower Cretaceous reservoir architecture in the Jeanne d'Arc Basin, with some comparisons from the Porcupine and Moray Firth Basins, *in* Croker, P.F. and Shannon, P.M. eds., The Petroleum Geology of Ireland's Offshore Basins, Geological Society of London Special Publication, p. 467–490, doi:10.1144/GSL.SP.1995.093.01.37.

Sinclair, I.K., 1988, Evolution of Mesozoic-Cenozoic sedimentary basins in the Grand Banks area of Newfoundland and comparison with Falvey's (1974) rift model: Bulletin of Canadian Petroleum Geology, v. 36, p. 255–273.

Sinclair, I.K., 2010, Reconcilation? Oil industry data in light of revised Iberia-Newfoundland rift models: Geological Association of Canada, Newfoundland Section 2010 spring technical meeting, Abstracts, v. 46, p. 84.

Smyth, H.R., Morton, A., Richardson, N., and Scott, R.A., 2014, Sediment provenance studies in hydrocarbon exploration and production: an introduction, *in* Scott, R.A., Smyth, H.R., Morton, A., and Richardson, N. eds., Sediment Provenance Studies in Hydrocarbon Exploration and Production, Geological Society of London, v. 386, p. 1–6, doi:10.1144/SP386.21.

Soares, D.M., Alves, T.M., and Terrinha, P., 2012, The breakup sequence and associated lithospheric breakup surface: Their significance in the context of rifted continental margins (West Iberia and Newfoundland margins, North Atlantic): Earth and Planetary Science Letters, v. 355–356, p. 311–326, doi:10.1016/j.epsl.2012.08.036.

Sutra, E., Manatschal, G., Mohn, G., and Unternehr, P., 2013, Quantification and restoration of extensional deformation along the Western Iberia and Newfoundland rifted margins: Geochemistry, Geophysics, Geosystems, v. 14, p. 2575–2597, doi:10.1002/ggge.20135.

Tagami, T., 2005, Zircon fission-track thermochronology and applications to fault studies: Reviews in Mineralogy and Geochemistry, v. 58, p. 95–122, doi:10.2138/rmg.2005.58.4.

Tankard, A.J., Welsink, H.J., and Jenkins, W.A.., 1989, Structural styles and stratigaphy of Jeanne d'Arc Basin, Grand Banks of Newfoundland, *in* Tankard, A.J. and Balkwill, H.R. eds., Extensional Tectonics and Stratigraphy of the North Atlantic Margins, AAPG, p. 265–282, doi:https://doi.org/10.1306/M46497.

Tucholke, B.E., Sawyer, D.S., and Sibuet, J.-C., 2007, Breakup of the Newfoundland – Iberia rift, *in* Karner, G.D., Manatschal, G., and Pinheiro, L.M. eds., Imaging, Mapping and Modelling Continental Lithosphere Extension and Breakup, Geological Society of London Special Publication 282, p. 9–46, doi:https://doi.org/10.1144/SP282.2.

van de Poll, H., Yamada, R., and Laslett, G.M., 1995, Introduction: Upper Paleozoic rocks, *in* Williams, H. ed., Geology of the Appalachian-Caledonian Orogen in Canada and Greenland, Canada, Geological Survey of Canada, p. 449–455.

van Staal, C.R., and Barr, S.M., 2012, Lithospheric architecture and tectonic evolution of the Canadian Appalachians and associated Atlantic margin, *in* Percival, J.A., Cook, F.A., and Clowes, R.M. eds., Tectonic Styles in Canada: the LITHOPROBE Perspective, Geological Association of Canada, Special Paper 49, p. 41–95.

Vermeesch, P., 2021, Maximum depositional age estimation revisited: Geoscience Frontiers, v. 12, p. 843–850, doi:10.1016/j.gsf.2020.08.008.

Vermeesch, P., 2019, Statistics for Fission-Track Thermochronology, *in* Malusà, M.G. and Fitzgerald, P.G. eds., Fission-Track Thermochronology and its Application to Geology, Cham, Switzerland, Springer International Publishing AG, p. 109–122.

Waldron, J.W.F., Barr, S.M., Park, A.F., White, C.E., and Hibbard, J., 2015, Late Paleozoic strike-slip faults in Maritime Canada and their role in the reconfiguration of the northern Appalachian orogen: Tectonics, v. 34, p. 1661–1684, doi:10.1002/2015TC003882.

Waldron, J.W.F., White, C.E., Barr, S.M., Simonetti, A., and Heaman, L.M., 2009, Provenance of the Meguma terrane, Nova Scotia: Rifted margin of early Paleozoic Gondwana: Canadian Journal of Earth Sciences, v. 46, p. 1–8, doi:10.1139/E09-004.

Williams, B.P.J., Shannon, P.M., and Sinclair, I.K., 1999, Comparative Jurassic and Cretaceous tectono-stratigraphy and reservoir development in the Jeanne d'Arc and Porcupine basins: Petroleum Geology Conference Proceedings, v. 5, p. 487–499, doi:10.1144/0050487.

Williams, G.L., Ascoli, P., Barss, M.S., Bujak, J.P., Davies, E.H., Fensome, R.A., and Williamson, M.A., 1990, Biostratigraphy and related studies, in Keen, M. and Williams,

G.L. eds., Geology of the Continental Margin of Eastern Canada, Geological Survey of Canada, p. 87–137.

Williams, H., 1979, Appalachian Orogen in Canada: Canadian Journal of Earth Sciences, v. 16, p. 792–807, doi:10.1139/e79-070.

Willner, A.P., Thomson, S.N., Glodny, J., Massonne, H.J., Romer, R.L., van Staal, C.R., and Zagorevski, A., 2019, Zircon fission-track ages from Newfoundland—A proxy for high geothermal gradients and exhumation before opening of the Central Atlantic Ocean: Terra Nova, v. 31, p. 1–10, doi:10.1111/ter.12361.

CHAPTER 2: EXHUMATION HISTORY AND EARLY CRETACEOUS PALEOGEOGRAPHY OF THE JEANNE D'ARC BASIN REGION, OFFSHORE NEWFOUNDLAND, CANADA: NEW INSIGHTS ON MAGMA-POOR RIFT DEVELOPMENT FROM DETRITAL ZIRCON U-PB AND FISSION-TRACK DOUBLE-DATING OF HIBERNIA FORMATION STRATA

2.1 Abstract

Syn-rift strata in the Grand Banks of Atlantic Canada have been broadly correlated with the Mesozoic tectonic evolution of the Newfoundland-Iberia conjugate margins, but the precise timing of regional exhumation events and their global significance to the stepwise development of magma-poor rift systems remain uncertain. New detrital zircon U-Pb (n = 518) and double-dating fission-track (FT) and U-Pb (n = 269) results from syn-rift, Hibernia Formation sandstone units constrain the timing of proximal domain rift processes in the Grand Banks and develop working hypotheses for the Early Cretaceous paleogeography of the Jeanne d'Arc basin region during the onset of hyperextension, mantle exhumation, and outboard development of the necking and distal domains. Most DZ grains (~70%) were recycled through upper Paleozoic strata from pre-rift, Appalachian basins in Atlantic Canada and are characterized by Neoarchean to Paleozoic U-Pb ages and Neoproterozoic to Paleozoic FT cooling ages. The Berriasian to Valanginian strata yield Archean to Paleozoic detrital zircon grains with Triassic to Jurassic and Early Cretaceous exhumation-cooling ages and indicate moderate to rapid tectonic exhumation of Appalachian basement or thermally-reset sedimentary rocks along active rift flanks or uplifts. Syn-depositional, Early Cretaceous DZ grains indicate provenance from volcanic centers along the SW Grand Banks transform fault and are consistent with north-directed paleoflow from the Avalon Uplift region

into the Jeanne d'Arc basin. Mesozoic FT cooling populations in Hibernia Formation strata support rift-related exhumation being temporally tied to proximal, necking, and distal domain deformation events that are more generally recognized by marine seismic studies of deep-water areas outboard of the Grand Banks. Syn-rift strata from proximal domain basins can therefore provide insights into the timing of exhumation events coincident with phases of magma-poor rift system development.

2.2 Introduction

Passive or rifted continental margins result from extensional processes that affect the entire lithosphere and provide insights into the nature of continental rifting, lithospheric breakup, and formation of divergent plate boundaries (e.g., McKenzie, 1978; Lister et al., 1986; Bradley, 2008). Although early rift models were based on tectonic scenarios where stretching is instantaneous and uniform for all layers of the lithosphere (McKenzie, 1978), there is now consensus for non-plume-related rift development to include polyphase, depth-dependent stretching that is decoupled between lithospheric layers (e.g., Davis and Kusznir et al., 2004, Lavier and Manatschal 2006, Huismans and Beaumont, 2014). Continental extension in polyphase rift scenarios takes place over >100 Myr and includes discrete modes of lithospheric stretching-thinning, hyperextension and mantle exhumation, and lithospheric breakup (e.g., Péron-Pinvidic and Manatschal, 2009). The full progression through these extensional modes results in margin-parallel architectural elements (proximal, necking, distal, outer, and oceanic domains) that collectively record continental margin development (e.g., Lavier and Manatschal, 2006, Péron-Pinvidic and Manatschal, 2009; Péron-Pinvidic et al., 2013; Huismans and Beaumont, 2014). The Newfoundland (SE Grand Banks)-Iberia conjugate margins (Fig. 2-1A) record the protracted breakup of supercontinent Pangea and opening of the North Atlantic Ocean and are used as the basis for most theoretical models of

magma-poor rift evolution (e.g., Whitmarsh et al., 2001; Péron-Pinvidic et al., 2013; Sutra et al., 2013). Marine seismic (e.g., Dean et al., 2000; Van Avendonk et al., 2006; Pereira and Alves, 2011; Deemer et al., 2009) and scientific drilling (e.g., Boillot et al., 1980; Müntener and Manatschal, 2006) results have been used to identify Triassic to Jurassic stretching and thinning (proximal and necking domains), Early to mid-Cretaceous hyperextension and mantle exhumation (distal domain), and mid-Cretaceous breakup-related (outer domain) events along the Newfoundland and Iberian margins (Fig. 2-1B; e.g., Pérez-Gussinyé and Reston, 2001; Bronner et al.., 2010; Péron-Pinvidic et al., 2013).

The Jeanne d'Arc basin is an asymmetric graben in the proximal domain (Grand Banks) of the Newfoundland margin and contains up to 18 km of Upper Triassic to Upper Cretaceous strata (Fig. 2-1B; Enachescu, 1988) that have been broadly correlated with rift episodes in the North Atlantic region (e.g., Hiscott et al., 1990; Shannon et al., 1995; Williams et al., 1999; Tucholke et al., 2007). However, the precise depositional age, provenance, and tectonic significance of these proximal domain units with respect to coincident Late Jurassic to Cretaceous growth of outboard (necking, distal, outer) domains and Mesozoic paleodrainage evolution are uncertain (e.g., Hutter and Beranek, 2020). Upper Jurassic to Lower Cretaceous braided fluvial strata of the Jeanne d'Arc Formation were sourced from volcanic centers along the SW Grand Banks transform fault and Appalachian highlands within the Avalon Uplift to the south of the Jeanne d'Arc basin as a result of rift-related tectonism in the proximal domain during the necking phase (Fig. 2-1B; e.g., Hutter and Beranek, 2020). Overlying Lower Cretaceous shallow-marine strata of the Hibernia Formation have untested source-to-sink histories and geological connections with deformation events that involved hyperextension and mantle exhumation (distal domain) outboard of the modern Grand Banks.

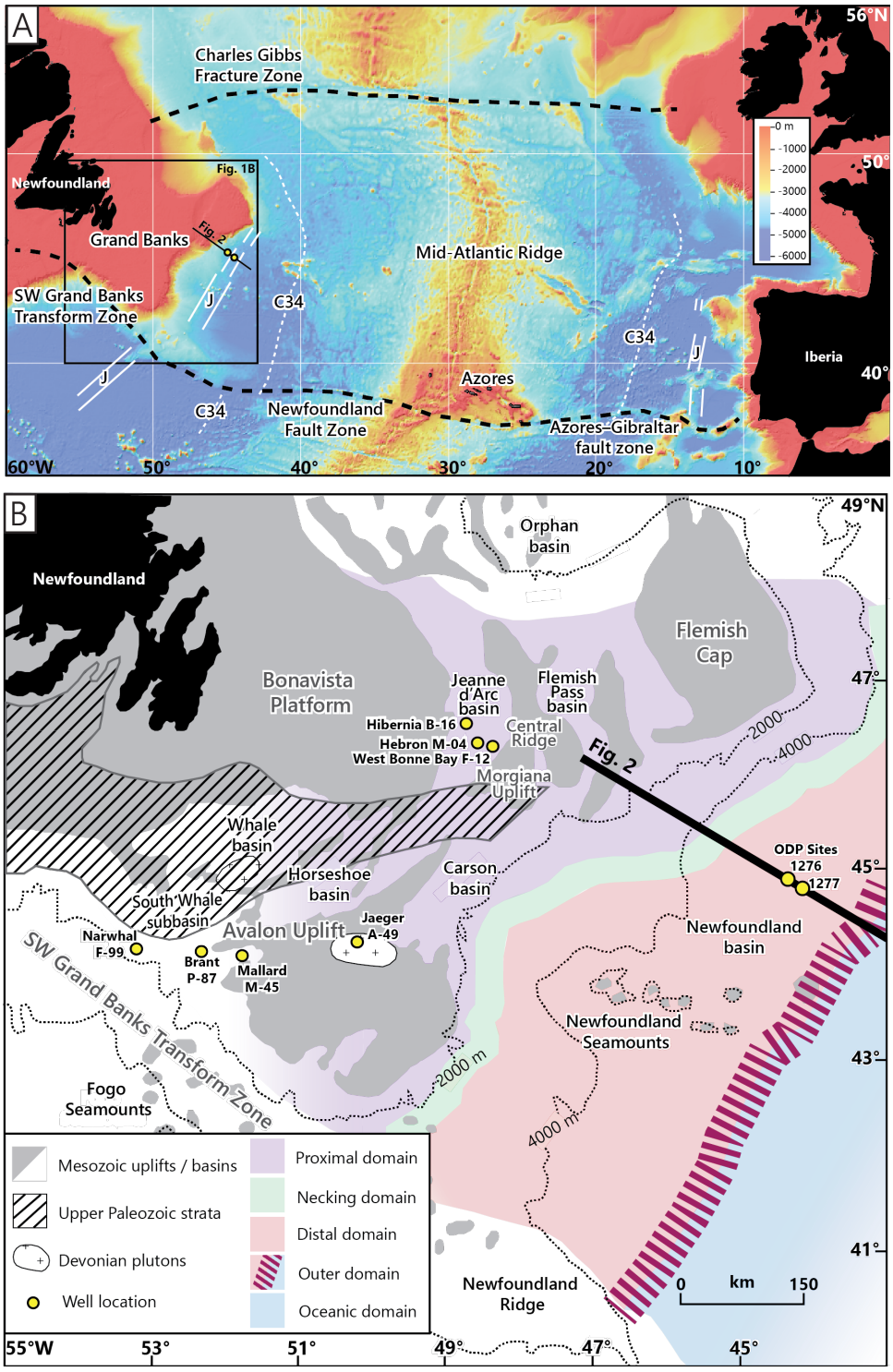

Figure 2-1: (a) Bathymetric map of the southern North Atlantic Ocean and primary features of the Newfoundland-Iberia rift system compiled from Ryan et al. (2009) and Bronner et al. (2011), (b) Locations of Mesozoic architectural elements, upper Paleozoic strata, and Devonian plutons of the Grand Banks and nearby regions after Grant and McAlpine (1990), Bell and Howie (1990) and Péron-Pinvidic et al. (2013).

New studies of Jeanne d'Arc basin strata are required to identify the timing of regional exhumation and source-to-sink connections along this archetypal magma-poor rift system. In this article, detrital zircon U-Pb and fission-track double-dating investigations of Hibernia Formation strata are used to constrain Early Cretaceous and older exhumation- and magmatic-cooling events (e.g., Carter and Moss, 1999; Montario and Garver, 2009; Enkelmann et al., 2019), sediment provenance signatures, and maximum depositional ages of syn-rift rocks deposited in a proximal domain setting. The results allow us to test published rift models for the Newfoundland margin, including predictions for proximal domain evolution during hyperextension and mantle exhumation (e.g., Péron-Pinvidic et al., 2013; Sutra et al., 2013), establish Berriasian to Valanginian depositional ages for Hibernia Formation strata, and develop working hypotheses for the Early Cretaceous paleogeography of the Grand Banks region to include north-flowing fluvial and deltaic systems that drained exhumed Appalachian cover assemblages of the Avalon Uplift and coeval, syn-rift volcanic-plutonic complexes along the SW Grand Banks transform fault.

2.3 Geological Background

2.3.1 North Atlantic rift evolution

Magma-poor rift systems are underlain by several margin-parallel architectural domains that have predictable geological elements and geophysical signatures worldwide (e.g., Péron-Pinvidic et al., 2013). In the southern North Atlantic Ocean, the Newfoundland and Iberian margins transition seaward from thick, undisturbed continental crust into proximal, necking, distal, outer, and oceanic domains that progressively developed during the Late Triassic to Late Cretaceous periods (Fig. 2-2; Péron-Pinvidic et al., 2013; Sutra et al., 2013). The Jeanne d'Arc basin, located in the Grand Banks continental platform of Newfoundland (proximal domain), records a polyphase subsidence history that resulted from episodic tectonism during the breakup of eastern North

America, Africa, UK, Ireland, and Iberia (Sinclair, 1988; Tankard et al., 1989; Soares et al., 2012; Péron-Pinvidic et al., 2013; Sutra et al., 2013; Nirrengarten et al., 2018). The proximal domains of the Newfoundland-Iberia system initially formed by widely distributed, upper crustal extension that resulted in the formation of intracontinental rift basins, including the Jeanne d'Arc basin, over a vast region without significant thinning (Tucholke et al., 2007). Thermal subsidence and slow extensional motion between Newfoundland and Iberia (<2.0 cm/year) subsequently occurred during the Early Jurassic (Sinclair, 1988; Nirrengarten et al., 2018). The transition from decoupled to coupled deformation and early development of the necking domain at the outer edge of the Grand Banks began by the early Late Jurassic (Péron-Pinvidic et al., 2013; Sutra et al., 2013). Renewed tectonic exhumation and subsidence in the Jeanne d'Arc basin and adjacent rift grabens at this time were accommodated by north- to north-northeast-trending normal faults (Tankard et al., 1989, Sinclair, 1988). The necking phase culminated with Early Cretaceous hyperextension and/or mantle exhumation episodes, which promoted the development of the distal domain and penetration of faults through the entire crust and mantle lithosphere (Fig. 2-2; Péron-Pinvidic et al., 2013). Berriasian and Hauterivian rift episodes recognized in the Jeanne d'Arc basin may correlate with the rupture of crust in the southern and northern parts of the Newfoundland-Iberia rift system, respectively (Tucholke et al., 2007; Nirrengarten et al., 2018).

Early to mid-Cretaceous exhumation of continental mantle lithosphere resulted in wide transition zones of serpentinized mafic-ultramafic rocks in the distal and outer domains prior to lithospheric breakup (Fig. 2-2; Péron-Pinvidic et al., 2013). The principal stress orientation in the Jeanne d'Arc basin shifted to a northeast-southwest direction by the mid-Cretaceous and drove dip-slip motion along transfer faults that previously accommodated strike-slip displacement (Tankard et al., 1989). Final lithospheric breakup between Newfoundland and Iberia occurred by

the late Aptian (e.g., Tankard et al., 1989; Sutra et al., 2013; Eddy et al., 2017) and was in part triggered by a high-volume magmatic event in the outer domain, a region with high relief that includes thickened crust and underplated, exhumed mantle lithosphere (Fig. 2-2; Bronner et al., 2011). This magmatic event produced a large-magnitude, linear magnetic anomaly (J anomaly; Fig. 2-1A) that has a long-lived and complicated history of syn- to post-breakup magmatism (Nirrengarten et al., 2018).

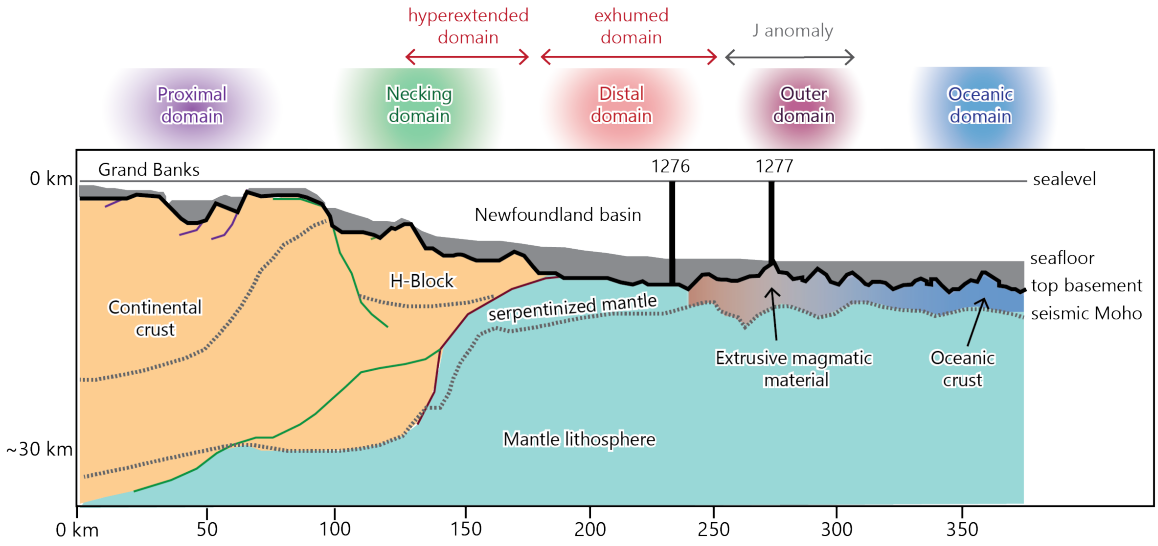

Figure 2-2: Schematic cross-section of the Newfoundland margin after Péron-Pinvidic et al. (2013). Location of J anomaly from Bronner et al. (2011).

Lithospheric breakup and the onset of seafloor spreading in the southern North Atlantic Ocean likely began in the south near the Newfoundland-Azores-Gibraltar fracture zone and propagated northwards (e.g., Alves et al., 2006; Bronner et al., 2011). The C34 anomaly (~85 Ma) represents the oceanward extent of the outer domain and is the oldest undisputed seafloor spreading isochron in the modern oceanic domain (Fig. 2-1A Bronner et al., 2011). Syn-breakup and off-axis, post-breakup magmatism persisted in the outer domain until at least 70 Ma (e.g., Jagoutz et al., 2007; Nirrengarten et al., 2018). Lithospheric breakup in the proximal domain is manifested by an unconformity referred to as the U reflection, a prominent seismic reflector at the

Aptian-Albian boundary in the Jeanne d'Arc basin and elsewhere (Tankard et al., 1989; Péron-Pinvidic et al., 2013; Sutra et al., 2013; Nirrengarten et al., 2018). Thermal subsidence dominated the Jeanne d'Arc basin after regional breakup-related uplift (e.g., Soares et al., 2014) and extension in the adjacent Orphan basin (Sinclair, 1988, Tucholke et al., 2007).

2.3.2 Newfoundland margin

The Newfoundland margin is underlain by Proterozoic to Paleozoic rocks of the Appalachian orogen that span the onshore and offshore portions of eastern North America and record the accretion of arcs and microcontinents prior to the final Laurentia-Gondwana collision and assembly of supercontinent Pangea (Fig. 2-3; e.g., van Staal and Barr, 2012). The Canadian Appalachians comprise the northern extent of the orogen and are subdivided into several lithotectonic components that from west to east represent the ancient Laurentian margin, peri-Laurentian arc and ophiolite fragments, peri-Gondwanan arc fragments, and the peri-Gondwanan Gander, Avalon, and Meguma terranes (e.g., Williams, 1979). Paleozoic events associated with the Taconic (500-450 Ma), Salinic (440-420 Ma), Acadian (420-400 Ma), Neoacadian (400-350 Ma), and Alleghenian (340-260 Ma) orogenies generated collision-related igneous suites and orogen-proximal basins that record Appalachian evolution (e.g., van Staal and Barr, 2012). In Atlantic Canada, the late Paleozoic Alleghenian orogeny included dextral-oblique convergence and filling of strike-slip basins with Upper Devonian to Permian strata (Fig. 2-3; van de Poll et al., 1995; Gibling et al., 2008; Waldron et al., 2015). Proterozoic to Paleozoic rocks in central and western Newfoundland yield Late Triassic zircon fission-track (Willner et al., 2019) and Jurassic and older apatite fission-track (Hendriks et al., 1993) ages, respectively, that are consistent with Mesozoic exhumation of Appalachian infrastructure and recycling of basement and cover assemblages into the Jeanne d'Arc and related rift basins.

The Grand Banks is a ~500 km-wide platform of submerged continental crust that consists of Neoproterozoic (760-550 Ma) igneous and meta-sedimentary basement units assigned to Avalonia and Cambrian to Ordovician (537-475 Ma) meta-sedimentary strata and Late Devonian plutons assigned to Meguma (Fig. 2-3; Bell and Howie, 1990; Tucholke et al., 2007; van Staal and Barr, 2012). The SW Grand Banks fault zone is part of a margin-normal, strike-slip fault system that transitions onshore into the Cobequid-Chedabucto or Minas fault zone in Nova Scotia that bounds Avalonia and Meguma (Fig. 2-3; Pe-Piper and Piper, 2004; Murphy et al., 2011).

Lower Paleozoic cover assemblages of Avalonia yield 550-750 Ma and 2000-2200 Ma detrital zircon age populations and indicate provenance from underlying arc basement and recycling of peri-Gondwanan cratonal signatures (e.g., Pollock et al., 2009, Barr et al., 2012). Cambrian to Ordovician cover assemblages in Meguma yield 550-750, 2000-2200, and 2500-3000 Ma detrital zircon age populations (e.g., Waldron et al., 2009; Krogh and Keppie, 1990) and are intruded by Late Devonian (ca. 375-370 Ma) plutons (e.g., Keppie and Krogh, 1999; Maclean et al., 2003; Kontak et al., 2004). Upper Paleozoic terrestrial to marine strata derived from the Canadian Appalachians represent overlap assemblages that sit unconformably on basement and may also have originally covered the Grand Banks region (Fig. 2-3; Bell and Howie, 1990; Gibling et al., 2008). Upper Paleozoic strata in Nova Scotia yield 370-380, 500-700, and 2000-2200 Ma detrital zircon populations that indicate recycling from clastic rocks of the Avalon and Meguma terranes with minor contributions from Appalachian igneous suites (e.g., Murphy and Hamilton, 2000; Force and Barr, 2012). Upper Paleozoic foreland basin strata derived from the Iberian Variscides may have also covered the Grand Banks region (e.g., Hiscott et al., 2008) and Carboniferous strata in southern Portugal yield 300-450, 500-750, and 900-1100 Ma detrital zircon populations (Rodrigues et al., 2015).

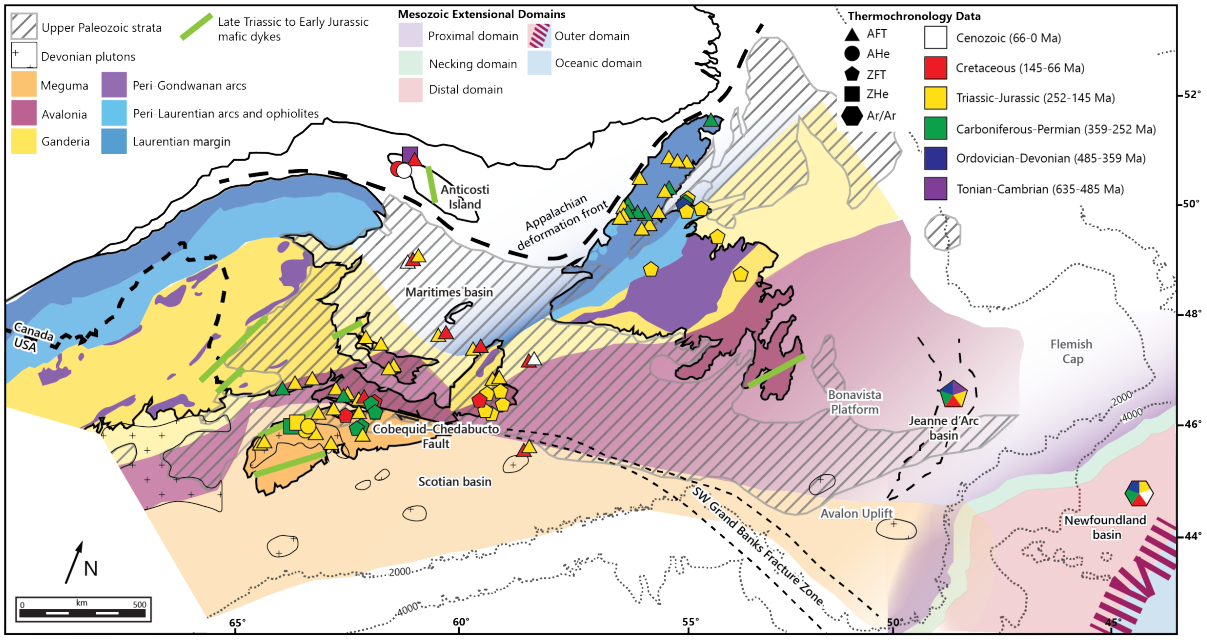

Figure 2-3: Compiled mica 40Ar-39Ar, zircon fission-track and (U-Th)/He, and apatite fission-track and (U-Th)/He ages from Cretaceous and older rocks in Atlantic Canada modified from Willner et al. (2019) and sources in Table 2-6. Tectonic map of northern Appalachians basement and early Paleozoic lithotectonic elements after van Staal and Barr (2012). Inferred extensions into offshore Nova Scotia and Newfoundland after Bell and Howie (1990). Early Triassic–Late Jurassic mafic dyke locations after Greenough (1995).

Triassic to Cretaceous syn-rift strata unconformably overlie upper Paleozoic and older rocks and filled multiple basins (e.g., Jeanne d'Arc, Flemish Pass, Whale, and Orphan basins) during North Atlantic rift evolution (e.g., Sinclair, 1988). Some syn-rift units are preserved on uplifted sediment ridges that now separate depocenters (e.g. Central Ridge, Morgiana Uplift; Enachescu, 1987, 1988). Extensional deformation and tectonic subsidence alternated with periods of thermal subsidence and are tied to the development of the proximal, necking, distal, and outer domain phases (Fig. 2-4; e.g., Sinclair, 1988; Tankard et al., 1989; Tucholke et al., 2007). Late Jurassic to Early Cretaceous tectonic subsidence in the Jeanne d'Arc basin was episodic and evidenced by stacked depositional successions, intervening unconformities, and isopach-thickening toward extensional faults (Tankard et al., 1989; Shannon et al., 1995). Multiple erosional surfaces coalesce at Mesozoic basin margins into a regional unconformity that records

50-60 Myr of rift-related deformation, uplift, and erosion in the Grand Banks (Avalon unconformity, e.g., Grant and McAlpine, 1990). Sedimentary wedges were deposited above rotated fault blocks during the growth of north-northeast-trending normal faults and rotation of subsiding blocks (Shannon et al., 1995; Williams et al., 1999).

Late Jurassic to Cretaceous igneous rocks locally crop out in onshore regions of Newfoundland (Peace et al., 2018) and western Portugal (Grange et al., 2008), and more prominently along the offshore SW Grand Banks fault zone where they include volcanic centers with mafic to felsic dykes, sills, and pyroclastic flows (e.g., Pe-Piper et al., 1994; e.g., Bowman et al., 2012). Upper Jurassic fluvial strata in the Jeanne d'Arc and Flemish Pass basins yield ca. 159-145 Ma detrital zircon grains that indicate rift-related magmatism in the Grand Banks during the development of the necking and distal domains (Lowe et al., 2011; Hutter and Beranek, 2020).

2.3.3 Hibernia Formation stratigraphy

Lower Cretaceous rock units of the Jeanne d'Arc basin mostly consist of nonmarine to shallow-marine siliciclastic strata (Tankard et al., 1989) that superceded north-directed, Upper Jurassic braided fluvial systems with headwaters in the Avalon Uplift (Fig. 2-1B; e.g., Hiscott et al., 1990a; Shannon et al., 1995). The Jurassic-Cretaceous contact is a disconformity that represents a brief hiatus across the basin (Tankard et al., 1989). Early Cretaceous rise of the Avalon Uplift renewed the clastic source area and resulted in the northward progradation of Hibernia Formation deltaic successions (Sinclair, 1988; Tankard et al., 1989; Hiscott et al., 1990b; Williams et al., 1999). The lower member of the Hibernia Formation (Lower Hibernia) is comprised of stacked fluvial channels in the southwest to delta-front bar facies and coastal deposits in the northeast (Sinclair, 1988; Hiscott et al., 1990b). The upper member of the Hibernia Formation (Upper Hibernia) consists of fine-grained, shallow-marine sandstone and mudstone units that

grade laterally to pro-delta shale in the northwest Hibernia oil field (Hiscott et al., 1990a). Biostratigraphic correlations based on palynomorphs, dinoflagellates, foraminifers, and ostracods indicate late Berriasian to Valanginian depositional ages in the type section of the Hibernia Formation (Williams et al., 1990).

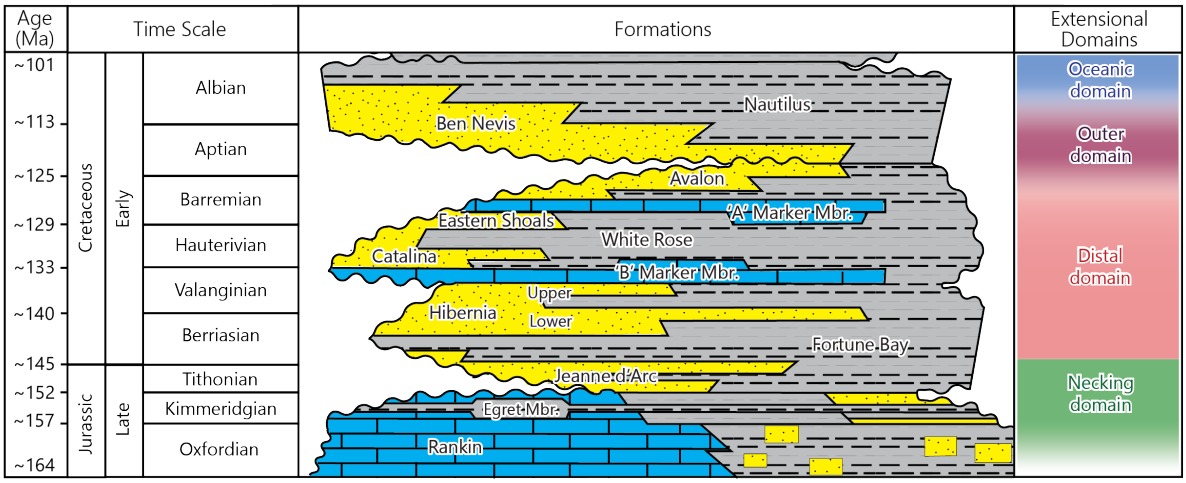

Figure 2-4: Upper Jurassic to Lower Cretaceous stratigraphy compiled by Sinclair et al. (1992) and Hutter & Beranek (2020) using the geological timescale of Cohen et al. (2013). Extensional domain development from Péron-Pinvidic et al. (2013).

2.4 Methods & Materials

2.4.1 Samples

Seven Hibernia Formation samples from the Hibernia B-16 55, Hibernia B-16 54W, Hebron M-04, and West Bonne Bay F-12 wells were collected from the Canada-Newfoundland and Labrador Offshore Petroleum Board Core Storage and Research Centre in St. John's, Newfoundland and Labrador (Fig. 2-5). These include two samples of the Lower Hibernia Formation from the Hibernia oil field and five samples of the Upper Hibernia Formation in the Hebron oil field and nearby areas (Table 1-1). Each sample consisted of ~500 g of medium- to coarse-grained sandstone from full-diameter core. Zircon grains were isolated from the samples using standard crushing, milling, sieving, magnetic separation, and heavy liquid separation (methylene iodide) techniques at Memorial University of Newfoundland.

Table 1-1: Location and lithological descriptions for Hibernia Formation detrital zircon samples.

Sample	Well Name	Core - Box Numbers	Core Depth (mMD)	Approx. True Vertical Depth (mTVD)	Formation - Member	Sample Description
20EJ01	West Bonne Bay F-12	#1 - 110-113	4009-4013	3431	Upper Hibernia	medium- to coarse-grained, subrounded to rounded, moderately-sorted, massive to normally graded, quartz arenite
20EJ02	West Bonne Bay F-12	#1 - 92-96	3994-3998	3416	Upper Hibernia	fine- to medium-grained, subrounded to rounded, well-sorted, massive to planar crossbedded, sublithic arenite
20EJ03	West Bonne Bay F-12	#1 - 24-30	3941-3947	3364	Upper Hibernia	fine- to medium-grained, subrounded to rounded, well-sorted, massive to planar crossbedded, sublithic arenite
20EJ08	Hebron M-04	#3 - 37-42	3028-3037	3032	Upper Hibernia	fine- to medium-grained, subrounded to rounded, well-sorted, massive to normally graded, sublithic arenite
20EJ09	Hebron M-04	#3 - 26-33	3015-3025	3020	Upper Hibernia	fine- to medium-grained, subrounded to rounded, poor- to moderately-sorted, wavy bedded, sublithic arenite
20EJ05	Hibernia B-16 55	#2 - 3	7245-7246	4618	Lower Hibernia	medium- to coarse-grained, subrounded to rounded, well-sorted, massive to planar crossbedded, quartz arenite
20EJ06	Hibernia B-16 54W	#1 - 1-3	6989-6986	4445	Lower Hibernia	fine- to medium-grained, subrounded to rounded, moderately- to well-sorted, massive to planar crossbedded, sublithic arenite

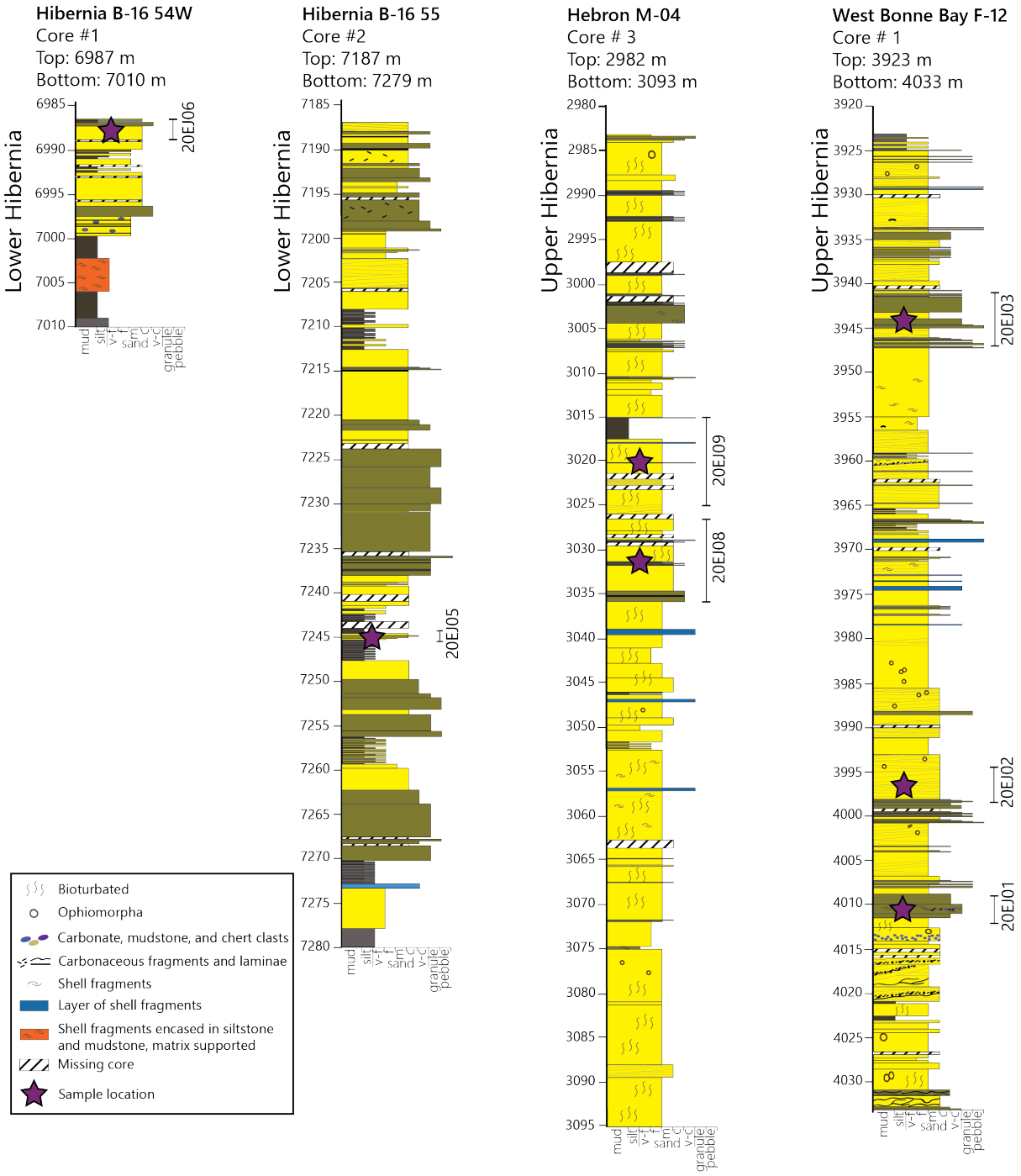

Figure 2-5: Stratigraphy and detrital zircon sample locations for Hibernia Formation samples in Hibernia B-16 55 and 54W, Hebron M-04, and West Bonne Bay F-12 wells.

2.4.2 Detrital zircon U-Pb and fission-track double-dating methods

Detrital zircon grains were analyzed using U-Pb and fission-track (FT) double-dating techniques at the Geo- and Thermochronology Laboratory, University of Calgary. Each rock sample was divided between two Teflon mounts and polished following the procedures of Tagami (2005). Mounts were polished with 6 μm, 3 μm, and 1 μm diamond paste and etched in a binary eutectic mixture of KOH:NaOH (in proportions by weight: 8.0 g KOH and 11.2 g NaOH) etchant at 228°C (Gleadow et al., 1976). Etching detrital zircon samples is a multi-step process devised to create as many countable grains as possible. Every zircon population has an unknown optimal etch time between 4-120+ hours dependent on variations in uranium concentration ([U]), radiation damage, and FT age (Garver and Brandon, 1994; Bernet and Garver, 2005; Kohn et al., 2019). In detrital samples, multiple zircon populations coexist and one etch time will not optimally etch all of the grains (Gleadow et al., 1976; Hasebe et al., 1994). One set of the mounts was etched for 10 hours before fission-track counting. At 10 h etch time, there were distinct populations of over-etched zircon (tracks were dense and uncountable; high [U] or old FT age) and under-etched zircon (tracks were too faint or infrequent to count; low [U] or young FT age). The second set of mounts was etched to 5, 7, and 12 hours, and counted at each etch point to capture these zircon populations.

Zircon samples were prepared for fission-track counting by cutting down to the size of a blank laser mount, marking with three reference points, flattening between glass for 20 minutes at 228°C, and allowed to cool for 45-60 minutes. After fission-track counting was completed, the samples were cleaned using 2% nitric acid (HNO_3) in a sonic bath for 30 minutes to remove surficial common Pb. A map of each sample mount was created using the three reference points and Trackworks program. A 30 μm grid was placed on each zircon under 160x magnification and the number of fission-tracks were recorded. The location of the grid was added to the mount map

and a photograph of the grain was saved to ensure the exact location was analyzed for U-Pb geochronology. Zircon grains with a crystal face large enough to fit a 30μm spot were mapped and photographed for U-Pb analysis only.

Six zircon reference materials were used for U-Pb dating by laser ablation inductively coupled plasma mass spectrometry (LA-ICP-MS; Appendix A) and a second mount of Fish Canyon Tuff was used for fission-track calibration. U-Pb age determinations and data-filtering followed procedures of Matthews and Guest (2016) and the reported measurement uncertainties include both random and systemic components. $^{206}Pb/^{238}U$ ages were used for dates <1.5 Ga and $^{207}Pb/^{206}Pb$ ages for dates >1.5 Ga, and analyses with a probability of concordance of <1% were eliminated from the dataset (Matthews and Guest, 2016). Fission-track ages were determined using the fundamental FT age equation modified for LA-ICP-MS-based data (Vermeesch, 2019):

$$t = \frac{1}{\lambda_D} \ln\left(1 + \frac{1}{2}\lambda_D \zeta \frac{N_s}{A[U]}\right)$$

Where λ_D is the decay constant of ^{238}U (1.55125 x 10-1 year-1; Jaffey et al., 1971), ζ is the zeta calibration calculated from Fish Canyon Tuff zircon standard, N_s is the counted fission tracks, A is the area of the analysis spot, and [U] is the uranium concentration (U/Si). FT analyses were eliminated that did not pass U-Pb data filtering protocols (Matthews and Guest, 2016) and three FT age outliers (819, 843, 899 Ma) were removed for age population analysis.

The youngest detrital zircon U-Pb age populations in each sample were statistically evaluated to constrain the maximum depositional age and compare to existing fossil constraints. Maximum depositional age (MDA) determinations vary and can be completed through a variety of statistical methods (e.g., Barbeau et al., 2009; Coutts et al., 2019; Vermeesch, 2021). MDA values were calculated using four methods: (1) the youngest statistical peak (YSP - Coutts et al.,

2019; Herriott et al., 2019) method, which calculates the MDA as the weighted average of the youngest sub-sample of two or more grains that yield a mean square weighted deviates (MSWD) of ~1; (2) the youngest grain cluster at 2σ method (YGC 2σ - Dickinson and Gehrels, 2009) method, which calculates the MDA from the youngest three or more ages that overlap within 2σ uncertainty; (3) the youngest graphical peak method (YPP - Dickinson and Gehrels, 2009), that uses the Age Pick macro (https://sites.google.com/laserchron.org/arizonalaserchroncenter/home) to calculate peaks for clusters of three or more overlapping ages at 2σ; and (4) the central value of the youngest peak determined by mixture modelling (Galbraith, 2005).

2.5 Results

2.5.1 U-Pb geochronology

Hibernia Formation rock samples yielded 787 U-Pb ages that show similar Archean to Tonian (3032-726 Ma), Cryogenian to Cambrian (707-493 Ma), Ordovician to Devonian (480-359 Ma), Carboniferous to Permian (358-275 Ma), and Early Cretaceous (143-123 Ma) detrital zircon populations regardless of lithology, grain size, geographic location, or stratigraphic position (Fig. 2-6). However, the proportion of grains that make up each of the U-Pb populations varied from well to well. The Lower Hibernia Formation samples from the Hibernia oil field (wells B-16 54W and B-16 55) in the western Jeanne d'Arc basin lack 358-275 Ma populations that are recognized in Upper Hibernia Formation strata, while also yielding relatively less and greater proportions of Cryogenian to Cambrian and Archean to Tonian zircon grains, respectively (Fig. 2-6). Upper Hibernia Formation strata from the eastern Jeanne d'Arc basin (West Bonne Bay F-12) contain greater 358-275 Ma U-Pb populations relative to 465-360 Ma populations, whereas central Jeanne d'Arc basin strata in the Hebron oil field (Hebron M-04) yield subequal portions of both Paleozoic age groupings (Fig. 2-6).

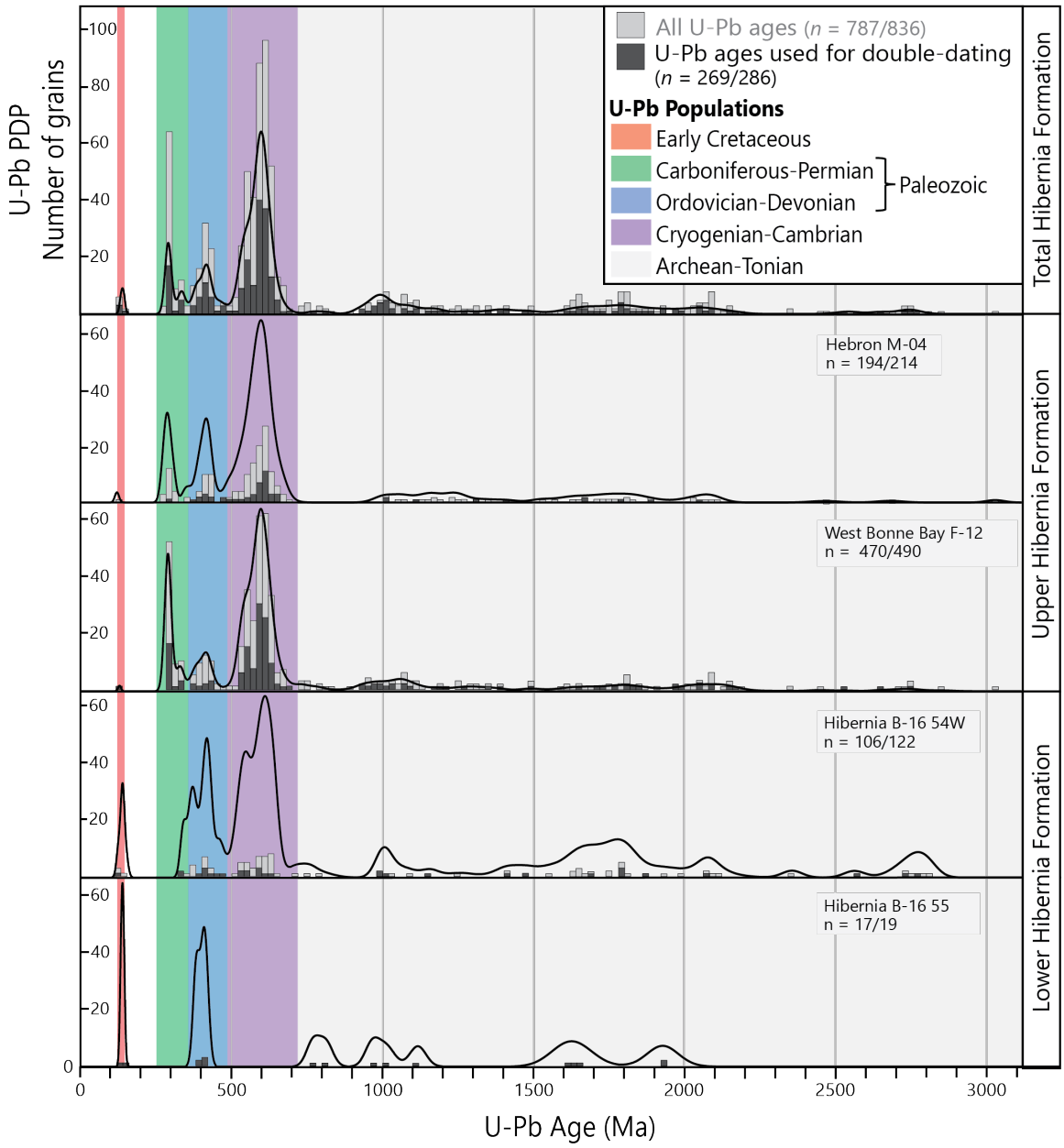

Figure 2-6: Probability density plots (PDP) and histograms of detrital zircon U-Pb results for Hibernia Formation samples. Data pooled for Hibernia B-16 55 (20EJ05) and 54W (20EJ06), Hebron M-04 (20EJ08 and 20EJ09), and West Bonne Bay F-12 (20EJ01, 20EJ02, and 20EJ03) samples.

2.5.3 Fission-track thermochronology

Hibernia Formation rock samples yielded 269 fission-track ages that comprise five cooling populations (CP) and age peaks: (1) Early Cretaceous (125 ± 3 Ma); (2) Triassic to Jurassic (198 ± 3 Ma); (3) Carboniferous to Permian (300 ± 3 Ma); (4) Ordovician to Devonian (415 ± 9 Ma); and (5) Cryogenian to Cambrian (538 ± 13 Ma)(Fig. 2-7 and Table 2-2). Upper Hibernia and Lower Hibernia Formation strata contain consistent FT age ranges, age dispersion, and CP peaks (Table 2-2).

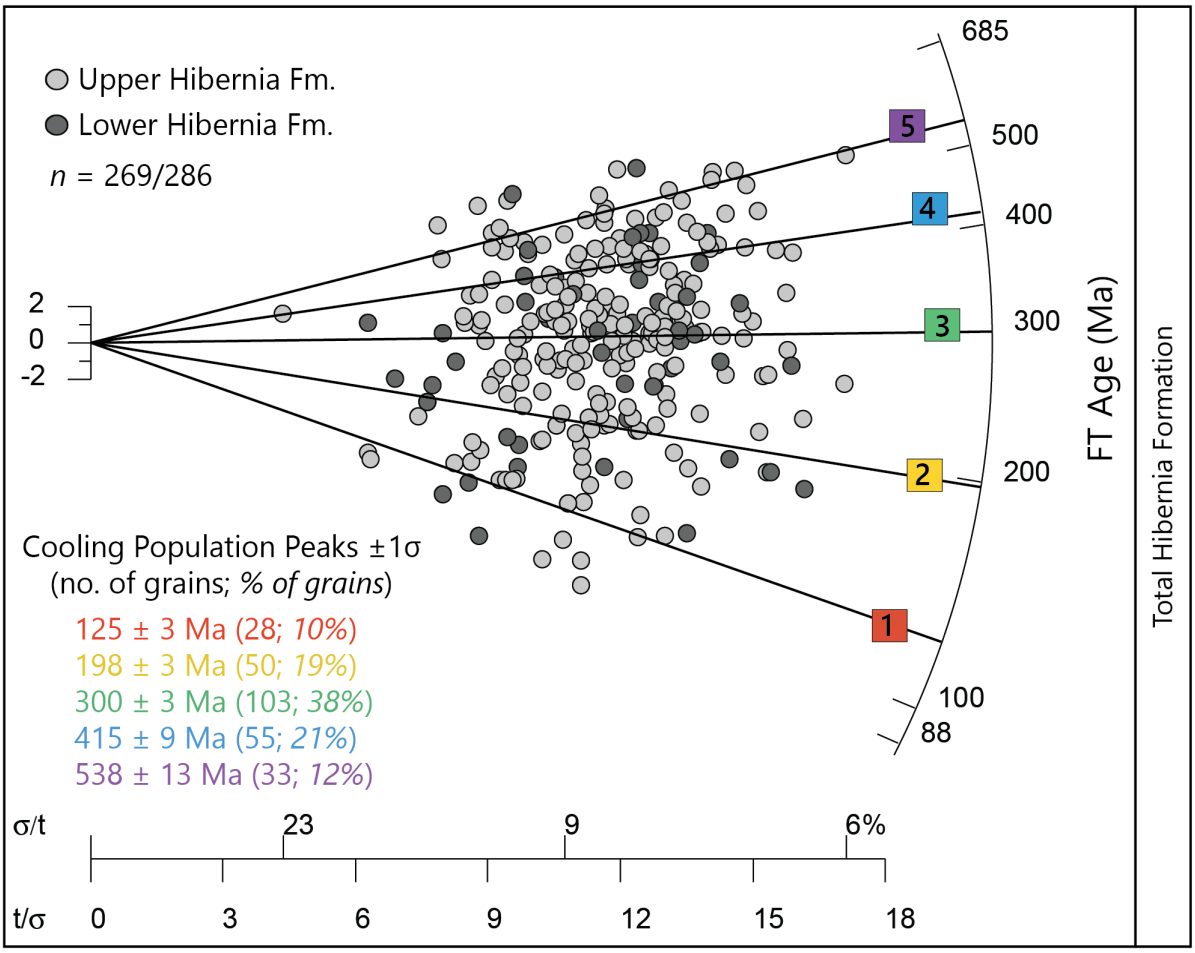

Figure 2-7: Radial plot and mixture modelling of detrital zircon fission-track results for Hibernia Formation samples. Data pooled for Lower Hibernia Formation (Hibernia B-16 55 and 54W wells) and Upper Hibernia Formation (Hebron M-04, and West Bonne Bay F-12 wells) samples.

Table 2-2: Detrital zircon fission-track age mixture modelling results for Lower Hibernia Formation (Hibernia B-16 55 and 54W wells) and Upper Hibernia Formation (Hebron M-04, and West Bonne Bay F-12 wells) samples.

Grouping	n (magmatic-cooled)	Central Value (Ma)	Dispersion (%)	Age Range (Ma)	Population 1 Peak ± 1σ (Ma) (% of grains) *(no. of grains)*	Population 2 Peak ± 1σ (Ma) (% of grains) *(no. of grains)*	Population 3 Peak ± 1σ (Ma) (% of grains) *(no. of grains)*	Population 4 Peak ± 1σ (Ma) (% of grains) *(no. of grains)*	Population 5 Peak ± 1σ (Ma) (% of grains) *(no. of grains)*
					Early Cretaceous 88-156 Ma	**Triassic-Jurassic** 157-239 Ma	**Carboniferous-Permian** 242-351 Ma	**Ordovician-Devonian** 355-473 Ma	**Cryogenian-Cambrian** 475-685 Ma
Upper Hibernia	218 (20)	296 ± 9	42	89-685	127 ± 3 (10)*(22)*	202 ± 4 (18)*(39)*	300 ± 3 (38)*(83)*	411 ± 10 (20)*(44)*	530 ± 12 (14)*(30)*
Lower Hibernia	51 (4)	272 ± 17	44	88-680	122 ± 6 (11)*(6)*	183 ± 6 (21)*(11)*	295 ± 7 (39)*(20)*	422 ± 14 (24)*(11)*	648 ± 42 (4)*(3)*
All Hibernia	**269 (24)**	**291 ± 8**	**42**	**88-685**	**125 ± 3 (10)*(28)***	**198 ± 3 (19)*(50)***	**300 ± 3 (38)*(103)***	**415 ± 9 (21)*(55)***	**538 ± 13 (12)*(33)***

2.6 Discussion

2.6.1 Depositional age of the Hibernia Formation and implications for the timing of magmatism in the Grand Banks

The youngest detrital zircon grains can constrain the maximum depositional ages, regional correlation, and geological significance of syn-rift strata (e.g., Cawood et al., 2012; Gehrels, 2014; Herriott et al., 2019). MDA estimates for the Lower and Upper Hibernia Formation ranged from Devonian to Early Cretaceous using four statistical routines (Table 2-3) and show no obvious trend with respect to geographic location in the Jeanne d'Arc basin. Devonian to Permian (ca. 364-280 Ma) MDA values calculated with the YSP, YGC 2σ, YPP, or central value methods are older than stratigraphic constraints and resulted from statistically low numbers of Mesozoic zircon grains in Hibernia Formation rocks. Upper Hibernia Formation strata from West Bonne Bay (sample 20EJ03) and Hebron oil field (sample 20EJ08) yielded Early Cretaceous ages using the central value method, whereas Lower Hibernia Formation strata from the Hibernia oil field (samples 20EJ05, 20EJ06) returned Early Cretaceous ages using both the YSP and central value methods (Table 2-3). Pooled MDA results from these Lower and Upper Hibernia Formation samples yield Berriasian-early Valanginian and late Valanginian-Barremian depositional ages, respectively,

which are consistent with published biostratigraphic correlations (Williams et al., 1990) and early Berriasian and older depositional age estimates for the underlying Jeanne d'Arc Formation (Hutter and Beranek, 2020). Berriasian to Barremian zircon grains from Hibernia Formation rocks indicate magmatism in the proximal domain during the development of the distal domain (Fig. 2-4).

Table 2-3: Maximum depositional age estimates for Hibernia Formation samples and other Upper Jurassic to Lower Cretaceous strata in the Jeanne d'Arc basin.

Sample	YSP (Ma)	MSWD	YGC 2σ (Ma)	YPP (Ma)	Central Age (Ma)	Mesozoic Grains (n)	MDA Range
Hibernia Samples							
20EJ01 (U)	289 ± 1	0.96	287 ± 2	292	299 ± 2	-	Permian-Pennsylvanian
20EJ02 (U)	292 ± 1	0.79	290 ± 3	293	332 ± 2	-	Permian-Mississippian
20EJ03 (U)	291 ± 1	1.02	287 ± 2	291	131 ± 6	1	Early Cretaceous-Permian
20EJ08 (U)	282 ± 2	1.08	280 ± 2	287	123 ± 8	1	Early Cretaceous-Permian
20EJ09 (U)	289 ± 3	0.2	289 ± 3	302	364 ± 3	-	Permian-Devonian
20EJ05 (L)	141 ± 2	1.67	413 ± 3	411	140 ± 4	2	Early Cretaceous-Devonian
20EJ06 (L)	135 ± 2	4.58	367 ± 3	139	138 ± 4	4	Early Cretaceous-Devonian
Formation							
Upper Hibernia Fm.	129 ± 2	2.92	282 ± 1	292	128 ± 5	2	Late Valanginian-Barremian
Lower Hibernia Fm.	140 ± 1	1.16	138 ± 2	139	139 ± 3	6	Berriasian-Early Valanginian
Jeanne d'Arc Fm.	141 ± 1	1.01	145 ± 1	145	145 ± 1	65	Tithonian-Berriasian

2.6.2 Interpreted zircon cooling populations, cooling types, and implications for exhumation

Hibernia Formation rock samples yielded 269 double-dated zircon grains that are assigned to five FT cooling populations (CP) and record ~400 Myr of tectonothermal events along the Atlantic Canadian margin (Table 2-4). Most of the zircon grains are classified as *exhumation-cooled* (91%; n = 245) and have U-Pb ages that are older than their corresponding FT ages (Fig. 2-8; Enkelmann et al., 2019). Exhumation-cooled grains occur below the 1:1 line on crystallization age versus cooling age plots and the difference between these values (ΔT) quantifies the time elapsed between zircon crystallization and the last time the zircon cooled through ~250ºC. The remaining zircon grains are classified as *magmatic-cooled* (9%; n = 24) and have U-Pb ages that

are statistically equal (within ≤2σ error) to their corresponding FT ages and occur close to the 1:1 line on crystallization age versus cooling age plots (Fig. 2-8; Enkelmann et al., 2019). Four magmatic-cooled peaks were calculated from the U-Pb ages of double-dated zircon grains: Early Cretaceous (137 ± 2 Ma), Carboniferous-Permian (298 ± 4 Ma), Silurian-Devonian (443 ± 9 Ma), and Ediacaran (576 ± 8 Ma) (Table 2-4 and Fig. 2-8). Magmatic-cooled grains may not only indicate derivation from volcanic units, but also shallow intrusive rocks in the top 0-5 km of the crust where magma cools quickly and results in similar FT and U-Pb ages (e.g., Malusà and Fitzgerald, 2019).

Hibernia Formation strata show vertical trends in crystallization age versus cooling age space that start with a magmatic-cooled cluster on the 1:1 line followed by Early Cretaceous and older FT ages (Fig. 2-8). Cryogenian to Cambrian and Carboniferous to Permian U-Pb populations show relatively continuous cooling ages since crystallization, whereas Ordovician to Devonian U-Pb populations have magmatic-cooled peaks followed by punctuated exhumation-cooled age clusters from the Carboniferous to Early Cretaceous (CP3 to CP1). Archean to Tonian zircon grains are characterised by only exhumation-cooled grains with $\Delta T > 300$ Ma and Early Cretaceous zircon grains only yield magmatic-cooled values. Horizontal trends in the crystallization age versus cooling age plot show each CP contains a spread of U-Pb ages equal to, or older than, the cooling ages and represents the signature of rocks that cooled within the time interval.

The Newfoundland-Iberia rift system evolved during Triassic to Jurassic stretching and thinning, Early to mid-Cretaceous mantle exhumation, and mid-Cretaceous breakup-related events that formed the proximal, necking, distal, and outer domains (e.g., Davis and Kusznir et al., 2004, Lavier and Manatschal, 2006, Péron-Pinvidic and Manatschal, 2009; Péron-Pinvidic et al., 2013;

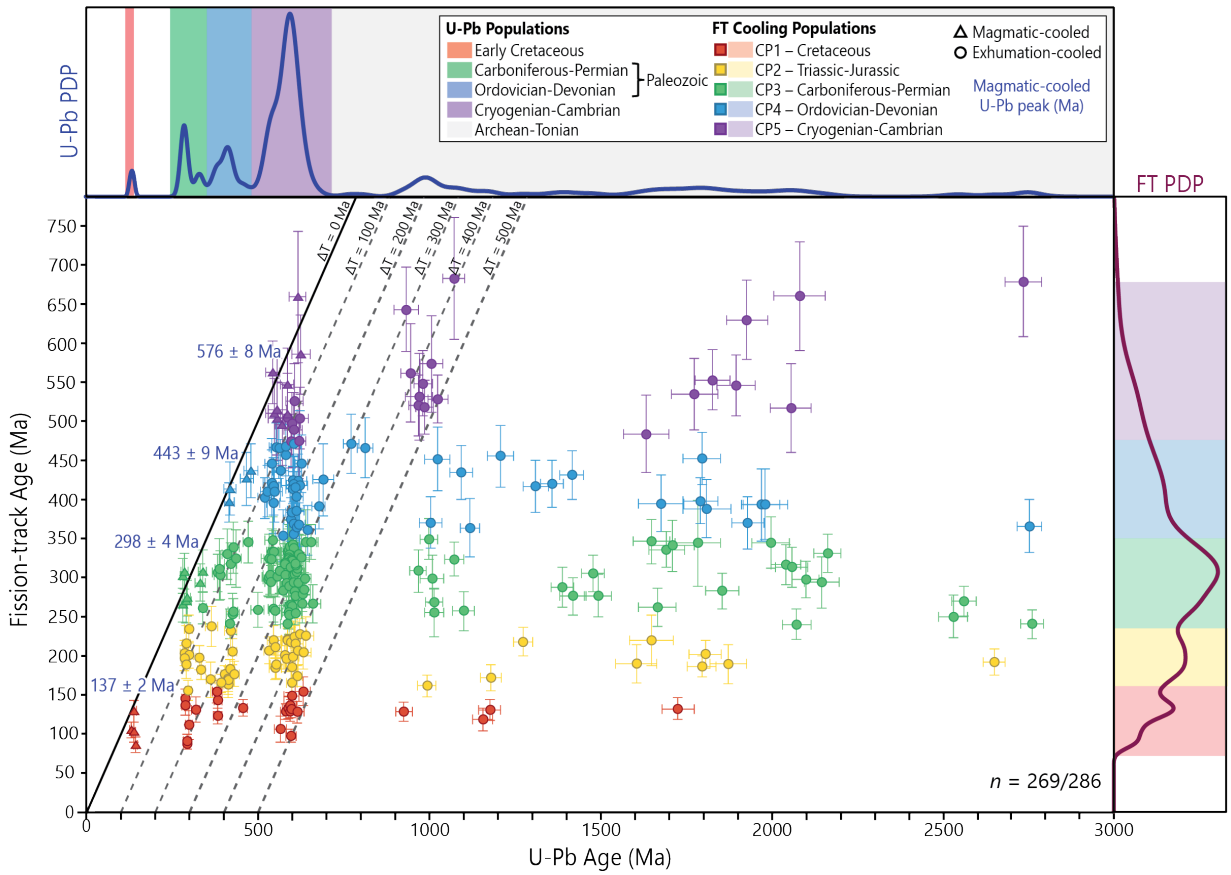

Figure 2-8: Crystallization age versus cooling age plot of detrital zircon U-Pb and FT double-dating results for Hibernia Formation samples. Data pooled for Lower Hibernia Formation (Hibernia B-16 55 and 54W wells) and Upper Hibernia Formation (Hebron M-04, and West Bonne Bay F-12 wells) samples.

Sutra et al., 2013; Huismans and Beaumont, 2014; Haupert et al., 2016). Lower Cretaceous Hibernia Formation strata from the Jeanne d'Arc basin record Grand Banks exhumation events that occurred during continued growth of the proximal domain and tectonic development of the necking and distal domains. Early Cretaceous CP1 and Triassic to Jurassic CP2 align with the timing of mantle exhumation (distal domain) and stretching-thinning (proximal and necking domain) phases of rift evolution between Newfoundland and Iberia, respectively (e.g., Tucholke et al., 2007; Péron-Pinvidic et al., 2013). Rift-related cooling was likely dominated by tectonic exhumation along normal faults and magmatic cooling of igneous rocks. The near-zero lag time observed between Early Cretaceous exhumation-cooled CP1 peak (129 ± 3 Ma; Table 2-4) and

estimated maximum depositional ages of Hibernia Formation strata (139-128 Ma) could result from fault displacements that caused rapid tectonic exhumation along rift flanks (e.g., Saylor et al., 2012). Early Cretaceous CP1 cooling ages align with the ~140 Ma onset of mantle exhumation along the Newfoundland margin (Sutra et al., 2013; Nirrengarten et al., 2018) and corresponding reactivation and attenuation of normal faults over geologically short time intervals within the Grand Banks (Berriasian rift episode; Sinclair, 1988; Tucholke et al., 2007). The lack of magmatic-cooled CP2 grains points to a zircon-poor, tectonothermal event that resulted in significant exhumation (e.g., Saylor et al., 2012), consistent with Late Triassic to Early Jurassic proximal domain development with wide corridors of upper crustal extension and mafic magmatism in Atlantic Canada (cf., Hodych and Hayatsu, 1988).

Carboniferous to Permian CP3 and Ordovician to Devonian CP4 align with the timing of the Alleghenian-Variscan and Taconic to Neoacadian orogenic cycles, respectively, and reflect various cooling events related to syn-orogenic magmatism, erosional exhumation, post-orogenic thermal relaxation and structurally-controlled exhumation along major shear zones and sutures. CP3 contains the most grains of all the cooling populations and may signal an increased rate of erosional exhumation (e.g., Pereira et al., 1998, Basler, 2020), increased zircon fertility from exposure of deeper plutons, and/or the indirect supply and recycling of Iberian-derived zircon grains through upper Paleozoic strata (Hiscott et al., 2008). Upper Paleozoic to Cretaceous sedimentary rocks in the Lusitanian basin of western Portugal yield Carboniferous to Permian (~300 Ma) detrital zircon fission-track ages (e.g., Pereira et al., 1998) and typically contain Carboniferous to Permian U-Pb populations (e.g., Rodrigues et al., 2015, Dinis et al., 2016) that are represented in Upper Hibernia Formation strata; however, the majority of the U-Pb ages in CP3 are Ordovician and older and do not distinguish between recycled Appalachian or Iberian

sources (Fig. 2-9). Cryogenian to Cambrian U-Pb ages (ca. 700-550) dominate Ordovician to Devonian CP4 (Fig. 2-9) and likely represent cooling of Avalonian arc successions during Acadian orogenesis. Silurian magmatic-cooled zircon grains in CP4 may show the introduction of composite Laurentian sources (e.g., Whalen, 1989); however, the persistent Cryogenian to Cambrian age population supports the hypothesis that the dominant signature reflects cooling of peri-Gondwanan terrane infrastructure.

Table 2-4: Detrital zircon double-dated mixture modelling results for exhumation-cooled FT, magmatic-cooled FT, and magmatic-cooled U-Pb ages for Hibernia Formation samples.

Grouping	**n**	**Central Value (Ma)**	**Dispersion (%)**	**Age Range (Ma)**	**Population 1 Peak ± 1σ (Ma)** (% of grains) *(no. of grains)*	**Population 2 Peak ± 1σ (Ma)** (% of grains) *(no. of grains)*	**Population 3 Peak ± 1σ (Ma)** (% of grains) *(no. of grains)*	**Population 4 Peak ± 1σ (Ma)** (% of grains) *(no. of grains)*	**Population 5 Peak ± 1σ (Ma)** (% of grains) *(no. of grains)*
					Early Cretaceous	**Triassic-Jurassic**	**Carboniferous-Permian**	**Ordovician-Devonian**	**Cryogenian-Cambrian**
Exhumation-cooled (FT)	245	288 ± 8	40	89-685	129 ± 3 (10)*(24)*	199 ± 3 (21)*(50)*	301 ± 4 (39)*(96)*	416 ± 10 (21)*(51)*	540 ± 16 (9)*(24)*
Magmatic-cooled (FT)	24	331 ± 38	56	88-660	107 ± 6 (17)*(4)*	-	292 ± 9 (29)*(7)*	423 ± 18 (19)*(4)*	542 ± 19 (35)*(9)*
Magmatic-cooled (U-Pb)	28	312 ± 34	58	131-625	137 ± 2 (29)*(8)*	-	298 ± 4 (25)*(7)*	443 ± 9 (14)*(4)*	576 ± 8 (32)*(9)*

Cryogenian to Cambrian CP5 aligns with the cessation of subduction along the peri-Gondwanan margin and end of Avalonian arc magmatism (e.g., Barr et al., 1990; Keppie et al., 1998). The U-Pb spectra for CP5 are characterized by three age populations (ca. 650-540, 1100-900, 2100-1600 Ma) and an age gap from 1600-1100 Ma that is consistent with West African crustal affinity and matches those recognized in Avalonia (Fig. 2-9; e.g., Linnemann et al., 2011, Pratt et al., 2015, Stephan et al., 2019).

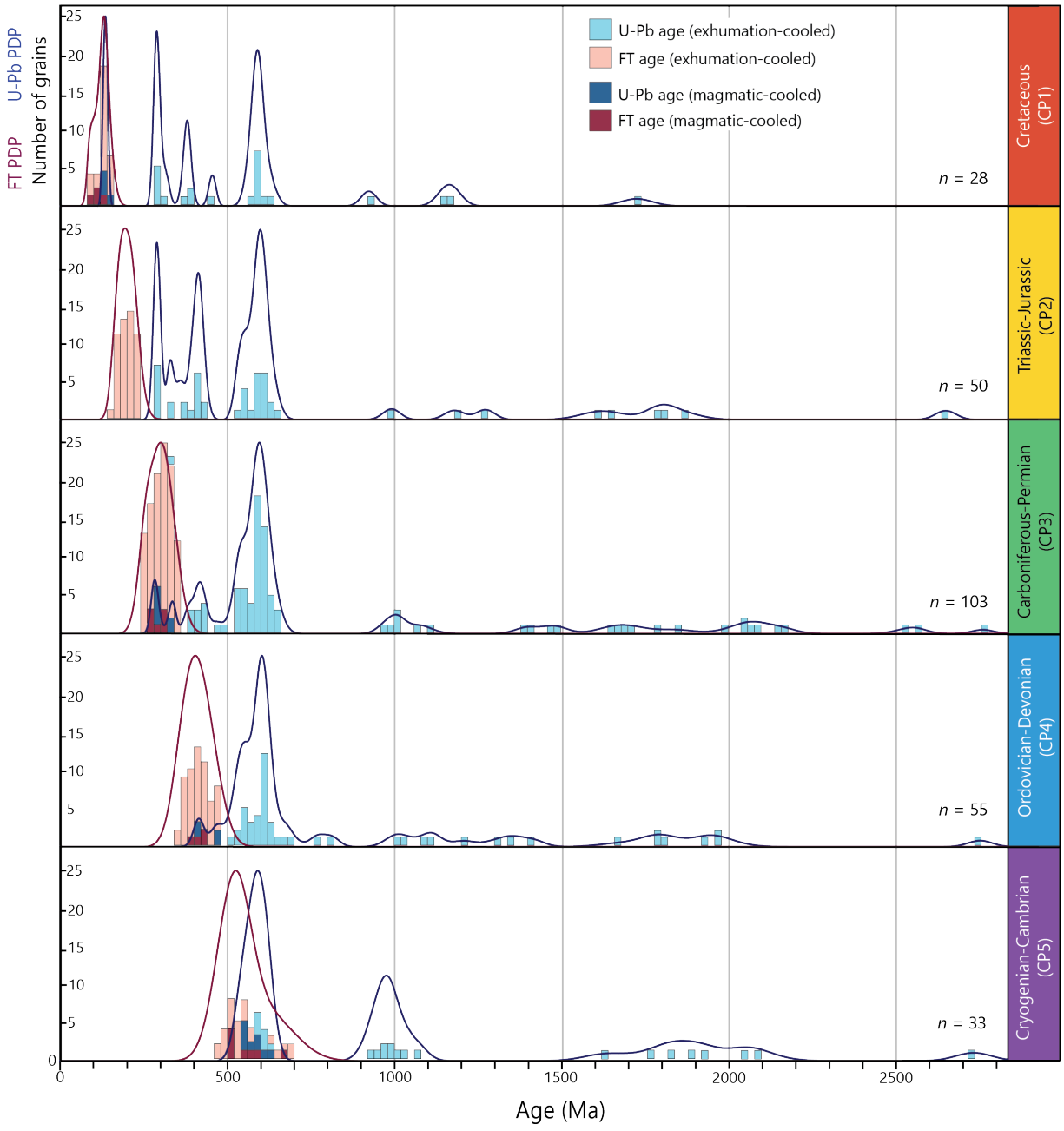

Figure 2-9: Probability density plots (PDP) and histograms of detrital zircon U-Pb and FT double-dating results for Hibernia Formation samples. Data pooled by FT cooling populations.

2.6.3 Interpreted zircon provenance signatures

2.6.3.1 Archean to Tonian

Archean to Tonian (ca. 3000-720 Ma) zircon grains make up 14-59% of each sample (mean = 27%) and have primary sources from the basement domains of eastern Laurentia and West

Gondwana (e.g., Stephan et al., 2019). Archean zircon grains (>2500 Ma) match the ages of magmatism in the Nain, Hearne, Superior, and related cratons of North America (e.g., Hoffman, 1988; Scott, 1995), and west Africa (e.g., Linnemann et al., 2011; Pratt et al., 2015; Marzoli et al., 2017). Early Paleoproterozoic zircon ages (ca. 2000-2200 Ma) are uncommon in eastern North America, but consistent with known magmatism in the West African craton (e.g., Sylvester and Attoh, 1992; Kuiper et al., 2017). Late Paleoproterozoic zircon grains match the ages of 2000-1800 Ma magmatism in the Torngat, Trans-Hudson, and related orogenic belts that assembled Laurentia (e.g., Hoffman, 1988; Scott, 1995; Whitmeyer and Karlstrom, 2007). Late Paleoproterozoic to early Neoproterozoic zircon grains (ca. 1700-720 Ma) are consistent with ages of Grenville basement and Tonian to Cryogenian rift episodes along the three margins of Laurentia. The Grenville orogen resulted from the successive accretion of Archean to late Mesoproterozoic arcs and microcontinents from ca. 1800 to 1300 Ma, such as those during the Yavapai and Mazatzal orogenies, and culminated with ca. 1000 Ma continent-continent collision and formation of supercontinent Rodinia (e.g., Rivers, 1997). Parts of eastern Labrador and western Newfoundland are underlain by Mesoproterozoic (1630-1460 Ma) Grenville basement rocks that were intruded by ca. 1130-1020 Ma and ca. 990-950 Ma plutons (e.g., Gower et al., 1991; Heaman et al., 2002; Rainbird et al., 2017). Possible recycled sources of Archean to Tonian zircon grains include those recognized in Ediacaran to lower Paleozoic strata from the Iapetan margin in Newfoundland (e.g., Cawood and Nemchin, 2001), peri-Gondwanan cover successions of Avalonia (e.g., Keppie et al., 1998; Pollock et al., 2009; Barr et al., 2012; Willner et al., 2013) and Meguma terrane (e.g., Krogh and Keppie, 1990; Waldron et al., 2009; Pothier et al., 2015), Appalachian-Variscan foreland and strike-slip basin strata (e.g., Gray and Zeitler, 1997; Thomas et al., 2004), and Grand Banks syn-rift successions (e.g., Hutter and Beranek, 2020).

Archean to Tonian zircon grains in the Hibernia Formation are classified as exhumation-cooled and yield FT ages that are 300-2500 Myr older than their crystallization ages (Fig. 2-8). The cooling ages correspond with the timing of several crustal cooling events, including peri-Gondwanan thermal relaxation (CP5), Acadian-Alleghanian orogenic uplift and erosion (CP4 and CP3), and Mesozoic rift-related tectonic exhumation (CP1 and CP2) (Fig. 2-10).

2.6.3.2 Cryogenian to Cambrian

Cryogenian to Cambrian zircon grains (ca. 720-485 Ma) make up 0-60% of each sample (mean = 49%) and have primary igneous sources within the Iapetan and peri-Gondwanan terrane basement domains of the Canadian Appalachians, such as those that underlie the Dunnage, Gander, and Avalon zones in Newfoundland (e.g. Krogh et al., 1988; Barr et al., 1990; Tucker and Mckerrow, 1995; O'Brien et al., 1996; Keppie et al., 1998; Rogers et al., 2006; Murphy et al., 2008). Recycled sources of late Neoproterozoic zircon grains include peri-Gondwanan cover assemblages (e.g., Krogh and Keppie, 1990; Murphy et al., 2004; Pollock et al., 2009; Waldron et al., 2009; Barr et al., 2012; Willner et al., 2013; Pothier et al., 2015), syn- to post-orogenic Paleozoic strata of the Maritimes basin (e.g., Murphy and Hamilton, 2000; Gibling et al., 2008; Waldron et al., 2015), and Grand Banks syn-rift successions (e.g., Hutter and Beranek, 2020).

Cryogenian to Cambrian zircon populations assigned to Cryogenian to Cambrian CP5 are characterized by magmatic-cooled grains derived from shallow intrusive rocks, and exhumation-cooled grains with $\Delta T < 100$ Ma that likely represent slow or lower crustal cooling of the intrusive bodies (Fig. 2-8; e.g., Campbell et al., 2005). Possible igneous sources in eastern Newfoundland include the 570 ± 6 Ma Berry Hills Granite (Kellett et al., 2014) and 585 ± 3 Ma Harbour Main Group (Krogh et al., 1988). Possible Variscan sources along the Iberian margin include 570-540 Ma rocks in the Ossa Morena and Central Iberian zones of Portugal (e.g., Henriques et al., 2015,

2016). The remaining FT ages for the Cryogenian to Cambrian U-Pb population are exhumation-cooled and reflect younger geological events (Fig. 2-10). Ordovician to Devonian CP4 and Carboniferous to Permian CP3 reflect episodes of uplift and erosion when Avalonia accreted during the Acadian orogeny and the final Gondwana-Laurentia collision during the Alleghanian-Variscan orogeny, respectively. Cryogenian to Cambrian zircon grains in Triassic to Jurassic CP2 and Early Cretaceous CP1 are consistent with tectonic exhumation events via normal faulting during proximal and distal domain development, respectively.

Table 2-5: Summary of potential primary and recycled detrital zircon sources for Hibernia Formation strata.

Age populations	Primary sources	Potential recycled sources in Atlantic Canada
Archean to Tonian		
>2500 Ma	Superior, North Atlantic, Nain cratons	Iapetan margin sandstones, Appalachian (peri-Laurentian & peri-Gondwanan) terrane cover assemblages
2200-2000 Ma	West Gondwanan cratons	Appalachian (Peri-Gondwanan) terrane cover assemblages
2000-720 Ma	Torngat, New Quebec, Trans-Hudson, Grenville and related orogens	Iapetan margin sandstones, Appalachian (Peri-Gondwanan) terrane cover assemblages, Appalachian foreland & strike-slip basins
Cryogenian to Cambrian		
720-485 Ma	Iapetan and Peri-Gondwanan terrane basement (Dunnage, Gander, Avalon)	Peri-Gondwanan terrane cover assemblages, Appalachian foreland & strike-slip basins, Mesozoic rift basins
Paleozoic		
540-280 Ma	Appalachian-Variscan igneous suites	Appalachian foreland & strike-slip basins, Mesozoic rift basins
Mesozoic		
148-123 Ma	North Atlantic rift assemblages	Tithonian to Valanginian strata, Grand Banks

2.6.3.3 Paleozoic

Early to late Paleozoic zircon grains (ca. 485-251 Ma) make up 19-29% of each sample (mean = 23%) and align with ages of Appalachian and Variscan igneous suites. Primary Taconic igneous sources include 467-452 Ma rocks in the peri-Laurentian realm (Fig. 2-3; e.g., Chorlton

and Dallmeyer, 1986; Dunning et al., 1990; Valverde-Vaquero et al., 2006; van Staal et al., 2007) and equivalent Iberian 490-470 Ma magmatism in the Ossa-Morena and Central Iberian zones (e.g., Solá et al., 2008; Henriques et al., 2015, 2016). Salinic rocks in the Gander zone include 435-419 Ma igneous suites and 425-410 Ma metamorphic complexes (e.g., O'Brien et al., 1991, Heaman et al., 2002, Dunning et al., 1990). Acadian and Neoacadian igneous rocks that record the docking of Avalonia and Meguma are characterized by 396-357 Ma granitic plutons that span from New England to Newfoundland, including the Grand Banks (e.g., Bell and Howie, 1990; Dunning et al., 1990; O'Brien et al., 1991; Keppie and Krogh, 1999; Maclean et al., 2003; Kontak et al., 2004; Kellett et al., 2014; Kellett et al., 2021). Primary Alleghanian sources include 300-265 Ma granitic plutons along the Appalachians (e.g., Tomascak 1996, Pe-Piper et al., 2010) and Iberian Variscides (e.g., Fernández-Suárez et al., 2000; Carracedo et al., 2009). Recycled sources for the Hibernia Formation include upper Paleozoic foreland and strike-slip basin strata (e.g., Hiscott et al., 2008; Piper et al., 2012) and Grand Banks syn-rift successions (e.g., Hutter and Beranek, 2020).

Early to late Paleozoic detrital zircon grains in the Hibernia Formation yield FT ages that correspond to CP4 to CP1 (Fig. 2-8). A Late Ordovician to early Silurian (443 ± 9 Ma; CP4) magmatic-cooled peak matches igneous crystallization ages in composite Laurentia (ca. 445-435 Ma; Whalen, 1989), Ganderia (ca. 440-419 Ma; e.g., Dunning et al., 1990), Avalonia (ca. 440 Cape St. Mary's sills; Greenough et al., 1993; Hodych and Buchan, 1998), and Meguma (ca. 440 Ma; White Rock Formation; Keppie and Krogh, 2000; MacDonald et al., 2002). A Carboniferous to Permian (298 ± 4 Ma; CP3) magmatic-cooled peak matches the emplacement ages of Alleghanian plutons in the northern Appalachians (e.g., Tomascak 1996, Pe-Piper et al., 2010) and Iberian Variscides (e.g., Fernandez-Suarez et al. 2000, Carracedo et al., 2008). Exhumation-cooled Paleozoic zircon grains are assigned to three cooling populations and correspond to tectonic

processes associated with the Alleghenian orogeny (CP3) and Triassic to Jurassic (CP2) and Early Cretaceous extensional deformation (CP1).

Carboniferous to Permian exhumation-cooled grains show a continuous cooling trend and grains with $\Delta T < 100$ Ma may reflect slow magmatic cooling of the pluton(s) identified by the magmatic-cooled grains (Figs. 2-8 and 2-10; Campbell et al., 2015). In contrast, Ordovician to Devonian zircon have intermittent FT age clusters with mostly $\Delta T \geq 100$ Ma that reflect later exhumation events (Figs. 2-8 and 2-10).

2.6.3.4 Early Cretaceous

Cretaceous zircon grains comprise 0-12% of each sample (mean = 1%) and have magmatic-cooled signatures that are assigned to CP1 (Fig. 2-8). The U-Pb ages of Cretaceous zircon grains corroborate the interpreted timing of syn-rift magmatism in the southern Grand Banks region, including volcanic centers along the SW Grand Banks transfer zone that are recognized in offshore drillcore and mapped by marine seismic investigations (e.g., Pe-Piper et al., 1994, Bowman et al., 2012). For example, mafic to felsic sills, lavas, pyroclastic flows, and volcaniclastic rocks have yielded whole-rock K-Ar ages of 135 ± 6 Ma to 133 ± 3 Ma in Brant P-87 and Mallard M-45 (Fig. 2-1B; e.g., Jansa and Pe-Piper, 1988; Pe-Piper et al., 1994). Amphibolite units drilled at Ocean Drilling Program sites 1067 and 1068, which are currently located in the distal regions of the Iberian conjugate margin, have similarly yielded $^{40}Ar/^{39}Ar$ mineral ages of 142–132 Ma (Jagoutz et al., 2007). Mafic-ultramafic intrusive rocks associated with the Budgell Harbour Stock in central Newfoundland yield Late Jurassic to mid-Cretaceous K-Ar ages (e.g., Helwig et al., 1974; Peace et al., 2018), whereas alkaline mafic rocks in western Portugal yield titanite U-Pb ages of 147-142 Ma (Grange et al., 2008).

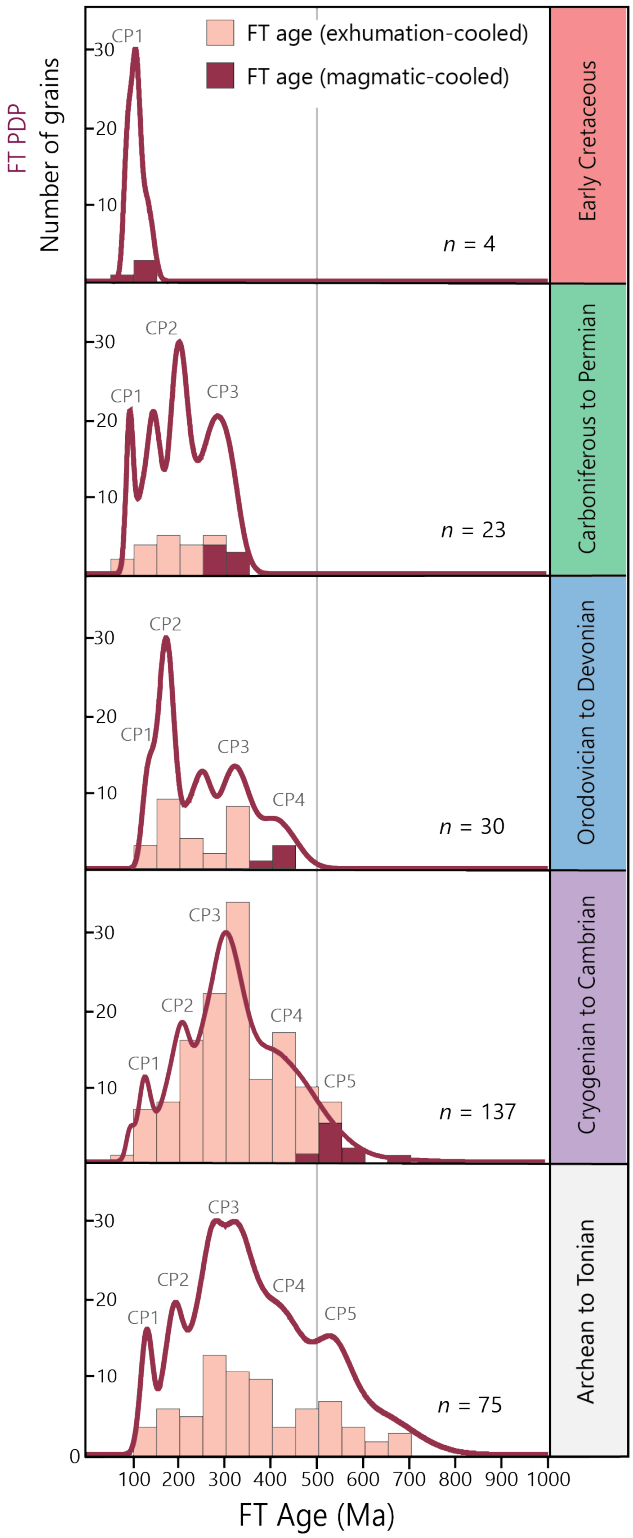

Figure 2-10: Probability density plots (PDP) and histograms of detrital zircon U-Pb and FT double-dating results for Hibernia Formation samples. Data pooled by U-Pb age populations.

2.6.4 Thermal history of the Atlantic margin and significance of Hibernia Formation cooling populations

Thermal history studies of basement and cover rocks that underlie the Atlantic Canadian margin have yielded Carboniferous to Cretaceous cooling ages (Fig. 2-3, Table 2-6; e.g., Ravenhurst et al., 1989; Hendriks et al., 1993; Ryan and Zentilli, 1993). The continuity of zircon and apatite fission-track and (U-Th)/He age results along the magma-poor Newfoundland and magma-rich Nova Scotian margins suggests that the rocks experienced similar Paleozoic thermal events. However, Paleozoic orogen-related thermal events capable of resetting low-temperature thermochronometers did not have a blanketing affect across Atlantic Canada. Appalachian collision-related deformation, metamorphism, and magmatism generally migrated eastwards along with the sequential accretion of volcanic arcs and microcontinents (van Staal et al., 2009) and the western limit of deformation is illustrated by Neoproterozoic ZHe ages in Grenville basement rocks from Anticosti Island (eastern Quebec) (Fig. 2-3; Powell et al., 2018). Acadian (ca. 420-400 Ma) and Neoacadian (ca. 400-350 Ma) deformation reached hundreds of kilometers west (inboard) of the Avalonian suture and overprinted older Taconic and Salinic fabrics (van Staal et al., 2009) demonstrated by Devonian to early Carboniferous cooling in the Gander zone of central Newfoundland (Chorlton and Dallmeyer, 1986) and Devonian syn-tectonic magmatism and cooling in the Humber zone (e.g; Anderson et al., 2000; Sandeman and Dunning, 2016). Carboniferous rocks of the Maritimes basin typically yield cooling ages that are younger than their depositional ages and indicate post-deposition thermal resetting (e.g., Ravenhurst et al., 1989; Hendriks et al., 1993; Ryan and Zentilli, 1993). Late Devonian to Pennsylvanian heating events associated with the Alleghenian orogenic cycle in the Canadian (e.g., Hendriks et al., 1993; Kuiper et al., 2017; Willner et al., 2019) and U.S. Appalachians (e.g., Naeser et al., 2016; Basler, 2020) are debated, but could reflect burial and/or high heat flow during the erosion of the Appalachians

and filling of adjacent foreland basins (Ravenhurst et al., 1989; Hendriks et al., 1993; Willner et al., 2019). Thermal history studies inferred that rocks at the present-day surface were buried >4-5 km depth by Carboniferous to Permian cover assemblages, and combined with a higher geothermal gradient, could have reset the zircon FT system (Grist and Zentilli, 2003). Evidence for Permian felsic magmatism in the northern U.S. Appalachians similarly indicates that high temperature conditions capable of triggering anatexis persisted until ~270 Ma (Tomascak et al., 1996). High temperatures during Carboniferous orogenesis and magmatism are also recognized in Iberia (e.g., Carracedo et al., 2009) and detrital zircon FT studies in central Portugal and Morocco likewise show a dominant ~300 Ma peak that represents unroofing of Variscan granitoids and adjacent basement (Pereira et al., 1998; Pratt et al., 2015). Thermal resetting of the zircon FT system during Alleghanian orogenesis is evident onshore Atlantic Canada and presumably extends into offshore regions including the Avalon Uplift, the proposed source area for most Hibernia Formation sediment (Fig. 2-3). Mesozoic deformation and magmatism along the SW Grand Banks transform and Avalon Uplift could also have reset zircon grains in Mesozoic and older strata by elevated geothermal gradients (<200 Ma; e.g. Kohn et al., 1993). Hibernia Formation strata contain a range of cooling ages, including those that pre-date the Acadian, Neoacadian, and Alleghanian orogenic cycles, indicating if thermal resetting occurred on the Avalon Uplift it did not affect all rocks.

Most Hibernia Formation detrital zircon grains (~70%) are interpreted to be recycled from Maritimes basin strata and characterized by long lag times (difference between cooling age and depositional age) that reflect tectono-thermal events older than those that freed the zircon from its most recent bedrock source (e.g., Bernet and Garver, 2005, Campbell et al., 2005). Apatite FT transects in the western Newfoundland Appalachians concluded that older, Permian-Carboniferous (ca. 343-283 Ma) cooling ages are typical at the highest elevations and younger, Triassic to Jurassic

Table 2-6: Mica ^{40}Ar-^{39}Ar, zircon fission-track and (U-Th)/He, and apatite fission-track and (U-Th)/He ages from Cretaceous and older rocks in Atlantic Canada.

Dating Method	Mica $^{40}Ar/^{39}Ar$	Zircon fission-track (ZFT)	Zircon (U-Th)/He (ZHe)	Apatite fission-track (AFT)	Apatite (U-Th)/He (AHe)
Closure/Annealing Temperature (°C)	300-400°C[(1)]	210-290°C[(2)]	160-200°C[(3)]	100-120°C[(4)]	40-80°C[(5)]
Western & Central Newfoundland		235-212 Ma[(6)] ($\bar{x}$ = 227 Ma)		343-152 Ma[(7)] ($\bar{x}$ = 232 Ma)	
Offshore Newfoundland	50-430 Ma[(8)]	122-648 Ma			
Onshore Nova Scotia		342-217 Ma[(13)(14)] ($\bar{x}$ = 225 Ma)	290-192 Ma[(15)] ($\bar{x}$ = 220 Ma)	244-165 Ma[(9)(10)(11)(12)(13)] ($\bar{x}$ = 213 Ma)	211-165 Ma[(15)] ($\bar{x}$ = 180)
Offshore Nova Scotia				200 Ma[(16)]	
Anticosti Island			761-581 Ma[(17)] ($\bar{x}$ = 655 Ma)	125 Ma[(17)]	48-16 Ma[(17)] ($\bar{x}$ = 33 Ma)

(1) Hames and Bowring (1994); (2) Tagami et al. (1998); Tagami (2005); (3) Reiners et al. (2004); (4) Green et al. (1986); Ketcham et al. (1999); (5) Farley (2000); (6) Willner et al. (2019); (7) Hendriks et al. (1993); (8) Wilson and Hiscott (2007); (9) Ryan and Zentilli (2003); Ryan (1993); (10) Ravenhurst et al. (1990); (11) Arne et al. (1990); (12) Grist and Zentilli (2003); (13) Ravenhurst et al. (1989); (14) Willner et al. (2015); (15) Chang (2017); (16) Grist et al. (1991); (17) Powell et al., (2018).

(ca. 241-194 Ma) ages are recognized at lower elevations (Hendriks et al., 1993). This relationship predicts that syn-rift strata of the Grand Banks would yield a range of similar, or perhaps even older, cooling ages representative of an exhumed mountain belt. Syn-rift strata from offshore Newfoundland are correspondingly characterized by Paleozoic to Mesozoic cooling ages, consistent with significant recycling of onshore Appalachian basement and cover rocks (Hiscott and Wilson, 2007).

It is uncertain if upper Paleozoic sedimentary rocks of the Avalon Uplift were thermally reset after deposition, prior to their Mesozoic exhumation. However, the U-Pb signatures for exhumation-cooled Triassic-Cretaceous (CP2) and Early Cretaceous (CP1) zircon grains could reflect such an event (Fig. 2-9). Localized thermal-resetting from Alleghanian-Variscan burial and deformation or Mesozoic deformation and magmatism along the SW Grand Banks transform could have affected some Avalon Uplift rocks. Subsequent Early Cretaceous tectonic exhumation and

erosion that supplied Hibernia Formation strata may have tapped into both thermally-reset and un-reset rocks resulting in the observed Paleozoic to Mesozoic cooling ages.

2.6.5 Early Cretaceous paleogeography

Early Cretaceous CP1 zircon grains that cooled near the time of deposition indicate at least two sediment sources for the Hibernia Formation. Early Cretaceous magmatic-cooled zircon grains are likely first-cycle and point to sources to the south of the Jeanne d'Arc basin where Berriasian and younger intrusive and extrusive igneous rocks are known or inferred along the SW Grand Banks transform fault (Fig. 2-11; e.g., Pe-Piper et al., 1994, Bowman et al., 2012). Paleozoic and older exhumation-cooled zircon grains reflect cooling during Early Cretaceous uplift of igneous basement sources or thermally-reset upper Paleozoic strata (e.g., Keen et al., 1987; Enachescu, 1988; Tankard et al., 1989).

Hibernia Formation detrital zircon grains mostly yield Cryogenian to Jurassic cooling (CP5 to CP2) and Permian to Archean U-Pb crystallization ages that are much older than Early Cretaceous deposition and characteristic of well-mixed, continental-scale drainage systems with multiple recycled sources (e.g., Cawood et al, 2012); however, the Hibernia Formation was deposited during extensional deformation when tectonic subsidence dominated and the likely sources were local rift flanks. The mature compositional and textural traits of Hibernia Formation rocks, in conjunction with an inferred local source region in the southern Grand Banks, support the hypothesis that Lower Cretaceous units were sourced from mature siliciclastic strata that comprised local rift flanks and uplifts. Syn-rift, Upper Jurassic to Lower Cretaceous sandstone units of the Jeanne d'Arc, Flemish Pass, and Orphan basins yield similar Archean to Mesoproterozoic (>2500-1000 Ma), late Neoproterozoic (ca. 760-540 Ma), early to late Paleozoic (ca. 540-250 Ma), and Mesozoic (ca. 159-137) detrital zircon U-Pb age populations (McDonough

et al., 2010; Lowe et al., 2011; Hutter and Beranek, 2020). The repeatability of these age spectra supports the hypothesis that the main sediment sources were pre-existing, Carboniferous to Jurassic strata that covered Avalonia and Meguma basement in the Grand Banks and adjacent regions of Atlantic Canada (Hendriks et al., 1993; Gibling et al., 2008; Hiscott et al., 2008; Hutter and Beranek, 2020).

Carboniferous to Permian (ca. 358-275 Ma) detrital zircon grains that are unique to Upper Hibernia Formation strata may reflect the change from predominantly southern (Avalon Uplift) to southeastern (Morgiana Uplift) sediment sources between Berriasian to early Valanginian and late Valanginian to Barremian time, respectively (Fig. 2-11; e.g., Sinclair, 1988). Furthermore, Upper Hibernia Formation strata from the eastern Jeanne d'Arc basin (West Bonne Bay F-12) contain higher proportions of 358-275 Ma zircon grains than those from Hebron M-04 and may indicate greater proximity to an eastern source (Fig. 2-11). Southern to southeastern source regions are interpreted for Tithonian to Berriasian Jeanne d 'Arc Formation strata (Terra Nova oil field; Fig. 2-11) that contain Carboniferous to Permian detrital zircon grains (Hutter and Beranek, 2020), similar to Upper Hibernia Formation strata.

The FT ages of Carboniferous to Permian zircon grains in the Hibernia Formation show a magmatic-cooled cluster followed by younger, exhumation-cooled ages that are indicative of cooling of igneous rocks in the upper crust (CP 3) and later Mesozoic tectonic exhumation (CP 2 and 1) (Fig. 2-10). Carboniferous to Permian igneous rocks are recognized along the Alleghanian-Varisican orogenic belt in the U.S., Atlantic Canada, and Portugal (e.g., Carracedo et al., 2009; Pe-Piper et al., 2010), however, it is uncertain if such rocks underlie offshore parts of the eastern Newfoundland margin. The location of the Alleghanian-Variscan suture along the Newfoundland margin is unknown (e.g., Lefort et al., 1993), but it is possible that late Paleozoic plutons underlie

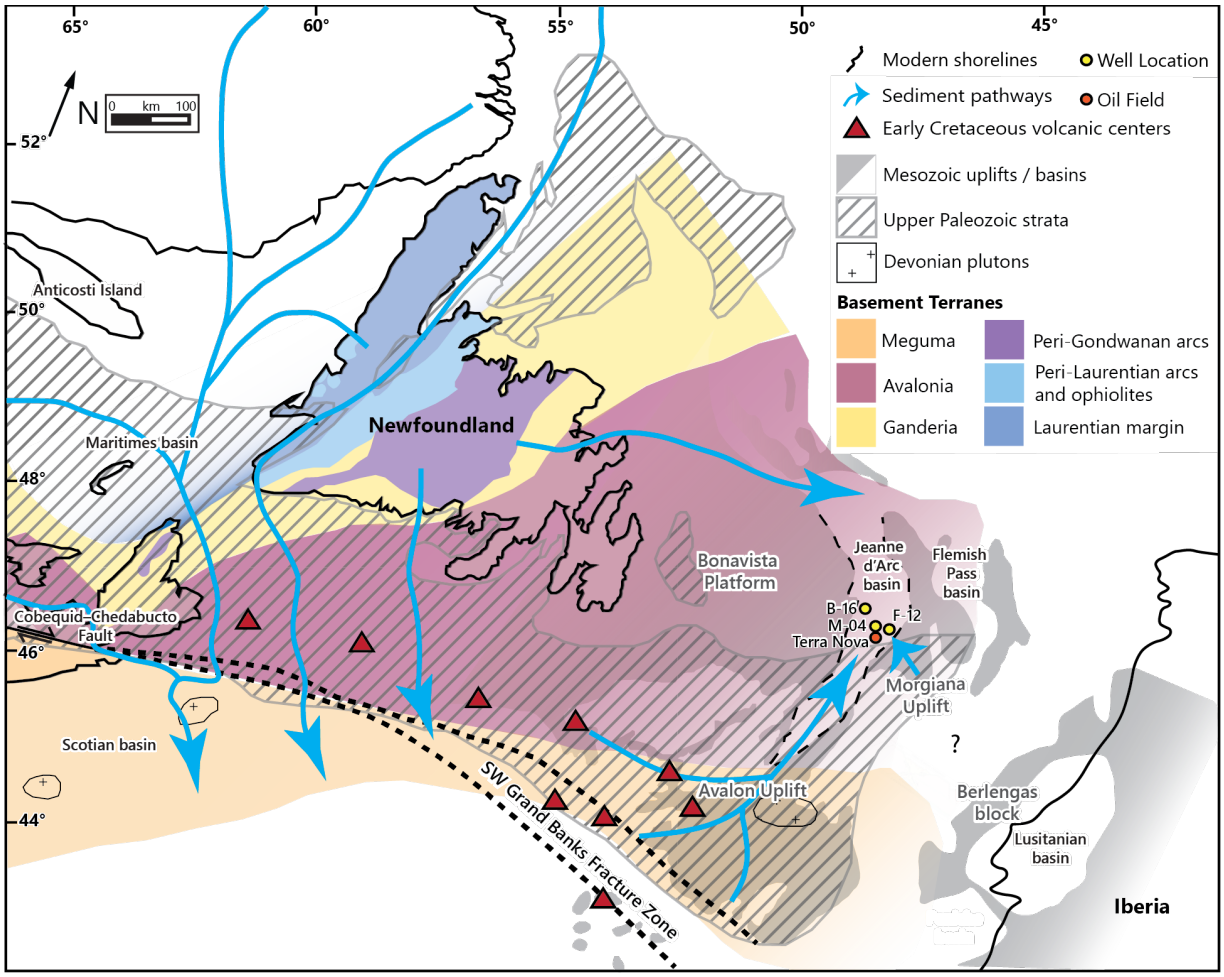

Figure 2-11: Early Cretaceous paleogeography of Atlantic Canada modified from Lowe et al. (2011) and Piper et al. (2012). Early Cretaceous volcanic centers from Bowman et al. (2012). North Atlantic Early Cretaceous reconstruction from Nirrengarten et al. (2017). Iberian Mesozoic architectural elements from Dinis et al. (2021). Hibernia Formation strata are mostly sourced from Avalon Uplift and SW Grand Banks fault zone regions with potential southeastern input from Morgiana Uplift and Variscan foreland-hinterland elements.

areas to the east of the Jeanne d'Arc basin (Fig. 2-11). Crustal thinning may have facilitated upper-crustal emplacement of late Paleozoic igneous rocks during the orogenic collapse of the Variscan orogen in western and offshore Portugal (e.g., Berlengas block; Dinis et al., 2021)(Fig. 2-11). Subsquent rapid exhumation of these late Paleozoic plutons during Triassic to Early Cretaceous extension would agree with the FT ages of Carboniferous to Permian zircon grains from the Hibernia Formation. Alternatively, Iberia was adjacent to the SE Grand Banks during the Early

Cretaceous and such late Paleozoic zircon grains may have been recycled through Alleghanian-Variscan foreland basin (e.g., Hiscott et al., 2008) or Triassic to Jurassic syn-rift strata. The scenario for reworked strata requires the mixing of two sources: (1) un-reset sedimentary rocks that preserve the ages of magmatic-cooled Carboniferous to Permian zircon; and (2) fully reset sedimentary rocks that lack evidence for Variscan uplift and erosion and instead yield Mesozoic cooling ages.

2.7 Conclusions

Detrital zircon U-Pb and FT double-dating studies of syn-rift, Lower Cretaceous Hibernia Formation strata establish source-to-sink connections for the Jeanne d'Arc basin and constrain the timing of regional exhumation during Mesozoic tectonic development of the Grand Banks region. Early Cretaceous magmatic-cooled zircon grains (131-143 Ma) identify the presence of syn-depositional igneous rocks within the drainage system that fed the Jeanne d'Arc basin and confirm Berriasian to early Valanginian and late Valanginian to Barremian depositional ages for Lower and Upper Hibernia Formation strata, respectively. Most Hibernia Formation detrital zircon grains (~70%) were recycled through older, upper Paleozoic strata of the Maritimes basin in Atlantic Canada and yield Paleozoic to Neoarchean (281-2753 Ma) U-Pb ages and Paleozoic to Cryogenian (252-685 Ma) FT ages. Early Cretaceous magmatic-cooled and exhumation-cooled zircon grains indicate southern Grand Banks source areas for the Hibernia Formation that included exhumed igneous basement or thermally-reset Appalachian cover assemblages of the Avalon Uplift and coeval, syn-rift volcanic-plutonic complexes along the SW Grand Banks transform fault. Detrital zircon double-dating results identify discrete exhumation-cooling events in the Newfoundland-Iberia magma-poor rift system and record the timing of Triassic to Jurassic stretching and thinning processes in the proximal domain and Early Cretaceous hyperextension and mantle exhumation in

the necking and distal domains at the edge of the Grand Banks. Syn-rift strata with exhumation-related cooling signals in proximal domain regions can be useful archives along other magma-poor rift margins around the world.

2.8 References

Alves, T.M., Moita, C., Sandnes, F., Cunha, T., Monteiro, J.H., and Pinheiro, L.M., 2006, Mesozoic-Cenozoic evolution of North Atlantic continental-slope basins: The Peniche basin, western Iberian margin: AAPG Bulletin, v. 90, p. 31–60, doi:10.1306/08110504138.

Anderson, S.D., Jamieson, R.A., Reynolds, P.H., and Dunning, G.R., 2001, Devonian extension in Northwestern Newfoundland: 40Ar/39Ar and U-Pb data from the Ming's Bight area, Baie Verte Peninsula: Journal of Geology, v. 109, p. 191–211, doi:10.1086/319237.

Arne, D.C., Duddy, I.R., and Sangster, D.F., 1990, Thermochronologic constraints on ore formation at the Gays River Pb- Zn deposit, Nova Scotia, Canada, from apatite fission track analysis: Canadian Journal of Earth Sciences, v. 27, p. 1013–1022, doi:10.1139/e90-105.

Barbeau, D.L., Olivero, E.B., Swanson-Hysell, N.L., Zahid, K.M., Murray, K.E., and Gehrels, G.E., 2009, Detrital-zircon geochronology of the eastern Magallanes foreland basin: Implications for Eocene kinematics of the northern Scotia Arc and Drake Passage: Earth and Planetary Science Letters, v. 284, p. 489–503, doi:10.1016/j.epsl.2009.05.014.

Barham, M., Kirkland, C.L., and Danišík, M., 2019, Assessing volcanic origins within detrital zircon populations – A case study from the Mesozoic non-volcanic margin of southern Australia: Geoscience Frontiers, v. 10, p. 1371–1381, doi:10.1016/j.gsf.2019.01.003.

Barr, S.M., Dunning, G.R., Raeside, R.P., and Jamieson, R.A., 1990, Contrasting U-Pb ages from plutons in the Bras d'Or and Mira terranes of Cape Breton Island, Nova Scotia: Canadian Journal of Earth Sciences, v. 27, p. 1200–1208, doi:10.1139/e90-127.

Barr, S.M., Hamilton, M.A., Samson, S.D., Satkoski, A.M., and White, C.E., 2012, Provenance variations in northern Appalachian Avalonia based on detrital zircon age patterns in Ediacaran and Cambrian sedimentary rocks, New Brunswick and Nova Scotia, Canada: Canadian Journal of Earth Sciences, v. 49, p. 533–546, doi:10.1139/E11-070.

Basler, L.C., 2020, Spatially variable syn- and post-orogenic exhumation of the Appalachian Mountains from apatite and zircon (U-Th)/He thermochronology [Honours Thesis]: Bowdoin College, https://digitalcommons.bowdoin.edu/honorsprojects/174.

Bell, J.S., and Howie, R.D., 1990, Paleozoic geology, *in* Keen, M.J. and Williams, G.L. eds., Geology of the Continental Margin of Eastern Canada, Geological Survey of Canada, p. 141–165.

Bernet, M., and Garver, J.I., 2005, Fission-track analysis of detrital zircon: Reviews in Mineralogy and Geochemistry, v. 58, p. 205–238, doi:10.2138/rmg.2005.58.8.

Boillot, G., Grimaud, S., Mauffret, A., Mougenot, D., Kornprobst, J., Mergoil-Daniel, J., and Torrent, G., 1980, Ocean-continent boundary off the Iberian margin: a serpentinite diapir west of the Galicia Bank: Earth and Planetary Letters, v. 48, p. 23-34, doi: https://doi.org/10.1016/0012-821X(80)90166-1.

Bowman, S.J., Pe-Piper, G., Piper, D.J.W., Fensome, R.A., and King, E.L., 2012, Early cretaceous volcanism in the Scotian Basin: Canadian Journal of Earth Sciences, v. 49, p. 1523–1539, doi:10.1139/e2012-063.

Bradley, D.C., 2008, Passive margins through earth history: Earth-Science Reviews, v. 91, p. 1–26, doi:10.1016/j.earscirev.2008.08.001.

Bronner, A., Sauter, D., Manatschal, G., Péron-Pinvidic, G., and Munschy, M., 2011, Magmatic breakup as an explanation for magnetic anomalies at magma-poor rifted margins: Nature Geoscience, v. 4, p. 549–553, doi:10.1038/NGEO1201.

Burton, W.C., and Southworth, S., 2010, A model for Iapetan rifting of Laurentia based on Neoproterozoic dikes and related rocks: Memoir of the Geological Society of America Bulletin, v. 206, p. 455–476, doi:10.1130/2010.1206(20).

Campbell, I.H., Reiners, P.W., Allen, C.M., Nicolescu, S., and Upadhyay, R., 2005, He-Pb double dating of detrital zircons from the Ganges and Indus Rivers: Implication for quantifying sediment recycling and provenance studies: Earth and Planetary Science Letters, v. 237, p. 402–432, doi:10.1016/j.epsl.2005.06.043.

Carracedo, M., Paquette, J.L., Alonso Olazabal, A., Santos Zalduegui, J.F., García de Madinabeitia, S., Tiepolo, M., and Gil Ibarguchi, J.I., 2009, U-Pb dating of granodiorite and granite units of the Los Pedroches batholith. Implications for geodynamic models of the southern Central Iberian Zone (Iberian Massif): International Journal of Earth Sciences, v. 98, p. 1609–1624, doi:10.1007/s00531-008-0317-0.

Carter, A., and Moss, S.J., 1999, Combined detrital-zircon fission-track and U-Pb dating: A new approach to understanding hinterland evolution: Geology, v. 27, p. 235–238, doi:https://doi.org/10.1130/0091-7613(1999)027<0235:CDZFTA>2.3.CO;2.

Cawood, P.A., Hawkesworth, C.J., and Dhuime, B., 2012, Detrital zircon record and tectonic setting: Geology, v. 40, p. 875–878, doi:10.1130/G32945.1.

Cawood, P.A., McCausland, P.J.A., and Dunning, G.R., 2001, Opening Iapetus: Constraints from the Laurentian margin in Newfoundland: Geological Society of America Bulletin, v. 113, p. 443–453, doi:10.1130/0016-7606(2001)113<0443:OICFTL>2.0.CO;2.

Cawood, P.A., and Nemchin, A.A., 2001, Paleogeographic development of the East Laurentian margin: Constraints from U-Pb dating of detrital zircons in the Newfoundland Appalachians: Geological Society of America Bulletin, v. 113, p. 1234–1246, doi:10.1130/0016-7606(2001)113<1234:PDOTEL>2.0.CO;2.

Chang, C., 2017, Low Temperature Thermal History Of Mainland Nova Scotia Using Apatite And Zircon (U-Th)/He Thermochronology [Honours Thesis]: Dalhousie University.

Chorlton, L.B., and Dallmeyer, R.D., 1986, Geochronology of early to middle Paleozoic tectonic development in the southwest Newfoundland Gander zone: Journal of Geology, v. 94, p. 67–89, doi:10.1086/629010.

Cohen, K.M., Finney, S.C., Gibbard, P.L., and Fan, J.-X., 2013 (updated), The ICS International Chronostratigraphic Chart: Episodes, v. 36, p. 199-204.

Coutts, D.S., Matthews, W.A., and Hubbard, S.M., 2019, Assessment of widely used methods to derive depositional ages from detrital zircon populations: Geoscience Frontiers, v. 10, p. 1421–1435, doi:10.1016/j.gsf.2018.11.002.

Culshaw, N., and Reynolds, P., 1997, 40Ar/39Ar age of shear zones in the southwest Meguma Zone between Yarmouth and Meteghan, Nova Scotia: Canadian Journal of Earth Sciences, v. 34, p. 848–853.

Davis, M., and Kusznir, N., 2004, Depth-Dependent Lithospheric Stretching at Rifted Continental Margins, *in* Karner, G.D. ed., Proceedings of NSF Rifted Margins Theoretical Institute, New York, Columbia University Press, p. 92–137, doi:10.7312/karn12738-005.

Dean, S.M., Minshull, T.A., Whitmarsh, R.B., and Louden, K.E., 2000, Deep structure of the ocean-continent transition in the southern Iberia Abyssal Plain from seismic refraction profiles: The IAM-9 transect at 40°20′N: Journal of Geophysical Research, v. 105, p. 5859–5885, doi:10.1029/1999jb900301.

Deemer, S., Hall, J., Solvason, K., Helen Lau, K.W., Louden, K., Srivastava, S., and Sibuet, J.-C., 2009, Structure and development of the southeast Newfoundland continental passive margin: Derived from SCREECH Transect 3: Geophysical Journal International, v. 178, p. 1004–1020, doi:10.1111/j.1365-246X.2009.04162.x.

Dickinson, W.R., and Gehrels, G.E., 2009, Use of U-Pb ages of detrital zircons to infer maximum depositional ages of strata: A test against a Colorado Plateau Mesozoic database: Earth and Planetary Science Letters, v. 288, p. 115–125, doi:10.1016/j.epsl.2009.09.013.

Dinis, P.A., Dinis, J., Tassinari, C., Carter, A., Callapez, P., and Morais, M., 2016, Detrital zircon geochronology of the Cretaceous succession from the Iberian Atlantic Margin: palaeogeographic implications: International Journal of Earth Sciences, v. 105, p. 727–745, doi:10.1007/s00531-015-1221-z.

Dinis, P.A., Vermeesch, P., Duarte, L. V., Cunha, P.P., Barbarano, M., and Garzanti, E., 2021, The Variscan basement in the western shoulder of the Lusitanian Basin (West Iberian Margin): insights from detrital-zircon geochronology of Jurassic strata: Journal of Iberian Geology, doi:10.1007/s41513-021-00177-w.

Dunn, A.M., Reynolds, P.H., Clarke, D.B., and Ugidos, J.M., 1998, A comparison of the age and composition of the Shelburne dyke, Nova Scotia, and the Messejana dyke, Spain: Canadian Journal of Earth Sciences, v. 35, p. 1110–1115, doi:10.1139/e98-058.

Dunning, G.R., O'Brien, S.J., Colman-Sadd, S.P., Blackwood, R.F., Dickson, W.L., O'Neill, P.P., and Krogh, T.E., 1990, Silurian orogeny in the Newfoundland Appalachians: Journal of Geology, v. 98, p. 895–913, doi:10.1086/629460.

Eddy, M.P., Jagoutz, O., and Ibañez-Mejia, M., 2017, Timing of initial seafloor spreading in the Newfoundland-Iberia rift: Geology, v. 45, p. 527–530, doi:10.1130/G38766.1.

Enachescu, M.E., 1987, Tectonic and Structural Framework of the Northeast Newfoundland Continental Margin, *in* Beaumont, C. and Tankard, A.J. eds., Sedimentary Basins and Basin-Forming Mechanisms, Canadian Society of Petroleum Geologists, Memoir 12, p. 117–146.

Enachescu, M.E., 1988, Extended basement beneath the intracratonic rifted basins of the Grand

Banks of Newfoundland: Canadian Journal of Exploration Geophysics, v. 24, p. 48–65.

Enkelmann, E., and Garver, J.I., 2016, Low-temperature thermochronology applied to ancient settings: Journal of Geodynamics, v. 93, p. 17–30, doi:10.1016/j.jog.2015.11.001.

Enkelmann, E., Lohff, S.K.S., and Finzel, E.S., 2019, Detrital zircon double-dating of forearc basin strata reveals magmatic, exhumational, and thermal history of sediment source areas: Geological Society of America Bulletin, v. 131, p. 1364–1384, doi:10.1130/B35043.1.

Farley, K.A., 2000, Helium diffusion from apatite: General behavior as illustrated by Durango fluorapatite: Journal of Geophysical Research: Solid Earth, v. 105, p. 2903–2914, doi:10.1029/1999jb900348.

Fernández-Suárez, J., Dunning, G.R., Jenner, G.A., and Gutiérrez-Alonso, G., 2000, Variscan collisional magmatism and deformation in NW Iberia: Constraints from U-Pb geochronology of granitoids: Journal of the Geological Society, London, v. 157, p. 565–576, doi:10.1144/jgs.157.3.565.

Force, E.R., and Barr, S.M., 2012, Provenance of the Lower Carboniferous Horton Group, Petit-de-Grat Island, Nova Scotia, as revealed by detrital zircon ages: Atlantic Geology, v. 48, p. 137–145, doi:10.4138/atlgeol.2012.007.

Franke, D., 2013, Rifting, lithosphere breakup and volcanism: Comparison of magma-poor and volcanic rifted margins: Marine and Petroleum Geology, v. 43, p. 63–87, doi:10.1016/j.marpetgeo.2012.11.003.

Galbraith, R.F., 2005, Statistics for Fission Track Analysis (R. F. Galbraith, Ed.): Boca Raton, Florida, Chapman & Hall/CRC, 224 p.

Garver, J.I., and Brandon, M.T., 1994, Erosional denudation of the British Columbia Coast Ranges as determined from fission-track ages of detrital zircon from the Tofino Basin, Olympic Peninsula, Washington: Geological Society of America Bulletin, v. 106, p. 1398–1412, doi:10.1130/0016-7606(1994)106<1398:EDOTBC>2.3.CO;2.

Gibling, M.R., Culshaw, N., Rygel, M.C., and Pascucci, V., 2008, Chapter 6 The Maritimes Basin of Atlantic Canada: Basin Creation and Destruction in the Collisional Zone of Pangea: Elsevier, v. 5, 211–244 p., doi:10.1016/S1874-5997(08)00006-3.

Gleadow, A.J.W., Hurford, A.J., and Quaife, R.D., 1976, Fission track dating of zircon: Improved etching techniques: Earth and Planetary Science Letters, v. 33, p. 273–276, doi:10.1016/0012-821X(76)90235-1.

Gower, C.F., Heaman, L.M., Loveridge, W.D., Schärer, U., and Tucker, R.D., 1991, Grenvillian magmatism in the eastern Grenville Province, Canada: Precambrian Research, v. 51, p. 315–336, doi:10.1016/0301-9268(91)90106-K.

Grange, M., Schärer, U., Cornen, G., and Girardeau, J., 2008, First alkaline magmatism during Iberia-Newfoundland rifting: Terra Nova, v. 20, p. 494–503, doi:10.1111/j.1365-3121.2008.00847.x.

Grant, A.C., and McAlpine, K.D., 1990, The continental margin around Newfoundland, *in* Keen, M.J. and Williams, G.L. eds., Geology of the Continental Margin of Eastern Canada,

Geological Survey of Canada, p. 239–292.

Gray, M.B., and Zeitler, P.K., 1997, Comparison of clastic wedge provenance in the Appalachian foreland using U/Pb ages of detrital zircons: Tectonics, v. 16, p. 151–160, doi:10.1029/96TC02911.

Green, P.F., Duddy, I.R., Gleadow, A.J.W., Tingate, P.R., and Laslett, G.M., 1986, Thermal annealing of fission tracks in apatite, 1. A qualitative description: Chemical Geology: Isotope Geoscience Section, v. 59, p. 237–253, doi:10.1016/0168-9622(88)90019-X.

Greenough, J.D., Kamo, S.L., and Krogh, T.E., 1993, A Silurian U-Pb age for the Cape St. Mary's sills, Avalon Peninsula, Newfoundland, Canada: implications for Silurian orogenesis in the Avalon Zone: Canadian Journal of Earth Sciences, v. 30, p. 1607–1612, doi:10.1139/e93-138.

Grist, A.M., Reynolds, P.H., Zentilli, M., and Beaumont, C., 1992, The Scotian Basin offshore Nova Scotia: thermal history and provenance of sandstones from apatite fission track and 40Ar/39Ar data: Canadian Journal of Earth Sciences, v. 29, p. 909–924, doi:10.1139/e92-077.

Grist, A.M., and Zentilli, M., 2003, Post-Paleocene cooling in the southern Canadian Atlantic region: Evidence from apatite fission track models: Canadian Journal of Earth Sciences, v. 40, p. 1279–1297, doi:10.1139/e03-045.

Hames, W.E., and Bowring, S.A., 1994, An empirical evaluation of the argon diffusion geometry in muscovite: Earth and Planetary Science Letters, v. 124, p. 161–169, doi:10.1016/0012-821X(94)00079-4.

Hasebe, N., Tagami, T., and Nishimura, S., 1994, Towards zircon fission-track thermochronology: Reference framework for confined track length measurements: Chemical Geology, v. 112, p. 169–178, doi:10.1016/0009-2541(94)90112-0.

Haupert, I., Manatschal, G., Decarlis, A., and Unternehr, P., 2016, Upper-plate magma-poor rifted margins: Stratigraphic architecture and structural evolution: Marine and Petroleum Geology, v. 69, p. 241–261, doi:10.1016/j.marpetgeo.2015.10.020.

Heaman, L.M., Erdmer, P., and Owen, J. V., 2002, U-Pb geochronologic constraints on the crustal evolution of the Long Range Inlier, Newfoundland: Canadian Journal of Earth Sciences, v. 39, p. 845–865, doi:10.1139/e02-015.

Helwig, J., Aronson, J., and Day, D.S., 1974, A Late Jurassic Mafic Pluton in Newfoundland: Canadian Journal of Earth Sciences, v. 11, p. 1314–1319, doi:10.1139/e74-123.

Hendriks, M., Jamieson, R.A., Willett, S.D., and Zentilli, M., 1993, Burial and exhumation of the Long Range Inlier and its surroundings, western Newfoundland: results of an apatite fission-track study: Canadian Journal of Earth Sciences, v. 30, p. 1594–1606, doi:10.1139/e93-137.

Henriques, S.B.A., Neiva, A.M.R., Ribeiro, M.L., Dunning, G.R., and Tajčmanová, L., 2016, Corrigendum to "Evolution of a Neoproterozoic suture in the Iberian Massif, Central Portugal: New U-Pb ages of igneous and metamorphic events at the contact between the Ossa Morena Zone and Central Iberian Zone" (Lithos 220–223 (2015) 43–59]: Lithos, v.

264, p. 595, doi:10.1016/j.lithos.2016.08.032.

Henriques, S.B.A., Neiva, A.M.R., Ribeiro, M.L., Dunning, G.R., and Tajčmanová, L., 2015, Evolution of a Neoproterozoic suture in the Iberian Massif, Central Portugal: New U-Pb ages of igneous and metamorphic events at the contact between the Ossa Morena Zone and Central Iberian Zone: Lithos, v. 220–223, p. 43–59, doi:10.1016/j.lithos.2015.02.001.

Herriott, T.M., Crowley, J.L., Schmitz, M.D., Wartes, M.A., and Gillis, R.J., 2019, Exploring the law of detrital zircon: LA-ICP-MS and CA-TIMS geochronology of Jurassic forearc strata, Cook Inlet, Alaska, USA: Geology, v. 47, p. 1044–1048, doi:10.1130/G46312.1.

Hicks, R.J., Jamieson, R.A., and Reynolds, P.H., 1999, Detrital and metamorphic 40Ar/39Ar ages from muscovite and whole-rock samples, Meguma Supergroup, southern Nova Scotia: Canadian Journal of Earth Sciences, v. 36, p. 23–32, doi:10.1139/e98-081.

Hiscott, R.N., Marsaglia, K.M., Wilson, R.C.L., Robertson, A.H.F., Karner, G.D., Tucholke, B.E., Pletsch, T., and Petschick, R., 2008, Detrital sources and sediment delivery to the early post-rift (Albian-Cenomanian) Newfoundland Basin east of the Grand Banks: Results from ODP Leg 210: Bulletin of Canadian Petroleum Geology, v. 56, p. 69–92, doi:10.2113/gscpgbull.56.2.69.

Hiscott, R.N., Wilson, R.C.L., Gradstein, F.M., Pujalte, V., Garcia-Mondejar, J., Boudreau, R.R., and Wishart, H.A., 1990a, Comparative stratigraphy and subsidence history of Mesozoic rift basins of North Atlantic: AAPG Bulletin, v. 74, p. 60–76.

Hiscott, R.N., Wilson, R.C.L., Harding, S.C., Pujalte, V., and Kitson, D., 1990b, Contrasts in early Cretaceous depositional environments of marine sandbodies, Grand Banks-Iberian corridor: Bulletin of Canadian Petroleum Geology, v. 38, p. 203–214.

Hodych, J.P., and Buchan, K.L., 1998, Palaeomagnetism of the ca. 440 Ma Cape St Mary's sills of the Avalon Peninsula of Newfoundland: implications for Iapetus Ocean closure: Geophysical Journal International, v. 135, p. 155–164, doi:10.1046/j.1365-246X.1998.00263.x.

Hodych, J.P., and Hayatsu, A., 1988, Paleomagnetism and K-Ar isochron dates of Early Jurassic basaltic flows and dikes of Atlantic Canada: Canadian Journal of Earth Sciences, v. 25, p. 1972–1989, doi:10.1139/e88-185.

Hoffman, P.F., 1988, United States of America, The Birth of a Craton : Early Proterozoic Assembly and Growth of Laurentia: Annual Review of Earth and Planetary Sciences, v. 16, p. 543–603.

Huismans, R.S., and Beaumont, C., 2014, Rifted continental margins: The case for depth-dependent extension: Earth and Planetary Science Letters, v. 407, p. 148–162, doi:10.1016/j.epsl.2014.09.032.

Hutter, A., and Beranek, L., 2020, Provenance of Upper Jurassic to Lower Cretaceous synrift strata in the Terra Nova oil field, Jeanne d'Arc basin, offshore Newfoundland: A new detrital zircon U-Pb-Hf reference frame for the Atlantic Canadian margin: AAPG Bulletin, v. 104, p. 2325–2349, doi:10.1306/02232018241.

Hyde, R.S., 1995, Upper Paleozoic rocks, Newfoundland, *in* Williams, H. ed., Geology of the

Appalachian-Caledonian Orogen in Canada and Greenland, Canada, Geological Survey of Canada, p. 523–552.

Jaffey, A.H., Flynn, K.F., Glendenin, L.E., Bentley, W.C., and Essling, A.M., 1971, Precision measurement of half-lives and specific activities of 235U and 238U: Physical Review C, v. 4, p. 1889–1906, doi:10.1103/PhysRevC.4.1889.

Jagoutz, O., Müntener, O., Manatschal, G., Rubatto, D., Péron-Pinvidic, G., Turrin, B.D., and Villa, I.M., 2007, The rift-to-drift transition in the North Altantic: A stuttering start of the MORB machine? Geology, v. 35, p. 1087–1090, doi:10.1130/G23613A.1.

Jansa, L.F., and Pe-Piper, G., 1988, Middle Jurassic to Early Cretaceous igneous rocks along eastern North American Continental Margin.: AAPG Bulletin, v. 72, p. 347–366, doi:10.1306/703c8c27-1707-11d7-8645000102c1865d.

Keen, C.E., Boutilier, R., Voogd, B.D.E., Mudford, B., and Enachescu, M.E., 1987, Crustal Geometry and Extensional Models for the Grand Banks, Eastern Canada: Constraints from Deep Seismic Reflection Data, *in* Beaumont, C. and Tankard, A.J. eds., Sedimentary Basins and Basin-Forming Mechanisms, Canadian Society of Petroleum Geologists, Memoir 12, p. 101–115.

Kellett, D.A., Piette-Lauzière, N., Mohammadi, N., Bickerton, L., Kontak, D., Rogers, N., and Larson, K., 2021. Spatio-temporal distribution of Devonian post-accretionary granitoids in the Canadian Appalachians: implications for tectonic controls on intrusion-related mineralization; *in* Plouffe, A. and Schetselaar, E. eds., Targeted Geoscience Initiative 5: Contributions to the understanding and exploration of porphyry deposits, Geological Survey of Canada, Bulletin 616, p. 7-23, https://doi.org/10.4095/327955.

Kellett, D.A., Rogers, N., McNicoll, V., Kerr, A., and van Staal, C., 2014, New age data refine extent and duration of Paleozoic and Neoproterozoic plutonism at Ganderia–Avalonia boundary, Newfoundland: Canadian Journal of Earth Sciences, v. 51, p. 943–972, doi:10.1139/cjes-2014-0090.

Keppie, J.D., Davis, D.W., and Krogh, T.E., 1998, U-Pb geochronological constraints on Precambrian stratified units in the Avalon Composite Terrane of Nova Scotia, Canada: tectonic implications: Canadian Journal of Earth Sciences, v. 35, p. 222–236, doi:10.1139/cjes-35-3-222.

Keppie, J.D., and Krogh, T.E., 2000, 440 Ma igneous activity in the Meguma terrane, Nova Scotia, Canada: Part of the Appalachian overstep sequence? American Journal of Science, v. 300, p. 528–538, doi:10.2475/ajs.300.6.528.

Keppie, J.D., and Krogh, T.E., 1999, U-Pb Geochronology of Devonian Granites in the Meguma Terrane of Nova Scotia, Canada: Evidence for Hotspot Melting of a Neoproterozoic Source: Journal of Geology, v. 107, p. 555–568, doi:10.1086/314369.

Ketcham, R.A., Donelick, R.A., and Carlson, W.D., 1999, Variability of apatite fission-track annealing kinetics: II. Crystallographic orientation effects: American Mineralogist, v. 84, p. 1224–1234, doi:10.2138/am-1999-0902.

King, L.H., Fader, G.B.J., Jenkins, W.A.M., and King, E.L., 1986, Occurrence and regional

geological setting of Paleozoic rocks on the Grand Banks of Newfoundland: Canadian Journal of Earth Sciences, v. 23, p. 504–526, doi:10.1139/e86-052.

Kohn, B., Chung, L., and Gleadow, A., 2019, Fission-Track Analysis: Field Collection, Sample Preparation and Data Acquisition, *in* Malusà, M.G. and Fitzgerald, P.G. eds., Fission-Track Thermochronology and its Application to Geology, Cham, Switzerland, Springer International Publishing AG, p. 25–48, doi:https://doi.org/10.1007/978-3-319-89421-8_2.

Kontak, D.J., Ham, L.J., and Dunning, G., 2004, U-Pb dating of the Musquodoboit Batholith, southern Nova Scotia: Evidence for a protracted magmatic-hydrothermal event in a Devonian intrusion: Atlantic Geology, v. 40, p. 207–216, doi:10.4138/1040.

Krogh, T.E., Strong, D.F., O'Brien, S.J., and Papezik, V.S., 1988, Precise U-Pb zircon dates from the Avalon Terrane in Newfoundland: Canadian Journal of Earth Sciences, v. 25, p. 442–453, http://www.nrcresearchpress.com/doi/abs/10.1139/e88-045.

Krogh, T.E., and Keppie, J.D., 1990, Age of detrital zircon and titanite in the Meguma Group, southern Nova Scotia, Canada: Clues to the origin of the Meguma Terrane: Tectonophysics, v. 177, p. 307–323, doi:10.1016/0040-1951(90)90287-I.

Kroner, U., and Romer, R.L., 2013, Two plates - Many subduction zones: The Variscan orogeny reconsidered: Gondwana Research, v. 24, p. 298–329, doi:10.1016/j.gr.2013.03.001.

Kuiper, Y.D., Thompson, M.D., Barr, S.M., White, C.E., Hepburn, J.C., and Crowley, J.L., 2017, Detrital zircon evidence for Paleoproterozoic West African crust along the eastern North American continental margin, Georges Bank, offshore Massachusetts, USA: Geology, v. 45, p. 811–814, doi:10.1130/G39203.1.

Lavier, L.L., and Manatschal, G., 2006, A mechanism to thin the continental lithosphere at magma-poor margins: Nature, v. 440, p. 324–328, doi:10.1038/nature04608.

Lefort, J.P., Miller, H.G., and Wiseman, R., 1993, Reconstitution of east-facing Variscan nappes between the Grand Banks of Newfoundland and Spain - Reply: Tectonophysics, v. 217, p. 331–341, doi:10.1016/0040-1951(94)90216-X.

Linnemann, U., Ouzegane, K., Drareni, A., Hofmann, M., Becker, S., Gärtner, A., and Sagawe, A., 2011, Sands of West Gondwana: An archive of secular magmatism and plate interactions - A case study from the Cambro-Ordovician section of the Tassili Ouan Ahaggar (Algerian Sahara) using U-Pb-LA-ICP-MS detrital zircon ages: Lithos, v. 123, p. 188–203, doi:10.1016/j.lithos.2011.01.010.

Lister, G.S., Etheridge, M.A., and Symonds, P.A., 1986, Detachment faulting and the evolution of passive continental margins: Geology, v. 14, p. 246–250, doi:10.1130/0091-7613(1986)14<890:CARODF>2.0.CO;2.

Lowe, D.G., Sylvester, P.J., and Enachescu, M.E., 2011, Provenance and paleodrainage patterns of Upper Jurassic and Lower Cretaceous synrift sandstones in the Flemish Pass Basin, offshore Newfoundland, east coast of Canada: AAPG Bulletin, v. 95, p. 1295–1320, doi:10.1306/12081010005.

MacDonald, L.A., Barr, S.M., White, C.E., and Ketchum, J.W.F., 2002, Petrology, age, and tectonic setting of the White Rock Formation, Meguma terrane, Nova Scotia: Evidence for

Silurian continental rifting: Canadian Journal of Earth Sciences, v. 39, p. 259–277, doi:10.1139/e01-074.

Maclean, N.J., Barr, S.M., White, C.E., and Ketchum, J.W.F., 2003, New U-Pb (zircon) age and geochemistry of the Wedgeport pluton, Meguma terrane, Nova Scotia: Atlantic Geology, v. 39, p. 239–253.

Malusà, M.G., and Fitzgerald, P.G., 2019, From Cooling to Exhumation: Setting the Reference Frame for the Interpretation of Thermochronologic Data, *in* Malusà, M.G. and Fitzgerald, P.G. eds., Fission-Track Thermochronology and its Application to Geology, Cham, Switzerland, Springer International Publishing AG, p. 147–164.

Manatschal, G., Lavier, L., and Chenin, P., 2015, The role of inheritance in structuring hyperextended rift systems: Some considerations based on observations and numerical modeling: Gondwana Research, v. 27, p. 140–164, doi:10.1016/j.gr.2014.08.006.

Marzoli, A. et al., 2017, Proterozoic to Mesozoic evolution of North-West Africa and Peri-Gondwana microplates: Detrital zircon ages from Morocco and Canada: Lithos, v. 278–281, p. 229–239, doi:10.1016/j.lithos.2017.01.016.

Matthews, W.A., and Guest, B., 2016, A Practical Approach for Collecting Large-n Detrital Zircon U-Pb Data sets by Quadrupole LA-ICP-MS: Geostandards and Geoanalytical Research, v. 41, p. 161–180, doi:10.1111/ggr.12146.

Mattinson, J.M., 1987, U-Pb ages of zircons: A basic examination of error propagation: Chemical Geology: Isotope Geoscience Section, v. 66, p. 151–162, doi:10.1016/0168-9622(87)90037-6.

McDonough, M., Sylvester, P., Bruder, N., Lo, J., and O'Sullivan, P., 2010, Provenance of reservoir sandstones in the Flemish Pass and Orphan Basins (Canada): U-Pb dating of detrital zircons using the laser ablation method: Central & North Atlantic Conjugate Margins Conference, v. 5, p. 181–184, http://metododirecto.pt/CM2010.

McKenzie, D., 1978, Some remarks on the development of sedimentary basins: Earth and Planetary Science Letters, v. 40, p. 25–32, doi:10.1016/0012-821X(78)90071-7.

Montario, M.J., and Garver, J.I., 2009, The thermal evolution of the grenville terrane revealed through U-Pb and fission-track analysis of detrital zircon from cambro-ordovician quartz arenites of the potsdam and galway formations: Journal of Geology, v. 117, p. 595–614, doi:10.1086/605778.

Müntener, O., and Manatschal, G., 2006, High degrees of melt extraction recorded by spinel harzburgite of the Newfoundland margin: The role of inheritance and consequences for the evolution of the southern North Atlantic: Earth and Planetary Science Letters, v. 252, p. 437–452, doi:10.1016/j.epsl.2006.10.009.

Murphy, J.B., Waldron, J.W.F., Kontak, D.J., Pe-Piper, G., and Piper, D.J.W., 2011, Minas Fault Zone: Late Paleozoic history of an intra-continental orogenic transform fault in the Canadian Appalachians: Journal of Structural Geology, v. 33, p. 312–328, doi:10.1016/j.jsg.2010.11.012.

Murphy, J.B., Fernández-Suárez, J., Jeffries, T.E., and Strachan, R.A., 2004, U-Pb (LA-ICP-MS) dating of detrital zircons from Cambrian clastic rocks in Avalonia: Erosion of a Neoproterozoic arc along the northern Gondwanan margin: Journal of the Geological Society, London, v. 161, p. 243–254, doi:10.1144/0016-764903-064.

Murphy, J.B., and Hamilton, M.A., 2000, Orogenesis and Basin development: U-Pb detrital zircon age constraints on evolution of the Late Paleozoic St. Marys Basin, Central Mainland Nova Scotia: Journal of Geology, v. 108, p. 53–71, doi:10.1086/314384.

Murphy, J.B., McCausland, P.J.A., O'Brien, S.J., Pisarevsky, S., and Hamilton, M.A., 2008, Age, geochemistry and Sm-Nd isotopic signature of the 0.76 Ga Burin Group: Compositional equivalent of Avalonian basement? Precambrian Research, v. 165, p. 37–48, doi:10.1016/j.precamres.2008.05.006.

Naeser, C.W., Naeser, N.D., Newell, W.L., Southworth, S., Edwards, L.E., and Weems, R.E., 2016, Erosional and depositional history of the Atlantic passive margin as recorded in detrital zircon fission-track ages and lithic detritus in Atlantic Coastal Plain sediments: American Journal of Science, v. 316, p. 110–168, doi:10.2475/02.2016.02.

Nirrengarten, M., Manatschal, G., Tugend, J., Kusznir, N., and Sauter, D., 2018, Kinematic Evolution of the Southern North Atlantic: Implications for the Formation of Hyperextended Rift Systems: Tectonics, v. 37, p. 89–118, doi:10.1002/2017TC004495.

O'Brien, B.H., O'Brien, S.J., and Dunning, G.R., 1991, Silurian cover, late Precambrian-early Ordovician basement, and the chronology of Silurian orogenesis in the Hermitage Flexure (Newfoundland Appalachians): American Journal of Science, v. 291, p. 760–799, doi:10.2475/ajs.291.8.760.

O'Brien, S.J., O'Brien, B.H., Dunning, G.R., and Tucker, R.D., 1996, Late Neoproterozoic Avalonian and related peri-Gondwanan rocks of the Newfoundland Appalachians, *in* Nance, R.D. and Thompson, M.D. eds., Boulder, Colorado, Geological Society of America Special Paper 304, v. 304, p. 9–28, doi:10.1130/0-8137-2304-3.9.

Pe-Piper, G., and Jansa, L.F., 1987, Geochemistry of late Middle Jurassic-Early Cretaceous igneous rocks on the eastern North American margin.: Geological Society of America Bulletin, v. 99, p. 803–813, doi:10.1130/0016-7606(1987)99<803:GOLMJC>2.0.CO;2.

Pe-Piper, G., Jansa, L.F., and Palacz, Z., 1994, Geochemistry and regional significance of the early Cretaceous bimodal basalt-felsic associations on Grand Banks, eastern Canada: Geological Society of America Bulletin, v. 106, p. 1319–1331, doi:10.1130/0016-7606(1994)106<1319:GARSOT>2.3.CO;2.

Pe-Piper, G., Kamo, S.L., and McCall, C., 2010, The German bank pluton, offshore SW Nova Scotia: Age, petrology, and regional signifi cance for Alleghanian plutonism: Geological Society of America Bulletin, v. 122, p. 690–700, doi:10.1130/B30031.1.

Pe-Piper, G., and Piper, D.J.W., 2004, The effects of strike-slip motion along the Cobequid - Chedabucto - Southwest Grand Banks fault system on the Cretaceous-Tertiary evolution of Atlantic Canada: Canadian Journal of Earth Sciences, v. 41, p. 799–808, doi:10.1139/E04-022.

Peace, A.L., Welford, J.K., Geng, M., Sandeman, H., Gaetz, B.D., and Ryan, S.S., 2018, Rift-related magmatism on magma-poor margins: Structural and potential-field analyses of the Mesozoic Notre Dame Bay intrusions, Newfoundland, Canada and their link to North Atlantic Opening: Tectonophysics, v. 745, p. 24–45, doi:10.1016/j.tecto.2018.07.025.

Pereira, R., and Alves, T.M., 2011, Margin segmentation prior to continental break-up: A seismic-stratigraphic record of multiphased rifting in the North Atlantic (Southwest Iberia): Tectonophysics, v. 505, p. 17–34, doi:10.1016/j.tecto.2011.03.011.

Pereira, A.J.S.C., Carter, A., Hurford, A.J., Neves, L.J.P.F., and Godinho, M.M., 1998, Evidence for the Unroofing History of Hercynian Granitoids in Central Portugal Derived from Late Palaeozoic and Mesozoic Sedimentary Zircons, *in* Van den haute, P. and De Corte, F. eds., Advances in Fission-Track Geochronology, Kluwer Academic Publishers, p. 173–186, doi:10.1007/978-94-015-9133-1_11.

Pereira, M.F., Gama, C., Chichorro, M., Silva, J.B., Gutiérrez-Alonso, G., Hofmann, M., Linnemann, U., and Gärtner, A., 2016, Evidence for multi-cycle sedimentation and provenance constraints from detrital zircon U–Pb ages: Triassic strata of the Lusitanian basin (western Iberia): Tectonophysics, v. 681, p. 318–331, doi:10.1016/j.tecto.2015.10.011.

Pérez-Gussinyé, M., and Reston, T.J., 2001, Rheological evolution during extension at nonvolcanic rifted margins: Onset of serpentinization and development of detachments leading to continental breakup: Journal of Geophysical Research: Solid Earth, v. 106, p. 3961–3975, doi:10.1029/2000JB900325.

Péron-Pinvidic, G., and Manatschal, G., 2009, The final rifting evolution at deep magma-poor passive margins from Iberia-Newfoundland: A new point of view: International Journal of Earth Sciences, v. 98, p. 1581–1597, doi:10.1007/s00531-008-0337-9.

Péron-Pinvidic, G., Manatschal, G., and Osmundsen, P.T., 2013, Structural comparison of archetypal Atlantic rifted margins: A review of observations and concepts: Marine and Petroleum Geology, v. 43, p. 21–47, doi:10.1016/j.marpetgeo.2013.02.002.

Piper, D.J.W., Pe-Piper, G., Tubrett, M., Triantafyllidis, S., and Strathdee, G., 2012, Detrital zircon geochronology and polycyclic sediment sources, upper Jurassic - lower Cretaceous of the scotian basin, Southeastern Canada: Canadian Journal of Earth Sciences, v. 49, p. 1540–1557, doi:10.1139/e2012-072.

Pollock, J.C., Hibbard, J.P., and Sylvester, P.J., 2009, Early Ordovician rifting of Avalonia and birth of the Rheic Ocean: U-Pb detrital zircon constraints from Newfoundland: Journal of the Geological Society, v. 166, p. 501–515, doi:10.1144/0016-76492008-088.

Pothier, H.D., Waldron, J.W.F., White, C.E., Dufrane, S.A., and Jamieson, R.A., 2015, Stratigraphy, provenance, and tectonic setting of the Lumsden dam and Bluestone Quarry formations (Lower Ordovician), Halifax Group, Nova Scotia, Canada: Atlantic Geology, v. 51, p. 51–83, doi:10.4138/atlgeol.2015.003.

Powell, J.W., Schneider, D.A., Desrochers, A., Flowers, R.M., Metcalf, J.R., Gaidies, F., and Stockli, D.F., 2018, Low-temperature thermochronology of Anticosti Island: A case study

on the application of conodont (U-Th)/He thermochronology to carbonate basin analysis: Marine and Petroleum Geology, v. 96, p. 441–456, doi:10.1016/j.marpetgeo.2018.05.018.

Pratt, J.R., Barbeau, D.L., Garver, J.I., Emran, A., and Izykowski, T.M., 2015, Detrital zircon geochronology of Mesozoic sediments in the Rif and Middle Atlas Belts of Morocco: Provenance constraints and refinement of the West African signature: Journal of Geology, v. 123, p. 177–200, doi:10.1086/681218.

Rainbird, R.H., Rayner, N.M., Hadlari, T., Heaman, L.M., Ielpi, A., Turner, E.C., and MacNaughton, R.B., 2017, Zircon provenance data record the lateral extent of pancontinental, early Neoproterozoic rivers and erosional unroofing history of the Grenville orogen: Geological Society of America Bulletin, v. 129, p. 1408–1423, doi:10.1130/B31695.1.

Ravenhurst, C.E., Donelick, R., Zentilli, M., Reynolds, P.H., and Beaumont, C., 1990, A fission track pilot study of thermal effects of rifting on the onshore Nova Scotian margin, Canada.: Nuclear Tracks Radiation Measurements, v. 17, p. 373–378, https://doi.org/10.1016/1359-0189(90)90060-B.

Ravenhurst, C.E., Reynolds, P.H., Zentilli, M., Krueger, H.W., and Blenkinsop, J., 1989, Formation of Carboniferous Pb-Zn and Barite Mineralization from Basin-Derived Fluids, Nova Scotia, Canada: Economic Geology, v. 84, p. 1471–1488.

Reiners, P.W., and Brandon, M.T., 2006, Using Thermochronology To Understand Orogenic Erosion: Annual Review of Earth and Planetary Sciences, v. 34, p. 419–466, doi:10.1146/annurev.earth.34.031405.125202.

Reiners, P.W., Spell, T.L., Nicolescu, S., and Zanetti, K.A., 2004, Zircon (U-Th)/He thermochronometry: He diffusion and comparisons with 40Ar/39Ar dating: Geochimica et Cosmochimica Acta, v. 68, p. 1857–1887, doi:10.1016/j.gca.2003.10.021.

Rivers, T., 1997, Lithotectonic elements of the Grenville Province: Review and tectonic implications: Precambrian Research, v. 86, p. 117–154, doi:10.1016/s0301-9268(97)00038-7.

Rodrigues, B., Chew, D.M., Jorge, R.C.G.S., Fernandes, P., Veiga-Pires, C., and Oliveira, J.T., 2015, Detrital zircon geochronology of the Carboniferous Baixo Alentejo Flysch Group (South Portugal); Constraints on the provenance and geodynamic evolution of the South Portuguese Zone: Journal of the Geological Society, v. 172, p. 294–308, doi:10.1144/jgs2013-084.

Ryan, R.J., 1993, Metallogenetic And Thermal Evolution Of The Upper Paleozoic Maritimes Basin: Evidence From The Cumberland Basin Of Nova Scotia: Dalhousie University.

Ryan, R.J., and Zentili, M., 1993, Allocyclic and thermochronological constraints on the evolution of the Maritimes Basin of eastern Canada: Atlantic Geology, v. 29, p. 187–197, doi:10.4138/2007.

Ryan, W.B.F. et al., 2009, Global multi-resolution topography synthesis: Geochemistry, Geophysics, Geosystems, v. 10, p. 1–9, doi:10.1029/2008GC002332.

Sandeman, H.A.I., and Dunning, G.R., 2016, Preliminary U-Pb Geochronology and Petrochemistry of Volcanic Rocks and Felsic Dykes of the Silurian Sops Arm Group, White Bay, Western Newfoundland (NTS 12H/10 and 15): Newfoundland and Labrador Department of Natural Resources Geological Survey, Report 16-1, p. 39–69, https://www.gov.nl.ca/iet/files/mines-geoscience-publications-currentresearch-2016-sandeman-2016.pdf.

Saylor, J.E., Stockli, D.F., Horton, B.K., Nie, J., and Mora, A., 2012, Discriminating rapid exhumation from syndepositional volcanism using detrital zircon double dating: Implications for the tectonic history of the Eastern Cordillera, Colombia: GSA Bulletin, v. 124, p. 762–779, doi:10.1130/B30534.1.Scott, D.J., 1995, U-Pb geochronology of a Paleoproterozoic continental magmatic arc on the western margin of the Archean Nain craton, northern Labrador, Canada: Canadian Journal of Earth Sciences, v. 32, p. 1870–1882, doi:10.1139/e95-144.

Shannon, P.M., Williams, B.P.J., and Sinclair, I.K., 1995, Tectonic controls on Upper Jurassic to Lower Cretaceous reservoir architecture in the Jeanne d'Arc Basin, with some comparisons from the Porcupine and Moray Firth Basins, *in* Croker, P.F. and Shannon, P.M. eds., The Petroleum Geology of Ireland's Offshore Basins, Geological Society of London Special Publication, p. 467–490, doi:10.1144/GSL.SP.1995.093.01.37.

Sinclair, I.K., 1988, Evolution of Mesozoic-Cenozoic sedimentary basins in the Grand Banks area of Newfoundland and comparison with Falvey's (1974) rift model: Bulletin of Canadian Petroleum Geology, v. 36, p. 255–273.

Sinclair, I.K., 2010, Reconcilation? Oil industry data in light of revised Iberia-Newfoundland rift models: Geological Association of Canada, Newfoundland Section 2010 spring technical meeting, Abstracts, v. 46, p. 84.

Sinclair, I.K., Shannon, P.M., Williams, B.P.J., Harker, S.D., and Moore, J.G., 1994, Tectonic control on sedimentary evolution of three North Atlantic borderland Mesozoic basins: Basin Research, v. 6, p. 193–217, doi:10.1111/j.1365-2117.1994.tb00085.x.

Soares, D.M., Alves, T.M., and Terrinha, P., 2012, The breakup sequence and associated lithospheric breakup surface: Their significance in the context of rifted continental margins (West Iberia and Newfoundland margins, North Atlantic): Earth and Planetary Science Letters, v. 355–356, p. 311–326, doi:10.1016/j.epsl.2012.08.036.

Solá, A.R., Pereira, M.F., Williams, I.S., Ribeiro, M.L., Neiva, A.M.R., Montero, P., Bea, F., and Zinger, T., 2008, New insights from U-Pb zircon dating of Early Ordovician magmatism on the northern Gondwana margin: The Urra Formation (SW Iberian Massif, Portugal): Tectonophysics, v. 461, p. 114–129, doi:10.1016/j.tecto.2008.01.011.

Stephan, T., Kroner, U., and Romer, R.L., 2019, The pre-orogenic detrital zircon record of the Peri-Gondwanan crust: Geological Magazine, v. 156, p. 281–307, doi:10.1017/S0016756818000031.

Sutra, E., Manatschal, G., Mohn, G., and Unternehr, P., 2013, Quantification and restoration of extensional deformation along the Western Iberia and Newfoundland rifted margins: Geochemistry, Geophysics, Geosystems, v. 14, p. 2575–2597, doi:10.1002/ggge.20135.

Sylvester, P.J., and Attoh, K., 1992, Lithostratigraphy and composition of 2.1 Ga greenstone belts of the West African craton and their bearing on crustal evolution and the Archean-Proterozoic boundary: Journal of Geology, v. 100, p. 377–393, doi:10.1086/629593.

Tagami, T., 2005, Zircon fission-track thermochronology and applications to fault studies: Reviews in Mineralogy and Geochemistry, v. 58, p. 95–122, doi:10.2138/rmg.2005.58.4.

Tagami, T., Galbraith, R.F., Yamada, R., and Laslett, G.M., 1998, Revised annealing kinetics of fission tracks in zircon and geological implications, *in* Van den haute, P. and De Corte, F. eds., Advances in Fission - Track Geochronology, p. 99–112, doi:http://dx.doi.org/10.1007/978-94-015-9133-1 8.

Tankard, A.J., Welsink, H.J., and Jenkins, W.A.., 1989, Structural styles and stratigaphy of Jeanne d'Arc Basin, Grand Banks of Newfoundland, *in* Tankard, A.J. and Balkwill, H.R. eds., Extensional Tectonics and Stratigraphy of the North Atlantic Margins, AAPG, p. 265–282, doi:https://doi.org/10.1306/M46497.

Thomas, W.A., Becker, T.P., Samson, S.D., and Hamilton, M.A., 2004, Detrital zircon evidence of a recycled orogenic foreland provenance for Alleghanian clastic-wedge sandstones: Journal of Geology, v. 112, p. 23–37, doi:10.1086/379690.

Tomascak, P.B., Krogstad, E.J., and Walker, R.J., 1996, U-Pb monazite geochronology of granitic rocks from Maine: Implications for Late Paleozoic tectonics in the northern Appalachians: Journal of Geology, v. 104, p. 185–195, doi:10.1086/629813.

Tucholke, B.E., Sawyer, D.S., and Sibuet, J.-C., 2007, Breakup of the Newfoundland – Iberia rift, *in* Karner, G.D., Manatschal, G., and Pinheiro, L.M. eds., Imaging, Mapping and Modelling Continental Lithosphere Extension and Breakup, Geological Society of London Special Publication 282, p. 9–46, doi:https://doi.org/10.1144/SP282.2.

Tucker, R.D., and Mckerrow, W.S., 1995, Early Paleozoic chronology: a review in light of new U - Pb zircon ages from Newfoundland and Britain: Canadian Journal of Earth Sciences, v. 32, p. 368–379.

Valverde-Vaquero, P., van Staal, C.R., McNicoll, V., and Dunning, G., 2006, Mid – Late Ordovician magmatism and metamorphism along the Gander margin in central Newfoundland: Journal of the Geological Society, London, v. 163, p. 347–362.

Van Avendonk, H.J.A., Holbrook, W.S., Nunes, G.T., Shillington, D.J., Tucholke, B.E., Louden, K.E., Larsen, H.C., and Hopper, J.R., 2006, Seismic velocity structure of the rifted margin of the eastern Grand Banks of Newfoundland, Canada: Journal of Geophysical Research, v. 111, p. 1–26, doi:10.1029/2005JB004156.

van de Poll, H., Yamada, R., and Laslett, G.M., 1995, Introduction: Upper Paleozoic rocks, *in* Williams, H. ed., Geology of the Appalachian-Caledonian Orogen in Canada and Greenland, Canada, Geological Survey of Canada, p. 449–455.

van Staal, C.R., and Barr, S.M., 2012, Lithospheric architecture and tectonic evolution of the Canadian Appalachians and associated Atlantic margin, *in* Percival, J.A., Cook, F.A., and Clowes, R.M. eds., Tectonic Styles in Canada: the LITHOPROBE Perspective, Geological Association of Canada, Special Paper 49, p. 41–95.

van Staal, C.R., Whalen, J.B., McNicoll, V.J., Pehrsson, S., Lissenberg, C.J., Zagorevski, A., Van Breemen, O., and Jenner, G.A., 2007, The Notre Dame arc and the Taconic orogeny in Newfoundland, *in* Hatcher, R.D.J., Carlson, M.P., McBride, J.H., and Martínez Catalán, J.R. eds., 4-D Framework of Continental Crust, Geological Society of America, p. 511–552, doi:10.1130/2007.1200(26).

van Staal, C.R., Whalen, J.B., Valverde-Vaquero, P., Zagorevski, A., and Rogers, N., 2009, Pre-Carboniferous, episodic accretion-related, orogenesis along the Laurentian margin of the northern Appalachians, *in* Murphy, J.B., Keppie, J.D., and Hynes, A.J. eds., Ancient Orogens and Modern Analogues, Geological Society of London, Special Publication, v. 327, p. 271–316, doi:10.1144/SP327.13.

Vermeesch, P., 2021, Maximum depositional age estimation revisited: Geoscience Frontiers, v. 12, p. 843–850, doi:10.1016/j.gsf.2020.08.008.

Vermeesch, P., 2009, RadialPlotter: A Java application for fission track, luminescence and other radial plots: Radiation Measurements, v. 44, p. 409–410, doi:10.1016/j.radmeas.2009.05.003.

Vermeesch, P., 2019, Statistics for Fission-Track Thermochronology, *in* Malusà, M.G. and Fitzgerald, P.G. eds., Fission-Track Thermochronology and its Application to Geology, Cham, Switzerland, Springer International Publishing AG, p. 109–122.

Waldron, J.W.F., Barr, S.M., Park, A.F., White, C.E., and Hibbard, J., 2015, Late Paleozoic strike-slip faults in Maritime Canada and their role in the reconfiguration of the northern Appalachian orogen: Tectonics, v. 34, p. 1661–1684, doi:10.1002/2015TC003882.

Waldron, J.W.F., and van Staal, C.R., 2001, Taconian orogeny and the accretion of the Dashwoods block: A peri-Laurentian microcontinent in the lapetus Ocean: Geology, v. 29, p. 811–814, doi:10.1130/0091-7613(2001)029<0811:TOATAO>2.0.CO;2.

Waldron, J.W.F., White, C.E., Barr, S.M., Simonetti, A., and Heaman, L.M., 2009, Provenance of the Meguma terrane, Nova Scotia: Rifted margin of early Paleozoic Gondwana: Canadian Journal of Earth Sciences, v. 46, p. 1–8, doi:10.1139/E09-004.

Whalen, J.B., 1989, The Topsails igneous suite, western Newfoundland: an Early Silurian subduction-related magmatic suite? Canadian Journal of Earth Sciences, v. 26, p. 2421–2434, doi:10.1139/e89-207.

Whitmeyer, S.J., and Karlstrom, K.E., 2007, Tectonic model for the Proterozoic growth of North America: Geosphere, v. 3, p. 220–259, doi:10.1130/GES00055.1.

Williams, B.P.J., Shannon, P.M., and Sinclair, I.K., 1999, Comparative Jurassic and Cretaceous tectono-stratigraphy and reservoir development in the Jeanne d'Arc and Porcupine basins: Petroleum Geology Conference Proceedings, v. 5, p. 487–499, doi:10.1144/0050487.

Williams, G.L., Ascoli, P., Barss, M.S., Bujak, J.P., Davies, E.H., Fensome, R.A., and Williamson, M.A., 1990, Biostratigraphy and related studies, in Keen, M. and Williams, G.L. eds., Geology of the Continental Margin of Eastern Canada, Geological Survey of Canada, p. 87–137.

Williams, H., 1979, Appalachian Orogen in Canada: Canadian Journal of Earth Sciences, v. 16,

p. 792–807, doi:10.1139/e79-070.

Willner, A.P., Bar, S.M., Gerdes, A., Massonne, H.J., and White, C.E., 2013, Origin and evolution of Avalonia: Evidence from U-Pb and Lu-Hf isotopes in zircon from the Mira terrane, Canada, and the Stavelot-Venn Massif, Belgium: Journal of the Geological Society of London, v. 170, p. 769–784, doi:10.1144/jgs2012-152.

Willner, A.P., Barr, S.M., Glodny, J., Massonne, H.-J., Sudo, M., Thomson, S.N., Van Staal, C.R., and White, C.E., 2015, Effects of fluid flow, cooling and deformation as recorded by 40 Ar/ 39 Ar, Rb–Sr and zircon fission track ages in very low- to low-grade metamorphic rocks in Avalonian SE Cape Breton Island (Nova Scotia, Canada): Geological Magazine, v. 152, p. 767–787, doi:10.1017/S0016756814000508.

Willner, A.P., Thomson, S.N., Glodny, J., Massonne, H.J., Romer, R.L., van Staal, C.R., and Zagorevski, A., 2019, Zircon fission-track ages from Newfoundland—A proxy for high geothermal gradients and exhumation before opening of the Central Atlantic Ocean: Terra Nova, v. 31, p. 1–10, doi:10.1111/ter.12361.

Wilson, R.C.L., and Hiscott, R.N., 2007, Ar/Ar dating of white mica clasts in early to late postrift sediments sampled during ODP Leg 210 off Newfoundland, *in* Tucholke, B.E., Sibuet, J.-C., and Klaus, A. eds., Proceedings of the Ocean Drilling Program: Scientific Results, College Station, TX (Ocean Drilling Program), v. 210, p. 1–13, doi:10.2973/odp.proc.sr.210.106.2007.

Whitmarsh, R.B., Manatschal, G., and Minshall, T.A., 2001, Evolution of magma-poor continental margins from rifting to seafloor spreading: Nature, v. 413, p. 150-154, doi: https://doi.org/10.1038/35093085.

CHAPTER 3: SUMMARY AND FUTURE RESEARCH

The Newfoundland-Iberia rift system developed during the protracted breakup of supercontinent Pangea and opening of the North Atlantic Ocean and evolved through Triassic to Jurassic stretching and thinning (proximal and necking), Early to mid-Cretaceous hyperextension and mantle exhumation (distal), and mid-Cretaceous breakup-related (outer) events (e.g., Davis and Kusznir et al., 2004, Lavier and Manatschal, 2006, Péron-Pinvidic and Manatschal, 2009; Péron-Pinvidic et al., 2013; Sutra et al., 2013; Huismans and Beaumont, 2014; Haupert et al., 2016). Syn-rift, Hibernia Formation strata were deposited in the Jeanne d'Arc basin on the SE Grand Banks (proximal domain) during Early Cretaceous distal domain development along the Newfoundland margin. Detrital zircon U-Pb and fission-track (FT) double-dating results from Hibernia Formation strata provide new insights into proximal domain evolution during outboard development of the distal domains and constrain the timing and significance of regional exhumation events, magmatic activity, and paleodrainage. Seven Hibernia Formation samples from the Hibernia B-16 55, Hibernia B-16 54W, Hebron M-04, and West Bonne Bay F-12 wells in the Jeanne d'Arc basin were analyzed and include two samples of the Lower Hibernia Formation from the Hibernia oil field and five samples of the Upper Hibernia Formation in the Hebron oil field and nearby areas. Pooled maximum depositional age (MDA) results for Lower and Upper Hibernia Formation samples yielded Berriasian to early Valanginian and late Valanginian to Barremian depositional ages, respectively, which are consistent with published biostratigraphic correlations (Williams et al., 1990) and early Berriasian and older depositional age estimates for the underlying Jeanne d'Arc Formation (Hutter and Beranek, 2020).

Hibernia Formation detrital zircon samples record exhumation-related cooling events that occurred in the Grand Banks during continued growth of the proximal domain and tectonic

development of the necking and distal domains. FT cooling populations align with the timing of Triassic to Jurassic stretching and thinning and Early Cretaceous hyperextension and/or mantle exhumation processes along the Newfoundland margin. The Late Triassic to Early Jurassic cooling population lacks magmatic-cooled zircon grains, which is consistent with proximal domain development characterized by wide corridors of upper crustal extension and mafic magmatism in Atlantic Canada (cf., Hodych and Hayatsu, 1988). Near syn-depositional, Early Cretaceous exhumation cooling signals indicate that rapid tectonic exhumation of rift flanks in the proximal domain occurred during distal domain development. Theoretical models for magma-poor rifting (e.g., Péron-Pinvidic et al., 2013; Sutra et al., 2013; Haupert et al., 2016) imply that extensional deformation migrated outboard and was localized in the distal domain; however, Hibernia Formation data suggest that extensional processes were similarly occurring in the proximal domain and included normal faulting that exhumed rocks from ~10-12 km depth followed by erosion and deposition over a 2-10 Myr interval. Results from the Hibernia Formation demonstrate that syn-rift strata in proximal domain basins can record evidence for rift-related regional exhumation events coincident with magma-poor rift system processes. Similar exhumation cooling signals may be recorded in analogous syn-rift strata of proximal domain basins around the world and may better constrain the timing of tectonic evolution of magma-poor rift systems globally.

Early Cretaceous magmatic-cooled zircon grains are likely first-cycle and point to a southern Grand Banks source where Berriasian and younger intrusive and extrusive igneous rocks are known or inferred (e.g., Pe-Piper et al., 1994, Bowman et al., 2012). North-flowing fluvial and deltaic systems drained exhumed upper Paleozoic cover assemblages and Appalachian basement within the Avalon Uplift and volcanic-plutonic assemblages along the SW Grand Banks transform fault and fed into the Jeanne d'Arc basin. Carboniferous to Permian (ca. 320-250 Ma) detrital

zircon grains that are unique to Upper Hibernia Formation strata may reflect a shift from a predominantly southern (Avalon Uplift) to southeastern (Morgiana Uplift) sediment sources between Berriasian to early Valanginian and late Valanginian to Barremian time, respectively (e.g., Sinclair, 1988), and hint at possible eastern sources from exhumed Alleghanian-Variscan foreland basin strata or late Paleozoic plutons to the east of the Jeanne d'Arc basin.

As of July 31, 2021, ~1 billion barrels of oil have been produced from the Hibernia Formation with ~220 million barrels of proven reserves remaining (Canada-Newfoundland and Labrador Offshore Petroleum Board, 2021). The mature quartz arenite units of the Hibernia Formation are in part the result of sourcing from predominantly mature sedimentary rock units. U-Pb and FT ages from the Hibernia Formation indicate the main sediment sources were pre-existing, upper Paleozoic strata that covered Avalonia and Meguma basement units in the Grand Banks and adjacent regions of Atlantic Canada (Hendriks et al., 1993; Gibling et al., 2008; Hiscott et al., 2008; Hutter and Beranek, 2020). Most double-dated Hibernia zircon grains (~70%) have pre-rift cooling signals and are characterized by Paleozoic to Archean U-Pb ages and Paleozoic to Cryogenian FT ages that reflect Appalachian tectono-thermal events. The remaining zircon grains (~30%) have syn-rift cooling signals characterized by Mesozoic to Archean U-Pb ages and Mesozoic FT ages that reflect rift-related exhumation of Appalachian basement or thermally-reset upper Paleozoic strata. Localized thermal resetting from Alleghanian-Variscan burial and deformation or Mesozoic deformation and magmatism along the SW Grand Banks transform fault could have affected a subset of Avalon Uplift source rocks. Subsequent Early Cretaceous tectonic exhumation and erosion that supplied Hibernia Formation sediment to the Jeanne d'Arc basin may have tapped into both thermally-reset and un-reset rocks and resulted in the observed Paleozoic to Mesozoic cooling ages.

3.1 Future research

Detrital zircon U-Pb and FT double-dating ages from the Lower Cretaceous Hibernia Formation provide insight into exhumation events in the Grand Banks during Triassic to Early Cretaceous rifting and older Paleozoic mountain-building events. As part of the initial scope of this project, prior to the COVID-19 pandemic, core-logging and detrital zircon sampling of syn-rift Upper Jurassic to Early Cretaceous Jeanne d'Arc Formation and syn- to post-breakup mid-Cretaceous Ben Nevis and Nautilus formation units were completed. New detrital zircon U-Pb and FT double-dating studies of these samples would capture a longer (~40 Myr) interval of Jeanne d'Arc basin evolution and provide additional context for exhumation rates and timing in the proximal domain during Mesozoic rifting. Specific questions include: (1) Do the U-Pb and FT age population signatures change through the syn-rift to post-breakup stratigraphy? If so, can we use detrital zircon U-Pb ages as stratigraphic indicators? Are they indicative of specific reservoir units? (2) Do FT cooling populations remain consistent between stratigraphic units? (3) Do Mesozoic cooling populations align with proximal, necking, distal, and outer domain phases? If so, how do they evolve between stratigraphic units? (4) Using the lag time between maximum depositional age and youngest exhumation-cooled FT ages, do rates of exhumation change over the Late Jurassic to Early Cretaceous periods?

Future research of Appalachian-Variscan basement rock units in eastern Newfoundland and Portugal with zircon and/or apatite U-Pb,FT, and (U-Th)/He methods could investigate the timing, rates, and spatial extent of rock exhumation associated with Mesozoic rifting on either side of a conjugate margin pair. There have yet to be regional-scale studies that use a consistent low-temperature (< 300°C) thermochronological method to observe patterns and rates of basement exhumation in eastern Newfoundland and Portugal. Nor have there been cross-conjugate margin

studies that apply the modern geological framework to the timing of exhumation to test magma-poor rift models. Applying zircon U-Pb and FT double-dating to basement rocks would provide source fingerprints to compare with offshore detrital zircon double-dating studies such as those presented in this thesis. Specific questions include: (1) are there differential exhumation patterns across Newfoundland and Portugal, respectively, and if so, what are their spatial relationships to Mesozoic fault systems and Paleozoic suture zones?; (2) do exhumation histories across fault transects indicate fault reactivation and tectonic exhumation in the Mesozoic?; (3) do basement rocks yield cooling ages that correspond to the timing of Triassic to Cretaceous stretching and thinning, mantle exhumation, breakup, or post-breakup seafloor spreading?; (4) are there predictable exhumation patterns between the conjugate margins? If so, what are their spatial relationships to fault systems and the rift axis?; and (5) what predictions can be made about the evolution of other modern magma-poor rift margins?

3.2 References

Barr, S.M., Dunning, G.R., Raeside, R.P., and Jamieson, R.A., 1990, Contrasting U-Pb ages from plutons in the Bras d'Or and Mira terranes of Cape Breton Island, Nova Scotia: Canadian Journal of Earth Sciences, v. 27, p. 1200–1208, doi:10.1139/e90-127.

Bernet, M., and Garver, J.I., 2005, Fission-track analysis of detrital zircon: Reviews in Mineralogy and Geochemistry, v. 58, p. 205–238, doi:10.2138/rmg.2005.58.8.

Bowman, S.J., Pe-Piper, G., Piper, D.J.W., Fensome, R.A., and King, E.L., 2012, Early cretaceous volcanism in the Scotian Basin: Canadian Journal of Earth Sciences, v. 49, p. 1523–1539, doi:10.1139/e2012-063.

Campbell, I.H., Reiners, P.W., Allen, C.M., Nicolescu, S., and Upadhyay, R., 2005, He-Pb double dating of detrital zircons from the Ganges and Indus Rivers: Implication for quantifying sediment recycling and provenance studies: Earth and Planetary Science Letters, v. 237, p. 402–432, doi:10.1016/j.epsl.2005.06.043.

Canada-Newfoundland and Labrador Offshore Petroleum Board Estimates of Recoverable Reserves/Resources:, https://www.cnlopb.ca/resource/information/ (accessed September 2021).

Cawood, P.A., Hawkesworth, C.J., and Dhuime, B., 2012, Detrital zircon record and tectonic setting: Geology, v. 40, p. 875–878, doi:10.1130/G32945.1.

Davis, M., and Kusznir, N., 2004, Depth-Dependent Lithospheric Stretching at Rifted Continental Margins, *in* Karner, G.D. ed., Proceedings of NSF Rifted Margins Theoretical Institute, New York, Columbia University Press, p. 92–137, doi:10.7312/karn12738-005.

Gibling, M.R., Culshaw, N., Rygel, M.C., and Pascucci, V., 2008, Chapter 6 The Maritimes Basin of Atlantic Canada: Basin Creation and Destruction in the Collisional Zone of Pangea: Elsevier, v. 5, 211–244 p., doi:10.1016/S1874-5997(08)00006-3.

Haupert, I., Manatschal, G., Decarlis, A., and Unternehr, P., 2016, Upper-plate magma-poor rifted margins: Stratigraphic architecture and structural evolution: Marine and Petroleum Geology, v. 69, p. 241–261, doi:10.1016/j.marpetgeo.2015.10.020.

Hiscott, R.N., Marsaglia, K.M., Wilson, R.C.L., Robertson, A.H.F., Karner, G.D., Tucholke, B.E., Pletsch, T., and Petschick, R., 2008, Detrital sources and sediment delivery to the early post-rift (Albian-Cenomanian) Newfoundland Basin east of the Grand Banks: Results from ODP Leg 210: Bulletin of Canadian Petroleum Geology, v. 56, p. 69–92, doi:10.2113/gscpgbull.56.2.69.

Hendriks, M., Jamieson, R.A., Willett, S.D., and Zentilli, M., 1993, Burial and exhumation of the Long Range Inlier and its surroundings, western Newfoundland: results of an apatite fission-track study: Canadian Journal of Earth Sciences, v. 30, p. 1594–1606, doi:10.1139/e93-137.

Hodych, J.P., and Hayatsu, A., 1988, Paleomagnetism and K-Ar isochron dates of Early Jurassic basaltic flows and dikes of Atlantic Canada: Canadian Journal of Earth Sciences, v. 25, p. 1972–1989, doi:10.1139/e88-185.

Huismans, R.S., and Beaumont, C., 2014, Rifted continental margins: The case for depth-dependent extension: Earth and Planetary Science Letters, v. 407, p. 148–162, doi:10.1016/j.epsl.2014.09.032.

Hutter, A., and Beranek, L., 2020, Provenance of Upper Jurassic to Lower Cretaceous synrift strata in the Terra Nova oil field, Jeanne d'Arc basin, offshore Newfoundland: A new detrital zircon U-Pb-Hf reference frame for the Atlantic Canadian margin: AAPG Bulletin, v. 104, p. 2325–2349, doi:10.1306/02232018241.

Keppie, J.D., Davis, D.W., and Krogh, T.E., 1998, U-Pb geochronological constraints on Precambrian stratified units in the Avalon Composite Terrane of Nova Scotia, Canada: tectonic implications: Canadian Journal of Earth Sciences, v. 35, p. 222–236, doi:10.1139/cjes-35-3-222.

Lavier, L.L., and Manatschal, G., 2006, A mechanism to thin the continental lithosphere at magma-poor margins: Nature, v. 440, p. 324–328, doi:10.1038/nature04608.

Lowe, D.G., Sylvester, P.J., and Enachescu, M.E., 2011, Provenance and paleodrainage patterns of Upper Jurassic and Lower Cretaceous synrift sandstones in the Flemish Pass Basin, offshore Newfoundland, east coast of Canada: AAPG Bulletin, v. 95, p. 1295–1320, doi:10.1306/12081010005.

McDonough, M., Sylvester, P., Bruder, N., Lo, J., and O'Sullivan, P., 2010, Provenance of reservoir sandstones in the Flemish Pass and Orphan Basins (Canada): U-Pb dating of detrital zircons using the laser ablation method: Central & North Atlantic Conjugate Margins Conference, v. 5, p. 181–184, http://metododirecto.pt/CM2010.

Péron-Pinvidic, G., and Manatschal, G., 2009, The final rifting evolution at deep magma-poor passive margins from Iberia-Newfoundland: A new point of view: International Journal of Earth Sciences, v. 98, p. 1581–1597, doi:10.1007/s00531-008-0337-9.

Péron-Pinvidic, G., Manatschal, G., and Osmundsen, P.T., 2013, Structural comparison of archetypal Atlantic rifted margins: A review of observations and concepts: Marine and Petroleum Geology, v. 43, p. 21–47, doi:10.1016/j.marpetgeo.2013.02.002.

Pe-Piper, G., Jansa, L.F., and Palacz, Z., 1994, Geochemistry and regional significance of the early Cretaceous bimodal basalt-felsic associations on Grand Banks, eastern Canada: Geological Society of America Bulletin, v. 106, p. 1319–1331, doi:10.1130/0016-7606(1994)106<1319:GARSOT>2.3.CO;2.

Saylor, J.E., Stockli, D.F., Horton, B.K., Nie, J., and Mora, A., 2012, Discriminating rapid exhumation from syndepositional volcanism using detrital zircon double dating: Implications for the tectonic history of the Eastern Cordillera, Colombia: GSA Bulletin, v. 124, p. 762–779, doi:10.1130/B30534.1.Scott, D.J., 1995, U-Pb geochronology of a Paleoproterozoic continental magmatic arc on the western margin of the Archean Nain craton, northern Labrador, Canada: Canadian Journal of Earth Sciences, v. 32, p. 1870–1882, doi:10.1139/e95-144.

Sinclair, I.K., 1988, Evolution of Mesozoic-Cenozoic sedimentary basins in the Grand Banks area of Newfoundland and comparison with Falvey's (1974) rift model: Bulletin of

Canadian Petroleum Geology, v. 36, p. 255–273.

Sutra, E., Manatschal, G., Mohn, G., and Unternehr, P., 2013, Quantification and restoration of extensional deformation along the Western Iberia and Newfoundland rifted margins: Geochemistry, Geophysics, Geosystems, v. 14, p. 2575–2597, doi:10.1002/ggge.20135.

van Staal, C.R., and Barr, S.M., 2012, Lithospheric architecture and tectonic evolution of the Canadian Appalachians and associated Atlantic margin, *in* Percival, J.A., Cook, F.A., and Clowes, R.M. eds., Tectonic Styles in Canada: the LITHOPROBE Perspective, Geological Association of Canada, Special Paper 49, p. 41–95.

APPENDIX A: U-PB AND FISSION-TRACK DATA TABLES

A.1 Detrital zircon U-Pb isotopic ratios and ages

20EJ01 - West Bonne Bay F-12 – Hibernia Formation (Upper) – Core # 1, boxes 110-113

	Isotopic ratios[2]								Isotopic ages									
Spot Name	$^{207}Pb/^{206}Pb$	$2s_x$ (%)	$^{238}U/^{206}Pb$	$2s_x$ (%)	$^{207}Pb/^{235}Pb$	$2s_x$ (%)	$^{206}Pb/^{238}U$	$2s_x$ (%)	$^{207}Pb/^{206}Pb$	$2s_{total}$ (Ma)	$^{207}Pb/^{235}Pb$	$2s_{total}$ (Ma)	$^{206}Pb/^{238}U$	$2s_{total}$ (Ma)	Prob. Conc. (%)	% conc[3]	U-Pb Best Age[4]	$2s_{total}$ (Ma)
J01_1_Grain01	0.0630	5.9	9.9	3.7	0.9	6.9	0.1	3.7	708	129	641	34	622	24	29.97	12.17	622	24
J01_1_t2_Grain01	0.0521	7.1	21.6	4.0	0.3	8.1	0.0	4.0	NA	NA	291	21	291	12	98.87	NA	291	12
J01_1_t2_Grain02	0.0623	4.7	10.5	3.2	0.8	5.7	0.1	3.2	684	105	607	27	587	20	14.37	14.26	587	20
J01_1_t2_Grain03	0.0587	6.8	10.4	4.0	0.8	7.8	0.1	4.0	556	152	584	35	591	24	71.06	-6.28	591	24
J01_1_t2_Grain04	0.0574	5.4	9.6	3.5	0.8	6.4	0.1	3.5	507	123	612	30	641	23	7.88	-26.39	641	23
J01_1_t2_Grain05	0.0485	6.4	22.5	3.7	0.3	7.4	0.0	3.7	NA	NA	265	18	281	11	9.21	NA	281	11
J01_1_t2_Grain06	0.0588	4.1	11.3	2.9	0.7	5.1	0.1	2.9	560	97	549	22	546	17	83.73	2.44	546	17
J01_1_t2_Grain07	0.0597	5.5	10.2	3.5	0.8	6.5	0.1	3.5	593	123	601	30	603	22	89.42	-1.68	603	22
J01_1_t2_Grain08	0.0589	5.1	11.6	3.5	0.7	6.2	0.1	3.5	563	117	540	27	534	19	71.60	5.18	534	19
J01_1_t2_Grain09	0.0588	6.0	10.6	3.7	0.8	7.1	0.1	3.7	560	136	578	32	582	22	81.69	-4.00	582	22
J01_1_t2_Grain10	0.0582	5.8	10.5	3.6	0.8	6.8	0.1	3.6	537	132	576	31	586	21	57.12	-9.10	586	21
J01_1_t2_Grain11	0.0582	4.8	11.5	3.2	0.7	5.8	0.1	3.2	537	111	538	25	538	18	98.91	-0.20	538	18
J01_1_t2_Grain12	0.0571	5.4	10.3	3.4	0.8	6.4	0.1	3.4	495	125	576	29	597	21	19.90	-20.47	597	21
J01_1_t3_Grain01	0.0545	4.4	15.7	3.1	0.5	5.3	0.1	3.1	NA	NA	397	18	397	13	93.07	NA	397	13
J01_1_t3_Grain02	0.0617	3.8	7.7	2.7	1.1	4.7	0.1	2.7	664	87	755	26	786	23	4.45	-18.36	786	23
J01_1_t3_Grain03	0.0588	9.7	11.1	4.9	0.7	10.8	0.1	4.9	560	214	557	47	557	27	98.30	0.53	557	27
J01_1_t3_Grain04	0.0595	4.3	12.5	3.1	0.7	5.3	0.1	3.1	NA	NA	511	22	494	16	6.37	NA	494	16
J01_1_t3_Grain05	0.0770	15.8	6.3	7.7	1.7	17.6	0.2	7.7	1121	320	1000	112	946	69	41.17	15.66	946	69
J01_1_t3_Grain06	0.0517	7.9	14.6	4.4	0.5	9.1	0.1	4.4	NA	NA	403	31	426	19	14.04	NA	426	19
J01_1_t3_Grain07	0.0589	5.8	10.8	3.6	0.8	6.9	0.1	3.6	563	132	570	31	572	21	92.15	-1.54	572	21
J01_1_t3_Grain08	0.0863	2.4	4.4	2.3	2.7	3.3	0.2	2.3	1345	56	1336	27	1331	32	72.48	1.05	1331	32

J01_1_t3_Grain09	0.0519	4.9	14.9	3.1	0.5	5.8	0.1	3.1	NA	NA	399	20	419	14	5.42	NA	419	14
J01_1_t3_Grain10	0.0554	4.6	21.5	3.1	0.4	5.6	0.0	3.1	NA	NA	309	15	293	10	7.72	NA	293	10
J01_1_t3_Grain11	0.0604	3.6	10.4	2.5	0.8	4.4	0.1	2.5	618	84	597	21	591	16	63.93	4.37	591	16
J01_1_t3_Grain12	0.0488	7.9	21.1	4.3	0.3	9.0	0.0	4.3	NA	NA	281	22	299	13	15.08	NA	299	13
J01_1_t3_Grain13	0.0500	9.1	15.8	4.7	0.4	10.2	0.1	4.7	NA	NA	368	32	396	19	13.05	NA	396	19
J01_1_t3_Grain14	0.0625	3.9	9.3	2.8	0.9	4.8	0.1	2.8	691	89	664	24	656	20	52.38	5.03	656	20
J01_1_t3_Grain15	0.0634	5.9	10.6	3.8	0.8	7.1	0.1	3.8	722	130	609	33	579	23	8.70	19.75	579	23
J01_1_t3_Grain16	0.1107	3.5	3.3	3.1	4.6	4.7	0.3	3.1	1811	70	1744	41	1688	51	2.43	6.77	1811	70
J01_1_t3_Grain17	0.0532	5.9	22.4	3.5	0.3	6.9	0.0	3.5	NA	NA	288	18	282	10	50.51	NA	282	10
J01_1_t3_Grain18	0.0542	4.8	21.6	3.2	0.3	5.8	0.0	3.2	NA	NA	301	15	292	10	19.20	NA	292	10
J01_1_t3_Grain19	0.0659	6.5	10.2	4.1	0.9	7.7	0.1	4.1	803	140	647	37	603	25	4.14	24.97	603	25
J01_1_t3_Grain20	0.0594	3.6	10.3	2.7	0.8	4.5	0.1	2.7	582	86	594	21	597	17	80.19	-2.58	597	17
J01_1_t3_Grain22	0.0616	5.1	9.7	3.6	0.9	6.2	0.1	3.6	660	114	639	30	633	23	70.27	4.20	633	23
J01_1_t3_Grain23	0.0520	5.9	22.2	3.5	0.3	6.9	0.0	3.5	NA	NA	284	17	284	11	98.98	NA	284	11
J01_1_t3_Grain24	0.0579	6.9	10.3	4.0	0.8	8.0	0.1	4.0	526	155	581	36	595	24	49.70	-13.13	595	24
J01_1_t3_Grain25	0.0594	9.5	10.5	5.0	0.8	10.7	0.1	5.0	582	209	585	48	586	29	97.35	-0.76	586	29
J01_1_t3_Grain27	0.0600	6.2	9.9	3.9	0.8	7.3	0.1	3.9	604	139	617	34	621	24	83.31	-2.86	621	24
J01_1_t3_Grain28	0.0611	5.0	10.6	3.2	0.8	5.9	0.1	3.2	643	112	592	27	579	19	34.33	9.99	579	19
J01_1_t3_Grain29	0.0612	7.7	10.0	4.3	0.8	8.9	0.1	4.3	646	170	620	42	613	26	76.89	5.11	613	26
J01_1_t3_Grain30	0.0604	5.5	11.4	3.6	0.7	6.6	0.1	3.6	618	124	556	29	541	20	30.47	12.40	541	20
J01_1_t3_Grain31	0.0633	5.9	10.3	3.9	0.8	7.1	0.1	3.9	718	131	622	34	596	24	15.64	17.00	596	24
J01_1_t3_Grain32	0.0596	8.3	18.7	5.2	0.4	9.8	0.1	5.2	NA	NA	369	31	335	17	2.78	NA	335	17
J01_1_t3_Grain34	0.0615	5.2	10.5	3.5	0.8	6.3	0.1	3.5	657	116	601	29	587	21	38.68	10.65	587	21
J01_1_t3_Grain35	0.0529	6.6	22.2	3.1	0.3	7.3	0.0	3.1	NA	NA	289	19	284	9	69.92	NA	284	9
J01_1_t3_Grain36	0.0595	4.4	11.6	3.0	0.7	5.4	0.1	3.0	585	102	542	23	532	17	45.24	9.16	532	17
J01_1_t3_Grain38	0.0582	3.6	11.5	2.8	0.7	4.6	0.1	2.8	537	86	536	20	536	16	98.03	0.24	536	16
J01_1_t3_Grain39	0.0548	6.8	21.8	4.1	0.3	7.9	0.0	4.1	NA	NA	302	21	289	12	21.42	NA	289	12
J01_1_t3_Grain40	0.0571	6.2	10.7	3.9	0.7	7.3	0.1	3.9	495	141	558	32	574	22	35.84	-15.84	574	22
J01_1_t3_Grain41	0.0577	9.9	11.4	5.2	0.7	11.2	0.1	5.2	518	221	536	47	540	28	86.95	-4.20	540	28

J01_1_t3_Grain42	0.0509	5.6	21.2	3.5	0.3	6.6	0.0	3.5	NA	NA	290	17	297	11	44.18	NA	297	11
J01_1_t3_Grain43	0.0631	6.8	9.8	4.1	0.9	7.9	0.1	4.1	712	148	647	38	628	26	35.27	11.68	628	26
J01_1_t3_Grain44	0.0588	4.2	10.1	2.8	0.8	5.0	0.1	2.8	560	97	599	24	610	18	46.68	-8.94	610	18
J01_1_t3_Grain45	0.0526	5.8	21.6	3.4	0.3	6.7	0.0	3.4	NA	NA	294	17	292	10	81.21	NA	292	10
J01_1_t3_Grain46	0.0590	5.7	10.4	3.7	0.8	6.8	0.1	3.7	567	130	585	31	589	22	75.55	-3.89	589	22
J01_1_t3_Grain47	0.0515	4.4	19.1	2.8	0.4	5.2	0.1	2.8	NA	NA	321	15	329	10	33.05	NA	329	10
J01_1_t3_Grain48	0.0602	8.1	11.3	4.6	0.7	9.3	0.1	4.6	611	178	560	40	547	25	56.67	10.40	547	25
J01_1_t3_Grain49	0.0573	5.3	11.1	3.3	0.7	6.2	0.1	3.3	503	121	545	27	556	19	47.56	-10.42	556	19
J01_1_t3_Grain50	0.0812	1.8	4.7	1.9	2.4	2.6	0.2	1.9	1226	47	1238	21	1244	26	55.37	-1.46	1244	26
J01_1_t3_Grain51	0.0570	5.4	10.7	3.5	0.7	6.5	0.1	3.5	492	125	560	29	577	21	30.63	-17.47	577	21
J01_1_t3_Grain52	0.0595	6.9	15.3	4.2	0.5	8.1	0.1	4.2	NA	NA	436	29	408	17	6.71	NA	408	17
J01_1_t3_Grain53	0.0622	5.4	10.6	3.5	0.8	6.5	0.1	3.5	681	121	603	30	583	21	19.21	14.44	583	21
J01_1_t3_Grain54	0.0557	4.8	14.9	3.2	0.5	5.7	0.1	3.2	NA	NA	422	20	418	14	73.12	NA	418	14
J01_1_t3_Grain55	0.0516	5.2	21.5	3.2	0.3	6.1	0.0	3.2	NA	NA	291	16	294	10	74.02	NA	294	10
J01_1_t3_Grain56	0.0628	5.8	9.9	3.7	0.9	6.9	0.1	3.7	701	128	637	33	619	23	30.76	11.83	619	23
J01_1_t3_Grain57	0.1500	4.2	2.3753	4.1	8.7071	5.9	0.4210	4.1	2346	77	2308	55	2265	82	8.77	3.45	2346	77
J01_1_t3_Grain58	0.0609	3.8	9.7	2.7	0.9	4.7	0.1	2.7	636	89	632	23	631	18	92.83	0.77	631	18
J01_1_t3_Grain60	0.0536	4.2	21.3	2.8	0.3	5.0	0.0	2.8	NA	NA	302	14	295	9	33.73	NA	295	9
J01_1_t3_Grain61	0.0598	3.1	11.3	2.3	0.7	3.8	0.1	2.3	596	75	556	17	547	14	32.19	8.33	547	14
J01_1_t3_Grain62	0.0666	7.2	9.5	4.1	1.0	8.3	0.1	4.1	825	154	688	42	647	27	12.64	21.66	647	27
J01_1_t3_Grain64	0.0598	3.0	9.7	2.3	0.8	3.8	0.1	2.3	596	73	623	19	630	16	42.58	-5.68	630	16
J01_1_t3_Grain66	0.0497	7.7	21.6	4.3	0.3	8.8	0.0	4.3	NA	NA	279	22	291	13	32.95	NA	291	13
J01_1_t3_Grain67	0.0605	6.9	10.2	4.3	0.8	8.1	0.1	4.3	622	153	607	38	603	26	86.05	2.93	603	26
J01_1_t3_Grain68	0.0921	2.9	3.8	2.6	3.3	3.9	0.3	2.6	1469	63	1483	32	1493	39	61.37	-1.60	1493	39
J01_1_t3_Grain70	0.0933	2.1	3.9	2.2	3.3	3.0	0.3	2.2	1494	50	1489	26	1486	34	81.71	0.52	1486	34
J01_1_t3_Grain71	0.0551	4.8	18.7	3.0	0.4	5.7	0.1	3.0	NA	NA	346	17	336	11	23.03	NA	336	11
J01_1_t3_Grain72	0.0601	4.5	10.4	3.0	0.8	5.4	0.1	3.0	607	102	595	25	592	19	82.64	2.58	592	19
J01_1_t3_Grain73	0.0627	5.7	10.4	3.8	0.8	6.8	0.1	3.8	698	126	614	32	592	23	19.66	15.26	592	23
J01_1_t3_Grain74	0.0623	4.2	10.6	2.9	0.8	5.1	0.1	2.9	684	95	602	24	580	18	11.39	15.30	580	18

J01_1_t3_Grain76	0.1117	2.4	3.0	2.4	5.1	3.4	0.3	2.4	1827	52	1837	31	1846	44	59.83	-1.03	1827	52
J01_1_t3_Grain77	0.0620	5.2	10.4	3.5	0.8	6.3	0.1	3.5	674	117	607	29	589	21	27.96	12.60	589	21
J01_1_t3_Grain79	0.0535	8.4	20.9	4.4	0.4	9.5	0.0	4.4	NA	NA	307	25	301	14	65.57	NA	301	14
J01_1_t3_Grain80	0.0618	7.3	10.2	4.4	0.8	8.5	0.1	4.4	667	161	617	40	604	26	54.96	9.49	604	26
J01_1_t3_Grain81	0.0565	4.0	10.1	2.8	0.8	4.9	0.1	2.8	472	96	579	22	606	18	2.17	-28.41	606	18
J01_1_t3_Grain82	0.0507	3.8	20.9	2.7	0.3	4.7	0.0	2.7	NA	NA	293	12	301	9	17.83	NA	301	9
J01_1_t3_Grain83	0.1164	2.5	2.8	2.6	5.7	3.6	0.4	2.6	1902	53	1929	33	1954	49	21.18	-2.76	1902	53
J01_1_t3_Grain84	0.0578	6.6	11.6	4.1	0.7	7.8	0.1	4.1	522	150	530	33	532	22	91.63	-1.85	532	22
J01_1_t3_Grain85	0.0574	4.8	11.4	3.1	0.7	5.7	0.1	3.1	507	112	535	25	542	18	61.40	-6.90	542	18
J01_1_t3_Grain86	0.0639	12.2	10.6	6.4	0.8	13.8	0.1	6.4	738	262	614	64	580	36	40.44	21.40	580	36
J01_1_t3_Grain87	0.0516	4.4	20.9	3.0	0.3	5.3	0.0	3.0	NA	NA	298	14	302	10	58.70	NA	302	10
J01_1_t3_Grain88	0.0721	4.4	5.8	3.3	1.7	5.5	0.2	3.3	989	95	1013	36	1024	34	59.49	-3.59	1024	34
J01_1_t3_Grain89	0.1336	2.5	2.5	2.7	7.3	3.7	0.4	2.7	2146	51	2150	35	2154	55	84.05	-0.39	2146	51
J01_1_t3_Grain90	0.0554	4.9	14.9	3.1	0.5	5.8	0.1	3.1	NA	NA	421	21	420	14	91.89	NA	420	14
J01_1_t3_Grain91	0.0592	4.5	10.3	3.0	0.8	5.4	0.1	3.0	574	103	594	25	599	19	71.95	-4.30	599	19
J01_1_t3_Grain92	0.0651	8.5	11.7	5.0	0.8	9.8	0.1	5.0	778	182	579	44	529	26	5.28	31.91	529	26
J01_1_t3_Grain93	0.0996	2.9	3.5	2.7	3.9	3.9	0.3	2.7	1617	61	1617	34	1616	43	99.80	0.01	1617	61
J01_2_Grain01	0.0604	3.5	10.1	2.2	0.8	4.1	0.1	2.2	618	82	609	20	607	15	83	98	607	15
J01_2_Grain02	0.0633	5.0	10.2	2.8	0.9	5.8	0.1	2.8	718	112	629	28	604	18	4	84	604	18
J01_2_Grain03	0.0627	4.7	9.0	2.7	1.0	5.4	0.1	2.7	698	105	682	28	677	19	78	3	677	19
J01_2_Grain04	0.0532	5.0	19.2	2.5	0.4	5.6	0.1	2.5	NA	NA	329	16	328	9	90	NA	328	9
J01_2_Grain05	0.0601	7.5	10.8	3.3	0.8	8.2	0.1	3.3	607	166	577	37	570	20	70	94	570	20
J01_2_Grain06	0.0740	4.3	6.2	2.8	1.7	5.1	0.2	2.8	1041	92	991	34	968	28	22	7	968	28
J01_2_Grain07	0.0582	5.6	11.3	2.8	0.7	6.2	0.1	2.8	537	127	544	27	545	16	91	102	545	16
J01_2_Grain08	0.0498	7.2	22.1	3.0	0.3	7.8	0.0	3.0	NA	NA	275	19	286	9	29	NA	286	9
J01_2_Grain09	0.0605	5.3	10.5	2.8	0.8	6.0	0.1	2.8	622	120	594	28	587	17	63	94	587	17
J01_2_Grain10	0.0605	4.3	10.2	2.5	0.8	5.0	0.1	2.5	622	99	609	24	606	17	80	97	606	17
J01_2_Grain11	0.0578	4.9	10.3	2.5	0.8	5.5	0.1	2.5	522	112	581	25	596	16	20	114	596	16
J01_2_Grain12	0.0581	5.6	11.4	2.9	0.7	6.3	0.1	2.9	534	127	539	27	541	17	93	101	541	17

J01_2_Grain13	0.0495	7.1	21.5	2.9	0.3	7.6	0.0	2.9	NA	NA	281	19	294	9	20	NA	294	9
J01_2_Grain14	0.0729	3.7	6.0	2.4	1.7	4.4	0.2	2.4	1011	82	994	29	987	26	61	2	987	26
J01_2_Grain15	0.0628	5.6	9.8	2.8	0.9	6.2	0.1	2.8	701	123	644	30	627	18	30	11	627	18
J01_2_Grain16	0.0614	5.2	10.2	2.8	0.8	5.9	0.1	2.8	653	116	616	28	606	18	47	93	606	18
J01_2_Grain17	0.0562	5.1	9.9	2.6	0.8	5.7	0.1	2.6	460	118	587	26	620	18	2	-35	620	18
J01_2_Grain18	0.0722	4.7	5.5	2.7	1.8	5.4	0.2	2.7	992	101	1052	37	1081	30	15	-9	1081	30
Rejected Analyses																		
J01_1_t3_Grain37	0.0530	9.1	9.6061	5.0	0.7607	10.4	0.1041	5.0	329	211	574	46	638	31	0.79	-94.16		

20EJ02 - West Bonne Bay F-12 – Hibernia Formation (Upper) – Core # 1, boxes 92-96

	Isotopic ratios[2]								**Isotopic ages**									
Spot Name	$^{207}Pb/^{206}Pb$	$2s_x$ (%)	$^{238}U/^{206}Pb$	$2s_x$ (%)	$^{207}Pb/^{235}Pb$	$2s_x$ (%)	$^{206}Pb/^{238}U$	$2s_x$ (%)	$^{207}Pb/^{206}Pb$	$2s_{total}$ (Ma)	$^{207}Pb/^{235}Pb$	$2s_{total}$ (Ma)	$^{206}Pb/^{238}U$	$2s_{total}$ (Ma)	Prob. Conc. (%)	% conc[3]	U-Pb Best Age[4]	$2s_{total}$ (Ma)
J02_1_Grain01	0.0601	4.2	9.6805	2.9	0.8560	5.1	0.1033	2.9	607	96	628	25	634	20	65.94	-4.37	634	20
J02_1_Grain02	0.1135	2.2	3.0488	2.1	5.1330	3.1	0.3280	2.1	1856	48	1842	28	1829	40	50.94	1.48	1856	48
J02_1_t2_Grain01	0.0541	6.3	22.1239	3.8	0.3372	7.4	0.0452	3.8	NA	NA	295	19	285	11	32.83	NA	285	11
J02_1_t2_Grain02	0.0601	4.7	11.2994	3.2	0.7334	5.6	0.0885	3.2	607	106	559	25	547	18	42.71	9.97	547	18
J02_1_t2_Grain03	0.0635	4.5	11.2108	3.1	0.7810	5.5	0.0892	3.1	725	101	586	25	551	18	1.18	24.03	551	18
J02_1_t2_Grain04	0.0615	3.3	10.6157	2.4	0.7988	4.1	0.0942	2.4	657	78	596	19	580	16	9.46	11.64	580	16
J02_1_t2_Grain05	0.0566	5.0	10.2459	3.2	0.7617	5.9	0.0976	3.2	476	115	575	27	600	20	10.49	-26.12	600	20
J02_1_t2_Grain06	0.0502	4.8	18.7441	3.0	0.3693	5.7	0.0534	3.0	NA	NA	319	16	335	11	6.87	NA	335	11
J02_1_t2_Grain07	0.0612	4.0	10.1317	2.9	0.8329	4.9	0.0987	2.9	646	92	615	24	607	19	45.63	6.11	607	19
J02_1_t2_Grain08	0.0597	4.5	10.3627	3.0	0.7943	5.4	0.0965	3.0	593	103	594	25	594	19	98.81	-0.19	594	19
J02_1_t2_Grain09	0.0577	3.9	11.1982	2.7	0.7104	4.8	0.0893	2.7	518	92	545	21	551	16	57.71	-6.37	551	16
J02_1_t3_Grain01	0.0580	4.6	10.9529	3.0	0.7301	5.5	0.0913	3.0	530	106	557	24	563	18	64.49	-6.32	563	18
J02_1_t3_Grain03	0.0623	6.6	10.4384	4.0	0.8229	7.7	0.0958	4.0	684	145	610	36	590	24	34.74	13.83	590	24
J02_1_t3_Grain05	0.0598	3.5	10.3093	2.6	0.7998	4.4	0.0970	2.6	596	83	597	21	597	17	99.30	-0.08	597	17
J02_1_t3_Grain06	0.0572	5.4	14.5560	3.2	0.5418	6.3	0.0687	3.2	NA	NA	440	23	428	15	26.27	NA	428	15

J02_1_t3_Grain07	0.0557	6.9	15.3610	3.9	0.5000	7.9	0.0651	3.9	NA	NA	412	27	407	16	73.36	NA	407	16
J02_1_t3_Grain08	0.0589	6.4	13.1926	3.8	0.6156	7.5	0.0758	3.8	NA	NA	487	29	471	18	26.73	NA	471	18
J02_1_t3_Grain09	0.0598	3.3	9.8619	2.5	0.8361	4.2	0.1014	2.5	596	80	617	20	623	17	59.92	-4.40	623	17
J02_1_t3_Grain10	0.0618	5.7	10.0604	3.6	0.8470	6.7	0.0994	3.6	667	126	623	32	611	22	48.66	8.44	611	22
J02_1_t3_Grain101	0.0600	8.9	9.7561	4.9	0.8480	10.2	0.1025	4.9	604	197	624	48	629	30	82.24	-4.22	629	30
J02_1_t3_Grain102	0.0913	3.3	3.8344	2.7	3.2831	4.3	0.2608	2.7	1453	69	1477	35	1494	41	39.44	-2.83	1494	41
J02_1_t3_Grain104	0.0531	5.9	15.4560	3.6	0.4737	6.9	0.0647	3.6	NA	NA	394	23	404	15	43.40	NA	404	15
J02_1_t3_Grain105	0.0539	6.3	21.0970	3.8	0.3523	7.4	0.0474	3.8	NA	NA	306	20	299	12	48.93	NA	299	12
J02_1_t3_Grain106	0.0579	5.2	11.2108	3.2	0.7121	6.1	0.0892	3.2	526	118	546	26	551	18	68.73	-4.72	551	18
J02_1_t3_Grain107	0.0539	9.1	10.1937	5.1	0.7291	10.4	0.0981	5.1	367	210	556	45	603	30	5.71	-64.43	603	30
J02_1_t3_Grain108	0.0600	6.5	10.9170	3.9	0.7578	7.6	0.0916	3.9	604	145	573	34	565	23	67.31	6.39	565	23
J02_1_t3_Grain109	0.0514	6.2	21.1864	3.6	0.3345	7.2	0.0472	3.6	NA	NA	293	19	297	11	62.86	NA	297	11
J02_1_t3_Grain11	0.0764	4.8	5.4585	3.6	1.9298	6.0	0.1832	3.6	1106	102	1091	41	1084	38	77.85	1.91	1084	38
J02_1_t3_Grain110	0.0509	5.7	21.5983	3.3	0.3249	6.6	0.0463	3.3	NA	NA	286	17	292	10	48.70	NA	292	10
J02_1_t3_Grain111	0.0709	4.5	6.2775	3.2	1.5573	5.5	0.1593	3.2	955	97	953	35	953	30	97.90	0.17	953	30
J02_1_t3_Grain112	0.0578	6.1	11.2740	3.7	0.7069	7.1	0.0887	3.7	522	139	543	31	548	21	78.03	-4.91	548	21
J02_1_t3_Grain114	0.0585	3.2	10.3306	2.4	0.7808	4.0	0.0968	2.4	549	77	586	19	596	16	31.77	-8.58	596	16
J02_1_t3_Grain115	0.1007	2.3	3.5186	2.0	3.9460	3.0	0.2842	2.0	1637	51	1623	27	1612	35	55.19	1.50	1637	51
J02_1_t3_Grain116	0.0558	7.1	11.0742	4.0	0.6947	8.2	0.0903	4.0	444	162	536	34	557	23	23.05	-25.40	557	23
J02_1_t3_Grain117	0.0614	4.6	10.2881	3.1	0.8229	5.6	0.0972	3.1	653	105	610	26	598	20	40.56	8.46	598	20
J02_1_t3_Grain118	0.0588	8.0	9.7371	4.4	0.8326	9.1	0.1027	4.4	560	178	615	42	630	27	46.56	-12.60	630	27
J02_1_t3_Grain119	0.0614	8.2	8.1967	4.7	1.0328	9.5	0.1220	4.7	653	180	720	49	742	34	48.12	-13.59	742	34
J02_1_t3_Grain12	0.0549	6.8	10.8932	4.0	0.6949	7.9	0.0918	4.0	408	158	536	34	566	23	8.31	-38.72	566	23
J02_1_t3_Grain120	0.0606	5.6	10.0200	3.7	0.8339	6.7	0.0998	3.7	625	125	616	31	613	23	87.53	1.89	613	23
J02_1_t3_Grain121	0.0589	5.0	11.4155	3.4	0.7114	6.0	0.0876	3.4	563	114	546	26	541	19	75.91	3.92	541	19
J02_1_t3_Grain122	0.0561	5.5	14.8148	3.3	0.5221	6.5	0.0675	3.3	NA	NA	427	23	421	15	69.15	NA	421	15
J02_1_t3_Grain123	0.0616	7.0	10.3627	4.2	0.8196	8.1	0.0965	4.2	660	154	608	38	594	25	48.70	10.05	594	25
J02_1_t3_Grain124	0.0616	8.2	10.8814	4.7	0.7805	9.4	0.0919	4.7	660	179	586	42	567	27	41.75	14.16	567	27
J02_1_t3_Grain125	0.0585	6.8	10.4275	4.1	0.7735	7.9	0.0959	4.1	549	153	582	36	590	24	67.90	-7.62	590	24

J02_1_t3_Grain126	0.0725	6.2	6.4185	3.8	1.5574	7.3	0.1558	3.8	1000	129	953	46	933	35	45.12	6.66	933	35
J02_1_t3_Grain127	0.0592	6.0	9.7276	3.7	0.8391	7.0	0.1028	3.7	574	135	619	33	631	24	52.44	-9.81	631	24
J02_1_t3_Grain128	0.1240	1.5	2.7226	1.7	6.2798	2.3	0.3673	1.7	2015	38	2016	23	2017	38	93.55	-0.11	2015	38
J02_1_t3_Grain129	0.0871	3.1	4.4228	2.7	2.7153	4.1	0.2261	2.7	1363	66	1333	32	1314	36	30.51	3.57	1314	36
J02_1_t3_Grain13	0.0616	5.3	11.5207	3.2	0.7372	6.2	0.0868	3.2	660	118	561	27	537	18	13.44	18.73	537	18
J02_1_t3_Grain130	0.1345	1.8	2.5873	2.0	7.1676	2.7	0.3865	2.0	2158	41	2132	27	2107	43	13.11	2.36	2158	41
J02_1_t3_Grain131	0.0579	5.1	10.5374	3.4	0.7576	6.1	0.0949	3.4	526	117	573	27	584	20	45.84	-11.12	584	20
J02_1_t3_Grain132	0.0528	6.2	21.5517	3.7	0.3378	7.3	0.0464	3.7	NA	NA	295	19	292	11	74.78	NA	292	11
J02_1_t3_Grain133	0.0990	3.3	3.5958	2.8	3.7961	4.3	0.2781	2.8	1605	67	1592	36	1582	44	58.88	1.47	1605	67
J02_1_t3_Grain134	0.0564	7.7	11.2994	4.3	0.6882	8.8	0.0885	4.3	468	174	532	37	547	23	50.05	-16.77	547	23
J02_1_t3_Grain135	0.0567	6.2	9.8912	3.8	0.7904	7.2	0.1011	3.8	480	141	591	33	621	24	10.91	-29.38	621	24
J02_1_t3_Grain136	0.0592	4.3	9.9010	2.9	0.8244	5.2	0.1010	2.9	574	99	611	25	620	19	49.01	-7.97	620	19
J02_1_t3_Grain137	0.0564	11.9	11.2613	6.1	0.6905	13.4	0.0888	6.1	468	268	533	56	548	33	60.83	-17.15	548	33
J02_1_t3_Grain138	0.0598	4.6	10.7527	3.0	0.7668	5.5	0.0930	3.0	596	105	578	25	573	18	73.99	3.87	573	18
J02_1_t3_Grain139	0.0578	4.4	11.4416	2.9	0.6965	5.3	0.0874	2.9	522	103	537	23	540	17	75.62	-3.44	540	17
J02_1_t3_Grain14	0.0616	12.6	11.2994	6.5	0.7517	14.2	0.0885	6.5	660	275	569	62	547	35	52.82	17.20	547	35
J02_1_t3_Grain140	0.0586	3.9	11.4548	2.7	0.7054	4.8	0.0873	2.7	552	92	542	21	540	16	84.13	2.30	540	16
J02_1_t3_Grain141	0.0605	4.0	9.9602	2.7	0.8375	4.8	0.1004	2.7	622	93	618	23	617	18	94.01	0.76	617	18
J02_1_t3_Grain142	0.1290	1.9	2.5720	2.1	6.9154	2.9	0.3888	2.1	2084	44	2101	28	2117	45	37.85	-1.58	2084	44
J02_1_t3_Grain143	0.0516	6.1	14.3266	3.7	0.4966	7.1	0.0698	3.7	NA	NA	409	24	435	17	5.87	NA	435	17
J02_1_t3_Grain144	0.0586	9.5	21.5983	4.8	0.3741	10.7	0.0463	4.8	NA	NA	323	30	292	14	7.31	NA	292	14
J02_1_t3_Grain145	0.0595	4.8	10.4493	3.0	0.7851	5.7	0.0957	3.0	585	109	588	26	589	19	96.19	-0.64	589	19
J02_1_t3_Grain146	0.0510	5.9	21.4638	3.3	0.3276	6.8	0.0466	3.3	NA	NA	288	17	294	10	55.11	NA	294	10
J02_1_t3_Grain147	0.0609	5.5	10.0301	3.5	0.8372	6.5	0.0997	3.5	636	124	618	31	613	22	76.06	3.63	613	22
J02_1_t3_Grain148	0.0683	6.4	7.3584	4.1	1.2798	7.6	0.1359	4.1	878	136	837	44	821	33	54.05	6.41	821	33
J02_1_t3_Grain149	0.0719	8.7	7.4349	4.5	1.3334	9.8	0.1345	4.5	983	180	860	57	813	36	18.17	17.25	813	36
J02_1_t3_Grain15	0.0640	7.3	9.7276	4.3	0.9071	8.5	0.1028	4.3	742	158	656	41	631	27	32.77	14.94	631	27
J02_1_t3_Grain150	0.0609	4.1	9.7847	2.9	0.8582	5.0	0.1022	2.9	636	95	629	24	627	19	88.75	1.32	627	19
J02_1_t3_Grain152	0.0585	7.7	12.1065	4.4	0.6662	8.9	0.0826	4.4	549	172	518	36	512	23	72.68	6.73	512	23

J02_1_t3_Grain153	0.0595	8.2	9.9108	4.5	0.8278	9.4	0.1009	4.5	585	183	612	44	620	28	76.48	-5.85	620	28
J02_1_t3_Grain154	0.0585	4.0	10.9051	2.8	0.7397	4.9	0.0917	2.8	549	94	562	22	566	17	79.07	-3.11	566	17
J02_1_t3_Grain155	0.0586	6.0	11.3766	3.4	0.7102	6.9	0.0879	3.4	552	135	545	30	543	19	91.66	1.66	543	19
J02_1_t3_Grain156	0.0714	4.2	5.4083	3.1	1.8203	5.2	0.1849	3.1	969	91	1053	35	1094	34	3.66	-12.88	1094	34
J02_1_t3_Grain158	0.1300	3.2	2.6511	3.2	6.7611	4.5	0.3772	3.2	2098	63	2081	42	2063	61	58.02	1.66	2098	63
J02_1_t3_Grain159	0.0595	4.0	10.2775	2.7	0.7982	4.8	0.0973	2.7	585	93	596	22	599	17	83.13	-2.24	599	17
J02_1_t3_Grain16	0.0748	3.0	5.5340	2.5	1.8636	3.9	0.1807	2.5	1063	67	1068	27	1071	28	88.52	-0.72	1071	28
J02_1_t3_Grain160	0.0611	6.5	10.7296	3.8	0.7852	7.5	0.0932	3.8	643	144	588	34	574	22	50.13	10.63	574	22
J02_1_t3_Grain161	0.0541	8.6	15.2207	4.8	0.4901	9.8	0.0657	4.8	NA	NA	405	33	410	20	77.83	NA	410	20
J02_1_t3_Grain162	0.0497	6.4	21.9298	3.6	0.3125	7.4	0.0456	3.6	NA	NA	276	18	287	11	27.15	NA	287	11
J02_1_t3_Grain163	0.1039	2.9	3.3647	2.5	4.2576	3.8	0.2972	2.5	1695	60	1685	33	1677	43	74.99	1.03	1695	60
J02_1_t3_Grain164	0.0650	5.5	8.1169	3.5	1.1041	6.5	0.1232	3.5	774	120	755	36	749	27	75.58	3.28	749	27
J02_1_t3_Grain165	0.0505	6.8	21.7391	4.0	0.3203	7.9	0.0460	4.0	NA	NA	282	20	290	12	50.02	NA	290	12
J02_1_t3_Grain166	0.0596	5.7	10.2145	3.2	0.8045	6.5	0.0979	3.2	589	128	599	30	602	20	88.52	-2.21	602	20
J02_1_t3_Grain17	0.1149	4.9	3.2103	4.1	4.9349	6.4	0.3115	4.1	1878	93	1808	55	1748	67	9.66	6.93	1878	93
J02_1_t3_Grain18	0.0595	5.8	9.9404	3.8	0.8253	6.9	0.1006	3.8	585	130	611	32	618	24	68.96	-5.55	618	24
J02_1_t3_Grain19	0.0580	5.7	10.9170	3.5	0.7325	6.7	0.0916	3.5	530	129	558	29	565	20	68.17	-6.65	565	20
J02_1_t3_Grain20	0.0601	6.9	10.2564	4.3	0.8079	8.1	0.0975	4.3	607	153	601	37	600	26	93.65	1.22	600	26
J02_1_t3_Grain21	0.0617	5.7	11.4679	3.7	0.7418	6.8	0.0872	3.7	664	127	563	30	539	21	14.47	18.80	539	21
J02_1_t3_Grain22	0.0612	4.9	9.0744	3.3	0.9299	5.9	0.1102	3.3	646	111	668	30	674	23	69.94	-4.28	674	23
J02_1_t3_Grain23	0.0638	6.8	10.5597	4.5	0.8331	8.2	0.0947	4.5	735	149	615	38	583	26	9.09	20.64	583	26
J02_1_t3_Grain25	0.0530	5.4	14.8368	3.4	0.4925	6.4	0.0674	3.4	NA	NA	407	22	420	15	19.21	NA	420	15
J02_1_t3_Grain26	0.0831	2.9	4.5208	2.4	2.5345	3.7	0.2212	2.4	1272	64	1282	29	1288	32	70.42	-1.31	1288	32
J02_1_t3_Grain29	0.0531	5.0	21.5378	3.1	0.3399	5.9	0.0464	3.1	NA	NA	297	16	293	10	60.96	NA	293	10
J02_1_t3_Grain30	0.0576	5.9	19.7628	3.6	0.4019	6.9	0.0506	3.6	NA	NA	343	21	318	12	2.10	NA	318	12
J02_1_t3_Grain31	0.0812	3.8	5.2938	3.1	2.1149	4.8	0.1889	3.1	1226	80	1154	35	1115	34	7.59	9.04	1115	34
J02_1_t3_Grain32	0.0593	4.8	10.2459	3.3	0.7980	5.8	0.0976	3.3	578	110	596	27	600	20	71.43	-3.84	600	20
J02_1_t3_Grain33	0.0583	5.3	10.0200	3.2	0.8022	6.2	0.0998	3.2	541	120	598	28	613	20	39.30	-13.34	613	20
J02_1_t3_Grain34	0.0651	7.4	9.8232	4.2	0.9138	8.5	0.1018	4.2	778	159	659	42	625	26	10.70	19.63	625	26

J02_1_t3_Grain35	0.0592	7.1	10.2775	4.2	0.7942	8.3	0.0973	4.2	574	159	594	38	599	25	81.13	-4.20	599	25
J02_1_t3_Grain36	0.0521	7.1	15.0602	4.0	0.4770	8.1	0.0664	4.0	NA	NA	396	27	414	17	24.63	NA	414	17
J02_1_t3_Grain37	0.0599	7.3	9.8912	4.3	0.8350	8.5	0.1011	4.3	600	162	616	40	621	27	83.84	-3.48	621	27
J02_1_t3_Grain38	0.0618	10.6	10.3842	5.7	0.8206	12.0	0.0963	5.7	667	230	608	55	593	33	60.48	11.17	593	33
J02_1_t3_Grain39	0.0591	5.1	11.1483	3.2	0.7309	6.1	0.0897	3.2	571	117	557	27	554	19	81.40	2.98	554	19
J02_1_t3_Grain41	0.0594	5.0	10.2249	3.3	0.8010	6.0	0.0978	3.3	582	115	597	28	602	20	77.93	-3.39	602	20
J02_1_t3_Grain42	0.0605	6.4	10.0908	3.9	0.8267	7.5	0.0991	3.9	622	142	612	35	609	24	88.62	1.99	609	24
J02_1_t3_Grain43	0.0632	6.0	10.2459	3.9	0.8505	7.1	0.0976	3.9	715	131	625	34	600	23	20.93	16.03	600	23
J02_1_t3_Grain44	0.1299	1.5	2.6774	1.9	6.6896	2.4	0.3735	1.9	2097	38	2071	24	2046	40	8.67	2.42	2097	38
J02_1_t3_Grain45	0.0669	4.0	6.7843	2.9	1.3596	4.9	0.1474	2.9	835	89	872	30	886	26	42.13	-6.20	886	26
J02_1_t3_Grain46	0.0609	5.6	10.6496	3.6	0.7885	6.6	0.0939	3.6	636	124	590	30	579	21	47.54	8.99	579	21
J02_1_t3_Grain47	0.0559	10.3	10.2145	5.4	0.7546	11.7	0.0979	5.4	448	234	571	51	602	32	26.22	-34.28	602	32
J02_1_t3_Grain48	0.0593	5.2	9.9305	3.4	0.8234	6.2	0.1007	3.4	578	118	610	29	619	22	57.70	-6.98	619	22
J02_1_t3_Grain49	0.0599	5.4	10.3306	3.5	0.7995	6.4	0.0968	3.5	600	121	597	30	596	21	95.33	0.72	596	21
J02_1_t3_Grain50	0.0591	8.1	9.5785	4.6	0.8507	9.3	0.1044	4.6	571	181	625	44	640	29	58.68	-12.15	640	29
J02_1_t3_Grain51	0.0513	5.4	21.2766	3.6	0.3324	6.5	0.0470	3.6	NA	NA	291	17	296	11	54.89	NA	296	11
J02_1_t3_Grain52	0.0609	6.0	10.9051	3.7	0.7700	7.1	0.0917	3.7	636	134	580	32	566	22	42.05	11.03	566	22
J02_1_t3_Grain53	0.1129	3.0	3.1046	2.7	5.0140	4.1	0.3221	2.7	1847	62	1822	37	1800	48	41.07	2.53	1847	62
J02_1_t3_Grain54	0.0607	5.4	10.4384	3.4	0.8018	6.4	0.0958	3.4	629	121	598	29	590	21	62.47	6.18	590	21
J02_1_t3_Grain55	0.0609	7.5	9.2251	4.5	0.9102	8.8	0.1084	4.5	636	166	657	43	663	30	79.00	-4.36	663	30
J02_1_t3_Grain56	0.0771	4.4	5.5772	3.2	1.9061	5.5	0.1793	3.2	1124	94	1083	38	1063	34	32.12	5.40	1063	34
J02_1_t3_Grain57	0.1104	2.1	3.0798	2.3	4.9426	3.1	0.3247	2.3	1806	48	1810	29	1813	42	82.52	-0.37	1806	48
J02_1_t3_Grain58	0.1895	2.9	1.8868	3.1	13.8480	4.2	0.5300	3.1	2738	53	2739	42	2741	76	94.89	-0.13	2738	53
J02_1_t3_Grain59	0.0600	7.8	10.0503	4.4	0.8231	8.9	0.0995	4.4	604	172	610	41	611	27	94.58	-1.31	611	27
J02_1_t3_Grain60	0.0580	6.7	11.0011	3.9	0.7269	7.8	0.0909	3.9	530	151	555	34	561	22	72.19	-5.87	561	22
J02_1_t3_Grain61	0.0524	6.8	18.6567	3.6	0.3873	7.7	0.0536	3.6	NA	NA	332	22	337	13	73.26	NA	337	13
J02_1_t3_Grain62	0.0985	2.3	3.6179	2.2	3.7538	3.2	0.2764	2.2	1596	52	1583	28	1573	36	58.20	1.42	1596	52
J02_1_t3_Grain64	0.0695	2.9	6.4767	2.4	1.4796	3.8	0.1544	2.4	914	69	922	25	926	24	77.76	-1.31	926	24
J02_1_t3_Grain65	0.0528	4.0	21.4592	2.9	0.3393	5.0	0.0466	2.9	NA	NA	297	13	294	9	63.07	NA	294	9

J02_1_t3_Grain66	0.0582	4.5	11.0497	3.0	0.7262	5.4	0.0905	3.0	537	103	554	24	558	18	75.91	-3.94	558	18
J02_1_t3_Grain67	0.0610	5.9	9.9701	3.6	0.8436	7.0	0.1003	3.6	639	132	621	33	616	23	80.06	3.61	616	23
J02_1_t3_Grain68	0.0767	6.1	5.5679	4.1	1.8993	7.3	0.1796	4.1	1113	126	1081	50	1065	42	61.86	4.37	1065	42
J02_1_t3_Grain69	0.0543	9.7	15.9236	5.3	0.4702	11.1	0.0628	5.3	NA	NA	391	36	393	21	93.40	NA	393	21
J02_1_t3_Grain70	0.0649	7.4	10.1833	4.5	0.8787	8.7	0.0982	4.5	771	160	640	42	604	27	12.73	21.69	604	27
J02_1_t3_Grain71	0.1270	2.2	2.6911	2.4	6.5070	3.3	0.3716	2.4	2057	48	2047	31	2037	49	59.65	0.97	2057	48
J02_1_t3_Grain72	0.0560	6.3	16.4745	3.6	0.4687	7.2	0.0607	3.6	NA	NA	390	24	380	14	44.75	NA	380	14
J02_1_t3_Grain73	0.0553	6.1	11.4548	3.7	0.6656	7.2	0.0873	3.7	424	142	518	30	540	21	14.54	-27.14	540	21
J02_1_t3_Grain75	0.1371	3.1	2.5336	3.0	7.4612	4.3	0.3947	3.0	2191	60	2168	41	2145	61	46.04	2.11	2191	60
J02_1_t3_Grain76	0.0711	3.4	5.6625	2.7	1.7313	4.3	0.1766	2.7	960	76	1020	29	1048	29	12.54	-9.17	1048	29
J02_1_t3_Grain77	0.0621	6.1	9.9502	3.9	0.8605	7.2	0.1005	3.9	678	134	630	35	617	24	52.58	8.89	617	24
J02_1_t3_Grain78	0.0515	6.7	20.2840	3.7	0.3501	7.7	0.0493	3.7	NA	NA	305	20	310	12	66.51	NA	310	12
J02_1_t3_Grain79	0.0592	4.0	10.5263	2.9	0.7754	4.9	0.0950	2.9	574	94	583	23	585	18	85.83	-1.84	585	18
J02_1_t3_Grain80	0.0641	5.5	10.0806	3.7	0.8767	6.6	0.0992	3.7	745	120	639	32	610	23	9.25	18.15	610	23
J02_1_t3_Grain81	0.0614	4.4	10.4712	2.9	0.8085	5.3	0.0955	2.9	653	101	602	25	588	18	29.41	9.99	588	18
J02_1_t3_Grain82	0.0617	8.1	10.2669	4.7	0.8286	9.3	0.0974	4.7	664	177	613	43	599	28	62.04	9.73	599	28
J02_1_t3_Grain83	0.0605	3.5	9.8912	2.6	0.8433	4.3	0.1011	2.6	622	82	621	21	621	17	99.03	0.10	621	17
J02_1_t3_Grain84	0.0550	4.8	22.1729	3.2	0.3420	5.7	0.0451	3.2	NA	NA	299	15	284	10	10.51	NA	284	10
J02_1_t3_Grain85	0.0532	5.7	21.2495	3.5	0.3452	6.7	0.0471	3.5	NA	NA	301	18	296	11	60.07	NA	296	11
J02_1_t3_Grain86	0.0574	6.1	10.5485	3.8	0.7503	7.2	0.0948	3.8	507	138	568	32	584	23	36.75	-15.18	584	23
J02_1_t3_Grain87	0.0597	3.7	9.8522	2.7	0.8355	4.6	0.1015	2.7	593	88	617	22	623	18	60.18	-5.14	623	18
J02_1_t3_Grain88	0.0612	5.5	10.6724	3.5	0.7907	6.5	0.0937	3.5	646	123	592	30	577	21	38.49	10.66	577	21
J02_1_t3_Grain89	0.0725	4.9	5.8106	3.6	1.7204	6.1	0.1721	3.6	1000	105	1016	40	1024	37	71.11	-2.37	1024	37
J02_1_t3_Grain90	0.0590	8.8	9.3110	4.7	0.8737	10.0	0.1074	4.7	567	196	638	48	658	31	46.28	-15.96	658	31
J02_1_t3_Grain91	0.0820	3.0	4.9727	2.5	2.2737	3.9	0.2011	2.5	1246	65	1204	29	1181	31	14.96	5.16	1181	31
J02_1_t3_Grain93	0.0618	5.5	9.7943	3.7	0.8700	6.6	0.1021	3.7	667	123	636	32	627	23	60.31	6.07	627	23
J02_1_t3_Grain94	0.0598	3.6	9.7371	2.7	0.8468	4.5	0.1027	2.7	596	85	623	22	630	18	51.61	-5.68	630	18
J02_1_t3_Grain96	0.0605	4.4	9.9404	3.0	0.8392	5.3	0.1006	3.0	622	100	619	25	618	20	95.88	0.58	618	20
J02_1_t3_Grain97	0.0576	8.6	16.0514	4.8	0.4948	9.9	0.0623	4.8	NA	NA	408	34	390	19	28.36	NA	390	19

J02_1_t3_Grain98	0.0645	9.4	9.5057	4.9	0.9356	10.6	0.1052	4.9	758	203	671	53	645	31	33.70	14.94	645	31
J02_1_t3_Grain99	0.0584	5.2	9.9206	3.3	0.8117	6.2	0.1008	3.3	545	119	603	29	619	21	33.98	-13.64	619	21
J02_2_Grain01	0.0563	7.7	11.3507	3.4	0.6839	8.4	0.0881	3.4	464	174	529	35	544	19	36	-17	544	19
J02_2_Grain02	0.0589	4.0	10.3842	2.4	0.7821	4.7	0.0963	2.4	563	94	587	22	593	16	62	-5	593	16
J02_2_Grain03	0.0864	3.0	4.1580	2.3	2.8650	3.8	0.2405	2.3	1347	65	1373	30	1389	34	30	-3	1389	34
J02_2_Grain05	0.0533	6.0	14.9701	2.7	0.4909	6.6	0.0668	2.7	NA	NA	406	23	417	12	37	NA	417	12
J02_2_Grain06	0.1301	1.7	2.6330	2.0	6.8129	2.6	0.3798	2.0	2099	40	2087	26	2075	43	49	1	2099	40
J02_2_Grain07	0.1913	1.6	1.9150	2.1	13.7738	2.6	0.5222	2.1	2753	36	2734	28	2709	55	28	2	2753	36
J02_2_Grain08	0.0626	4.8	10.2564	2.7	0.8416	5.5	0.0975	2.7	695	108	620	26	600	17	15	14	600	17
J02_2_Grain09	0.0503	5.9	21.6450	2.8	0.3204	6.6	0.0462	2.8	NA	NA	282	16	291	9	33	NA	291	9
J02_2_Grain10	0.0716	5.3	5.5249	2.9	1.7869	6.0	0.1810	2.9	975	112	1041	40	1072	31	15	-10	1072	31
J02_2_Grain11	0.0604	4.8	9.9800	2.7	0.8345	5.5	0.1002	2.7	618	110	616	26	616	18	97	0	616	18
J02_2_Grain12	0.0863	2.9	4.2626	2.3	2.7915	3.7	0.2346	2.3	1345	63	1353	29	1359	33	76	-1	1359	33
J02_2_Grain13	0.0597	4.8	11.6009	2.5	0.7095	5.4	0.0862	2.5	593	109	544	23	533	15	35	10	533	15
J02_2_Grain14	0.1048	3.0	3.3190	2.4	4.3537	3.8	0.3013	2.4	1711	62	1704	34	1698	41	79	1	1711	62
J02_2_Grain15	0.1014	2.4	3.4758	2.2	4.0223	3.3	0.2877	2.2	1650	54	1639	29	1630	37	65	1	1650	54
J02_2_Grain16	0.0744	4.4	6.0753	2.6	1.6885	5.1	0.1646	2.6	1052	95	1004	34	982	26	28	7	982	26
J02_2_Grain17	0.0856	2.4	4.5746	2.0	2.5800	3.1	0.2186	2.0	1329	55	1295	25	1274	28	14	4	1274	28
J02_2_Grain18	0.0534	5.8	21.9298	2.7	0.3357	6.4	0.0456	2.7	NA	NA	294	17	287	9	47	NA	287	9
J02_2_Grain19	0.0513	5.6	21.2314	2.8	0.3331	6.3	0.0471	2.8	NA	NA	292	16	297	9	52	NA	297	9
Rejected Analyses																		
J02_1_t3_Grain04	0.0665	1.9	9.2166	2.6	0.9948	3.2	0.1085	2.6	822	51	701	17	664	18	0.00	19.23		
J02_1_t3_Grain103	0.0575	4.3	16.6945	3.4	0.4749	5.5	0.0599	3.4	NA	NA	395	18	375	13	0.92	NA		
J02_1_t3_Grain24	0.1990	11.7	9.4251	8.3	2.9112	14.3	0.1061	8.3	2818	194	1385	109	650	52	0.00	76.93		
J02_1_t3_Grain40	0.0889	3.8	4.6707	3.1	2.6243	4.9	0.2141	3.1	1402	78	1307	37	1251	38	0.23	10.80		
J02_1_t3_Grain63	0.0926	5.7	8.5324	5.1	1.4964	7.7	0.1172	5.1	1480	113	929	47	714	36	0.00	51.72		
J02_1_t3_Grain92	0.1547	1.8	2.5381	2.2	8.4040	2.8	0.3940	2.2	2399	40	2276	28	2141	47	0.00	10.72		

20EJ03 - West Bonne Bay F-12 – Hibernia Formation (Upper) – Core # 1, boxes 24-30

	Isotopic ratios[2]								Isotopic ages									
Spot Name	$^{207}Pb/^{206}Pb$	$2s_x$ (%)	$^{238}U/^{206}Pb$	$2s_x$ (%)	$^{207}Pb/^{235}Pb$	$2s_x$ (%)	$^{206}Pb/^{238}U$	$2s_x$ (%)	$^{207}Pb/^{206}Pb$	$2s_{total}$ (Ma)	$^{207}Pb/^{235}Pb$	$2s_{total}$ (Ma)	$^{206}Pb/^{238}U$	$2s_{total}$ (Ma)	Prob. Conc. (%)	% conc[3]	U-Pb Best Age[4]	$2s_{total}$ (Ma)
J03_1_Grain01	0.0606	4.1	10.3627	2.7	0.8063	4.9	0.0965	2.7	625	95	600	23	594	17	64.22	4.99	594	17
J03_1_Grain02	0.1259	1.9	2.7367	2.1	6.3430	2.9	0.3654	2.1	2041	44	2024	28	2008	43	33.65	1.65	2041	44
J03_1_t2_Grain01	0.0541	6.6	14.5349	3.8	0.5132	7.7	0.0688	3.8	NA	NA	421	27	429	17	52.70	NA	429	17
J03_1_t2_Grain04	0.0727	4.0	5.9172	3.2	1.6940	5.1	0.1690	3.2	1006	87	1006	34	1007	32	98.48	-0.10	1007	32
J03_1_t2_Grain06	0.0603	5.0	10.4384	3.1	0.7965	5.9	0.0958	3.1	614	112	595	27	590	19	73.51	4.01	590	19
J03_1_t2_Grain08	0.0766	3.4	5.8005	2.8	1.8208	4.4	0.1724	2.8	1111	74	1053	30	1025	29	12.09	7.69	1025	29
J03_1_t2_Grain09	0.0729	3.0	5.5218	2.4	1.8203	3.8	0.1811	2.4	1011	68	1053	26	1073	27	25.78	-6.11	1073	27
J03_1_t3_Grain01	0.0562	6.2	10.4493	3.8	0.7416	7.3	0.0957	3.8	460	143	563	32	589	23	14.85	-28.00	589	23
J03_1_t3_Grain02	0.0621	5.7	10.1937	3.6	0.8400	6.8	0.0981	3.6	678	127	619	32	603	22	40.60	10.96	603	22
J03_1_t3_Grain03	0.0745	5.6	5.9067	3.9	1.7391	6.9	0.1693	3.9	1055	117	1023	45	1008	39	58.51	4.43	1008	39
J03_1_t3_Grain04	0.0614	4.7	10.6610	3.3	0.7941	5.7	0.0938	3.3	653	107	593	27	578	20	31.52	11.53	578	20
J03_1_t3_Grain05	0.1027	2.9	3.4904	2.6	4.0569	3.9	0.2865	2.6	1673	61	1646	34	1624	43	24.15	2.96	1673	61
J03_1_t3_Grain06	0.0529	8.2	17.2414	4.9	0.4230	9.5	0.0580	4.9	NA	NA	358	29	363	18	77.04	NA	363	18
J03_1_t3_Grain07	0.0603	4.6	10.0200	3.0	0.8298	5.5	0.0998	3.0	614	105	613	26	613	19	98.65	0.18	613	19
J03_1_t3_Grain08	0.0599	4.2	10.7527	2.9	0.7681	5.1	0.0930	2.9	600	97	579	23	573	18	66.42	4.45	573	18
J03_1_t3_Grain09	0.0821	3.9	4.9068	3.0	2.3070	4.9	0.2038	3.0	1248	81	1214	36	1196	36	42.73	4.18	1196	36
J03_1_t3_Grain10	0.0551	8.0	21.7391	4.1	0.3495	9.0	0.0460	4.1	NA	NA	304	24	290	12	21.08	NA	290	12
J03_1_t3_Grain100	0.1319	1.5	2.5253	2.0	7.2018	2.5	0.3960	2.0	2123	38	2137	25	2151	44	36.45	-1.28	2123	38
J03_1_t3_Grain101	0.1593	1.1	2.1146	1.6	10.3869	1.9	0.4729	1.6	2448	32	2470	22	2496	43	3.68	-1.96	2448	32
J03_1_t3_Grain102	0.0603	6.2	11.3895	3.9	0.7300	7.3	0.0878	3.9	614	138	557	32	543	21	44.81	11.69	543	21
J03_1_t3_Grain103	0.0677	4.4	8.3472	3.3	1.1183	5.5	0.1198	3.3	859	97	762	30	729	24	2.48	15.12	729	24
J03_1_t3_Grain105	0.0528	4.1	21.2404	2.7	0.3427	4.9	0.0471	2.7	NA	NA	299	13	297	9	70.78	NA	297	9
J03_1_t3_Grain106	0.0521	9.2	21.6920	4.9	0.3312	10.5	0.0461	4.9	NA	NA	290	27	291	14	99.55	NA	291	14
J03_1_t3_Grain107	0.0587	6.1	9.7847	3.7	0.8272	7.1	0.1022	3.7	556	137	612	33	627	23	45.10	-12.82	627	23
J03_1_t3_Grain108	0.0587	4.1	10.5152	2.8	0.7697	5.0	0.0951	2.8	556	97	580	23	586	17	62.66	-5.33	586	17

J03_1_t3_Grain109	0.0626	6.6	10.1420	3.8	0.8510	7.6	0.0986	3.8	695	145	625	36	606	24	36.97	12.74	606	24
J03_1_t3_Grain11	0.0585	4.7	11.3636	3.2	0.7098	5.7	0.0880	3.2	549	107	545	25	544	18	94.41	0.88	544	18
J03_1_t3_Grain110	0.0558	5.9	16.3132	3.5	0.4716	6.8	0.0613	3.5	NA	NA	392	23	384	14	49.26	NA	384	14
J03_1_t3_Grain111	0.0565	6.5	15.6006	3.8	0.4994	7.5	0.0641	3.8	NA	NA	411	26	401	16	46.86	NA	401	16
J03_1_t3_Grain112	0.0580	22.0	10.8932	9.4	0.7341	23.9	0.0918	9.4	530	498	559	103	566	52	89.23	-6.87	566	52
J03_1_t3_Grain113	0.0604	4.4	10.5485	3.0	0.7895	5.3	0.0948	3.0	618	101	591	25	584	18	64.81	5.51	584	18
J03_1_t3_Grain115	0.0669	10.1	9.6061	5.5	0.9602	11.4	0.1041	5.5	835	213	683	57	638	34	19.44	23.51	638	34
J03_1_t3_Grain116	0.0505	6.3	19.3798	3.6	0.3593	7.3	0.0516	3.6	NA	NA	312	20	324	12	17.17	NA	324	12
J03_1_t3_Grain117	0.0524	6.3	18.4843	3.5	0.3909	7.2	0.0541	3.5	NA	NA	335	21	340	12	68.79	NA	340	12
J03_1_t3_Grain118	0.0545	6.3	21.8341	3.4	0.3442	7.2	0.0458	3.4	NA	NA	300	19	289	10	24.62	NA	289	10
J03_1_t3_Grain119	0.0553	5.3	21.0526	3.4	0.3622	6.3	0.0475	3.4	NA	NA	314	17	299	11	10.47	NA	299	11
J03_1_t3_Grain12	0.0544	6.0	15.1515	3.5	0.4950	6.9	0.0660	3.5	NA	NA	408	24	412	15	76.81	NA	412	15
J03_1_t3_Grain120	0.2041	1.8	1.7665	2.3	15.9308	3.0	0.5661	2.3	2859	39	2873	31	2892	62	48.59	-1.14	2859	39
J03_1_t3_Grain121	0.0570	5.8	13.7931	3.8	0.5698	6.9	0.0725	3.8	NA	NA	458	26	451	18	58.14	NA	451	18
J03_1_t3_Grain122	0.0589	3.1	10.3093	2.4	0.7877	3.9	0.0970	2.4	563	76	590	19	597	16	46.60	-5.93	597	16
J03_1_t3_Grain123	0.0524	5.4	21.7817	3.2	0.3317	6.3	0.0459	3.2	NA	NA	291	16	289	10	84.80	NA	289	10
J03_1_t3_Grain124	0.0599	6.6	9.9800	4.1	0.8276	7.7	0.1002	4.1	600	147	612	36	616	25	87.52	-2.60	616	25
J03_1_t3_Grain126	0.0591	5.0	9.8522	3.1	0.8271	5.9	0.1015	3.1	571	115	612	28	623	20	48.78	-9.18	623	20
J03_1_t3_Grain127	0.1103	2.9	3.1476	2.8	4.8316	4.0	0.3177	2.8	1804	60	1790	36	1778	48	53.40	1.43	1804	60
J03_1_t3_Grain128	0.0747	6.5	6.1576	4.2	1.6727	7.7	0.1624	4.2	1060	134	998	50	970	39	28.17	8.52	970	39
J03_1_t3_Grain129	0.0559	6.3	17.3913	3.6	0.4432	7.3	0.0575	3.6	NA	NA	372	23	360	14	35.48	NA	360	14
J03_1_t3_Grain13	0.0756	4.2	5.3533	3.6	1.9472	5.6	0.1868	3.6	1084	91	1097	39	1104	39	64.61	-1.80	1104	39
J03_1_t3_Grain130	0.0512	8.5	21.2766	4.7	0.3318	9.7	0.0470	4.7	NA	NA	291	25	296	14	62.49	NA	296	14
J03_1_t3_Grain131	0.0640	4.1	8.3682	2.8	1.0545	4.9	0.1195	2.8	742	93	731	27	728	21	83.99	1.88	728	21
J03_1_t3_Grain132	0.1673	2.0	2.1142	2.3	10.9108	3.1	0.4730	2.3	2531	42	2516	31	2497	56	35.42	1.35	2531	42
J03_1_t3_Grain133	0.0536	5.1	21.4731	3.1	0.3442	6.0	0.0466	3.1	NA	NA	300	16	293	10	44.21	NA	293	10
J03_1_t3_Grain134	0.0591	6.3	14.0449	3.7	0.5802	7.3	0.0712	3.7	NA	NA	465	28	443	17	18.88	NA	443	17
J03_1_t3_Grain135	0.0598	6.3	10.5263	3.9	0.7833	7.4	0.0950	3.9	596	142	587	34	585	23	89.90	1.90	585	23
J03_1_t3_Grain136	0.0604	3.2	9.2678	2.4	0.8986	4.0	0.1079	2.4	618	77	651	20	661	17	40.12	-6.89	661	17

J03_1_t3_Grain139	0.1092	3.2	3.2468	2.9	4.6374	4.3	0.3080	2.9	1786	65	1756	38	1731	49	36.28	3.09	1786	65
J03_1_t3_Grain14	0.0872	2.1	4.1615	2.1	2.8892	3.0	0.2403	2.1	1365	51	1379	25	1388	31	49.98	-1.71	1388	31
J03_1_t3_Grain140	0.0612	3.9	10.2041	2.7	0.8269	4.8	0.0980	2.7	646	91	612	23	603	18	46.51	6.75	603	18
J03_1_t3_Grain141	0.0571	4.5	11.3895	2.9	0.6912	5.3	0.0878	2.9	495	104	534	23	543	17	52.21	-9.51	543	17
J03_1_t3_Grain142	0.0642	7.1	9.9900	4.2	0.8861	8.3	0.1001	4.2	748	154	644	40	615	26	21.45	17.81	615	26
J03_1_t3_Grain143	0.0550	5.5	22.0410	3.3	0.3441	6.5	0.0454	3.3	NA	NA	300	17	286	10	14.13	NA	286	10
J03_1_t3_Grain144	0.0552	5.9	11.5075	3.6	0.6614	6.9	0.0869	3.6	420	137	515	28	537	20	19.92	-27.80	537	20
J03_1_t3_Grain146	0.0815	4.0	4.4248	3.2	2.5396	5.1	0.2260	3.2	1234	84	1283	38	1314	41	19.66	-6.48	1314	41
J03_1_t3_Grain147	0.0783	4.4	4.8544	3.2	2.2240	5.5	0.2060	3.2	1154	93	1189	39	1207	39	43.46	-4.59	1207	39
J03_1_t3_Grain148	0.0547	4.5	14.3678	2.9	0.5249	5.4	0.0696	2.9	NA	NA	428	19	434	13	61.40	NA	434	13
J03_1_t3_Grain149	0.0572	5.1	10.1937	3.2	0.7737	6.0	0.0981	3.2	499	117	582	27	603	20	15.53	-20.83	603	20
J03_1_t3_Grain15	0.0603	4.7	9.7561	3.1	0.8522	5.6	0.1025	3.1	614	107	626	27	629	20	84.60	-2.39	629	20
J03_1_t3_Grain150	0.0585	5.1	9.7182	3.4	0.8300	6.1	0.1029	3.4	549	117	614	29	631	22	30.42	-15.10	631	22
J03_1_t3_Grain151	0.0623	7.3	10.1937	4.1	0.8427	8.4	0.0981	4.1	684	161	621	40	603	25	41.15	11.86	603	25
J03_1_t3_Grain152	0.0750	4.2	5.8685	3.1	1.7621	5.2	0.1704	3.1	1069	90	1032	35	1014	32	33.56	5.07	1014	32
J03_1_t3_Grain153	0.1099	1.7	3.0941	1.9	4.8975	2.5	0.3232	1.9	1798	42	1802	24	1805	36	81.08	-0.42	1798	42
J03_1_t3_Grain155	0.0598	6.5	11.0254	3.9	0.7478	7.6	0.0907	3.9	596	145	567	34	560	22	71.86	6.15	560	22
J03_1_t3_Grain156	0.1334	1.5	2.6233	1.8	7.0115	2.3	0.3812	1.8	2143	38	2113	24	2082	40	6.14	2.86	2143	38
J03_1_t3_Grain157	0.0617	8.0	9.2593	4.0	0.9188	8.9	0.1080	4.0	664	174	662	44	661	27	98.21	0.39	661	27
J03_1_t3_Grain158	0.0745	3.1	5.5835	2.5	1.8397	4.0	0.1791	2.5	1055	70	1060	28	1062	28	86.74	-0.66	1062	28
J03_1_t3_Grain159	0.0508	4.5	21.2089	3.0	0.3303	5.4	0.0472	3.0	NA	NA	290	14	297	10	36.12	NA	297	10
J03_1_t3_Grain160	0.0615	6.4	10.2881	4.0	0.8242	7.6	0.0972	4.0	657	142	610	35	598	24	54.95	8.95	598	24
J03_1_t3_Grain161	0.0716	2.2	6.3613	2.1	1.5519	3.1	0.1572	2.1	975	55	951	21	941	22	18.62	3.43	941	22
J03_1_t3_Grain17	0.0603	10.0	11.3895	5.4	0.7300	11.3	0.0878	5.4	614	219	557	49	543	29	61.88	11.69	543	29
J03_1_t3_Grain19	0.1912	2.7	1.9305	3.2	13.6559	4.2	0.5180	3.2	2753	51	2726	42	2691	76	18.25	2.25	2753	51
J03_1_t3_Grain20	0.0706	4.3	6.0496	2.9	1.6091	5.1	0.1653	2.9	946	93	974	33	986	29	48.87	-4.26	986	29
J03_1_t3_Grain21	0.0578	10.3	10.8225	5.4	0.7364	11.7	0.0924	5.4	522	230	560	51	570	31	74.14	-9.10	570	31
J03_1_t3_Grain22	0.0571	7.3	9.6339	4.4	0.8172	8.5	0.1038	4.4	495	165	606	39	637	28	15.55	-28.51	637	28
J03_1_t3_Grain23	0.0689	9.2	9.8328	5.4	0.9661	10.6	0.1017	5.4	896	192	686	54	624	33	4.42	30.30	624	33

J03_1_t3_Grain24	0.1108	2.1	3.1124	2.2	4.9085	3.0	0.3213	2.2	1813	47	1804	28	1796	40	65.22	0.91	1813	47
J03_1_t3_Grain25	0.0535	7.9	16.3132	4.5	0.4522	9.1	0.0613	4.5	NA	NA	379	29	384	17	78.87	NA	384	17
J03_1_t3_Grain26	0.0612	4.2	10.0301	2.8	0.8413	5.1	0.0997	2.8	646	96	620	24	613	18	65.13	5.20	613	18
J03_1_t3_Grain27	0.0616	6.0	10.0402	3.7	0.8459	7.1	0.0996	3.7	660	134	622	34	612	23	56.73	7.30	612	23
J03_1_t3_Grain28	0.0632	6.7	9.6899	4.1	0.8993	7.8	0.1032	4.1	715	146	651	38	633	26	43.71	11.45	633	26
J03_1_t3_Grain29	0.0553	8.1	15.9236	4.4	0.4788	9.2	0.0628	4.4	NA	NA	397	31	393	17	77.71	NA	393	17
J03_1_t3_Grain30	0.0497	8.7	48.6381	4.4	0.1409	9.7	0.0206	4.4	NA	NA	134	12	131	6	68.52	NA	131	6
J03_1_t3_Grain31	0.0532	7.1	21.0970	4.1	0.3477	8.2	0.0474	4.1	NA	NA	303	22	299	13	71.89	NA	299	13
J03_1_t3_Grain32	0.0594	5.0	10.4603	3.4	0.7830	6.0	0.0956	3.4	582	114	587	28	589	21	93.08	-1.17	589	21
J03_1_t3_Grain33	0.0559	7.9	11.1235	4.3	0.6929	9.0	0.0899	4.3	448	179	535	38	555	24	31.29	-23.76	555	24
J03_1_t3_Grain34	0.0565	4.7	14.6413	3.0	0.5321	5.6	0.0683	3.0	NA	NA	433	20	426	14	48.52	NA	426	14
J03_1_t3_Grain35	0.1067	4.0	3.2468	3.2	4.5312	5.1	0.3080	3.2	1744	78	1737	44	1731	53	85.30	0.74	1744	78
J03_1_t3_Grain36	0.0601	3.8	11.2486	2.8	0.7367	4.7	0.0889	2.8	607	88	560	21	549	16	35.96	9.58	549	16
J03_1_t3_Grain37	0.0551	6.0	16.3132	3.6	0.4657	7.0	0.0613	3.6	NA	NA	388	23	384	14	71.22	NA	384	14
J03_1_t3_Grain38	0.0615	5.1	8.3893	3.5	1.0108	6.2	0.1192	3.5	657	114	709	32	726	26	31.85	-10.53	726	26
J03_1_t3_Grain39	0.0528	5.2	21.5983	3.2	0.3371	6.1	0.0463	3.2	NA	NA	295	16	292	10	70.22	NA	292	10
J03_1_t3_Grain40	0.0600	6.5	16.5563	4.1	0.4997	7.7	0.0604	4.1	NA	NA	411	26	378	16	2.45	NA	378	16
J03_1_t3_Grain42	0.0597	5.8	10.2041	3.5	0.8067	6.7	0.0980	3.5	593	130	601	31	603	21	90.74	-1.68	603	21
J03_1_t3_Grain43	0.1287	3.6	2.5253	3.6	7.0271	5.0	0.3960	3.6	2080	69	2115	46	2151	69	24.68	-3.38	2080	69
J03_1_t3_Grain44	0.0558	7.9	14.2248	4.0	0.5409	8.8	0.0703	4.0	NA	NA	439	32	438	18	95.51	NA	438	18
J03_1_t3_Grain45	0.0582	6.3	10.5263	3.6	0.7623	7.3	0.0950	3.6	537	143	575	33	585	22	58.89	-8.89	585	22
J03_1_t3_Grain46	0.0632	4.7	10.2459	3.1	0.8505	5.7	0.0976	3.1	715	105	625	27	600	20	11.57	16.03	600	20
J03_1_t3_Grain47	0.0536	4.9	16.3399	3.1	0.4523	5.8	0.0612	3.1	NA	NA	379	19	383	13	71.58	NA	383	13
J03_1_t3_Grain49	0.0622	4.5	11.8765	2.9	0.7221	5.4	0.0842	2.9	681	102	552	24	521	16	3.64	23.47	521	16
J03_1_t3_Grain50	0.1872	1.4	1.9531	1.9	13.2153	2.4	0.5120	1.9	2718	34	2695	26	2665	51	8.11	1.93	2718	34
J03_1_t3_Grain51	0.0599	6.3	9.1491	4.2	0.9027	7.6	0.1093	4.2	600	141	653	37	669	28	45.43	-11.45	669	28
J03_1_t3_Grain52	0.0778	1.9	5.2438	1.8	2.0457	2.6	0.1907	1.8	1142	48	1131	20	1125	23	56.10	1.45	1125	23
J03_1_t3_Grain53	0.0807	2.9	4.9950	2.5	2.2276	3.9	0.2002	2.5	1214	65	1190	29	1176	31	32.49	3.11	1176	31
J03_1_t3_Grain54	0.0512	5.9	21.8293	3.4	0.3234	6.8	0.0458	3.4	NA	NA	285	17	289	10	66.08	NA	289	10

J03_1_t3_Grain55	0.0549	6.1	14.6199	3.6	0.5178	7.1	0.0684	3.6	NA	NA	424	25	427	16	82.81	NA	427	16
J03_1_t3_Grain56	0.0524	6.4	16.5563	3.7	0.4364	7.4	0.0604	3.7	NA	NA	368	23	378	14	45.90	NA	378	14
J03_1_t3_Grain57	0.0588	2.3	9.7847	2.0	0.8286	3.1	0.1022	2.0	560	61	613	15	627	14	3.60	-12.08	627	14
J03_1_t3_Grain58	0.0671	4.4	9.0662	3.1	1.0205	5.4	0.1103	3.1	841	97	714	28	674	21	1.85	19.79	674	21
J03_1_t3_Grain59	0.0600	4.0	9.6061	2.8	0.8612	4.9	0.1041	2.8	604	93	631	24	638	19	58.65	-5.77	638	19
J03_1_t3_Grain60	0.0637	8.2	10.0301	4.5	0.8757	9.4	0.0997	4.5	732	177	639	45	613	28	28.82	16.27	613	28
J03_1_t3_Grain61	0.0605	5.4	10.1317	3.4	0.8233	6.4	0.0987	3.4	622	121	610	30	607	21	83.33	2.37	607	21
J03_1_t3_Grain62	0.0572	4.8	10.1833	3.2	0.7745	5.8	0.0982	3.2	499	112	582	26	604	20	10.05	-20.95	604	20
J03_1_t3_Grain63	0.0532	4.7	18.5529	3.0	0.3954	5.6	0.0539	3.0	NA	NA	338	16	338	11	98.69	NA	338	11
J03_1_t3_Grain64	0.1014	2.5	3.6765	2.4	3.8028	3.5	0.2720	2.4	1650	54	1593	30	1551	38	1.13	6.00	1650	54
J03_1_t3_Grain65	0.1057	2.1	3.2394	2.1	4.4990	3.0	0.3087	2.1	1727	47	1731	27	1734	39	77.86	-0.45	1727	47
J03_1_t3_Grain66	0.0567	11.0	10.3093	5.4	0.7583	12.3	0.0970	5.4	480	248	573	54	597	31	45.10	-24.36	597	31
J03_1_t3_Grain67	0.0564	5.0	10.8108	3.2	0.7193	5.9	0.0925	3.2	468	116	550	26	570	19	16.54	-21.82	570	19
J03_1_t3_Grain68	0.0519	3.5	21.6450	2.5	0.3306	4.2	0.0462	2.5	NA	NA	290	11	291	8	84.83	NA	291	8
J03_1_t3_Grain69	0.0591	3.6	10.1523	2.7	0.8026	4.5	0.0985	2.7	571	86	598	21	606	17	44.68	-6.10	606	17
J03_1_t3_Grain70	0.0581	7.6	9.7943	4.4	0.8179	8.7	0.1021	4.4	534	169	607	40	627	27	40.62	-17.46	627	27
J03_1_t3_Grain71	0.1250	1.4	2.7601	1.7	6.2442	2.3	0.3623	1.7	2029	37	2011	23	1993	38	20.78	1.76	2029	37
J03_1_t3_Grain72	0.1216	3.4	2.8377	3.2	5.9084	4.7	0.3524	3.2	1980	67	1962	42	1946	58	56.77	1.71	1980	67
J03_1_t3_Grain73	0.0656	3.1	7.7580	3.0	1.1659	4.3	0.1289	3.0	794	73	785	25	782	24	67.77	1.52	782	24
J03_1_t3_Grain74	0.0703	7.2	8.8496	4.5	1.0953	8.5	0.1130	4.5	937	151	751	46	690	31	2.11	26.36	690	31
J03_1_t3_Grain75	0.0532	8.0	18.9753	4.3	0.3866	9.0	0.0527	4.3	NA	NA	332	26	331	15	95.71	NA	331	15
J03_1_t3_Grain76	0.0581	4.4	11.2233	2.9	0.7138	5.3	0.0891	2.9	534	101	547	23	550	17	81.80	-3.13	550	17
J03_1_t3_Grain77	0.0509	5.1	21.5564	3.1	0.3256	6.0	0.0464	3.1	NA	NA	286	15	292	10	43.45	NA	292	10
J03_1_t3_Grain78	0.1241	3.2	2.8169	3.0	6.0744	4.4	0.3550	3.0	2016	63	1987	40	1958	55	30.76	2.86	2016	63
J03_1_t3_Grain79	0.1108	4.6	3.1556	3.7	4.8413	5.9	0.3169	3.7	1813	89	1792	51	1775	60	56.65	2.10	1813	89
J03_1_t3_Grain80	0.0621	3.8	10.4493	2.8	0.8194	4.7	0.0957	2.8	678	88	608	22	589	17	8.47	13.05	589	17
J03_1_t3_Grain81	0.1280	3.9	2.8273	3.5	6.2423	5.3	0.3537	3.5	2071	75	2010	48	1952	64	7.08	5.72	2071	75
J03_1_t3_Grain82	0.0674	10.1	10.2987	5.6	0.9024	11.5	0.0971	5.6	850	213	653	56	597	33	8.76	29.73	597	33
J03_1_t3_Grain83	0.0581	6.0	8.2169	3.8	0.9749	7.1	0.1217	3.8	534	137	691	36	740	28	2.31	-38.76	740	28

J03_1_t3_Grain84	0.0618	5.7	10.2249	3.7	0.8334	6.8	0.0978	3.7	667	127	615	32	602	22	44.94	9.85	602	22
J03_1_t3_Grain85	0.0570	6.0	11.6144	3.6	0.6767	7.0	0.0861	3.6	492	137	525	29	532	20	67.21	-8.32	532	20
J03_1_t3_Grain86	0.0771	4.4	5.3362	3.2	1.9922	5.4	0.1874	3.2	1124	92	1113	38	1107	35	81.52	1.47	1107	35
J03_1_t3_Grain87	0.0837	4.1	4.5351	3.0	2.5447	5.1	0.2205	3.0	1286	86	1285	39	1285	39	98.75	0.08	1285	39
J03_1_t3_Grain88	0.0526	4.4	21.7817	2.9	0.3330	5.2	0.0459	2.9	NA	NA	292	14	289	9	73.48	NA	289	9
J03_1_t3_Grain89	0.0592	5.0	9.9108	3.2	0.8236	5.9	0.1009	3.2	574	114	610	28	620	21	56.64	-7.87	620	21
J03_1_t3_Grain90	0.0654	4.9	10.2145	3.2	0.8828	5.8	0.0979	3.2	787	107	642	29	602	20	2.21	23.52	602	20
J03_1_t3_Grain91	0.0548	5.6	21.1864	3.3	0.3566	6.5	0.0472	3.3	NA	NA	310	18	297	10	24.29	NA	297	10
J03_1_t3_Grain92	0.0647	6.7	10.2669	4.0	0.8689	7.8	0.0974	4.0	765	145	635	37	599	24	11.31	21.64	599	24
J03_1_t3_Grain93	0.0725	3.3	5.6593	2.6	1.7663	4.2	0.1767	2.6	1000	75	1033	29	1049	28	38.96	-4.89	1049	28
J03_1_t3_Grain94	0.0537	6.2	15.1286	3.5	0.4894	7.2	0.0661	3.5	NA	NA	405	24	413	15	51.88	NA	413	15
J03_1_t3_Grain95	0.1070	14.0	4.3103	8.3	3.4227	16.2	0.2320	8.3	1749	260	1510	129	1345	102	4.56	23.10	1345	102
J03_1_t3_Grain97	0.0579	4.8	11.4286	3.2	0.6985	5.8	0.0875	3.2	526	111	538	25	541	18	84.01	-2.81	541	18
J03_1_t3_Grain98	0.1068	3.5	3.4855	3.1	4.2248	4.7	0.2869	3.1	1746	71	1679	40	1626	48	4.85	6.85	1746	71
J03_1_t3_Grain99	0.0602	4.5	10.0908	3.1	0.8226	5.5	0.0991	3.1	611	104	609	26	609	19	98.18	0.27	609	19
J03_2_Grain01	0.0555	6.6	10.0301	3.0	0.7629	7.2	0.0997	3.0	432	151	576	32	613	19	4	-42	613	19
J03_2_Grain02	0.0589	4.2	10.3093	2.4	0.7877	4.9	0.0970	2.4	563	98	590	23	597	16	63	-6	597	16
J03_2_Grain03	0.0595	4.8	11.6686	2.6	0.7031	5.4	0.0857	2.6	585	109	541	23	530	15	37	9	530	15
J03_2_Grain04	0.1349	1.7	2.5323	2.0	7.3451	2.6	0.3949	2.0	2163	40	2154	26	2146	43	60	1	2163	40
J03_2_Grain05	0.1797	1.1	1.9589	1.8	12.6487	2.1	0.5105	1.8	2650	32	2654	24	2659	49	75	0	2650	32
J03_2_Grain06	0.0593	5.9	10.1626	3.1	0.8045	6.7	0.0984	3.1	578	133	599	31	605	19	74	-5	605	19
J03_2_Grain07	0.0597	7.0	10.5263	3.1	0.7820	7.6	0.0950	3.1	593	155	587	35	585	19	94	1	585	19
J03_2_Grain08	0.0605	4.8	10.2041	2.6	0.8175	5.4	0.0980	2.6	622	108	607	25	603	17	80	3	603	17
J03_2_Grain09	0.0518	7.3	22.4215	3.1	0.3185	7.9	0.0446	3.1	NA	NA	281	20	281	9	96	NA	281	9
J03_2_Grain10	0.1288	4.0	2.7701	3.0	6.4110	5.0	0.3610	3.0	2082	75	2034	45	1987	56	9	5	2082	75
J03_2_Grain11	0.1228	2.7	2.7847	2.4	6.0802	3.6	0.3591	2.4	1997	55	1987	33	1978	47	68	1	1997	55
J03_2_Grain12	0.1085	3.4	3.1447	2.6	4.7573	4.3	0.3180	2.6	1774	68	1777	38	1780	46	92	0	1774	68
J03_2_Grain13	0.0569	5.5	10.0100	2.7	0.7838	6.1	0.0999	2.7	488	125	588	28	614	18	9	-26	614	18
J03_2_Grain14	0.1209	2.6	2.8482	2.4	5.8527	3.5	0.3511	2.4	1970	53	1954	32	1940	46	46	2	1970	53

J03_2_Grain15	0.0572	3.9	10.2669	2.4	0.7682	4.6	0.0974	2.4	499	92	579	21	599	16	10	-20	599	16
J03_2_Grain16	0.1270	3.0	2.6810	2.6	6.5315	4.0	0.3730	2.6	2057	60	2050	37	2044	51	75	1	2057	60
J03_2_Grain18	0.0683	6.0	6.3291	3.0	1.4879	6.7	0.1580	3.0	878	129	925	42	946	29	38	-8	946	29
J03_2_Grain19	0.0592	5.0	10.5932	2.6	0.7705	5.6	0.0944	2.6	574	114	580	26	582	16	93	-1	582	16
J03_2_Grain20	0.0520	6.7	22.1043	2.8	0.3244	7.3	0.0452	2.8	NA	NA	285	18	285	9	100	NA	285	9
J03_2_Grain21	0.0598	5.5	11.3379	2.6	0.7272	6.1	0.0882	2.6	596	125	555	27	545	16	47	9	545	16
Rejected Analyses																		
J03_1_t2_Grain07	0.1175	1.6	3.0941	1.9	5.2361	2.4	0.3232	1.9	1919	39	1859	24	1805	36	0.00	5.90		
J03_1_t3_Grain104	0.0573	4.6	21.1864	3.1	0.3729	5.6	0.0472	3.1	NA	NA	322	16	297	10	0.15	NA		
J03_1_t3_Grain114	0.1158	2.7	3.3979	2.6	4.6989	3.8	0.2943	2.6	1892	56	1767	33	1663	43	0.00	12.12		
J03_1_t3_Grain137	0.0823	8.3	7.9239	5.1	1.4321	9.8	0.1262	5.1	1253	167	902	59	766	38	0.01	38.84		
J03_1_t3_Grain138	0.0691	5.2	10.4712	3.5	0.9099	6.3	0.0955	3.5	902	113	657	31	588	21	0.01	34.79		
J03_1_t3_Grain145	~~0.0821~~	~~3.6~~	~~5.5556~~	~~3.1~~	~~2.0376~~	~~4.8~~	~~0.1800~~	~~3.1~~	~~1248~~	~~77~~	~~1128~~	~~34~~	~~1067~~	~~33~~	0.01	14.50		
J03_1_t3_Grain154	0.1847	2.5	2.7693	2.9	9.1959	3.9	0.3611	2.9	2696	49	2358	38	1987	55	0.00	26.27		
J03_1_t3_Grain16	~~0.0892~~	~~5.0~~	~~5.0839~~	~~3.7~~	~~2.4192~~	~~6.2~~	~~0.1967~~	~~3.7~~	~~1408~~	~~100~~	~~1248~~	~~46~~	~~1158~~	~~42~~	0.02	17.81		
J03_1_t3_Grain18	0.1142	2.0	3.8986	2.4	4.0388	3.1	0.2565	2.4	1867	45	1642	28	1472	37	0.00	21.17		
J03_1_t3_Grain48	0.0645	5.3	10.8460	3.6	0.8200	6.4	0.0922	3.6	758	117	608	30	569	21	0.65	25.00		
J03_1_t3_Grain96	0.0759	4.5	8.7873	2.9	1.1909	5.4	0.1138	2.9	1092	96	796	31	695	21	0.00	36.40		
J03_2_Grain17	0.1198	1.6	3.0893	2.0	5.3469	2.5	0.3237	2.0	1953	40	1876	25	1808	38	0	7		
J03_2_Grain22	0.1587	1.5	2.2784	2.0	9.6038	2.5	0.4389	2.0	2442	37	2398	26	2346	47	0	4		

20EJ05 – Hibernia B-16 55 – Hibernia Formation (Lower) – Core # 2, box 3

	Isotopic ratios[2]								**Isotopic ages**									
Spot Name	$^{207}Pb/^{206}Pb$	$2s_x$ (%)	$^{238}U/^{206}Pb$	$2s_x$ (%)	$^{207}Pb/^{235}Pb$	$2s_x$ (%)	$^{206}Pb/^{238}U$	$2s_x$ (%)	$^{207}Pb/^{206}Pb$	$2s_{total}$ (Ma)	$^{207}Pb/^{235}Pb$	$2s_{total}$ (Ma)	$^{206}Pb/^{238}U$	$2s_{total}$ (Ma)	Prob. Conc. (%)	% conc[3]	U-Pb Best Age[4]	$2s_{total}$ (Ma)
J05_2_Grain01	0.0563	4.2	16.3132	2.5	0.4759	4.9	0.0613	2.5	NA	NA	395	17	384	11	13	NA	384	11
J05_2_Grain02	0.1181	3.0	2.9429	2.5	5.5332	3.9	0.3398	2.5	1928	60	1906	35	1886	46	34	2	1928	60
J05_2_Grain03	0.0651	5.4	7.8616	2.8	1.1417	6.1	0.1272	2.8	778	118	773	34	772	23	94	1	772	23

J05_2_Grain05	0.0723	4.7	5.8685	2.7	1.6987	5.4	0.1704	2.7	994	100	1008	36	1014	28	77	-2	1014	28
J05_2_Grain06	0.1183	2.2	2.8393	2.1	5.7448	3.1	0.3522	2.1	1931	48	1938	29	1945	43	71	-1	1931	48
J05_2_Grain07	0.0543	6.0	15.0830	2.9	0.4964	6.7	0.0663	2.9	NA	NA	409	23	414	13	69	NA	414	13
J05_2_Grain08	0.0542	5.9	15.0830	2.8	0.4955	6.5	0.0663	2.8	NA	NA	409	22	414	12	63	NA	414	12
J05_2_Grain09	0.0558	7.2	15.2439	3.1	0.5047	7.8	0.0656	3.1	NA	NA	415	27	410	14	73	NA	410	14
J05_2_Grain10	0.0633	4.7	7.4294	2.7	1.1748	5.4	0.1346	2.7	718	105	789	31	814	23	14	-13	814	23
J05_2_Grain11	0.0990	2.8	3.4542	2.3	3.9517	3.6	0.2895	2.3	1605	60	1624	31	1639	38	46	-2	1605	60
J05_2_t2_Grain01	0.0474	11.6	46.4037	3.7	0.1408	12.1	0.0216	3.7	NA	NA	134	15	137	5	66	NA	137	5
J05_2_t2_Grain03	0.1014	3.1	3.5727	2.5	3.9133	3.9	0.2799	2.5	1650	64	1616	34	1591	40	22	4	1650	64
J05_2_t2_Grain04	0.0736	3.4	6.1728	2.3	1.6440	4.1	0.1620	2.3	1031	76	987	27	968	24	23	6	968	24
J05_2_t2_Grain05	0.0504	7.6	16.1551	3.0	0.4302	8.2	0.0619	3.0	NA	NA	363	25	387	12	7	NA	387	12
J05_2_t2_Grain06	0.1005	3.2	3.5524	2.5	3.9007	4.0	0.2815	2.5	1633	66	1614	34	1599	40	48	2	1633	66
J05_2_t2_Grain07	0.0785	3.0	5.2770	2.3	2.0511	3.8	0.1895	2.3	1160	67	1133	28	1119	27	31	4	1119	27
J05_2_t2_Grain08	0.0446	8.9	44.4444	3.3	0.1384	9.5	0.0225	3.3	NA	NA	132	12	143	5	7	NA	143	5
Rejected Analyses																		
J05_2_Grain04	0.0669	5.5	10.6838	2.9	0.8634	6.2	0.0936	2.9	835	119	632	30	577	18	0	31		
J05_2_t2_Grain02	0.1006	1.9	3.6778	2.0	3.7715	2.8	0.2719	2.0	1635	46	1587	25	1550	34	1	5		

20EJ06 – Hibernia B-16 54W – Hibernia Formation (Lower) – Core # 1, box 1-3

	Isotopic ratios[2]								**Isotopic ages**									
Spot Name	$^{207}Pb/^{206}Pb$	$2s_x$ (%)	$^{238}U/^{206}Pb$	$2s_x$ (%)	$^{207}Pb/^{235}Pb$	$2s_x$ (%)	$^{206}Pb/^{238}U$	$2s_x$ (%)	$^{207}Pb/^{206}Pb$	$2s_{total}$ (Ma)	$^{207}Pb/^{235}Pb$	$2s_{total}$ (Ma)	$^{206}Pb/^{238}U$	$2s_{total}$ (Ma)	Prob. Conc. (%)	% conc[3]	U-Pb Best Age[4]	$2s_{total}$ (Ma)
J06_1_Grain01	0.0731	3.1	5.8617	2.3	1.7195	3.8	0.1706	2.3	1017	70	1016	26	1015	25	98.13	0.13	1015	25
J06_1_Grain02	0.1098	1.7	3.1338	1.9	4.8309	2.6	0.3191	1.9	1796	42	1790	24	1785	36	64.52	0.60	1796	42
J06_1_Grain03	0.0596	3.9	10.5485	2.8	0.7790	4.8	0.0948	2.8	589	91	585	22	584	17	93.19	0.89	584	17
J06_1_Grain04	0.1973	1.4	1.8242	1.8	14.9131	2.3	0.5482	1.8	2804	34	2810	25	2818	52	69.53	-0.49	2804	34
J06_1_Grain05	0.0558	4.4	14.9254	2.9	0.5155	5.2	0.0670	2.9	NA	NA	422	19	418	13	74.75	NA	418	13
J06_1_Grain06	0.1922	1.3	1.8643	1.8	14.2149	2.2	0.5364	1.8	2761	33	2764	25	2768	51	80.19	-0.26	2761	33

J06_1_t2_Grain01	0.0570	6.7	11.7371	3.9	0.6696	7.7	0.0852	3.9	492	151	520	32	527	21	71.15	-7.23	527	21
J06_1_t2_Grain03	0.1091	3.2	3.1133	2.7	4.8317	4.2	0.3212	2.7	1784	66	1790	37	1796	47	84.82	-0.62	1784	66
J06_1_t2_Grain05	0.1039	3.1	3.4941	2.9	4.1000	4.2	0.2862	2.9	1695	63	1654	36	1623	45	13.10	4.27	1695	63
J06_1_t2_Grain06	0.0543	4.1	15.4631	2.8	0.4842	5.0	0.0647	2.8	NA	NA	401	17	404	12	76.44	NA	404	12
J06_1_t3_Grain01	0.0587	4.5	10.0100	3.0	0.8085	5.4	0.0999	3.0	556	103	602	25	614	19	39.57	-10.40	614	19
J06_1_t3_Grain02	0.1016	3.0	3.5945	2.7	3.8972	4.1	0.2782	2.7	1654	63	1613	35	1582	42	11.17	4.31	1654	63
J06_1_t3_Grain03	0.0505	9.6	46.2321	4.7	0.1506	10.7	0.0216	4.7	NA	NA	142	14	138	7	57.61	NA	138	7
J06_1_t3_Grain04	0.1015	2.7	3.2279	2.8	4.3356	3.9	0.3098	2.8	1652	58	1700	34	1740	47	2.64	-5.33	1652	58
J06_1_t3_Grain05	0.0617	4.8	9.9404	3.1	0.8558	5.7	0.1006	3.1	664	108	628	27	618	20	52.19	6.90	618	20
J06_1_t3_Grain06	0.0630	4.4	10.4712	3.1	0.8296	5.4	0.0955	3.1	708	99	613	26	588	19	4.92	16.98	588	19
J06_1_t3_Grain08	0.0641	4.7	9.7182	3.3	0.9094	5.8	0.1029	3.3	745	105	657	29	631	22	8.75	15.24	631	22
J06_1_t3_Grain09	0.0668	7.2	10.4275	4.3	0.8833	8.4	0.0959	4.3	832	154	643	40	590	25	2.89	29.01	590	25
J06_1_t3_Grain10	0.0606	6.3	10.1317	3.7	0.8247	7.3	0.0987	3.7	625	141	611	34	607	23	85.55	2.92	607	23
J06_1_t3_Grain100	0.0576	7.5	11.2740	4.3	0.7044	8.7	0.0887	4.3	515	168	541	37	548	24	72.39	-6.46	548	24
J06_1_t3_Grain11	0.0547	8.5	15.1976	4.5	0.4963	9.6	0.0658	4.5	NA	NA	409	33	411	19	93.07	NA	411	19
J06_1_t3_Grain12	0.0622	6.5	9.6712	3.9	0.8868	7.6	0.1034	3.9	681	143	645	37	634	25	63.29	6.86	634	25
J06_1_t3_Grain13	0.0637	9.6	10.9051	4.7	0.8054	10.7	0.0917	4.7	732	208	600	49	566	26	20.64	22.70	566	26
J06_1_t3_Grain14	0.0600	4.7	11.2486	3.0	0.7355	5.6	0.0889	3.0	604	108	560	25	549	17	47.03	9.04	549	17
J06_1_t3_Grain15	0.1227	2.7	2.7894	2.9	6.0651	4.0	0.3585	2.9	1996	56	1985	36	1975	54	65.65	1.04	1996	56
J06_1_t3_Grain16	0.0604	3.2	9.5785	2.5	0.8694	4.1	0.1044	2.5	618	77	635	20	640	17	60.31	-3.59	640	17
J06_1_t3_Grain17	0.0555	7.4	14.8588	4.3	0.5150	8.6	0.0673	4.3	NA	NA	422	30	420	18	90.02	NA	420	18
J06_1_t3_Grain18	0.0630	6.6	10.1010	3.8	0.8600	7.7	0.0990	3.8	708	145	630	37	609	24	30.93	14.08	609	24
J06_1_t3_Grain19	0.0539	4.8	15.2672	3.1	0.4868	5.7	0.0655	3.1	NA	NA	403	19	409	13	57.36	NA	409	13
J06_1_t3_Grain20	0.1288	5.2	2.8011	4.1	6.3399	6.6	0.3570	4.1	2082	96	2024	59	1968	73	21.51	5.46	2082	96
J06_1_t3_Grain21	0.0531	5.4	16.6667	3.4	0.4393	6.4	0.0600	3.4	NA	NA	370	20	376	13	62.11	NA	376	13
J06_1_t3_Grain23	0.0595	4.8	10.3520	3.4	0.7925	5.9	0.0966	3.4	585	109	593	27	594	21	89.04	-1.54	594	21
J06_1_t3_Grain24	0.0620	4.8	10.1729	3.2	0.8403	5.8	0.0983	3.2	674	109	619	28	604	20	31.26	10.34	604	20
J06_1_t3_Grain25	0.1892	2.9	1.9231	3.3	13.5652	4.4	0.5200	3.3	2735	54	2720	43	2699	78	53.02	1.32	2735	54
J06_1_t3_Grain26	0.1102	2.2	3.0395	2.2	4.9989	3.1	0.3290	2.2	1803	48	1819	28	1834	41	41.49	-1.71	1803	48

J06_1_t3_Grain27	0.0998	6.3	3.6232	4.5	3.7979	7.7	0.2760	4.5	1620	121	1592	63	1571	66	60.48	3.03	1620	121
J06_1_t3_Grain28	0.0552	8.9	11.4155	5.1	0.6667	10.2	0.0876	5.1	420	202	519	42	541	27	32.17	-28.79	541	27
J06_1_t3_Grain29	0.0612	4.7	10.8460	3.2	0.7780	5.7	0.0922	3.2	646	107	584	26	569	19	27.83	12.03	569	19
J06_1_t3_Grain30	0.0643	5.1	8.0906	3.4	1.0958	6.2	0.1236	3.4	752	113	751	34	751	26	99.69	0.03	751	26
J06_1_t3_Grain31	0.1898	2.9	1.8248	3.1	14.3410	4.2	0.5480	3.1	2740	54	2773	42	2817	77	20.38	-2.79	2740	54
J06_1_t3_Grain32	0.1068	3.1	3.2289	2.7	4.5605	4.1	0.3097	2.7	1746	64	1742	36	1739	47	90.20	0.36	1746	64
J06_1_t3_Grain33	0.0527	4.4	17.0940	3.0	0.4251	5.3	0.0585	3.0	NA	NA	360	17	366	12	43.49	NA	366	12
J06_1_t3_Grain34	0.1282	1.8	2.6638	2.1	6.6357	2.8	0.3754	2.1	2073	42	2064	27	2055	44	57.01	0.90	2073	42
J06_1_t3_Grain35	0.0632	9.4	9.9206	5.1	0.8784	10.7	0.1008	5.1	715	203	640	51	619	31	48.13	13.41	619	31
J06_1_t3_Grain36	0.0508	9.0	12.3153	4.7	0.5687	10.1	0.0812	4.7	232	211	457	38	503	23	1.71	#####	503	23
J06_1_t3_Grain38	0.0564	7.1	11.4416	4.3	0.6797	8.3	0.0874	4.3	468	162	527	35	540	23	44.46	-15.38	540	23
J06_1_t3_Grain39	0.1095	2.4	3.1066	2.4	4.8600	3.3	0.3219	2.4	1791	51	1795	30	1799	43	85.01	-0.44	1791	51
J06_1_t3_Grain40	0.0582	5.8	11.4548	3.7	0.7005	6.9	0.0873	3.7	537	132	539	29	540	20	97.84	-0.42	540	20
J06_1_t3_Grain42	0.0626	5.0	8.6281	3.4	1.0004	6.0	0.1159	3.4	695	112	704	31	707	24	88.20	-1.76	707	24
J06_1_t3_Grain43	0.0596	6.2	9.9010	3.9	0.8300	7.3	0.1010	3.9	589	140	614	34	620	24	71.35	-5.29	620	24
J06_1_t3_Grain45	0.0924	4.7	4.1203	3.6	3.0920	5.9	0.2427	3.6	1476	95	1431	47	1401	48	28.72	5.08	1401	48
J06_1_t3_Grain46	0.1065	2.4	3.2938	2.4	4.4581	3.4	0.3036	2.4	1740	53	1723	31	1709	41	42.44	1.79	1740	53
J06_1_t3_Grain47	0.0772	4.4	5.4795	3.0	1.9426	5.3	0.1825	3.0	1126	92	1096	37	1081	33	55.53	4.06	1081	33
J06_1_t3_Grain48	0.0730	3.2	6.0024	2.5	1.6769	4.1	0.1666	2.5	1014	72	1000	27	993	26	71.15	2.03	993	26
J06_1_t3_Grain49	0.1704	1.4	2.0708	1.9	11.3456	2.3	0.4829	1.9	2562	35	2552	25	2540	48	54.03	0.85	2562	35
J06_1_t3_Grain51	0.0498	12.3	43.1034	5.8	0.1593	13.6	0.0232	5.8	NA	NA	150	19	148	9	82.76	NA	148	9
J06_1_t3_Grain52	0.0537	5.7	16.7785	3.5	0.4413	6.7	0.0596	3.5	NA	NA	371	21	373	14	86.93	NA	373	14
J06_1_t3_Grain53	0.1016	2.2	3.3636	2.2	4.1648	3.1	0.2973	2.2	1654	51	1667	28	1678	38	53.27	-1.47	1654	51
J06_1_t3_Grain54	0.1003	2.0	3.4990	2.0	3.9524	2.9	0.2858	2.0	1630	47	1624	26	1621	35	81.38	0.56	1630	47
J06_1_t3_Grain55	0.1026	3.2	3.4698	2.8	4.0770	4.2	0.2882	2.8	1672	65	1650	36	1633	44	44.08	2.34	1672	65
J06_1_t3_Grain56	0.0583	4.2	11.3122	2.8	0.7106	5.1	0.0884	2.8	541	99	545	22	546	16	93.70	-0.93	546	16
J06_1_t3_Grain57	0.0530	7.7	17.4520	4.2	0.4187	8.7	0.0573	4.2	NA	NA	355	27	359	15	80.40	NA	359	15
J06_1_t3_Grain58	0.0597	5.3	9.6154	3.5	0.8561	6.4	0.1040	3.5	593	120	628	30	638	23	54.96	-7.61	638	23
J06_1_t3_Grain59	0.1304	2.8	2.6035	2.6	6.9059	3.8	0.3841	2.6	2103	56	2099	36	2095	53	86.77	0.38	2103	56

J06_1_t3_Grain60	0.0557	7.0	10.6157	4.1	0.7234	8.1	0.0942	4.1	440	159	553	35	580	24	13.27	-31.76	580	24
J06_1_t3_Grain61	0.1093	2.3	3.1260	2.5	4.8210	3.4	0.3199	2.5	1788	51	1789	31	1789	44	97.03	-0.08	1788	51
J06_1_t3_Grain62	0.0929	3.0	4.0584	2.6	3.1562	4.0	0.2464	2.6	1486	65	1447	33	1420	37	19.91	4.44	1420	37
J06_1_t3_Grain63	0.1038	2.3	3.5075	2.3	4.0803	3.2	0.2851	2.3	1693	52	1650	29	1617	38	7.37	4.50	1693	52
J06_1_t3_Grain64	0.1966	1.6	1.8529	2.1	14.6298	2.7	0.5397	2.1	2798	37	2791	28	2782	57	66.33	0.57	2798	37
J06_1_t3_Grain66	0.0763	5.7	4.6490	4.2	2.2629	7.0	0.2151	4.2	1103	118	1201	51	1256	50	6.04	-13.87	1256	50
J06_1_t3_Grain68	0.0623	3.3	10.1112	2.4	0.8495	4.1	0.0989	2.4	684	79	624	20	608	16	17.73	11.17	608	16
J06_1_t3_Grain69	0.0598	6.4	11.7647	4.0	0.7008	7.5	0.0850	4.0	596	143	539	32	526	21	40.68	11.81	526	21
J06_1_t3_Grain70	0.0612	4.2	9.7276	3.1	0.8675	5.2	0.1028	3.1	646	96	634	25	631	20	80.81	2.39	631	20
J06_1_t3_Grain72	0.0645	10.0	7.6628	5.7	1.1606	11.5	0.1305	5.7	758	215	782	63	791	44	81.29	-4.31	791	44
J06_1_t3_Grain73	0.1182	1.9	2.9438	2.1	5.5362	2.8	0.3397	2.1	1929	44	1906	27	1885	40	20.66	2.28	1929	44
J06_1_t3_Grain74	0.0547	5.5	14.8810	3.4	0.5068	6.4	0.0672	3.4	NA	NA	416	22	419	15	82.28	NA	419	15
J06_1_t3_Grain75	0.0581	6.3	14.4300	3.7	0.5552	7.3	0.0693	3.7	NA	NA	448	27	432	17	28.27	NA	432	17
J06_1_t3_Grain76	0.0606	5.2	11.5473	3.4	0.7236	6.2	0.0866	3.4	625	118	553	27	535	19	22.67	14.35	535	19
J06_1_t3_Grain77	0.1097	2.0	3.2175	2.0	4.7010	2.8	0.3108	2.0	1794	46	1767	26	1745	37	18.87	2.77	1794	46
J06_1_t3_Grain78	0.0572	5.3	15.0376	3.2	0.5245	6.2	0.0665	3.2	NA	NA	428	22	415	14	28.87	NA	415	14
J06_1_t3_Grain79	0.0532	6.5	17.1527	3.8	0.4276	7.5	0.0583	3.8	NA	NA	362	23	365	14	77.85	NA	365	14
J06_1_t3_Grain80	0.1882	2.2	1.9558	2.6	13.2677	3.4	0.5113	2.6	2726	45	2699	35	2662	64	19.88	2.36	2726	45
J06_1_t3_Grain82	0.0589	6.5	11.7096	3.9	0.6935	7.5	0.0854	3.9	563	145	535	32	528	21	73.50	6.23	528	21
J06_1_t3_Grain84	0.0500	8.8	45.9770	4.4	0.1499	9.9	0.0218	4.4	NA	NA	142	13	139	6	67.70	NA	139	6
J06_1_t3_Grain86	0.0526	12.6	51.0204	6.2	0.1421	14.1	0.0196	6.2	NA	NA	135	18	125	8	29.11	NA	125	8
J06_1_t3_Grain87	0.0580	10.5	10.8578	5.4	0.7365	11.8	0.0921	5.4	530	235	560	51	568	30	80.34	-7.21	568	30
J06_1_t3_Grain88	0.0611	3.7	9.7276	2.7	0.8660	4.6	0.1028	2.7	643	86	633	23	631	18	84.42	1.86	631	18
J06_1_t3_Grain89	0.0787	3.2	5.0916	2.5	2.1312	4.1	0.1964	2.5	1165	71	1159	30	1156	31	86.38	0.74	1156	31
J06_1_t3_Grain90	0.1285	0.8	2.6511	1.3	6.6831	1.6	0.3772	1.3	2078	31	2070	18	2063	33	33.05	0.69	2078	31
J06_1_t3_Grain91	0.0549	4.6	14.7710	3.0	0.5125	5.5	0.0677	3.0	NA	NA	420	19	422	14	82.80	NA	422	14
J06_1_t3_Grain92	0.0627	5.7	10.3413	3.8	0.8360	6.8	0.0967	3.8	698	126	617	32	595	23	18.98	14.76	595	23
J06_1_t3_Grain94	0.0617	4.6	9.9010	3.1	0.8592	5.5	0.1010	3.1	664	103	630	27	620	20	49.05	6.55	620	20
J06_1_t3_Grain96	0.0710	5.5	5.7770	3.6	1.6946	6.6	0.1731	3.6	957	117	1006	43	1029	37	39.69	-7.49	1029	37

J06_1_t3_Grain97	0.0541	6.6	16.3666	3.9	0.4558	7.6	0.0611	3.9	NA	NA	381	25	382	15	93.59	NA	382	15
J06_1_t3_Grain98	0.0959	2.3	3.6955	2.2	3.5781	3.2	0.2706	2.2	1546	53	1545	27	1544	35	96.61	0.13	1544	35
J06_1_t3_Grain99	0.1508	1.2	2.2341	1.6	9.3066	2.0	0.4476	1.6	2355	33	2369	22	2385	42	27.16	-1.26	2355	33
J06_2_Grain01	0.0563	4.0	13.6091	2.2	0.5704	4.6	0.0735	2.2	NA	NA	458	18	457	11	91	NA	457	11
J06_2_Grain02	0.0541	6.2	13.2100	2.9	0.5647	6.9	0.0757	2.9	NA	NA	455	26	470	15	24	NA	470	15
J06_2_Grain03	0.0730	3.6	5.9666	2.3	1.6869	4.3	0.1676	2.3	1014	79	1004	28	999	25	77	1	999	25
J06_2_Grain04	0.0935	2.4	3.8775	2.1	3.3248	3.2	0.2579	2.1	1498	54	1487	27	1479	33	63	1	1479	33
J06_2_Grain05	0.0543	7.5	18.5529	3.0	0.4035	8.1	0.0539	3.0	NA	NA	344	24	338	11	66	NA	338	11
J06_2_Grain06	0.1146	2.6	3.1270	2.2	5.0532	3.4	0.3198	2.2	1874	54	1828	31	1789	41	2	5	1874	54
J06_2_Grain07	0.0532	5.5	14.6628	2.7	0.5003	6.1	0.0682	2.7	NA	NA	412	21	425	12	25	NA	425	12
J06_2_Grain08	0.0598	5.0	10.2775	2.7	0.8023	5.7	0.0973	2.7	596	113	598	26	599	17	97	0	599	17
J06_2_Grain09	0.0615	4.1	9.6061	2.4	0.8827	4.7	0.1041	2.4	657	93	642	23	638	17	76	3	638	17
J06_2_Grain10	0.0525	6.5	18.4843	2.9	0.3916	7.1	0.0541	2.9	NA	NA	336	21	340	11	71	NA	340	11
Rejected Analyses																		
J06_1_t3_Grain07	0.0604	5.8	16.9779	3.4	0.4905	6.8	0.0589	3.4	NA	NA	405	23	369	13	0.54	NA		
J06_1_t3_Grain44	0.1918	1.8	2.0198	2.3	13.0931	2.9	0.4951	2.3	2758	39	2686	30	2593	57	0.01	5.98		
J06_1_t3_Grain50	0.1056	2.2	3.6617	2.3	3.9764	3.2	0.2731	2.3	1725	50	1629	28	1557	36	0.00	9.76		
J06_1_t3_Grain71	0.0652	5.3	10.6952	3.5	0.8405	6.3	0.0935	3.5	781	115	619	30	576	21	0.24	26.20		
J06_1_t3_Grain81	0.1071	2.0	3.0102	2.1	4.9056	2.9	0.3322	2.1	1751	46	1803	27	1849	40	0.36	-5.62		
J06_1_t3_Grain83	0.0479	9.1	14.3678	4.6	0.4597	10.2	0.0696	4.6	NA	NA	384	33	434	20	0.48	NA		
J06_1_t3_Grain95	0.1887	1.4	1.9716	2.0	13.1963	2.5	0.5072	2.0	2731	35	2694	27	2645	53	0.76	3.16		

20EJ08 – Hebron M-04 – Hibernia Formation (Upper) – Core # 3, box 37-42

	Isotopic ratios[2]								**Isotopic ages**									
Spot Name	$^{207}Pb/^{206}Pb$	$2s_x$ (%)	$^{238}U/^{206}Pb$	$2s_x$ (%)	$^{207}Pb/^{235}Pb$	$2s_x$ (%)	$^{206}Pb/^{238}U$	$2s_x$ (%)	$^{207}Pb/^{206}Pb$	$2s_{total}$ (Ma)	$^{207}Pb/^{235}Pb$	$2s_{total}$ (Ma)	$^{206}Pb/^{238}U$	$2s_{total}$ (Ma)	Prob. Conc. (%)	% conc[3]	U-Pb Best Age[4]	$2s_{total}$ (Ma)
J08_1_Grain01	0.0564	5.1	14.5773	3.1	0.5335	5.9	0.0686	3.1	NA	NA	434	21	428	14	59.02	NA	428	14
J08_1_Grain02	0.0595	3.8	10.0705	2.7	0.8146	4.7	0.0993	2.7	585	90	605	22	610	17	66.38	-4.25	610	17

J08_1_t2_Grain01	0.1271	2.2	2.6028	2.3	6.7329	3.2	0.3842	2.3	2058	48	2077	31	2096	48	36.64	-1.83	2058	48
J08_1_t2_Grain02	0.0576	5.3	10.2041	3.4	0.7783	6.3	0.0980	3.4	515	122	585	29	603	21	25.08	-17.12	603	21
J08_1_t2_Grain03	0.0628	5.0	9.7371	3.4	0.8893	6.0	0.1027	3.4	701	111	646	29	630	22	28.30	10.16	630	22
J08_1_t2_Grain04	0.0597	5.6	11.1607	3.5	0.7375	6.6	0.0896	3.5	593	127	561	29	553	20	65.29	6.67	553	20
J08_1_t2_Grain05	0.0596	5.8	11.9332	3.5	0.6886	6.7	0.0838	3.5	589	130	532	28	519	18	46.64	11.94	519	18
J08_1_t2_Grain06	0.0626	4.9	10.6724	3.3	0.8088	5.9	0.0937	3.3	695	110	602	28	577	19	10.34	16.88	577	19
J08_1_t3_Grain01	0.0586	4.5	10.5820	3.1	0.7635	5.4	0.0945	3.1	552	103	576	25	582	19	67.75	-5.40	582	19
J08_1_t3_Grain02	0.0509	6.5	17.3310	3.6	0.4049	7.4	0.0577	3.6	NA	NA	345	22	362	14	17.70	NA	362	14
J08_1_t3_Grain03	0.0638	5.8	10.7875	3.7	0.8155	6.9	0.0927	3.7	735	127	606	32	571	22	6.44	22.25	571	22
J08_1_t3_Grain04	0.1045	6.0	3.6364	4.6	3.9623	7.6	0.2750	4.6	1706	114	1627	62	1566	67	16.67	8.17	1706	114
J08_1_t3_Grain06	0.0963	2.2	3.7552	2.1	3.5359	3.1	0.2663	2.1	1554	50	1535	26	1522	34	42.66	2.04	1522	34
J08_1_t3_Grain07	0.0575	4.9	14.2857	3.3	0.5550	5.9	0.0700	3.3	NA	NA	448	22	436	15	29.25	NA	436	15
J08_1_t3_Grain08	0.0721	3.8	5.6433	2.9	1.7616	4.8	0.1772	2.9	989	84	1031	33	1052	31	28.76	-6.36	1052	31
J08_1_t3_Grain09	0.0540	7.1	14.8588	4.2	0.5011	8.3	0.0673	4.2	NA	NA	412	28	420	18	61.90	NA	420	18
J08_1_t3_Grain10	0.1067	1.6	3.3289	1.8	4.4194	2.5	0.3004	1.8	1744	41	1716	23	1693	34	10.04	2.90	1744	41
J08_1_t3_Grain100	0.0612	3.4	10.3627	2.5	0.8143	4.2	0.0965	2.5	646	79	605	20	594	16	26.78	8.11	594	16
J08_1_t3_Grain101	0.0591	5.7	11.1607	3.6	0.7301	6.7	0.0896	3.6	571	129	557	29	553	20	82.30	3.09	553	20
J08_1_t3_Grain102	0.1023	2.6	3.3124	2.5	4.2583	3.6	0.3019	2.5	1666	55	1685	31	1701	42	40.74	-2.07	1666	55
J08_1_t3_Grain103	0.0518	5.7	21.6920	3.5	0.3293	6.7	0.0461	3.5	NA	NA	289	17	291	11	87.42	NA	291	11
J08_1_t3_Grain104	0.0588	7.7	11.2108	4.4	0.7232	8.9	0.0892	4.4	560	172	553	38	551	24	93.73	1.59	551	24
J08_1_t3_Grain105	0.1122	1.9	3.0488	2.1	5.0742	2.8	0.3280	2.1	1835	44	1832	26	1829	40	85.17	0.36	1835	44
J08_1_t3_Grain106	0.0795	2.9	4.9358	2.4	2.2208	3.8	0.2026	2.4	1185	65	1188	28	1189	30	91.29	-0.39	1189	30
J08_1_t3_Grain107	0.0577	4.2	10.2881	3.0	0.7733	5.1	0.0972	3.0	518	97	582	24	598	19	12.57	-15.35	598	19
J08_1_t3_Grain108	0.0805	7.8	5.0736	4.8	2.1877	9.2	0.1971	4.8	1209	157	1177	65	1160	53	66.06	4.10	1160	53
J08_1_t3_Grain109	0.0597	3.4	9.9800	2.6	0.8248	4.3	0.1002	2.6	593	82	611	21	616	17	65.79	-3.86	616	17
J08_1_t3_Grain11	0.0621	4.8	9.3633	3.2	0.9145	5.8	0.1068	3.2	678	109	659	29	654	22	74.72	3.46	654	22
J08_1_t3_Grain110	0.0685	4.7	5.8893	3.4	1.6037	5.8	0.1698	3.4	884	103	972	37	1011	34	5.08	-14.40	1011	34
J08_1_t3_Grain112	0.0540	5.2	15.5521	3.4	0.4787	6.2	0.0643	3.4	NA	NA	397	21	402	14	64.80	NA	402	14
J08_1_t3_Grain12	0.0595	11.2	10.4384	5.8	0.7859	12.6	0.0958	5.8	585	248	589	57	590	34	97.61	-0.74	590	34

J08_1_t3_Grain13	0.0595	8.8	10.1317	4.8	0.8097	10.0	0.0987	4.8	585	194	602	46	607	29	85.11	-3.65	607	29
J08_1_t3_Grain14	0.0616	5.6	10.2775	3.5	0.8264	6.6	0.0973	3.5	660	126	612	31	599	21	51.59	9.34	599	21
J08_1_t3_Grain15	0.0528	6.3	21.1416	3.5	0.3443	7.2	0.0473	3.5	NA	NA	300	19	298	11	81.44	NA	298	11
J08_1_t3_Grain16	0.0605	5.1	10.9890	3.3	0.7591	6.1	0.0910	3.3	622	115	573	27	561	19	40.49	9.66	561	19
J08_1_t3_Grain17	0.0558	5.4	21.8818	3.5	0.3516	6.4	0.0457	3.5	NA	NA	306	17	288	11	4.51	NA	288	11
J08_1_t3_Grain18	0.0623	6.0	10.0503	3.7	0.8547	7.0	0.0995	3.7	684	132	627	33	611	23	44.68	10.66	611	23
J08_1_t3_Grain19	0.0741	4.5	5.9347	3.3	1.7215	5.6	0.1685	3.3	1044	96	1017	37	1004	33	55.87	3.86	1004	33
J08_1_t3_Grain20	0.0533	9.6	11.1607	5.3	0.6585	10.9	0.0896	5.3	342	221	514	44	553	29	10.80	-61.94	553	29
J08_1_t3_Grain22	0.0597	6.0	10.3093	3.7	0.7984	7.0	0.0970	3.7	593	134	596	32	597	22	96.55	-0.69	597	22
J08_1_t3_Grain23	0.0591	4.4	10.6724	2.9	0.7635	5.3	0.0937	2.9	571	102	576	24	577	18	92.55	-1.16	577	18
J08_1_t3_Grain24	0.0561	5.6	10.1937	3.5	0.7588	6.6	0.0981	3.5	456	130	573	30	603	22	7.78	-32.20	603	22
J08_1_t3_Grain25	0.0587	5.3	10.4167	3.6	0.7770	6.4	0.0960	3.6	556	121	584	29	591	22	63.45	-6.28	591	22
J08_1_t3_Grain27	0.0587	3.4	10.9769	2.5	0.7373	4.2	0.0911	2.5	556	82	561	19	562	15	91.98	-1.09	562	15
J08_1_t3_Grain28	0.0777	2.4	5.0684	2.2	2.1137	3.2	0.1973	2.2	1139	56	1153	24	1161	28	56.49	-1.89	1161	28
J08_1_t3_Grain29	0.0646	6.6	9.5147	4.1	0.9361	7.7	0.1051	4.1	761	142	671	39	644	26	26.77	15.38	644	26
J08_1_t3_Grain30	0.0606	7.2	10.0604	4.1	0.8305	8.3	0.0994	4.1	625	159	614	39	611	25	87.63	2.27	611	25
J08_1_t3_Grain31	0.0622	6.9	9.9502	4.0	0.8619	8.0	0.1005	4.0	681	152	631	38	617	25	57.17	9.35	617	25
J08_1_t3_Grain32	0.1011	2.5	3.5945	2.4	3.8780	3.4	0.2782	2.4	1644	55	1609	30	1582	38	16.80	3.78	1644	55
J08_1_t3_Grain34	0.0517	6.1	22.6244	3.7	0.3151	7.1	0.0442	3.7	NA	NA	278	18	279	11	94.25	NA	279	11
J08_1_t3_Grain35	0.0574	6.4	9.8328	4.0	0.8049	7.5	0.1017	4.0	507	145	600	35	624	25	16.03	-23.16	624	25
J08_1_t3_Grain36	0.1160	2.7	3.0665	2.7	5.2157	3.8	0.3261	2.7	1895	56	1855	34	1819	47	14.22	4.01	1895	56
J08_1_t3_Grain37	0.0632	4.8	9.7561	3.3	0.8932	5.8	0.1025	3.3	715	106	648	28	629	21	21.13	12.02	629	21
J08_1_t3_Grain38	0.0574	8.2	11.3122	4.5	0.6996	9.3	0.0884	4.5	507	184	539	39	546	24	75.49	-7.72	546	24
J08_1_t3_Grain39	0.0572	5.9	10.4275	3.4	0.7563	6.8	0.0959	3.4	499	135	572	30	590	21	32.95	-18.24	590	21
J08_1_t3_Grain41	0.0553	6.7	22.9358	3.6	0.3324	7.6	0.0436	3.6	NA	NA	291	20	275	10	17.68	NA	275	10
J08_1_t3_Grain42	0.0593	9.5	10.9890	4.8	0.7440	10.6	0.0910	4.8	578	209	565	46	561	27	90.51	2.89	561	27
J08_1_t3_Grain43	0.0601	6.4	10.4058	4.0	0.7963	7.5	0.0961	4.0	607	142	595	34	592	24	86.46	2.58	592	24
J08_1_t3_Grain45	0.0539	5.9	22.2717	3.6	0.3337	6.9	0.0449	3.6	NA	NA	292	18	283	11	33.77	NA	283	11
J08_1_t3_Grain46	0.0639	5.5	10.6383	3.6	0.8282	6.6	0.0940	3.6	738	121	613	31	579	21	6.65	21.56	579	21

J08_1_t3_Grain47	0.0521	6.8	22.2222	3.9	0.3233	7.8	0.0450	3.9	NA	NA	284	20	284	11	95.55	NA	284	11
J08_1_t3_Grain48	0.0586	4.7	10.5152	3.2	0.7684	5.7	0.0951	3.2	552	109	579	26	586	19	65.84	-6.04	586	19
J08_1_t3_Grain49	0.0584	4.6	11.7233	3.0	0.6869	5.5	0.0853	3.0	545	106	531	23	528	17	81.69	3.14	528	17
J08_1_t3_Grain50	0.0589	6.7	11.4811	3.7	0.7074	7.6	0.0871	3.7	563	149	543	33	538	21	77.04	4.44	538	21
J08_1_t3_Grain51	0.1006	1.8	3.6127	1.9	3.8394	2.6	0.2768	1.9	1635	45	1601	24	1575	32	7.32	3.67	1635	45
J08_1_t3_Grain53	0.0568	9.4	8.9767	5.1	0.8724	10.7	0.1114	5.1	484	211	637	51	681	34	12.69	-40.74	681	34
J08_1_t3_Grain54	0.0460	13.0	51.8135	6.4	0.1224	14.5	0.0193	6.4	NA	NA	117	16	123	8	45.55	NA	123	8
J08_1_t3_Grain55	0.0572	5.8	10.3413	3.5	0.7626	6.8	0.0967	3.5	499	132	576	30	595	21	25.32	-19.19	595	21
J08_1_t3_Grain56	0.0600	5.1	10.1523	3.3	0.8149	6.1	0.0985	3.3	604	116	605	28	606	21	97.77	-0.34	606	21
J08_1_t3_Grain57	0.0546	6.5	22.6757	3.9	0.3320	7.5	0.0441	3.9	NA	NA	291	19	278	11	18.08	NA	278	11
J08_1_t3_Grain58	0.0635	4.3	10.3199	2.9	0.8484	5.2	0.0969	2.9	725	98	624	25	596	18	3.52	17.77	596	18
J08_1_t3_Grain61	0.0569	5.9	12.4224	3.8	0.6316	7.0	0.0805	3.8	NA	NA	497	28	499	19	89.92	NA	499	19
J08_1_t3_Grain62	0.0590	6.1	15.3610	3.6	0.5296	7.1	0.0651	3.6	NA	NA	432	25	407	15	10.35	NA	407	15
J08_1_t3_Grain63	0.0594	7.6	11.0865	4.2	0.7387	8.7	0.0902	4.2	582	168	562	38	557	24	78.29	4.31	557	24
J08_1_t3_Grain64	0.0756	3.9	5.3735	2.9	1.9399	4.9	0.1861	2.9	1084	84	1095	34	1100	33	80.00	-1.45	1100	33
J08_1_t3_Grain65	0.0570	5.5	14.4509	3.4	0.5439	6.4	0.0692	3.4	NA	NA	441	24	431	15	36.10	NA	431	15
J08_1_t3_Grain67	0.0608	5.4	10.3520	3.4	0.8098	6.4	0.0966	3.4	632	122	602	30	594	21	62.38	5.97	594	21
J08_1_t3_Grain68	0.0610	4.0	10.1937	2.7	0.8251	4.9	0.0981	2.7	639	93	611	23	603	18	57.96	5.63	603	18
J08_1_t3_Grain69	0.0611	4.9	10.1215	3.1	0.8323	5.8	0.0988	3.1	643	111	615	28	607	20	63.62	5.50	607	20
J08_1_t3_Grain71	0.0608	10.3	10.1420	5.4	0.8266	11.6	0.0986	5.4	632	226	612	54	606	32	86.80	4.11	606	32
J08_1_t3_Grain72	0.0626	6.1	10.4167	3.8	0.8286	7.2	0.0960	3.8	695	134	613	34	591	23	24.20	14.93	591	23
J08_1_t3_Grain73	0.0530	8.7	21.0970	3.8	0.3464	9.5	0.0474	3.8	NA	NA	302	25	299	12	79.53	NA	299	12
J08_1_t3_Grain74	0.0545	7.7	22.4719	4.4	0.3344	8.9	0.0445	4.4	NA	NA	293	23	281	13	33.80	NA	281	13
J08_1_t3_Grain75	0.0858	3.4	4.4346	2.9	2.6677	4.5	0.2255	2.9	1334	73	1320	35	1311	38	68.73	1.71	1311	38
J08_1_t3_Grain76	0.0592	4.0	11.4943	2.9	0.7101	5.0	0.0870	2.9	574	94	545	22	538	16	58.11	6.39	538	16
J08_1_t3_Grain78	0.0531	4.6	21.4408	3.0	0.3415	5.5	0.0466	3.0	NA	NA	298	15	294	9	55.80	NA	294	9
J08_1_t3_Grain79	0.0582	5.0	15.0512	2.7	0.5332	5.6	0.0664	2.7	NA	NA	434	20	415	12	6.90	NA	415	12
J08_1_t3_Grain80	0.0603	7.4	10.0705	4.2	0.8256	8.5	0.0993	4.2	614	163	611	40	610	26	96.56	0.66	610	26
J08_1_t3_Grain81	0.0577	5.1	9.6061	3.2	0.8282	6.0	0.1041	3.2	518	116	613	28	638	21	7.08	-23.15	638	21

J08_1_t3_Grain82	0.0617	3.4	9.8814	2.5	0.8609	4.2	0.1012	2.5	664	80	631	21	621	17	38.67	6.37	621	17
J08_1_t3_Grain84	0.0614	6.0	10.0705	3.7	0.8407	7.1	0.0993	3.7	653	134	620	33	610	23	63.80	6.58	610	23
J08_1_t3_Grain85	0.0573	5.1	10.9769	3.3	0.7197	6.1	0.0911	3.3	503	118	551	27	562	19	44.38	-11.72	562	19
J08_1_t3_Grain86	0.0532	6.4	20.9205	3.8	0.3506	7.4	0.0478	3.8	NA	NA	305	20	301	12	68.07	NA	301	12
J08_1_t3_Grain87	0.0577	3.6	10.1523	2.6	0.7836	4.5	0.0985	2.6	518	87	588	21	606	17	10.20	-16.83	606	17
J08_1_t3_Grain88	0.0597	4.0	10.0402	2.9	0.8199	4.9	0.0996	2.9	593	92	608	23	612	19	74.01	-3.26	612	19
J08_1_t3_Grain89	0.0583	4.9	14.8148	3.2	0.5426	5.9	0.0675	3.2	NA	NA	440	22	421	14	15.07	NA	421	14
J08_1_t3_Grain90	0.1109	2.9	3.3047	2.6	4.6270	3.9	0.3026	2.6	1814	59	1754	34	1704	44	1.40	6.06	1814	59
J08_1_t3_Grain93	0.0566	5.2	18.1818	3.6	0.4292	6.3	0.0550	3.6	NA	NA	363	20	345	13	6.59	NA	345	13
J08_1_t3_Grain96	0.0559	6.7	10.2775	4.0	0.7499	7.8	0.0973	4.0	448	153	568	34	599	24	10.75	-33.49	599	24
J08_1_t3_Grain98	0.0605	4.8	9.2764	3.2	0.8992	5.8	0.1078	3.2	622	108	651	28	660	22	58.95	-6.19	660	22
J08_1_t3_Grain99	0.0562	5.8	14.7493	3.5	0.5254	6.8	0.0678	3.5	NA	NA	429	24	423	15	66.88	NA	423	15
Rejected Analyses																		
J08_1_t3_Grain111	0.0770	6.6	10.3842	4.2	1.0224	7.9	0.0963	4.2	1121	136	715	41	593	25	0.00	47.14		
J08_1_t3_Grain26	0.0950	8.3	9.4073	3.6	1.3924	9.1	0.1063	3.6	1528	160	886	54	651	24	0.00	57.38		
J08_1_t3_Grain40	0.1309	3.8	2.8498	3.0	6.3332	4.8	0.3509	3.0	2110	72	2023	44	1939	55	0.14	8.11		
J08_1_t3_Grain52	0.1206	2.7	3.0497	2.7	5.4524	3.8	0.3279	2.7	1965	56	1893	35	1828	48	0.35	6.97		
J08_1_t3_Grain66	0.0603	6.2	21.9298	3.6	0.3791	7.2	0.0456	3.6	NA	NA	326	20	287	11	0.03	NA		
J08_1_t3_Grain70	0.0680	5.5	21.2766	3.5	0.4407	6.6	0.0470	3.5	NA	NA	371	21	296	11	0.00	NA		
J08_1_t3_Grain77	0.0747	4.2	15.3610	3.2	0.6705	5.3	0.0651	3.2	NA	NA	521	22	407	14	0.00	NA		
J08_1_t3_Grain83	0.1159	1.8	4.7281	2.0	3.3798	2.7	0.2115	2.0	1894	43	1500	23	1237	27	0.00	34.70		
J08_1_t3_Grain92	0.1046	2.5	5.7637	3.0	2.5023	3.9	0.1735	3.0	1707	53	1273	30	1031	32	0.00	39.59		
J08_1_t3_Grain95	0.0635	4.8	11.4416	3.4	0.7652	5.9	0.0874	3.4	725	106	577	26	540	19	0.71	25.50		

20EJ09 – Hebron M-04 – Hibernia Formation (Upper) – Core # 3, box 26-33

	Isotopic ratios[2]								Isotopic ages									
Spot Name	$^{207}Pb/^{206}Pb$	$2s_x$ (%)	$^{238}U/^{206}Pb$	$2s_x$ (%)	$^{207}Pb/^{235}Pb$	$2s_x$ (%)	$^{206}Pb/^{238}U$	$2s_x$ (%)	$^{207}Pb/^{206}Pb$	$2s_{total}$ (Ma)	$^{207}Pb/^{235}Pb$	$2s_{total}$ (Ma)	$^{206}Pb/^{238}U$	$2s_{total}$ (Ma)	Prob. Conc. (%)	% conc[3]	U-Pb Best Age[4]	$2s_{total}$ (Ma)
J09_1_Grain03	0.0532	4.0	15.9744	2.7	0.4592	4.8	0.0626	2.7	NA	NA	384	16	391	12	40.82	NA	391	12
J09_1_t2_Grain01	0.0897	2.5	4.0683	2.3	3.0400	3.4	0.2458	2.3	1419	56	1418	28	1417	34	95.99	0.17	1417	34
J09_1_t2_Grain02	0.0568	4.8	10.1833	3.1	0.7691	5.8	0.0982	3.1	484	113	579	26	604	20	6.98	-24.82	604	20
J09_1_t2_Grain03	0.0617	3.5	10.4822	2.7	0.8116	4.4	0.0954	2.7	664	81	603	21	587	17	11.83	11.50	587	17
J09_1_t3_Grain01	0.0973	2.1	3.4990	2.0	3.8342	2.9	0.2858	2.0	1573	48	1600	26	1621	35	16.15	-3.02	1573	48
J09_1_t3_Grain03	0.0647	4.8	9.5329	3.2	0.9358	5.8	0.1049	3.2	765	107	671	29	643	22	6.20	15.90	643	22
J09_1_t3_Grain04	0.0562	12.5	11.9904	6.1	0.6463	13.9	0.0834	6.1	460	281	506	56	516	31	72.23	-12.19	516	31
J09_1_t3_Grain05	0.0517	4.6	21.7108	3.0	0.3283	5.5	0.0461	3.0	NA	NA	288	14	290	9	78.30	NA	290	9
J09_1_t3_Grain06	0.0534	5.7	14.9925	3.4	0.4911	6.6	0.0667	3.4	NA	NA	406	23	416	15	38.85	NA	416	15
J09_1_t3_Grain07	0.0541	7.2	13.2979	4.1	0.5609	8.2	0.0752	4.1	NA	NA	452	31	467	19	38.70	NA	467	19
J09_1_t3_Grain08	0.0596	5.2	11.9760	3.1	0.6862	6.0	0.0835	3.1	589	117	530	25	517	17	35.06	12.24	517	17
J09_1_t3_Grain09	0.0804	3.2	4.7393	2.6	2.3391	4.1	0.2110	2.6	1207	71	1224	31	1234	33	55.21	-2.26	1234	33
J09_1_t3_Grain101	0.0523	6.9	21.7391	3.9	0.3317	7.9	0.0460	3.9	NA	NA	291	20	290	12	92.87	NA	290	12
J09_1_t3_Grain102	0.0524	4.7	21.9780	3.1	0.3287	5.7	0.0455	3.1	NA	NA	289	15	287	10	83.58	NA	287	10
J09_1_t3_Grain103	0.0647	3.7	9.0827	2.8	0.9822	4.6	0.1101	2.8	765	84	695	24	673	20	11.59	11.94	673	20
J09_1_t3_Grain104	0.1107	2.1	3.0893	2.3	4.9407	3.2	0.3237	2.3	1811	48	1809	29	1808	42	92.43	0.17	1811	48
J09_1_t3_Grain105	0.0547	4.0	21.0084	2.7	0.3590	4.8	0.0476	2.7	NA	NA	311	13	300	9	9.44	NA	300	9
J09_1_t3_Grain106	0.0602	3.7	11.0497	2.7	0.7512	4.6	0.0905	2.7	611	87	569	21	558	16	43.26	8.56	558	16
J09_1_t3_Grain11	0.0572	4.0	10.7296	2.8	0.7350	4.9	0.0932	2.8	499	95	560	22	574	17	23.97	-15.06	574	17
J09_1_t3_Grain12	0.0586	6.5	10.0503	4.0	0.8039	7.6	0.0995	4.0	552	147	599	35	611	24	53.63	-10.72	611	24
J09_1_t3_Grain14	0.0638	5.1	10.7643	3.4	0.8172	6.1	0.0929	3.4	735	113	606	29	573	20	3.16	22.09	573	20
J09_1_t3_Grain15	0.0744	4.9	5.9067	3.4	1.7367	5.9	0.1693	3.4	1052	103	1022	39	1008	34	56.73	4.19	1008	34
J09_1_t3_Grain16	0.0505	6.0	17.5131	3.7	0.3976	7.0	0.0571	3.7	NA	NA	340	21	358	14	8.37	NA	358	14
J09_1_t3_Grain17	0.0792	2.1	4.7619	2.1	2.2932	3.0	0.2100	2.1	1177	52	1210	23	1229	28	10.28	-4.39	1229	28
J09_1_t3_Grain18	0.0543	8.1	16.0256	4.7	0.4672	9.3	0.0624	4.7	NA	NA	389	30	390	18	95.14	NA	390	18

J09_1_t3_Grain19	0.1295	1.5	2.6724	1.8	6.6815	2.3	0.3742	1.8	2091	38	2070	24	2049	39	14.36	2.01	2091	38
J09_1_t3_Grain20	0.0610	4.3	9.3545	2.9	0.8991	5.2	0.1069	2.9	639	98	651	26	655	20	80.04	-2.42	655	20
J09_1_t3_Grain21	0.0620	6.4	10.3734	3.9	0.8241	7.4	0.0964	3.9	674	140	610	35	593	23	41.67	11.99	593	23
J09_1_t3_Grain22	0.1152	2.4	3.0760	2.4	5.1638	3.4	0.3251	2.4	1883	52	1847	31	1815	44	8.80	3.63	1883	52
J09_1_t3_Grain23	0.0527	3.7	20.0562	2.6	0.3623	4.6	0.0499	2.6	NA	NA	314	13	314	9	97.14	NA	314	9
J09_1_t3_Grain24	0.0551	6.3	14.7493	3.8	0.5151	7.4	0.0678	3.8	NA	NA	422	26	423	16	94.58	NA	423	16
J09_1_t3_Grain25	0.1835	2.2	1.9194	2.6	13.1818	3.4	0.5210	2.6	2685	45	2693	35	2703	65	65.10	-0.70	2685	45
J09_1_t3_Grain26	0.0553	6.3	9.8135	3.6	0.7770	7.2	0.1019	3.6	424	144	584	33	626	23	3.95	-47.40	626	23
J09_1_t3_Grain27	0.0599	5.3	9.9305	3.3	0.8317	6.3	0.1007	3.3	600	120	615	30	619	21	80.51	-3.09	619	21
J09_1_t3_Grain29	0.0567	6.6	15.2672	4.0	0.5121	7.8	0.0655	4.0	NA	NA	420	27	409	17	46.40	NA	409	17
J09_1_t3_Grain30	0.0560	4.9	11.1607	3.2	0.6918	5.8	0.0896	3.2	452	114	534	25	553	19	10.33	-22.28	553	19
J09_1_t3_Grain31	0.0609	5.1	9.7561	3.6	0.8607	6.2	0.1025	3.6	636	115	630	30	629	23	92.28	1.05	629	23
J09_1_t3_Grain32	0.0645	9.2	9.6618	5.5	0.9205	10.8	0.1035	5.5	758	199	663	53	635	35	33.08	16.25	635	35
J09_1_t3_Grain33	0.0601	3.1	9.7752	2.3	0.8477	3.8	0.1023	2.3	607	74	623	19	628	16	65.37	-3.41	628	16
J09_1_t3_Grain34	0.1305	1.6	2.5400	1.9	7.0840	2.4	0.3937	1.9	2105	39	2122	25	2140	42	28.40	-1.68	2105	39
J09_1_t3_Grain35	0.0730	2.5	5.5494	2.2	1.8138	3.4	0.1802	2.2	1014	60	1050	24	1068	26	14.61	-5.34	1068	26
J09_1_t3_Grain36	0.0609	7.1	12.9366	4.1	0.6491	8.2	0.0773	4.1	NA	NA	508	33	480	20	12.44	NA	480	20
J09_1_t3_Grain37	0.0583	7.6	12.2699	4.3	0.6551	8.7	0.0815	4.3	541	170	512	36	505	22	74.85	6.65	505	22
J09_1_t3_Grain38	0.0519	5.3	20.3252	3.5	0.3521	6.4	0.0492	3.5	NA	NA	306	17	310	11	68.67	NA	310	11
J09_1_t3_Grain39	0.0607	4.1	10.5485	2.8	0.7934	5.0	0.0948	2.8	629	95	593	23	584	17	50.63	7.12	584	17
J09_1_t3_Grain41	0.0815	3.3	4.6490	2.6	2.4171	4.2	0.2151	2.6	1234	72	1248	32	1256	33	66.60	-1.82	1256	33
J09_1_t3_Grain43	0.0602	4.1	10.0100	2.8	0.8292	4.9	0.0999	2.8	611	94	613	24	614	18	96.10	-0.50	614	18
J09_1_t3_Grain44	0.0616	8.2	10.6045	4.6	0.8009	9.4	0.0943	4.6	660	181	597	43	581	27	49.78	12.02	581	27
J09_1_t3_Grain47	0.0566	8.3	9.6525	4.7	0.8085	9.5	0.1036	4.7	476	188	602	44	635	29	20.54	-33.51	635	29
J09_1_t3_Grain48	0.0599	6.7	10.1420	4.1	0.8143	7.9	0.0986	4.1	600	150	605	36	606	25	94.83	-1.04	606	25
J09_1_t3_Grain49	0.0599	6.1	14.7929	3.8	0.5583	7.2	0.0676	3.8	NA	NA	450	27	422	17	6.10	NA	422	17
J09_1_t3_Grain50	0.0585	7.6	14.9477	4.3	0.5396	8.7	0.0669	4.3	NA	NA	438	31	417	18	24.49	NA	417	18
J09_1_t3_Grain51	0.0587	3.2	12.5786	2.4	0.6434	4.0	0.0795	2.4	NA	NA	504	17	493	13	14.99	NA	493	13
J09_1_t3_Grain52	0.0763	3.3	5.2411	2.6	2.0073	4.2	0.1908	2.6	1103	73	1118	30	1126	30	68.57	-2.06	1126	30

J09_1_t3_Grain53	0.1029	3.2	3.5026	2.9	4.0506	4.4	0.2855	2.9	1677	66	1644	37	1619	46	28.02	3.46	1677	66
J09_1_t3_Grain54	0.1247	2.5	2.8563	2.6	6.0195	3.6	0.3501	2.6	2025	52	1979	34	1935	50	1.37	4.42	2025	52
J09_1_t3_Grain55	0.0581	5.2	14.5138	3.2	0.5519	6.1	0.0689	3.2	NA	NA	446	23	430	14	23.44	NA	430	14
J09_1_t3_Grain56	0.0533	3.8	20.3500	2.8	0.3611	4.7	0.0491	2.8	NA	NA	313	13	309	9	54.37	NA	309	9
J09_1_t3_Grain57	0.1058	2.2	3.3003	2.2	4.4201	3.1	0.3030	2.2	1728	49	1716	28	1706	38	59.02	1.28	1728	49
J09_1_t3_Grain59	0.2272	0.8	1.6722	1.6	18.7331	1.8	0.5980	1.6	3032	28	3028	21	3022	50	59.72	0.35	3032	28
J09_1_t3_Grain60	0.0612	5.9	9.8619	3.7	0.8556	7.0	0.1014	3.7	646	132	628	33	623	24	77.26	3.66	623	24
J09_1_t3_Grain61	0.0616	5.6	9.5147	3.6	0.8927	6.7	0.1051	3.6	660	125	648	33	644	24	83.56	2.43	644	24
J09_1_t3_Grain62	0.1612	2.5	2.2124	2.9	10.0463	3.8	0.4520	2.9	2468	50	2439	37	2404	64	18.49	2.60	2468	50
J09_1_t3_Grain63	0.0624	5.2	10.3093	3.4	0.8346	6.2	0.0970	3.4	688	115	616	29	597	21	25.47	13.24	597	21
J09_1_t3_Grain64	0.1245	2.1	2.5913	2.3	6.6244	3.1	0.3859	2.3	2022	46	2063	30	2104	48	1.96	-4.06	2022	46
J09_1_t3_Grain65	0.0810	2.2	4.6232	2.1	2.4157	3.0	0.2163	2.1	1221	53	1247	24	1262	28	22.38	-3.34	1262	28
J09_1_t3_Grain67	0.0539	5.7	14.9254	3.4	0.4979	6.6	0.0670	3.4	NA	NA	410	23	418	15	60.53	NA	418	15
J09_1_t3_Grain68	0.0630	12.9	15.0602	6.5	0.5768	14.4	0.0664	6.5	NA	NA	462	54	414	27	9.81	NA	414	27
J09_1_t3_Grain69	0.0593	4.9	10.6270	3.2	0.7694	5.8	0.0941	3.2	578	111	579	26	580	19	98.21	-0.28	580	19
J09_1_t3_Grain71	0.0630	4.1	9.0090	2.9	0.9642	5.0	0.1110	2.9	708	93	685	26	679	20	62.85	4.19	679	20
J09_1_t3_Grain72	0.0882	3.3	4.2772	2.8	2.8432	4.3	0.2338	2.8	1387	69	1367	34	1354	38	55.34	2.34	1354	38
J09_1_t3_Grain73	0.0613	6.3	9.1241	4.0	0.9263	7.5	0.1096	4.0	650	141	666	37	670	27	82.41	-3.18	670	27
J09_1_t3_Grain74	0.0606	6.4	11.3766	3.9	0.7345	7.5	0.0879	3.9	625	143	559	33	543	21	46.22	13.11	543	21
J09_1_t3_Grain75	0.0551	6.9	16.1551	4.0	0.4703	8.0	0.0619	4.0	NA	NA	391	26	387	16	78.53	NA	387	16
J09_1_t3_Grain76	0.0616	4.4	10.7181	2.9	0.7924	5.2	0.0933	2.9	660	99	593	24	575	18	25.46	12.91	575	18
J09_1_t3_Grain77	0.0572	5.8	14.6413	3.8	0.5387	6.9	0.0683	3.8	NA	NA	438	25	426	17	36.64	NA	426	17
J09_1_t3_Grain79	0.0574	7.0	15.2207	4.1	0.5200	8.1	0.0657	4.1	NA	NA	425	28	410	17	39.17	NA	410	17
J09_1_t3_Grain80	0.1098	2.6	3.1716	2.5	4.7734	3.6	0.3153	2.5	1796	55	1780	32	1767	44	49.97	1.63	1796	55
J09_1_t3_Grain81	0.0577	6.4	10.1317	4.0	0.7852	7.6	0.0987	4.0	518	146	588	34	607	24	34.24	-17.05	607	24
J09_1_t3_Grain82	0.0832	3.3	5.0531	2.7	2.2702	4.3	0.1979	2.7	1274	71	1203	32	1164	32	2.63	8.63	1164	32
J09_1_t3_Grain83	0.0615	7.7	9.9206	4.3	0.8547	8.8	0.1008	4.3	657	169	627	42	619	26	74.74	5.74	619	26
J09_1_t3_Grain84	0.0535	4.6	14.7275	2.9	0.5009	5.5	0.0679	2.9	NA	NA	412	19	423	13	29.36	NA	423	13
J09_1_t3_Grain85	0.0558	4.6	15.9744	3.2	0.4816	5.6	0.0626	3.2	NA	NA	399	19	391	13	42.60	NA	391	13

J09_1_t3_Grain87	0.0610	5.8	10.0604	3.6	0.8360	6.8	0.0994	3.6	639	129	617	32	611	22	75.23	4.43	611	22
J09_1_t3_Grain89	0.0639	4.1	10.6610	2.8	0.8264	5.0	0.0938	2.8	738	93	612	24	578	17	1.46	21.72	578	17
J09_1_t3_Grain90	0.1083	2.8	3.3091	2.6	4.5126	3.9	0.3022	2.6	1771	59	1733	34	1702	44	23.60	3.89	1771	59
J09_1_t3_Grain91	0.0577	4.9	11.3250	3.2	0.7025	5.8	0.0883	3.2	518	113	540	25	545	18	72.37	-5.23	545	18
J09_1_t3_Grain93	0.1283	1.6	2.6062	1.9	6.7877	2.5	0.3837	1.9	2075	39	2084	25	2094	42	48.54	-0.90	2075	39
J09_1_t3_Grain96	0.0576	4.3	11.8203	3.0	0.6719	5.2	0.0846	3.0	515	100	522	22	524	16	88.98	-1.74	524	16
J09_1_t3_Grain98	0.0627	4.3	9.9602	3.0	0.8680	5.3	0.1004	3.0	698	97	634	26	617	20	17.97	11.65	617	20
J09_1_t3_Grain99	0.0613	8.6	10.8932	4.6	0.7759	9.7	0.0918	4.6	650	188	583	44	566	26	48.60	12.87	566	26
J09_2_Grain01	0.0610	3.9	10.0100	2.5	0.8402	4.6	0.0999	2.5	639	90	619	22	614	17	62	4	614	17
J09_2_Grain02	0.0608	5.4	10.1833	2.7	0.8232	6.0	0.0982	2.7	632	121	610	28	604	17	69	4	604	17
Rejected Analyses																		
J09_1_Grain01	0.1284	1.6	2.8686	1.9	6.1715	2.5	0.3486	1.9	2076	39	2000	25	1928	39	0.00	7.14		
J09_1_Grain02	0.1355	1.8	2.6504	2.0	7.0490	2.7	0.3773	2.0	2170	41	2118	27	2064	43	0.20	4.92		
J09_1_t3_Grain100	0.2014	1.2	1.9186	1.9	14.4732	2.3	0.5212	1.9	2838	32	2781	25	2704	52	0.00	4.70		
J09_1_t3_Grain40	0.1344	1.1	3.2362	3.0	5.7261	3.2	0.3090	3.0	2156	33	1935	30	1736	50	0.00	19.50		
J09_1_t3_Grain42	0.0573	5.0	22.7531	3.3	0.3472	6.0	0.0440	3.3	NA	NA	303	16	277	10	0.08	NA		
J09_1_t3_Grain45	0.1661	2.1	2.6316	2.8	8.7027	3.5	0.3800	2.8	2519	44	2307	34	2076	56	0.00	17.57		
J09_1_t3_Grain66	0.0611	2.1	11.5340	2.0	0.7304	2.9	0.0867	2.0	643	55	557	14	536	12	0.00	16.61		
J09_1_t3_Grain78	0.2263	0.8	1.7596	1.4	17.7322	1.6	0.5683	1.4	3026	28	2975	20	2901	45	0.00	4.14		
J09_1_t3_Grain95	0.0685	2.2	10.3627	2.9	0.9114	3.7	0.0965	2.9	884	55	658	19	594	18	0.00	32.80		
J09_2_Grain03	0.1643	1.5	2.3057	2.0	9.8249	2.5	0.4337	2.0	2500	37	2418	27	2322	47	0	7		

[1]Concentration uncertainty 5%

[2]Data not corrected for common lead

[3]Concordance calculated as ($^{206}Pb/^{238}U$ age/^{207}Pb-^{206}Pb Age)*100

[4]Accepted dates have probability of concordance >1%

Decay constants of Jaffey et al. (1971) used with modification after Mattinson (1987)

bd = below detection, NA = not available

s_x includes all random uncertainties (s_m, ε); s_{total} includes all random and systematic uncertainties (s_m, ε, ε', s_y, λ)

A.2 Detrital zircon fission-track and U-Pb data

20EJ01 - West Bonne Bay F-12 – Hibernia Formation (Upper) – Core # 1, boxes 110-113

Spot Name	U/Si	± 2SE	Ns	Area (um)	ξ	± 2SE	ZFT Age	2SE (Ma)	U-Pb Best Age[(4)]	$2s_{total}$ (Ma)	Cooling-Type
J01_1_Grain01	0.000606	0.000132	208	900	0.022746	0.001215	420	96	622	24	EXHUMATIONAL
J01_1_t2_Grain01	0.000984	0.000072	172	900	0.022746	0.001215	217	23	291	12	EXHUMATIONAL
J01_1_t2_Grain02	0.001000	0.000022	179	900	0.022746	0.001215	222	17	587	20	EXHUMATIONAL
J01_1_t2_Grain03	0.000502	0.000040	135	900	0.022746	0.001215	331	39	591	24	EXHUMATIONAL
J01_1_t2_Grain04	0.000728	0.000049	133	900	0.022746	0.001215	227	25	641	23	EXHUMATIONAL
J01_1_t2_Grain05	0.001127	0.000056	243	900	0.022746	0.001215	267	22	281	11	MAGMATIC
J01_1_t2_Grain06	0.001236	0.000024	261	900	0.022746	0.001215	261	17	546	17	EXHUMATIONAL
J01_1_t2_Grain07	0.000634	0.000015	221	900	0.022746	0.001215	426	30	603	22	EXHUMATIONAL
J01_1_t2_Grain08	0.000713	0.000017	176	900	0.022746	0.001215	304	24	534	19	EXHUMATIONAL
J01_1_t2_Grain09	0.000527	0.000025	198	900	0.022746	0.001215	458	39	582	22	EXHUMATIONAL
J01_1_t2_Grain10	0.000595	0.000030	248	900	0.022746	0.001215	506	41	586	21	EXHUMATIONAL
J01_1_t2_Grain11	0.000967	0.000018	232	900	0.022746	0.001215	296	20	538	18	EXHUMATIONAL
J01_1_t2_Grain12	0.000642	0.000012	197	900	0.022746	0.001215	377	28	597	21	EXHUMATIONAL
J01_1_t3_Grain03	0.000275	0.000023	117	900	0.022746	0.001215	517	65	557	27	MAGMATIC
J01_1_t3_Grain06	0.000510	0.000017	105	900	0.022746	0.001215	255	26	426	19	EXHUMATIONAL
J01_1_t3_Grain15	0.000578	0.000011	149	900	0.022746	0.001215	318	27	579	23	EXHUMATIONAL
J01_1_t3_Grain16	0.000362	0.000008	115	900	0.022746	0.001215	390	37	1811	70	EXHUMATIONAL
J01_1_t3_Grain19	0.000480	0.000007	134	900	0.022746	0.001215	343	30	603	25	EXHUMATIONAL
J01_1_t3_Grain22	0.000653	0.000026	108	900	0.022746	0.001215	206	21	633	23	EXHUMATIONAL
J01_1_t3_Grain25	0.000250	0.000008	105	900	0.022746	0.001215	511	52	586	29	MAGMATIC
J01_1_t3_Grain27	0.000496	0.000008	170	900	0.022746	0.001215	419	33	621	24	EXHUMATIONAL
J01_1_t3_Grain31	0.000505	0.000010	109	900	0.022746	0.001215	267	26	596	24	EXHUMATIONAL
J01_1_t3_Grain34	0.000731	0.000028	143	900	0.022746	0.001215	242	22	587	21	EXHUMATIONAL

J01_1_t3_Grain40	0.000509	0.000021	147	900	0.022746	0.001215	355	33	574	22	EXHUMATIONAL
J01_1_t3_Grain46	0.000607	0.000011	161	900	0.022746	0.001215	327	26	589	22	EXHUMATIONAL
J01_1_t3_Grain48	0.000339	0.000008	143	900	0.022746	0.001215	512	44	547	25	MAGMATIC
J01_1_t3_Grain49	0.000815	0.000019	200	900	0.022746	0.001215	303	22	556	19	EXHUMATIONAL
J01_1_t3_Grain68	0.000644	0.000034	145	900	0.022746	0.001215	279	27	1493	39	EXHUMATIONAL
J01_1_t3_Grain73	0.000539	0.000013	116	900	0.022746	0.001215	266	25	592	23	EXHUMATIONAL
J01_1_t3_Grain76	0.000600	0.000020	275	900	0.022746	0.001215	555	38	1827	52	EXHUMATIONAL
J01_1_t3_Grain84	0.000430	0.000007	114	900	0.022746	0.001215	326	31	532	22	EXHUMATIONAL
J01_1_t3_Grain89	0.000364	0.000009	87	900	0.022746	0.001215	295	33	2146	51	EXHUMATIONAL
J01_1_t3_Grain91	0.000925	0.000033	139	900	0.022746	0.001215	187	17	599	19	EXHUMATIONAL
J01_2_Grain01	0.001597	0.000022	263	900	0.025091	0.001302	226	14	607	15	EXHUMATIONAL
J01_2_Grain02	0.000736	0.000017	194	900	0.025091	0.001302	358	27	604	18	EXHUMATIONAL
J01_2_Grain03	0.000685	0.000017	199	900	0.025091	0.001302	393	30	677	19	EXHUMATIONAL
J01_2_Grain04	0.001710	0.000078	248	900	0.025091	0.001302	199	16	328	9	EXHUMATIONAL
J01_2_Grain05	0.000353	0.000021	131	900	0.025091	0.001302	498	53	570	20	MAGMATIC
J01_2_Grain06	0.000487	0.000010	190	900	0.025091	0.001302	522	39	968	28	EXHUMATIONAL
J01_2_Grain07	0.000649	0.000034	201	900	0.025091	0.001302	418	37	545	16	EXHUMATIONAL
J01_2_Grain08	0.000949	0.000028	216	900	0.025091	0.001302	310	23	286	9	MAGMATIC
J01_2_Grain09	0.000593	0.000015	146	900	0.025091	0.001302	334	29	587	17	EXHUMATIONAL
J01_2_Grain10	0.000979	0.000054	220	900	0.025091	0.001302	306	27	606	17	EXHUMATIONAL
J01_2_Grain11	0.000981	0.000025	157	900	0.025091	0.001302	219	18	596	16	EXHUMATIONAL
J01_2_Grain12	0.000600	0.000014	148	900	0.025091	0.001302	335	29	541	17	EXHUMATIONAL
J01_2_Grain13	0.000925	0.000035	187	900	0.025091	0.001302	276	23	294	9	MAGMATIC
J01_2_Grain14	0.000613	0.000011	238	900	0.025091	0.001302	520	35	987	26	EXHUMATIONAL
J01_2_Grain15	0.000557	0.000020	185	900	0.025091	0.001302	447	37	627	18	EXHUMATIONAL
J01_2_Grain16	0.000625	0.000041	193	900	0.025091	0.001302	417	40	606	18	EXHUMATIONAL
J01_2_Grain17	0.000700	0.000012	191	900	0.025091	0.001302	369	27	620	18	EXHUMATIONAL
Rejected Analyses											
J01_2_Grain18	0.000350	0.000017	226	900	0.025091	0.001302	843	69	1081	30	EXHUMATIONAL

20EJ02 - West Bonne Bay F-12 – Hibernia Formation (Upper) – Core # 1, boxes 92-96

Spot Name	U/Si	± 2SE	Ns	Area (um)	ξ	± 2SE	ZFT Age	2SE (Ma)	U-Pb Best Age[4]	$2s_{total}$ (Ma)	Cooling-Type
J02_1_Grain01	0.001057	0.000046	245	900	0.022746	0.001215	286	22	634	20	EXHUMATIONAL
J02_1_Grain02	0.000961	0.000040	221	900	0.022746	0.001215	284	23	1856	48	EXHUMATIONAL
J02_1_t2_Grain01	0.001199	0.000034	198	900	0.022746	0.001215	205	16	285	11	EXHUMATIONAL
J02_1_t2_Grain02	0.001053	0.000047	188	900	0.022746	0.001215	222	19	547	18	EXHUMATIONAL
J02_1_t2_Grain03	0.001091	0.000022	228	900	0.022746	0.001215	259	18	551	18	EXHUMATIONAL
J02_1_t2_Grain04	0.002196	0.000090	228	900	0.022746	0.001215	130	10	580	16	EXHUMATIONAL
J02_1_t2_Grain05	0.000836	0.000040	200	900	0.022746	0.001215	295	25	600	20	EXHUMATIONAL
J02_1_t2_Grain06	0.001772	0.000044	261	900	0.022746	0.001215	184	12	335	11	EXHUMATIONAL
J02_1_t2_Grain07	0.001248	0.000090	287	900	0.022746	0.001215	284	26	607	19	EXHUMATIONAL
J02_1_t2_Grain08	0.000962	0.000019	246	900	0.022746	0.001215	315	21	594	19	EXHUMATIONAL
J02_1_t2_Grain09	0.001530	0.000028	261	900	0.022746	0.001215	212	14	551	16	EXHUMATIONAL
J02_1_t3_Grain03	0.000485	0.000011	128	900	0.022746	0.001215	325	30	590	24	EXHUMATIONAL
J02_1_t3_Grain105	0.001084	0.000048	177	900	0.022746	0.001215	203	18	299	12	EXHUMATIONAL
J02_1_t3_Grain108	0.000448	0.000020	161	900	0.022746	0.001215	439	40	565	23	EXHUMATIONAL
J02_1_t3_Grain109	0.001228	0.000046	233	900	0.022746	0.001215	235	18	297	11	EXHUMATIONAL
J02_1_t3_Grain114	0.002016	0.000072	160	900	0.022746	0.001215	100	9	596	16	EXHUMATIONAL
J02_1_t3_Grain120	0.000526	0.000038	157	900	0.022746	0.001215	366	39	613	23	EXHUMATIONAL
J02_1_t3_Grain126	0.000285	0.000006	153	900	0.022746	0.001215	645	54	933	35	EXHUMATIONAL
J02_1_t3_Grain143	0.000756	0.000066	200	900	0.022746	0.001215	326	37	435	17	EXHUMATIONAL
J02_1_t3_Grain154	0.001278	0.000156	110	900	0.022746	0.001215	108	17	566	17	EXHUMATIONAL
J02_1_t3_Grain156	0.000493	0.000012	176	900	0.022746	0.001215	436	35	1094	34	EXHUMATIONAL
J02_1_t3_Grain18	0.000529	0.000018	184	900	0.022746	0.001215	425	35	618	24	EXHUMATIONAL
J02_1_t3_Grain20	0.000409	0.000007	168	900	0.022746	0.001215	499	39	600	26	EXHUMATIONAL
J02_1_t3_Grain29	0.002226	0.000144	163	900	0.022746	0.001215	92	9	293	10	EXHUMATIONAL
J02_1_t3_Grain30	0.001350	0.000120	143	900	0.022746	0.001215	132	16	318	12	EXHUMATIONAL
J02_1_t3_Grain33	0.000856	0.000015	89	900	0.022746	0.001215	130	14	613	20	EXHUMATIONAL

J02_1_t3_Grain34	0.000339	0.000013	165	900	0.022746	0.001215	587	51	625	26	MAGMATIC
J02_1_t3_Grain39	0.001122	0.000058	171	900	0.022746	0.001215	190	18	554	19	EXHUMATIONAL
J02_1_t3_Grain42	0.000431	0.000007	97	900	0.022746	0.001215	278	29	609	24	EXHUMATIONAL
J02_1_t3_Grain50	0.000287	0.000011	81	900	0.022746	0.001215	347	41	640	29	EXHUMATIONAL
J02_1_t3_Grain57	0.000839	0.000017	137	900	0.022746	0.001215	203	18	1806	48	EXHUMATIONAL
J02_1_t3_Grain60	0.000508	0.000021	195	900	0.022746	0.001215	468	39	561	22	EXHUMATIONAL
J02_1_t3_Grain64	0.001326	0.000039	138	900	0.022746	0.001215	130	12	926	24	EXHUMATIONAL
J02_1_t3_Grain70	0.000337	0.000016	136	900	0.022746	0.001215	491	48	604	27	EXHUMATIONAL
J02_1_t3_Grain72	0.001017	0.000017	127	900	0.022746	0.001215	156	14	380	14	EXHUMATIONAL
J02_1_t3_Grain80	0.000607	0.000024	156	900	0.022746	0.001215	317	28	610	23	EXHUMATIONAL
J02_1_t3_Grain81	0.001326	0.000078	143	900	0.022746	0.001215	135	14	588	18	EXHUMATIONAL
J02_1_t3_Grain89	0.000350	0.000008	130	900	0.022746	0.001215	453	41	1024	37	EXHUMATIONAL
J02_1_t3_Grain91	0.000939	0.000037	131	900	0.022746	0.001215	174	17	1181	31	EXHUMATIONAL
J02_1_t3_Grain93	0.000588	0.000023	156	900	0.022746	0.001215	327	29	627	23	EXHUMATIONAL
J02_2_Grain01	0.000388	0.000010	114	900	0.025091	0.001302	397	39	544	19	EXHUMATIONAL
J02_2_Grain02	0.001412	0.000039	133	900	0.025091	0.001302	130	12	593	16	EXHUMATIONAL
J02_2_Grain03	0.000623	0.000011	132	900	0.025091	0.001302	289	26	1389	34	EXHUMATIONAL
J02_2_Grain05	0.000946	0.000014	168	900	0.025091	0.001302	243	19	417	12	EXHUMATIONAL
J02_2_Grain06	0.000784	0.000012	172	900	0.025091	0.001302	299	23	2099	40	EXHUMATIONAL
J02_2_Grain07	0.000494	0.000015	134	900	0.025091	0.001302	368	34	2753	36	EXHUMATIONAL
J02_2_Grain08	0.000809	0.000019	192	900	0.025091	0.001302	322	24	600	17	EXHUMATIONAL
J02_2_Grain09	0.001410	0.000084	195	900	0.025091	0.001302	190	18	291	9	EXHUMATIONAL
J02_2_Grain10	0.000303	0.000025	157	900	0.025091	0.001302	685	78	1072	31	EXHUMATIONAL
J02_2_Grain11	0.000827	0.000013	179	900	0.025091	0.001302	295	23	616	18	EXHUMATIONAL
J02_2_Grain12	0.000666	0.000011	208	900	0.025091	0.001302	421	30	1359	33	EXHUMATIONAL
J02_2_Grain13	0.001065	0.000017	162	900	0.025091	0.001302	209	17	533	15	EXHUMATIONAL
J02_2_Grain14	0.000444	0.000007	112	900	0.025091	0.001302	342	33	1711	62	EXHUMATIONAL
J02_2_Grain15	0.000604	0.000011	155	900	0.025091	0.001302	348	29	1650	54	EXHUMATIONAL
J02_2_Grain16	0.000476	0.000012	196	900	0.025091	0.001302	550	42	982	26	EXHUMATIONAL

J02_2_Grain17	0.000962	0.000024	154	900	0.025091	0.001302	219	19	1274	28	EXHUMATIONAL
J02_2_Grain18	0.001342	0.000025	143	900	0.025091	0.001302	147	13	287	9	EXHUMATIONAL
J02_2_Grain19	0.001357	0.000016	155	900	0.025091	0.001302	157	13	297	9	EXHUMATIONAL
Rejected Analyses											
J02_1_t3_Grain161	0.000383	0.000024	149	900	0.022746	0.001215	473	49	410	20	
J02_1_t3_Grain58	0.000200	0.000005	153	900	0.022746	0.001215	899	77	2738	53	

20EJ03 - West Bonne Bay F-12 – Hibernia Formation (Upper) – Core # 1, boxes 24-30

Spot Name	U/Si	± 2SE	Ns	Area (um)	ξ	± 2SE	ZFT Age	2SE (Ma)	U-Pb Best Age[(4)]	$2s_{total}$ (Ma)	Cooling-Type
J03_1_Grain01	0.001446	0.000120	160	900	0.022750	0.001000	138	16	594	17	EXHUMATIONAL
J03_1_Grain02	0.000775	0.000029	200	900	0.022750	0.001000	318	25	2041	44	EXHUMATIONAL
J03_1_t2_Grain01	0.000677	0.000042	187	900	0.022750	0.001000	340	33	429	17	EXHUMATIONAL
J03_1_t2_Grain04	0.000569	0.000050	271	900	0.022750	0.001000	575	62	1007	32	EXHUMATIONAL
J03_1_t2_Grain06	0.000976	0.000035	202	900	0.022750	0.001000	257	20	590	19	EXHUMATIONAL
J03_1_t2_Grain08	0.000730	0.000011	319	900	0.022750	0.001000	530	31	1025	29	EXHUMATIONAL
J03_1_t2_Grain09	0.001004	0.000026	265	900	0.022750	0.001000	325	22	1073	27	EXHUMATIONAL
J03_1_t3_Grain01	0.000544	0.000042	149	900	0.022750	0.001000	337	38	589	23	EXHUMATIONAL
J03_1_t3_Grain02	0.000667	0.000014	184	900	0.022750	0.001000	340	26	603	22	EXHUMATIONAL
J03_1_t3_Grain04	0.000920	0.000038	150	900	0.022750	0.001000	203	19	578	20	EXHUMATIONAL
J03_1_t3_Grain06	0.000497	0.000018	96	900	0.022750	0.001000	239	26	363	18	EXHUMATIONAL
J03_1_t3_Grain102	0.000511	0.000012	145	900	0.022750	0.001000	349	30	543	21	EXHUMATIONAL
J03_1_t3_Grain106	0.000478	0.000017	105	900	0.022750	0.001000	272	28	291	14	MAGMATIC
J03_1_t3_Grain113	0.001004	0.000028	160	900	0.022750	0.001000	198	17	584	18	EXHUMATIONAL
J03_1_t3_Grain124	0.000376	0.000040	207	900	0.022750	0.001000	660	84	616	25	MAGMATIC
J03_1_t3_Grain126	0.000785	0.000022	145	900	0.022750	0.001000	229	20	623	20	EXHUMATIONAL
J03_1_t3_Grain128	0.000232	0.000008	102	900	0.022750	0.001000	533	56	970	39	EXHUMATIONAL
J03_1_t3_Grain132	0.000433	0.000005	88	900	0.022750	0.001000	252	27	2531	42	EXHUMATIONAL

J03_1_t3_Grain147	0.000366	0.000006	137	900	0.022750	0.001000	457	40	1207	39	EXHUMATIONAL
J03_1_t3_Grain150	0.000639	0.000017	80	900	0.022750	0.001000	156	18	631	22	EXHUMATIONAL
J03_1_t3_Grain27	0.000572	0.000013	143	900	0.022750	0.001000	308	27	612	23	EXHUMATIONAL
J03_1_t3_Grain30	0.001442	0.000025	123	900	0.022750	0.001000	107	10	131	6	MAGMATIC
J03_1_t3_Grain33	0.000407	0.000021	169	900	0.022750	0.001000	505	47	555	24	MAGMATIC
J03_1_t3_Grain47	0.001488	0.000021	148	900	0.022750	0.001000	124	10	383	13	EXHUMATIONAL
J03_1_t3_Grain53	0.000898	0.000019	95	900	0.022750	0.001000	132	14	1176	31	EXHUMATIONAL
J03_1_t3_Grain54	0.001501	0.000037	165	900	0.022750	0.001000	137	11	289	10	EXHUMATIONAL
J03_1_t3_Grain65	0.000943	0.000032	101	900	0.022750	0.001000	134	14	1727	47	EXHUMATIONAL
J03_1_t3_Grain72	0.000245	0.000005	79	900	0.022750	0.001000	396	45	1980	67	EXHUMATIONAL
J03_1_t3_Grain74	0.000266	0.000009	93	900	0.022750	0.001000	427	47	690	31	EXHUMATIONAL
J03_1_t3_Grain75	0.000644	0.000008	154	900	0.022750	0.001000	295	24	331	15	MAGMATIC
J03_1_t3_Grain76	0.001244	0.000024	185	900	0.022750	0.001000	185	14	550	17	EXHUMATIONAL
J03_1_t3_Grain77	0.002008	0.000031	143	900	0.022750	0.001000	89	8	292	10	EXHUMATIONAL
J03_1_t3_Grain85	0.000629	0.000012	154	900	0.022750	0.001000	302	25	532	20	EXHUMATIONAL
J03_1_t3_Grain89	0.000852	0.000072	333	900	0.022750	0.001000	476	48	620	21	EXHUMATIONAL
J03_1_t3_Grain90	0.000760	0.000023	188	900	0.022750	0.001000	305	24	602	20	EXHUMATIONAL
J03_1_t3_Grain92	0.000409	0.000013	109	900	0.022750	0.001000	329	33	599	24	EXHUMATIONAL
J03_1_t3_Grain94	0.000889	0.000029	123	900	0.022750	0.001000	173	17	413	15	EXHUMATIONAL
J03_2_Grain01	0.000580	0.000010	174	900	0.025091	0.001302	405	32	613	19	EXHUMATIONAL
J03_2_Grain02	0.001347	0.000026	131	900	0.025091	0.001302	134	12	597	16	EXHUMATIONAL
J03_2_Grain03	0.001000	0.000020	220	900	0.025091	0.001302	300	21	530	15	EXHUMATIONAL
J03_2_Grain04	0.000817	0.000015	200	900	0.025091	0.001302	332	24	2163	40	EXHUMATIONAL
J03_2_Grain05	0.000967	0.000014	136	900	0.025091	0.001302	193	17	2650	32	EXHUMATIONAL
J03_2_Grain06	0.000568	0.000013	200	900	0.025091	0.001302	473	35	605	19	EXHUMATIONAL
J03_2_Grain07	0.000517	0.000027	212	900	0.025091	0.001302	548	47	585	19	MAGMATIC
J03_2_Grain08	0.001015	0.000013	148	900	0.025091	0.001302	200	17	603	17	EXHUMATIONAL
J03_2_Grain09	0.001120	0.000041	250	900	0.025091	0.001302	304	22	281	9	MAGMATIC
J03_2_Grain10	0.000204	0.000007	102	900	0.025091	0.001302	662	70	2082	75	EXHUMATIONAL

J03_2_Grain11	0.000454	0.000008	116	900	0.025091	0.001302	347	33	1997	55	EXHUMATIONAL
J03_2_Grain12	0.000359	0.000007	144	900	0.025091	0.001302	536	46	1774	68	EXHUMATIONAL
J03_2_Grain13	0.000788	0.000013	181	900	0.025091	0.001302	312	24	614	18	EXHUMATIONAL
J03_2_Grain14	0.000493	0.000041	144	900	0.025091	0.001302	395	46	1970	53	EXHUMATIONAL
J03_2_Grain15	0.001320	0.000060	160	900	0.025091	0.001302	167	15	599	16	EXHUMATIONAL
J03_2_Grain16	0.000271	0.000013	105	900	0.025091	0.001302	518	57	2057	60	EXHUMATIONAL
J03_2_Grain18	0.000343	0.000025	145	900	0.025091	0.001302	564	62	946	29	EXHUMATIONAL
J03_2_Grain19	0.000902	0.000015	202	900	0.025091	0.001302	305	22	582	16	EXHUMATIONAL
J03_2_Grain20	0.001073	0.000014	155	900	0.025091	0.001302	198	16	285	9	EXHUMATIONAL
J03_2_Grain21	0.000836	0.000037	206	900	0.025091	0.001302	334	28	545	16	EXHUMATIONAL
Rejected Analyses											
J03_2_Grain22	0.000673	0.000013	87	900	0.025091	0.001302	178	19			
J03_2_Grain17	0.001175	0.000019	212	900	0.025091	0.001302	247	17			
J03_1_t2_Grain07	0.001410	0.000066	202	900	0.022750	0.001000	179	15			

20EJ05 – Hibernia B-16 55 – Hibernia Formation (Lower) – Core # 2, box 3

Spot Name	U/Si	± 2SE	Ns	Area (um)	ξ	± 2SE	ZFT Age	2SE (Ma)	U-Pb Best Age[(4)]	$2s_{total}$ (Ma)	Cooling-Type
J05_2_Grain01	0.001854	0.000138	195	900	0.025091	0.001302	145	15	384	11	EXHUMATIONAL
J05_2_Grain02	0.000347	0.000007	165	900	0.025091	0.001302	631	51	1928	60	EXHUMATIONAL
J05_2_Grain03	0.000471	0.000009	166	900	0.025091	0.001302	473	38	772	23	EXHUMATIONAL
J05_2_Grain05	0.000377	0.000008	71	900	0.025091	0.001302	257	31	1014	28	EXHUMATIONAL
J05_2_Grain06	0.000499	0.000014	137	900	0.025091	0.001302	372	34	1931	48	EXHUMATIONAL
J05_2_Grain07	0.000808	0.000029	100	900	0.025091	0.001302	170	18	414	13	EXHUMATIONAL
J05_2_Grain08	0.000843	0.000013	101	900	0.025091	0.001302	165	17	414	12	EXHUMATIONAL
J05_2_Grain09	0.000545	0.000023	133	900	0.025091	0.001302	332	32	410	14	EXHUMATIONAL
J05_2_Grain10	0.000497	0.000016	173	900	0.025091	0.001302	467	38	814	23	EXHUMATIONAL
J05_2_Grain11	0.000438	0.000007	61	900	0.025091	0.001302	191	25	1605	60	EXHUMATIONAL

J05_2_t2_Grain01	0.000914	0.000014	69	900	0.025091	0.001302	104	13	137	5	MAGMATIC
J05_2_t2_Grain03	0.000334	0.000017	54	900	0.025091	0.001302	221	32	1650	64	EXHUMATIONAL
J05_2_t2_Grain04	0.000750	0.000032	171	900	0.025091	0.001302	310	27	968	24	EXHUMATIONAL
J05_2_t2_Grain05	0.000540	0.000047	124	900	0.025091	0.001302	312	39	387	12	EXHUMATIONAL
J05_2_t2_Grain06	0.000315	0.000013	114	900	0.025091	0.001302	486	49	1633	66	EXHUMATIONAL
J05_2_t2_Grain07	0.000686	0.000049	185	900	0.025091	0.001302	365	37	1119	27	EXHUMATIONAL
J05_2_t2_Grain08	0.001343	0.000043	85	900	0.025091	0.001302	88	10	143	5	MAGMATIC
Rejected Analyses											
J05_2_Grain04	0.000666	0.000028	116	900	0.025091	0.001302	238	24			
J05_2_t2_Grain02	0.000974	0.000022	139	900	0.025091	0.001302	196	17			

20EJ06 – Hibernia B-16 54W – Hibernia Formation (Lower) – Core # 1, box 1-3

Spot Name	U/Si	± 2SE	Ns	Area (um)	ξ	± 2SE	ZFT Age	2SE (Ma)	U-Pb Best Age[4]	$2s_{total}$ (Ma)	Cooling-Type
J06_1_Grain01	0.001393	0.000030	304	900	0.022750	0.001000	270	17	1015	25	EXHUMATIONAL
J06_1_Grain02	0.001415	0.000026	214	900	0.022750	0.001000	188	13	1796	42	EXHUMATIONAL
J06_1_Grain03	0.001380	0.000072	329	900	0.022750	0.001000	294	22	584	17	EXHUMATIONAL
J06_1_Grain05	0.001643	0.000022	244	900	0.022750	0.001000	185	12	418	13	EXHUMATIONAL
J06_1_Grain06	0.000922	0.000017	180	900	0.022750	0.001000	242	19	2761	33	EXHUMATIONAL
J06_1_t2_Grain03	0.000858	0.000126	241	900	0.022750	0.001000	346	55	1784	66	EXHUMATIONAL
J06_1_t2_Grain06	0.001850	0.000023	264	900	0.022750	0.001000	178	11	404	12	EXHUMATIONAL
J06_1_t3_Grain100	0.000354	0.000008	119	900	0.022750	0.001000	411	39	548	24	EXHUMATIONAL
J06_1_t3_Grain17	0.000610	0.000014	158	900	0.022750	0.001000	319	26	420	18	EXHUMATIONAL
J06_1_t3_Grain18	0.000539	0.000040	94	900	0.022750	0.001000	217	28	609	24	EXHUMATIONAL
J06_1_t3_Grain25	0.000173	0.000004	98	900	0.022750	0.001000	680	71	2735	54	EXHUMATIONAL
J06_1_t3_Grain28	0.000295	0.000007	102	900	0.022750	0.001000	423	43	541	27	EXHUMATIONAL
J06_1_t3_Grain34	0.001230	0.000060	240	900	0.022750	0.001000	242	20	2073	42	EXHUMATIONAL
J06_1_t3_Grain39	0.000674	0.000019	220	900	0.022750	0.001000	400	29	1791	51	EXHUMATIONAL

J06_1_t3_Grain40	0.000633	0.000019	232	900	0.022750	0.001000	447	32	540	20	EXHUMATIONAL
J06_1_t3_Grain48	0.001048	0.000020	137	900	0.022750	0.001000	163	14	993	26	EXHUMATIONAL
J06_1_t3_Grain49	0.001003	0.000017	220	900	0.022750	0.001000	271	19	2562	35	EXHUMATIONAL
J06_1_t3_Grain60	0.000434	0.000008	167	900	0.022750	0.001000	469	37	580	24	EXHUMATIONAL
J06_1_t3_Grain62	0.000601	0.000007	135	900	0.022750	0.001000	278	24	1420	37	EXHUMATIONAL
J06_1_t3_Grain63	0.000817	0.000011	224	900	0.022750	0.001000	338	23	1693	52	EXHUMATIONAL
J06_1_t3_Grain71	0.000643	0.000026	202	900	0.022750	0.001000	386	31			
J06_1_t3_Grain82	0.000493	0.000008	166	900	0.022750	0.001000	412	33	528	21	EXHUMATIONAL
J06_1_t3_Grain84	0.001290	0.000078	135	900	0.022750	0.001000	131	14	139	6	MAGMATIC
J06_1_t3_Grain89	0.000771	0.000016	74	900	0.022750	0.001000	120	14	1156	31	EXHUMATIONAL
J06_1_t3_Grain97	0.000682	0.000007	170	900	0.022750	0.001000	308	24	382	15	EXHUMATIONAL
J06_2_Grain01	0.001858	0.000029	182	900	0.025091	0.001302	135	10	457	11	EXHUMATIONAL
J06_2_Grain02	0.000700	0.000013	179	900	0.025091	0.001302	347	27	470	15	EXHUMATIONAL
J06_2_Grain03	0.000746	0.000012	193	900	0.025091	0.001302	351	26	999	25	EXHUMATIONAL
J06_2_Grain04	0.000802	0.000014	181	900	0.025091	0.001302	307	23	1479	33	EXHUMATIONAL
J06_2_Grain05	0.000844	0.000042	192	900	0.025091	0.001302	310	27	338	11	MAGMATIC
J06_2_Grain06	0.000439	0.000014	61	900	0.025091	0.001302	191	25	1874	54	EXHUMATIONAL
J06_2_Grain07	0.000987	0.000011	149	900	0.025091	0.001302	207	17	425	12	EXHUMATIONAL
J06_2_Grain08	0.000664	0.000022	189	900	0.025091	0.001302	385	31	599	17	EXHUMATIONAL
J06_2_Grain09	0.000914	0.000013	202	900	0.025091	0.001302	301	22	638	17	EXHUMATIONAL
J06_2_Grain10	0.000888	0.000011	171	900	0.025091	0.001302	263	20	340	11	EXHUMATIONAL
Rejected Analyses											
J06_1_t2_Grain01	0.000580	0.000035	279	900	0.022750	0.001000	581	49	527	21	NA
J06_1_t2_Grain05	0.000425	0.000009	294	900	0.022750	0.001000	819	51	1695	63	EXHUMATIONAL
J06_1_t3_Grain57	0.000619	0.000055	286	900	0.022750	0.001000	559	60	359	15	NA

20EJ08 – Hebron M-04 – Hibernia Formation (Upper) – Core # 3, box 37-42

Spot Name	U/Si	± 2SE	Ns	Area (um)	ξ	± 2SE	ZFT Age	2SE (Ma)	U-Pb Best Age[4]	$2s_{total}$ (Ma)	Cooling-Type
J08_1_Grain01	0.001366	0.000036	285	900	0.022750	0.001000	259	17	428	14	EXHUMATIONAL
J08_1_Grain02	0.001558	0.000027	322	900	0.022750	0.001000	256	15	610	17	EXHUMATIONAL
J08_1_t2_Grain01	0.000627	0.000013	160	900	0.022750	0.001000	315	26	2058	48	EXHUMATIONAL
J08_1_t2_Grain02	0.000675	0.000012	229	900	0.022750	0.001000	415	28	603	21	EXHUMATIONAL
J08_1_t2_Grain03	0.000953	0.000041	216	900	0.022750	0.001000	280	23	630	22	EXHUMATIONAL
J08_1_t2_Grain04	0.000692	0.000017	266	900	0.022750	0.001000	469	31	553	20	EXHUMATIONAL
J08_1_t2_Grain05	0.000825	0.000019	272	900	0.022750	0.001000	404	26	519	18	EXHUMATIONAL
J08_1_t2_Grain06	0.000768	0.000020	200	900	0.022750	0.001000	321	24	577	19	EXHUMATIONAL
J08_1_t3_Grain02	0.000984	0.000102	135	900	0.022750	0.001000	171	23	362	14	EXHUMATIONAL
J08_1_t3_Grain09	0.000526	0.000016	99	900	0.022750	0.001000	234	24	420	18	EXHUMATIONAL
J08_1_t3_Grain102	0.000572	0.000011	122	900	0.022750	0.001000	264	24	1666	55	EXHUMATIONAL
J08_1_t3_Grain107	0.000943	0.000021	202	900	0.022750	0.001000	265	20	598	19	EXHUMATIONAL
J08_1_t3_Grain14	0.000714	0.000019	86	900	0.022750	0.001000	150	17	599	21	EXHUMATIONAL
J08_1_t3_Grain15	0.002202	0.000324	199	900	0.022750	0.001000	113	18	298	11	EXHUMATIONAL
J08_1_t3_Grain19	0.000452	0.000010	137	900	0.022750	0.001000	372	33	1004	33	EXHUMATIONAL
J08_1_t3_Grain24	0.000613	0.000009	111	900	0.022750	0.001000	225	22	603	22	EXHUMATIONAL
J08_1_t3_Grain25	0.000718	0.000016	169	900	0.022750	0.001000	291	23	591	22	EXHUMATIONAL
J08_1_t3_Grain36	0.000484	0.000010	219	900	0.022750	0.001000	548	39	1895	56	EXHUMATIONAL
J08_1_t3_Grain37	0.000802	0.000046	174	900	0.022750	0.001000	269	25	629	21	EXHUMATIONAL
J08_1_t3_Grain50	0.000691	0.000013	182	900	0.022750	0.001000	324	25	538	21	EXHUMATIONAL
J08_1_t3_Grain55	0.000673	0.000013	187	900	0.022750	0.001000	342	26	595	21	EXHUMATIONAL
J08_1_t3_Grain61	0.000704	0.000011	148	900	0.022750	0.001000	260	22	499	19	EXHUMATIONAL
J08_1_t3_Grain64	0.000526	0.000010	110	900	0.022750	0.001000	259	25	1100	33	EXHUMATIONAL
J08_1_t3_Grain65	0.000874	0.000015	125	900	0.022750	0.001000	178	16	431	15	EXHUMATIONAL
J08_1_t3_Grain72	0.000562	0.000010	115	900	0.022750	0.001000	254	24	591	23	EXHUMATIONAL
J08_1_t3_Grain75	0.000482	0.000008	165	900	0.022750	0.001000	418	33	1311	38	EXHUMATIONAL

J08_1_t3_Grain84	0.000459	0.000008	119	900	0.022750	0.001000	320	30	610	23	EXHUMATIONAL
J08_1_t3_Grain85	0.000751	0.000043	189	900	0.022750	0.001000	311	29	562	19	EXHUMATIONAL
J08_1_t3_Grain98	0.000586	0.000007	127	900	0.022750	0.001000	268	24	660	22	EXHUMATIONAL
Rejected Analyses											
J08_1_t3_Grain95	0.000655	0.000019	170	900	0.022750	0.001000	320	26			

20EJ09 – Hebron M-04 – Hibernia Formation (Upper) – Core # 3, box 26-33

Spot Name	U/Si	± 2SE	Ns	Area (um)	ξ	± 2SE	ZFT Age	2SE (Ma)	U-Pb Best Age[(4)]	$2s_{total}$ (Ma)	Cooling-Type
J09_1_Grain03	0.002076	0.000078	277	900	0.022750	0.001000	166	12	391	12	EXHUMATIONAL
J09_1_t2_Grain01	0.000903	0.000041	320	900	0.022750	0.001000	433	31	1417	34	EXHUMATIONAL
J09_1_t2_Grain02	0.000860	0.000053	296	900	0.022750	0.001000	421	36	604	20	EXHUMATIONAL
J09_1_t2_Grain03	0.001372	0.000040	244	900	0.022750	0.001000	221	16	587	17	EXHUMATIONAL
J09_1_t3_Grain06	0.000881	0.000016	286	900	0.022750	0.001000	398	25	416	15	MAGMATIC
J09_1_t3_Grain07	0.000497	0.000012	174	900	0.022750	0.001000	428	34	467	19	MAGMATIC
J09_1_t3_Grain11	0.001222	0.000027	281	900	0.022750	0.001000	284	18	574	17	EXHUMATIONAL
J09_1_t3_Grain12	0.000399	0.000010	126	900	0.022750	0.001000	387	36	611	24	EXHUMATIONAL
J09_1_t3_Grain15	0.000416	0.000009	101	900	0.022750	0.001000	300	31	1008	34	EXHUMATIONAL
J09_1_t3_Grain18	0.000458	0.000018	113	900	0.022750	0.001000	305	31	390	18	EXHUMATIONAL
J09_1_t3_Grain20	0.000937	0.000016	264	900	0.022750	0.001000	347	22	655	20	EXHUMATIONAL
J09_1_t3_Grain27	0.000709	0.000017	191	900	0.022750	0.001000	332	25	619	21	EXHUMATIONAL
J09_1_t3_Grain36	0.000473	0.000008	170	900	0.022750	0.001000	439	34	480	20	MAGMATIC
J09_1_t3_Grain48	0.000363	0.000014	158	900	0.022750	0.001000	528	47	606	25	EXHUMATIONAL
J09_1_t3_Grain50	0.000472	0.000010	160	900	0.022750	0.001000	415	34	417	18	MAGMATIC
J09_1_t3_Grain53	0.000383	0.000007	124	900	0.022750	0.001000	396	36	1677	66	EXHUMATIONAL
J09_1_t3_Grain60	0.000433	0.000010	180	900	0.022750	0.001000	506	39	623	24	EXHUMATIONAL
J09_1_t3_Grain61	0.000468	0.000007	138	900	0.022750	0.001000	362	31	644	24	EXHUMATIONAL
J09_1_t3_Grain63	0.000634	0.000017	247	900	0.022750	0.001000	475	33	597	21	EXHUMATIONAL

J09_1_t3_Grain74	0.000450	0.000007	210	900	0.022750	0.001000	564	40	543	21	MAGMATIC
J09_1_t3_Grain80	0.000524	0.000009	195	900	0.022750	0.001000	454	33	1796	55	EXHUMATIONAL
J09_1_t3_Grain98	0.000838	0.000018	140	900	0.022750	0.001000	208	18	617	20	EXHUMATIONAL
J09_2_Grain01	0.001400	0.000018	179	900	0.025091	0.001302	176	13	614	17	EXHUMATIONAL
J09_2_Grain02	0.000805	0.000029	220	900	0.025091	0.001302	370	28	604	17	EXHUMATIONAL
Rejected Analyses											
J09_2_Grain03	0.000737	0.000017	161	900	0.025091	0.001302	298	24			
J09_1_Grain01	0.001162	0.000022	348	900	0.022750	0.001000	368	21			
J09_1_Grain02	0.000921	0.000022	312	900	0.022750	0.001000	415	26			
J09_1_t3_Grain42	0.001542	0.000120	205	900	0.022750	0.001000	166	17			

APPENDIX B: FISSION-TRACK AGE AND U/SI

B.1 Fission-track age and U/Si of pooled Lower and Upper Hibernia Formation data (n = 269)

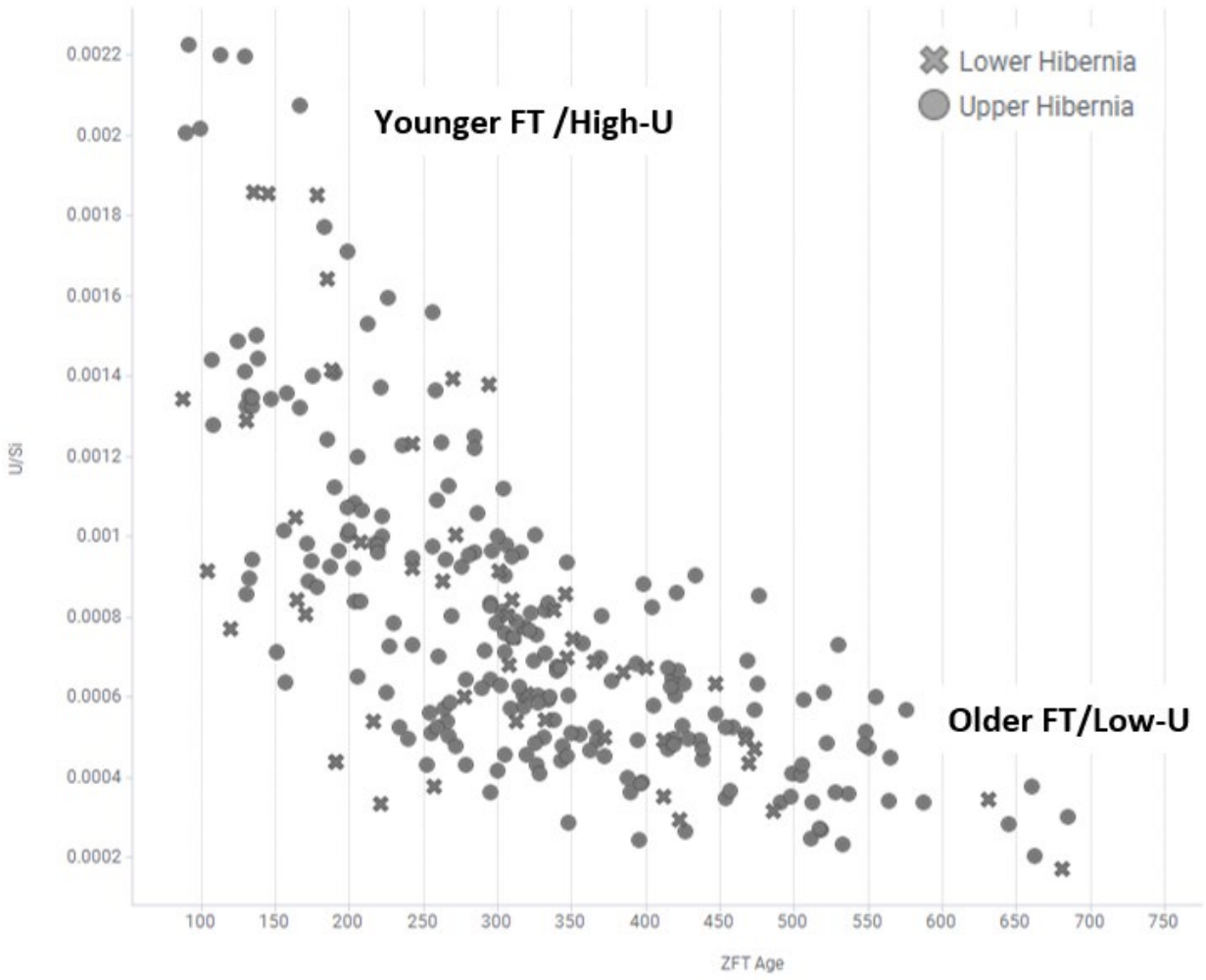

B.2 Fission-track age and U/Si of pooled Hibernia Formation data (n = 269) colored by etch time

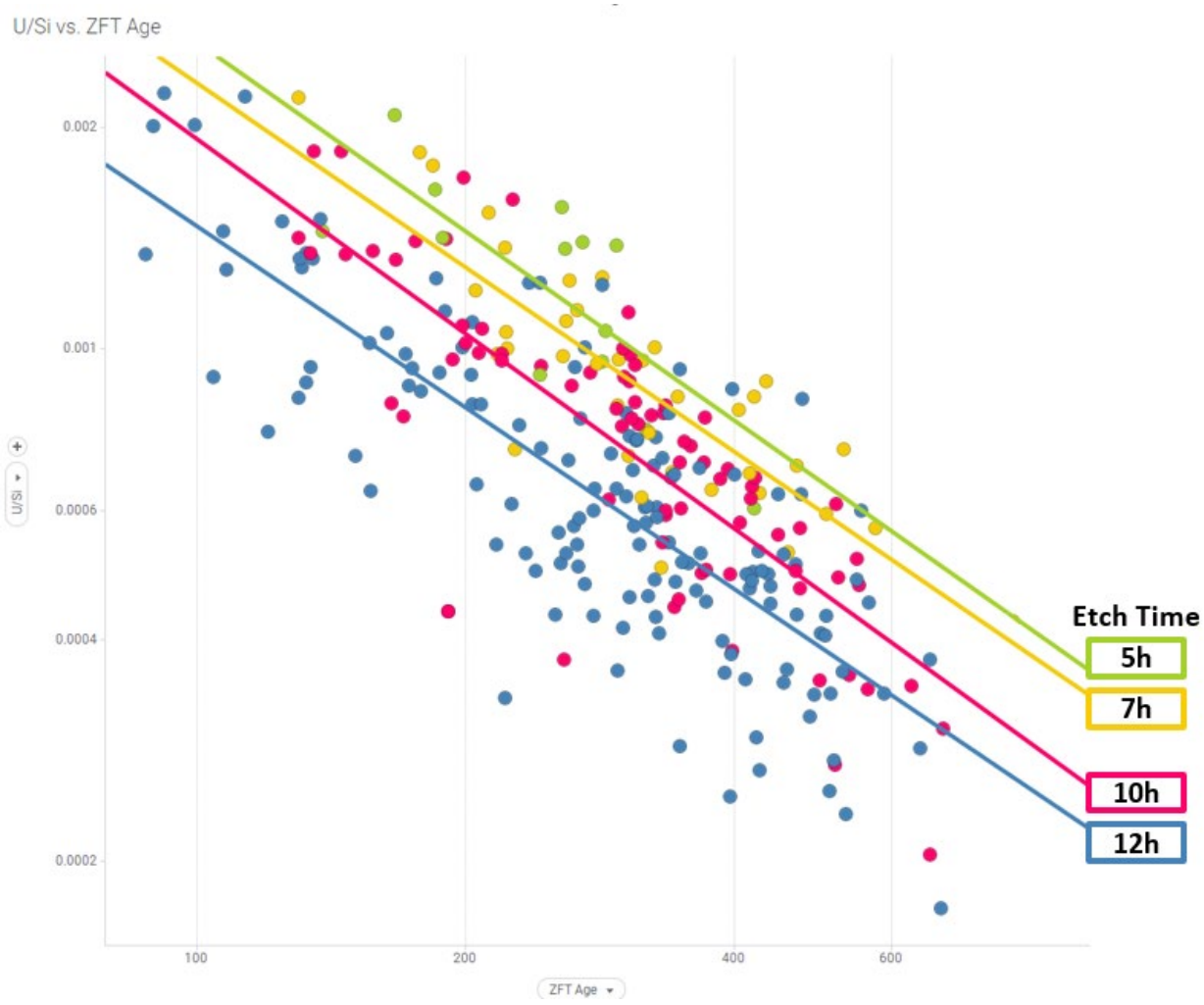

APPENDIX C: MAXIMUM DEPOSITIONAL AGE DIAGRAMS

C.1 Youngest Statistical Peak – Weighted Mean Plots

20EJ01 – West Bonne Bay F-12
(Upper Hibernia Formation)

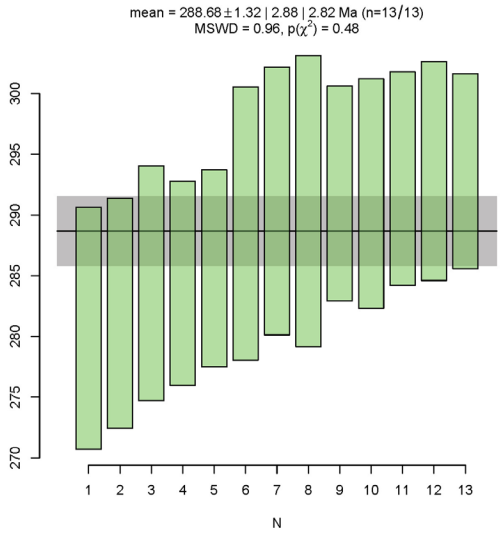

20EJ03 – West Bonne Bay F-12
(Upper Hibernia Formation)

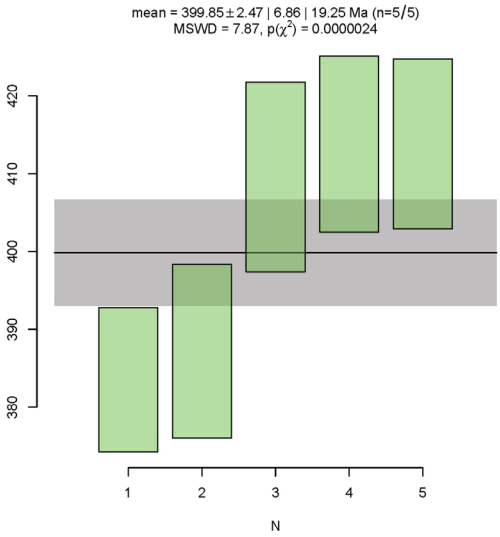

20EJ02 – West Bonne Bay F-12
(Upper Hibernia Formation)

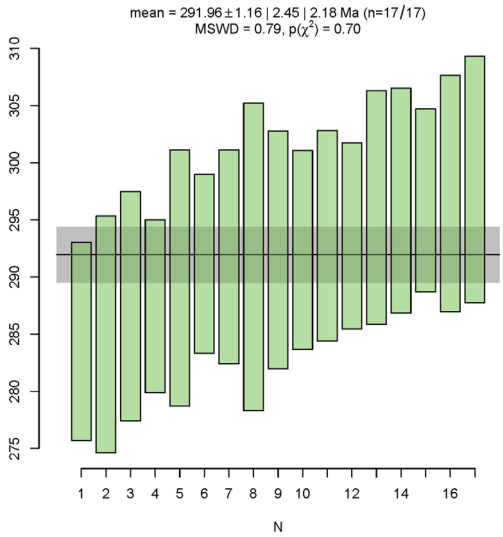

20EJ05 – Hibernia B-16 55
(Lower Hibernia Formation)

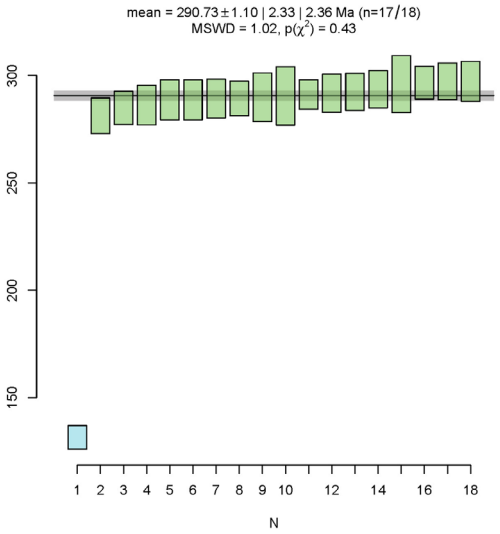

20EJ06 – Hibernia B-16 54W
(Lower Hibernia Formation)

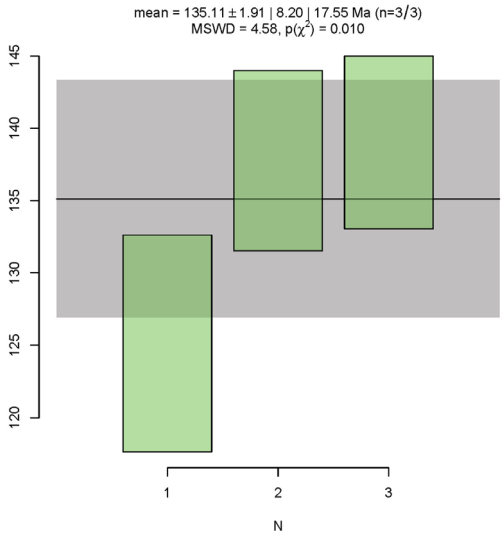

20EJ09 – Hebron M-04
(Upper Hibernia Formation)

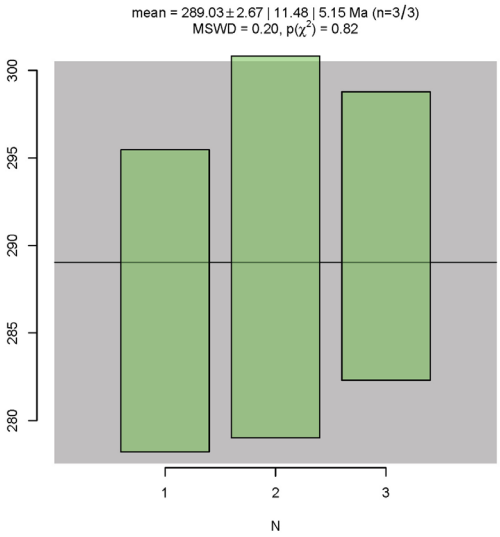

20EJ08 – Hebron M-04
(Upper Hibernia Formation)

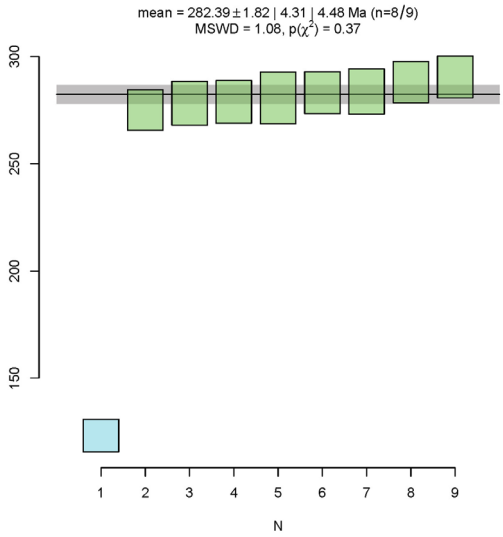

Lower Hibernia Formation (pooled)
(Hibernia B-16 55 and 54W)

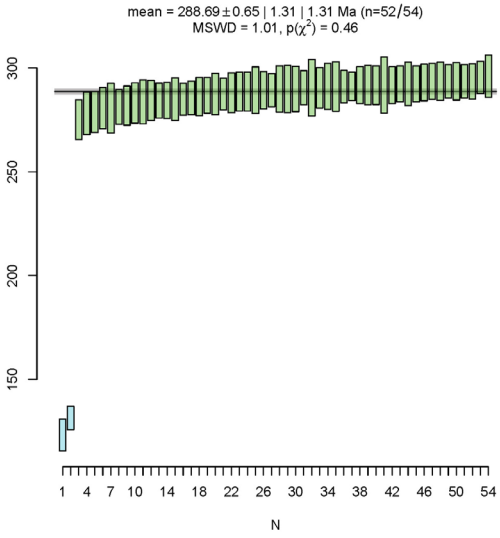

Upper Hibernia Formation (pooled)
(West Bonne Bay F-12 and Hebron M-04)

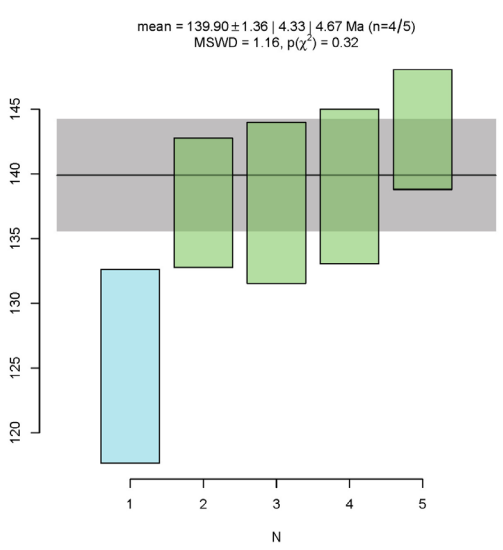

Jeanne d'Arc Formation (pooled)

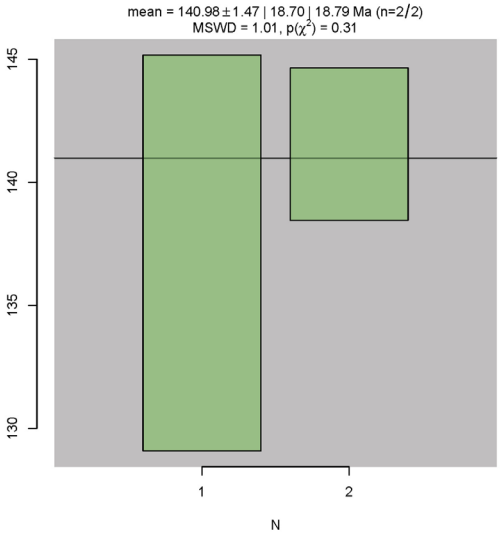

C.2 Youngest Grain Cluster – Weighted Mean Plots

20EJ01 – West Bonne Bay F-12
(Upper Hibernia Formation)

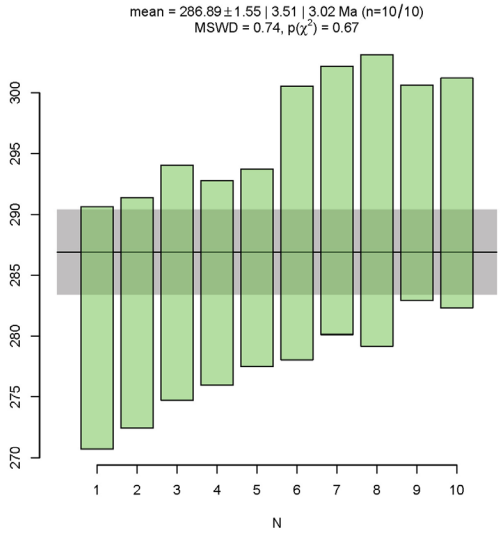

20EJ02 – West Bonne Bay F-12
(Upper Hibernia Formation)

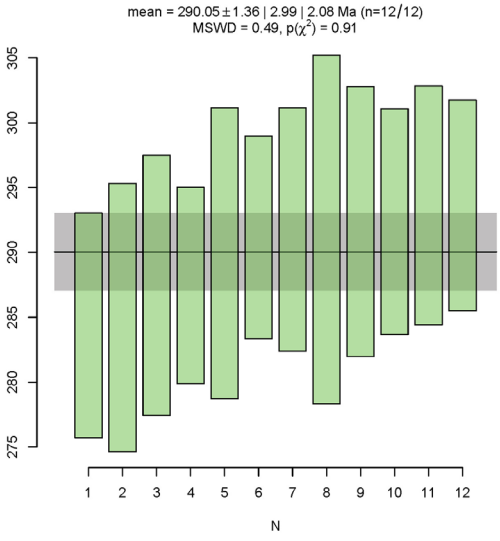

20EJ03 – West Bonne Bay F-12
(Upper Hibernia Formation)

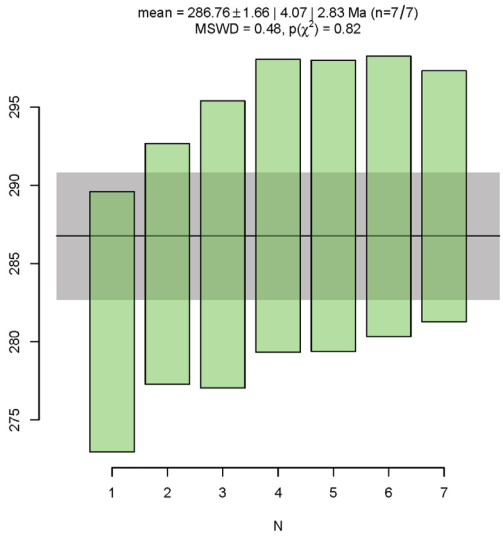

20EJ06 – Hibernia B-16 54W
(Lower Hibernia Formation)

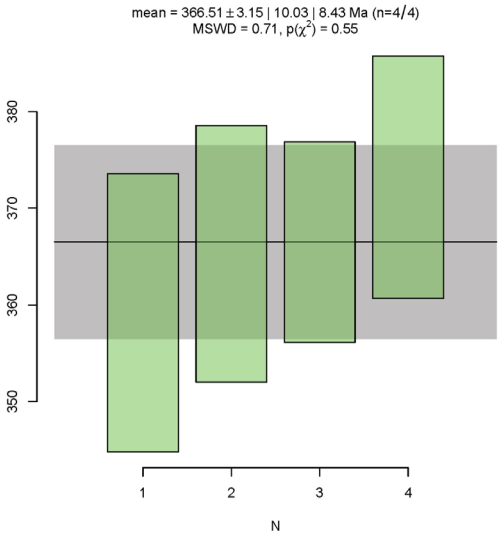

20EJ05 – Hibernia B-16 55
(Lower Hibernia Formation)

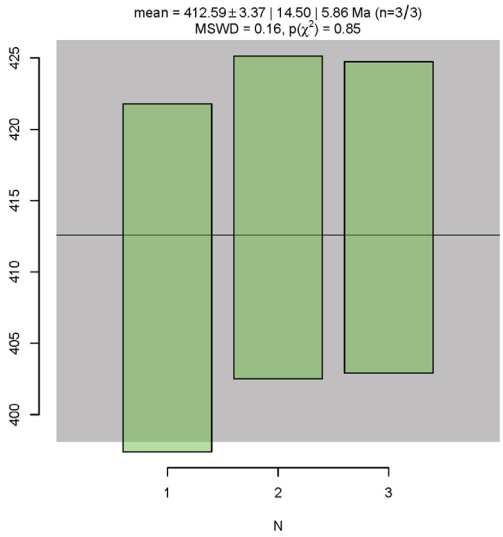

20EJ08 – Hebron M-04
(Upper Hibernia Formation)

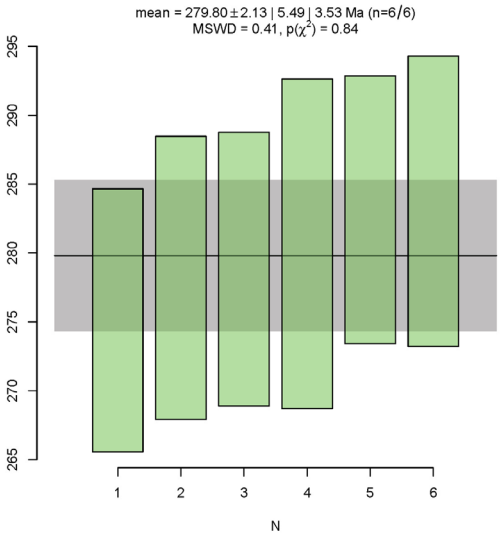

20EJ09 – Hebron M-04
(Upper Hibernia Formation)

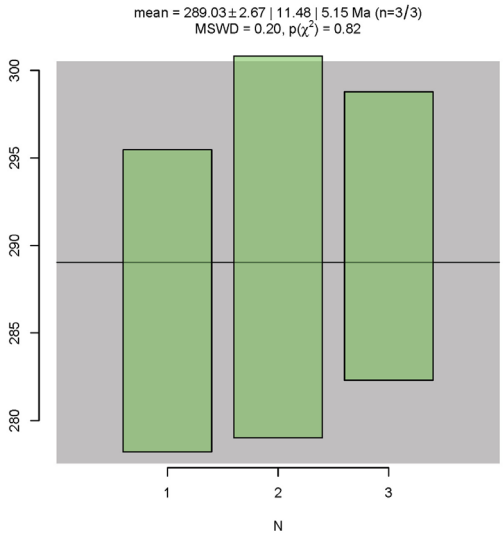

Upper Hibernia Formation (pooled)
(West Bonne Bay F-12 and Hebron M-04)

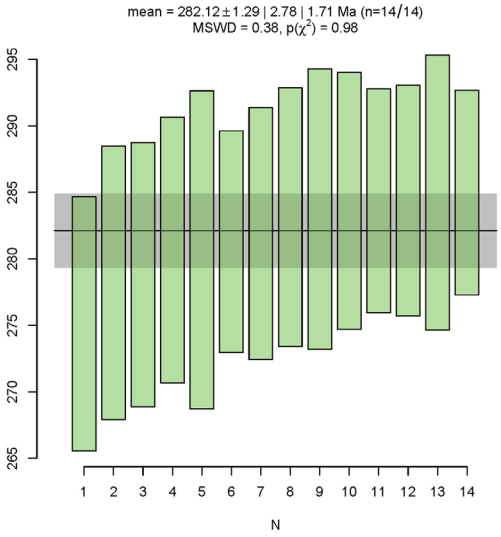

Lower Hibernia Formation (pooled)
(Hibernia B-16 55 and 54W)

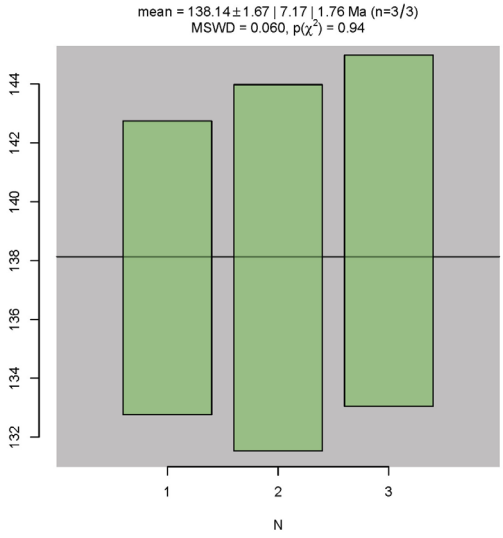

Jeanne d'Arc Formation (pooled)

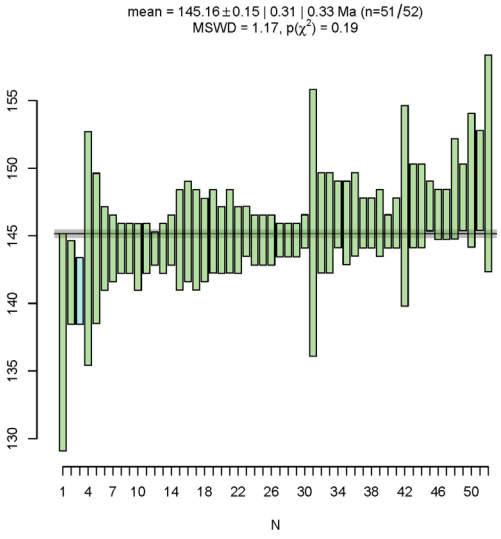

C.3 Radial Plots with peak-fitting, Peak 1 used for MDA estimates

20EJ03 – West Bonne Bay F-12
(Upper Hibernia Formation)

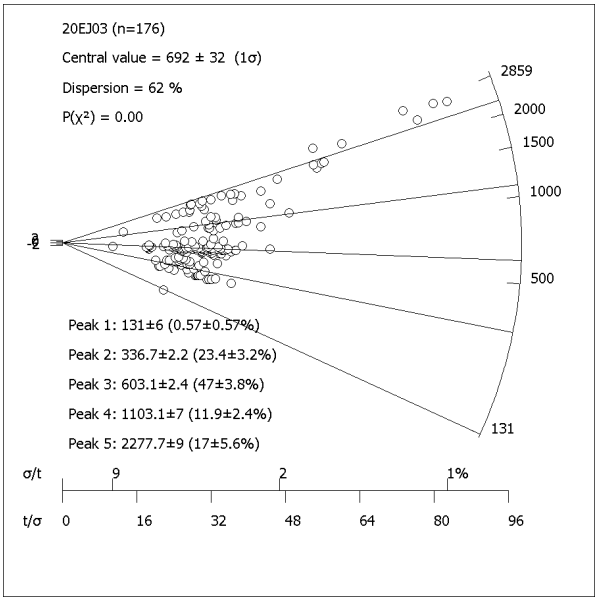

20EJ05 – Hibernia B-16 55
(Lower Hibernia Formation)

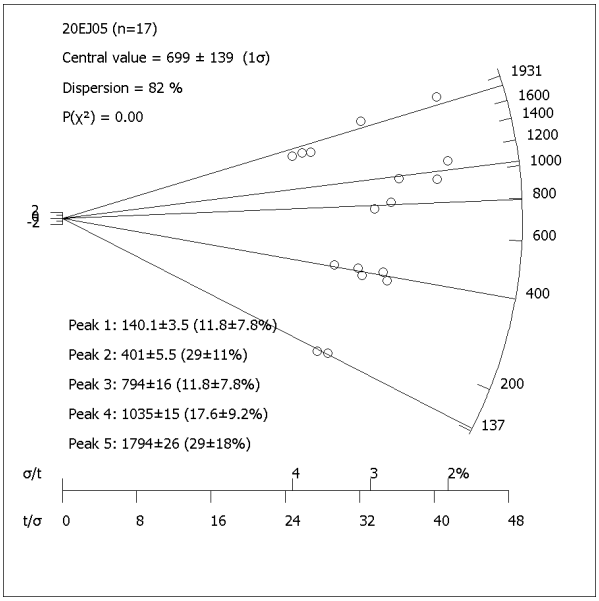

20EJ08 – Hebron M-04
(Upper Hibernia Formation)

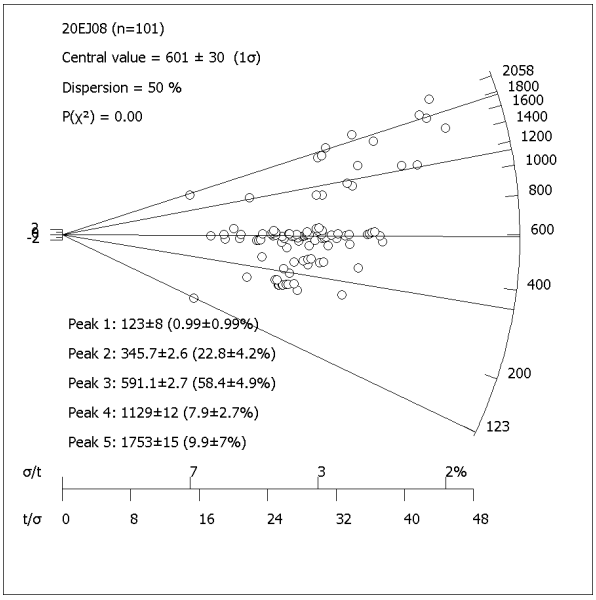

20EJ06 – Hibernia B-16 54W
(Lower Hibernia Formation)

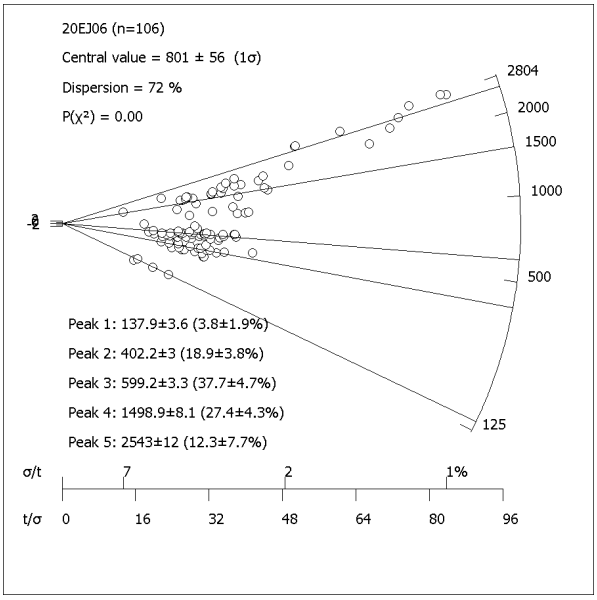

APPENDIX D: RADIALPLOTTER DIAGRAMS

D.1 Radial plots with peak-fitting for pooled Upper and Lower Hibernia Formation samples, respectively.

Lower Hibernia Formation
(Hibernia B-16 55 and 54W)

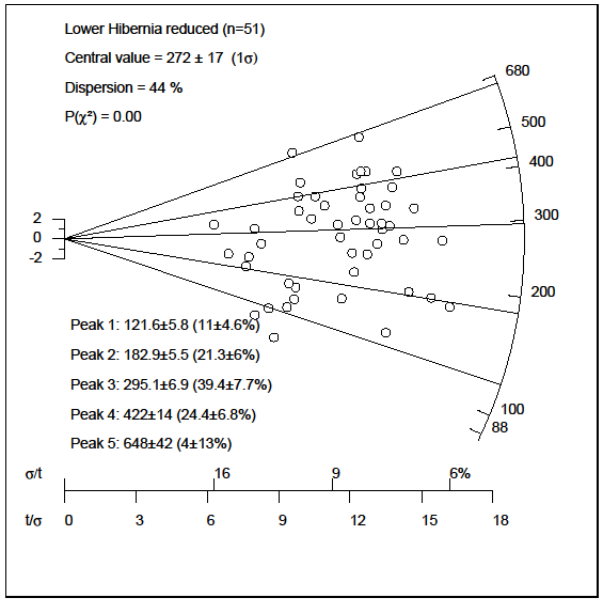

Upper Hibernia Formation
(West Bonne Bay F-12 and Hebron M-04)

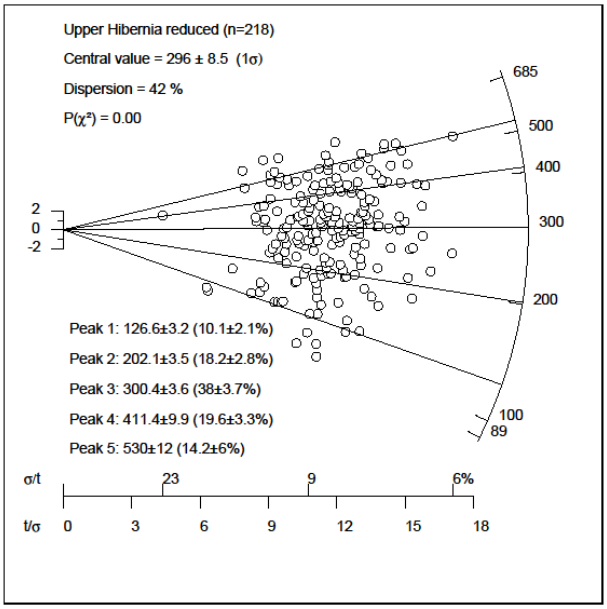

D.2 Radial plots with peak-fitting for double-dated detrital zircon FT and U-Pb ages by cooling type (exhumation- and magmatic-cooled)

FT Ages – Exhumation-cooled grains

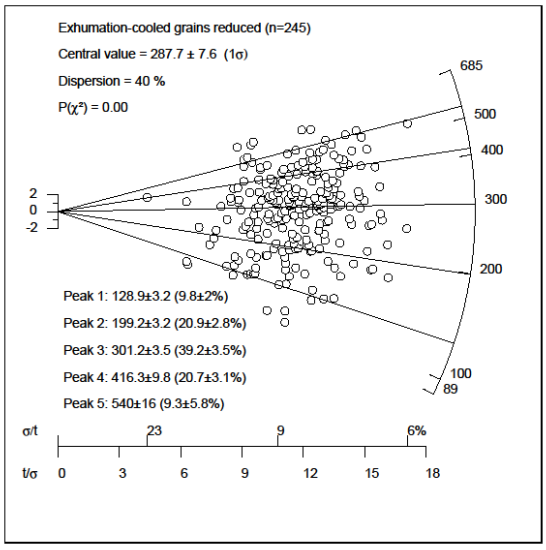

FT Ages – Magmatic-cooled grains

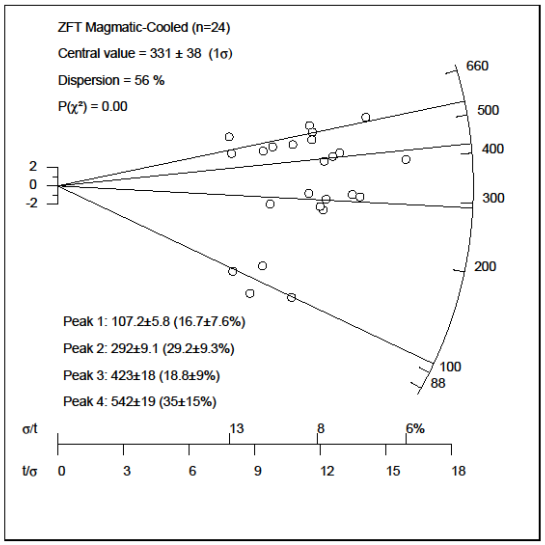

U-Pb Ages – Magmatic-cooled grains